MONTE CARLO CODE PREDICTING MODELS FOR NEUTRON ACTIVATION ANALYSIS AND EXPLORATIVE STUDY OF LARGE SAMPLE NEUTRON ACTIVATION ANALYSIS

by

Christian Amevi Adjei

A dissertation submitted to the faculty of
The University of Utah
in partial fulfillment of the requirements for the degree of

Doctor of Philosophy

in

Nuclear Engineering

Department of Civil and Environmental Engineering

The University of Utah

August 2015

The University of Utah Graduate School

STATEMENT OF DISSERTATION APPROVAL

The dissertation of **Christian Amevi Adjei**

has been approved by the following supervisory committee members:

Tatjana Jevremovic	, Chair	**05/04/15** Date Approved
Terry A. Ring	, Member	**05/04/15** Date Approved
Sivaraman Guruswamy	, Member	**02/26/15** Date Approved
Ilija Miskovic	, Member	**05/04/15** Date Approved
Roy Dunker	, Member	**05/11/15** Date Approved

and by **Michael E. Barber** , Chair/Dean of

the Department/College/School of **Civil and Environmental Engineering**

and by David B. Kieda, Dean of The Graduate School.

ABSTRACT

Neutron activation analysis is a nondestructive method used to determine elemental composition of samples by exposing them to neutron radiation, which leads to the activation of stable nuclei into radioactive nuclei. During deactivation of irradiated samples, element-signature gamma rays are emitted that are detected using gamma spectroscopy. The main goal of this dissertation is to develop detailed modeling of neutron activation analysis in predicting gamma spectra of various samples using MCNP6 and GEANT4 (version 4.9.6) codes. High precision physics models for neutron transport and ENDF/B-VII evaluated cross-sectional data library are used in both MCNP6 and GEANT4 simulations. These newly developed models are validated based on the experimental data of a National Institute of Standard and Technology (NIST) certified flyash sample and six samples with varying compositional matrices. These models predict the gamma spectra of activated samples with good agreement to measured gamma spectra. Thus, both codes, MCNP6 and GEANT4, can be used to predict neutron induced gamma emissions in samples of various compositions prior to neutron activation analysis taking place in the laboratory settings. The relative computational error is within 5 - 8%, which falls within the Monte Carlo accepted computational limit of 10%. Another goal of this dissertation is to develop an

explorative study of a large sample analysis based on neutron activation and to assess the feasibility of such experiments in research reactors, specifically the TRIGA Mark I type research reactors. The Utah Nuclear Engineering Program houses a 100 kW TRIGA Mark I research reactor with irradiation channels that were not studied for large sample neutron activation analysis. The newly developed MCNP6/GEANT4 models provide 3D point-wise spatial neutron flux distributions within irradiation channels. These models are adequate in simulating experiments prior to taking place in the laboratory. The neutron flux intensities are adequate for large sample analysis in one of the reactor irradiation channels.

TABLE OF CONTENTS

LIST OF TABLES

ACKNOWLEDGEMENTS

Glory and honour to God almighty for touching the heart of Professor Tatjana Jevremovic, and for using her to provide mentorship and the opportunity to take up a PhD at the University of Utah. I am indeed indebted to my advisor Professor Tatjana Jevremovic for her unconditional guidance, advice, and support she has provided for my academic development. Sincere gratitude to the members of my advisory committee: Professor Terry A. Ring, Professor Sivaraman Guruswamy, Professor Ilija Miskovic, and Dr. Roy Dunker for their commitment, support, and guidance. I would like to thank my colleagues at the Utah Nuclear Engineering Program (UNEP) and friends for their help and support. Finally, my heartfelt gratitude goes to my family for their prayers and support.

CHAPTER 1

INTRODUCTION

1.1. Motivation

Determination of the elemental composition of material samples can be performed with the technique of neutron activation analysis (NAA). The NAA involves the activation of material samples with neutrons; the isotopes present in the material are activated through neutron capture, transforming the sample into radioactive. The Utah Nuclear Engineering Program (UNEP) at the University of Utah has a Mark I General Atomic TRIGA Reactor (UUTR), licensed to operate at 100 kW thermal power. The UUTR is used for research, teaching, and training. The motivation for this research stems from the possibility of a computational and numerical model and simulation of the NAA process at the UUTR, with the goal of developing a realistic predictive computational model for gamma spectroscopy of NAA samples, and studying the possibility of large sample neutron activation analysis (LSNAA) at the UUTR.

In order to obtain a realistic gamma emitting spectra prediction model, detailed understanding of physics processes, UUTR reactor, detector design, and gamma spectroscopy is required. Developing the predictive simulation

models requires the study of different types of NAA (based on neutron energies), and physics process of NAA. It also requires the computational and numerical analysis of the neutron flux profiles within the main neutron irradiation channels of the UUTR. In addition to planning experiments, these predictive simulation models can be used for class teaching and training of students about NAA. The exploration study of large sample neutron activation analysis at the UUTR has never been performed. The NAA for large samples requires detailed understanding of neutron flux distribution in a designated irradiation channel, the limit of the large sample size, and if any, what will be the requirements in positioning such a sample in a designated irradiation channel. This newly developed MCNP6/GEANT4 model provides 3D point-wise spatial neutron flux distributions within the irradiation channel. These models are adequate in simulating experiments prior to their taking place in the laboratory. The neutron flux intensities are adequate for large sample analysis in one of the reactor irradiation channels of the UUTR.

1.2. Objectives

The main objectives of this research are:

1. Neutron flux profile characterization of the UUTR irradiation channels based on Monte Carlo N-Particle code version 6 (MCNP6) to ascertain the neutron flux within the irradiation port for neutron activation analysis modeling and prediction of gamma emitting spectra for

irradiated samples. Good prediction of the neutron flux 3D spatial profile within the UUTR is important for optimization of NAA experiments.

2. Numerical modeling and simulation of NAA at the UUTR, using Monte Carlo Codes – GEANT4 and MCNP6 for prediction of NAA gamma spectra of activated samples in comparison to experimentally measured gamma spectra. This includes a coupling of MCNP6 and GEANT4 in predicting the gamma spectra for activated samples. The coupling is required, because GEANT4 cannot be used for reactor modeling, only particle interactions.
3. Explorative study of large sample neutron activation analysis at the UUTR in assessing which of the irradiation channels can be used for such experiments and if there are limitations in regard to sample size, sample position within the channel, and sample heterogeneity.

1.3. Organization of the Dissertation

The basic concepts of NAA theory and the physics of thermal, epithermal, and fast NAA are discussed in Chapter 2. In Chapter 3, the specifics of the UUTR facility of interest to the objectives of this dissertation are presented. The computation analyses of spatial neutron flux profiles within the UUTR irradiation channels are discussed. The gamma flux characterization within the irradiation channels is also discussed. Chapter 4 gives descriptions of issues that pertain to uncertainty, error, and accuracy of

these newly developed models. Chapter 4 also provides the framework of quality control and quality assurance protocols as it could be implemented at the UUTR in regard to NAA. Chapter 5 presents the developed predictive models of the gamma spectrum for NAA. This includes the physics models and processes for both the MCNP and GEANT4 models and simulation results. Chapter 5 also includes the model of high purity germanium detector, and the comparison of predictive simulations with experimental NAA data. Chapter 6 outlines the feasibility of large sample neutron activation analysis in the UUTR irradiation channels. Homogeneity and heterogeneity of large samples are discussed as well. This chapter also includes descriptions and discussion about the physics of large sample activation, neutron and gamma self-shielding and attenuation, the methods of large sample analysis, and the simulation of neutron flux spatial distribution within large samples. The discussion and conclusion of this research, and future work are presented in Chapter 7.

CHAPTER 2

NEUTRON ACTIVATION ANALYSIS

2.1. Literature Review

The investigation of elemental composition of materials using neutron activation analysis (NAA) is not new. Through the discovery of neutrons by J. Chadwick in 1932 (Nobel prize, 1935) and the scientific research by F. Joliot and I. Curie in 1934, G. Hevesy and H. Levi in 1936 developed the NAA technique [1]. The NAA is used for qualitative and quantitative determination of elements based on the measurement of characteristic gamma radiation from radionuclides formed directly or indirectly by neutron irradiation of the sample, Figure 2-1. Neutron activation analysis provides researchers the ability to characterize with very low detection limits over 30 different elements, [2].

The NAA requires a source of neutrons, instrumentation for detecting gamma rays, and a detailed knowledge of the reactions that occur when neutrons interact with target nuclei. During neutron interaction with the nucleus of an atom, the neutron is either captured or scattered. When the neutron is captured (absorbed) by the nucleus, the isotope becomes an unstable radioactive isotope. The newly formed radioactive nuclide undergoes

decay in becoming stable. Possible decay modes include emitting excess energy through beta emission, positron emission, electron capture, and/or isomeric transition accompanied with the emission of photons. The high-energy photons emitted are then detected and counted with gamma spectroscopy detectors.

The NAA is neutron energy-dependent and therefore, it can be defined as thermal neutron activation analysis (TNAA), epithermal neutron activation analysis (ENAA), and fast neutron activation analysis (FNAA). The neutron capture reaction (n, γ) occurs with all isotopes and with no neutron energy threshold, [3].

2.2. Thermal Neutron Activation Analysis

TNAA employs the activation of material with low-energy neutrons (energies below 0.5 eV). Figure 2-2 shows an example of neutron cross-section distribution as a function of neutron energy indicating the most probable neutron interaction for this element in the low-energy region is radiative capture, [4, 5]. In the low-energy region, the cross-section for absorption generally varies as inversely proportional to neutron velocity. This energy region is therefore known as the $1/v$ region. In neutron capture, there is an increase in mass number of the nucleus [7] given as:

$$X_A^Z + n_0^1 \rightarrow X_A^{Z+1} \qquad (2.1)$$

The newly formed isotope becomes unstable and undergoes radioactive decay to become stable. The probability of decay for a single radioactive nuclide is known as the decay constant, λ, that is related to its half-life as follows:

Half-life: $t_{1/2}$ (sec), $$\lambda = \frac{\ln 2}{t_{1/2}} \tag{2.2}$$

The activity of a nuclide can be determined as a product of its decay constant and radioactive atoms (N). The activity: A (Becquerel's (Bq)) is then given as:

$$A(Bq) = \lambda N \tag{2.3}$$

$$\frac{dN}{dt} = -\lambda N \,, \quad A(t) = A_o e^{-\lambda t} \tag{2.4}$$

The probability of a single neutron interaction with nucleus is expressed as microscopic cross-section $(\sigma - barns\ or\ cm^2)$ and the total cross-section over a number of nuclei (N - $atoms/cm^3$) in a target per unit volume is defined as macroscopic cross-section - Σ.

$$\Sigma(cm^{-1}) = N\sigma \tag{2.5}$$

The probability of neutrons interacting with nuclei in a unit volume is calculated by multiplying the neutron flux (ϕ – $neutrons/cm^2$) with the neutron macroscopic cross-section. This gives a reaction rate (R) per second [8]. The activity of the daughter nuclide produced can be analytically determined and it is the basis on which the mass concentrations of the elements present within the sample are deduced and could be derived as [6]:

t_{irr} – irradiation time (sec), $\frac{dN}{dt} = \phi\Sigma - \lambda N$, $N(t) = \frac{\phi\Sigma}{\lambda}(1 - e^{-\lambda t_{irr}})$ (2.6)

Activity of daughter - A_D, λ_D – daughter decay constant (sec^{-1}):

$$A_D(t) = \phi\Sigma(1 - e^{-\lambda_D t_{irr}}) \tag{2.7}$$

Equations (2.6) and (2.7) are representative of the "one-group" activation, meaning that the neutron flux is monoenergetic [8]. The total reaction rate integrated over all possible neutron energies provides a more accurate activation equation given as:

$$R(n/cm^3 \cdot s) = N\int_0^\infty \varphi\sigma_{absorption}dE \tag{2.8}$$

$$\begin{aligned} A_D(t) &= (1 - e^{-\lambda_D t_{irr}})\sum_{i=0}^{n} N_i\varphi_i\sigma_{i,absorption} \\ A_D(t) &= N_p(1 - e^{-\lambda_D t_{irr}})\int_0^\infty \varphi\sigma_{absorption}dE \end{aligned} \tag{2.9}$$

The combination of equations (2.4) and (2.7) gives the activity of the daughter isotope after irradiation and decay:

$$A_D(t) = \phi\Sigma\left(1 - e^{-\lambda_D t_{irr}}\right)e^{-\lambda_D t_{decay}} \tag{2.10}$$

The total number of parent atoms (N_p) can be determined [7] as:

m – mass of sample (g); N_A – Avogadro's number; A_m – atomic mass $(g/mole)$,

$A_{\%}$ - atomic abundance ratio $$N_p(atoms) = m\frac{N_A}{A_m}A_{\%} \tag{2.11}$$

The modified NAA equation [7] is as follows:

$$A_D(t) = \phi\left[\frac{\sqrt{\pi}}{2}\sigma_p\sqrt{\frac{293}{T}}\right]m\frac{N_A}{A_m}A_{\%}(1-e^{-\lambda_D t_{irr}})e^{-\lambda_D t_{decay}} \qquad (2.12)$$

The mass *(m)*, concentration *(C)*, and number of parent isotope *(N_p)* can be calculated if the activity of the isotope, given time of irradiation and the neutron flux, is known.

$$N_p(atoms) = \frac{A_D(t)}{\sigma_p\phi\left(1-e^{-\lambda_D t_{irr}}\right)e^{-\lambda_D t_{decay}}} \qquad (2.13)$$

$$m(g) = \frac{A_D(t)}{\phi\sigma_p\frac{N_A}{A_m}A_{\%}\left(1-e^{-\lambda_D t_{irr}}\right)e^{-\lambda_D t_{decay}}} \qquad (2.14)$$

The concentration – C ($\mu g/g$ or ppm): $$C = \frac{A_D^{'}(t)}{\phi\sigma_p\frac{N_A}{A_m}A_{\%}\left(1-e^{-\lambda_D t_{irr}}\right)e^{-\lambda_D t_{decay}}} \qquad (2.15)$$

Most activated isotopes decay once to reach their stable configurations, but others go through multiple decays. Equations for calculation of grand-daughter nuclides [9] N_D – number of daughter atoms (*atoms/cm^3*);

$$\frac{dN_G(t)}{dt} = \phi\sigma_p N_p - \lambda_D N_D(t) - \lambda_G N_G(t) \qquad (2.16)$$

λ_G – grand-daughter decay constant *(sec^{-1})*, N_G – number of grand-daughter atoms *(atoms/cm^3)*, A_G – activity of grand-daughter,

$$A_G(t) = \frac{N_p\sigma_p\phi}{(\lambda_D-\lambda_G)}[\lambda_D\left(1-e^{-\lambda_D t_{irr}}\right)e^{-\lambda_D t_{decay}} - \lambda_G\left(1-e^{-\lambda_D t_{irr}}\right)e^{-\lambda_D t_{decay}}] \qquad (2.17)$$

$$N_p(atoms) = \frac{A_G(t)}{\frac{\sigma_p\phi}{(\lambda_D-\lambda_G)}[\lambda_D\left(1-e^{-\lambda_D t_{irr}}\right)e^{-\lambda_D t_{decay}} - \lambda_G\left(1-e^{-\lambda_D t_{irr}}\right)e^{-\lambda_D t_{decay}}]} \qquad (2.18)$$

$$C = \frac{A_D^i(t)}{\phi\left[\frac{\sqrt{\pi}}{2}\sigma\sqrt{\frac{293}{T}}\right]\frac{N_A}{A_m}A_{\%}\left(1-e^{-\lambda_D t_{irr}}\right)e^{-\lambda_D t_{decay}}} \qquad (2.19)$$

Another method of calculating the concentration of an element in a sample is by irradiating a certified standard sample similar to the unknown sample of interest. The mass/concentration of the standard can be multiplied by the ratio of the activity of the unknown sample over the activity of the standard, given as [8]:

$$C_{sample} = C_{standard}\frac{m_{standard}}{m_{sample}}\frac{A_{sample}}{A_{standard}} \qquad (2.20)$$

Example of thermal neutron activation analysis of Manganese Mn-56 which activates to $Mn^{56} + n' \rightarrow Mn^{57} + \gamma$: applying equation (2.15) with the following values:

Assuming the activity of daughter isotope is, *A' = 2.5164 x 10 $^{-3}$ (μCi/g);* Microscopic cross-section for radiation capture of Mn^{56} at thermal energy of 0.025 eV is, *σ = 13.412 barns;* Neutron flux within the reactor is, *ϕ = 3.7 x 10^{11} n/cm^{2}s;* at a temperature of, *T = 22^{o}C;* Half-life of Mn^{56} is, *$T_{1/2}$ = 2.57 hours;* Decay constant of Mn^{56} is, *λ = 7.46 x 10^{-5} s^{-1};* Time of irradiation of the Mn^{56} sample is, *t_{irr} = 360 secs;* and decay time - *t_{decay} = 1850 sec*

$$C = \frac{A_D^i(t)}{\phi\left[\frac{\sqrt{\pi}}{2}\sigma\sqrt{\frac{293}{T}}\right]\frac{N_A}{A_m}A_{\%}\left(1-e^{-\lambda_D t_{irr}}\right)e^{-\lambda_D t_{decay}}}$$

$$C = \frac{2.5164\times10^{-3}\,\mu Ci/g}{3.7\times10^{11}\,n/cm^2 s\left[\frac{\sqrt{\pi}}{2}\cdot 13.412\times10^{-24}\,cm^2\sqrt{\frac{293}{295.2}}\right]\frac{6.022\times10^{23}\,m^{-1}}{56\,g/m}\left(1-e^{-(7.46\times10^{-5}\cdot 360)}\right)e^{-7.46\times10^{-5}\cdot 1850}}$$

$$C = \underline{\underline{12.9801 ppm}}$$

The mass concentration of the Mn^{56} element within the sample is determined as 12.9801 parts-per-million (ppm).

2.3. Epithermal Neutron Activation Analysis

The ENAA is defined as analysis of samples when irradiated with neutrons of energies ranging from 0.5 eV to 100 keV. In this energy region, most of a nuclei's cross-section curves exhibit narrow peaks known as resonances (one example is shown in Figure 2-2). Epithermal neutrons are defined as neutrons with kinetic energy greater than that of thermal agitation [10]. Epithermal neutron activation is obtained by covering the sample with a cadmium or boron shield to absorb all thermal neutrons, but allowing epithermal and fast neutrons above 0.5 eV energies to pass through. Epithermal neutrons activate the sample and the fast neutrons traverse through the sample [11, 12]. Classical examples of nuclides with good resonance peaks include indium (peak energy at 1.46 eV) and gold (peak energy at 4.9 eV). Materials which are activated by exposure to epithermal neutrons can serve in principle as epithermal neutron detectors [10]. The resonance activation detectors provide experimental data on the epithermal neutron flux density in nuclear reactors for reactor physics calculations,

shielding experiments, and radiation damage studies. In performing ENAA, the following points have to be considered [10]: (a) activation response of the sample/detector with epithermal neutrons should always be separated from the response to thermal neutrons by the use of foil covers such as those made of cadmium; (b) the response that corresponds to the resonance peak in the cross-sections is generally perturbed by the response corresponding to the *1/v* part of the cross-section; (c) the resonance integral cross-sections are mostly insufficiently known; (d) the corrections for self-shielding are more complicated for epithermal neutrons; (e) the use of extremely thin cadmium foils necessary to reduce the self-shielding correction requires refined techniques and determination of the cadmium ratio.

Cadmium ratio: during irradiation of the sample in a reactor, the induced activity of the sample will be caused by both the thermal and epithermal neutrons. In order to distinguish between these two activations, the sample is covered with cadmium. The cadmium will absorb neutrons below a cut-off energy E_{cd} *(< 0.5 eV),* while neutrons above the energy pass through the cadmium. When the sample is not covered with cadmium, the sample will be activated by both the thermal and epithermal neutrons. The cadmium ratio is defined as the activity of the sample without the cadmium cover divided by the activity of the sample with cadmium:

$$R_{cd} = \frac{\int_0^{\infty} \phi(E)\sigma(E)dE}{\int_{E_{cd}}^{\infty} \phi(E)\sigma(E)dE} = \frac{\int_0^{\infty} \phi_{Max}(E)\sigma(E)dE + \int_{\mu kT}^{\infty} \phi_{\text{int}}(E)\sigma(E)dE}{\int_{E_{cd}}^{\infty} \phi_{\text{int}}(E)\sigma(E)dE} \qquad (2.21)$$

$$R_{cd} = \frac{\int_0^{\infty} \varphi_{Max}(E)\sigma E)\sigma(E + \int_{\mu kT}^{\infty} \varphi_{\text{int}}(E)\sigma E)\sigma(E}{\int_{E_{cd}}^{\infty} \varphi_{\text{int}}(E)\sigma E)\sigma(E} \qquad (2.22)$$

where $E = \mu kT$ – Maxwellian distribution and flux density ϕ_{epi} and $\phi_{Max}(E)$. Therefore, the cadmium ratio is given as: R_{cd} = (response of foil without cadmium cover)/(response of foil without cadmium cover).

ENAA technique is used to determine the thermal and epithermal neutron flux ratios within the reactor, and could also be used for the irradiation of geological and archeological samples to correct for isotope interference. The technique of ENAA with and without the thin cadmium foil could be determined using Monte Carlo code. This is achieved by simulating the realistic model of the reactor core, irradiation channels, and the sample of interest with and without the thin cadmium foil to determine the cadmium ratio.

2.4. Fast Neutron Activation Analysis

The FNAA is the most complicated approach as compared to thermal and epithermal neutron activation analysis. Measurement of fast neutron spectra can be obtained by using threshold activation detectors, the detectors that have threshold energies greater than 1 MeV. Due to the threshold energy being above 1 MeV, there is a significant gap between the energy range of resonance detectors and fast neutron threshold detectors. Most often the method of using threshold detectors suffers from poor energy resolution.

The energy distribution of fast neutrons activation analysis generally ranges from energies above 100 keV with a maximum fraction of the energies at 2 MeV. Fast neutron interaction with target nuclei transmutes by the following reactions: *(n, p), (n, 2n), (n, α), (n, n')*, and *(n, f)* reactions [11, 14]. The response of the threshold detectors by neutron activation is proportional to the product of differential activation cross-section, $\sigma(E)$, and differential flux spectrum $\phi(E)$ expressed as [10]:

$$A = \int_0^\infty \sigma(E)\varphi(E)dE \tag{2.23}$$

The choice of fast neutron detector depends on some of the following factors:

(a) Purpose of the study determines the type of detector to be used because fast neutrons induce different reactions in the detector; (b) duration of the irradiation and easy accessibility of the detectors after irradiation is very important because of the half-life of the produced nuclides. The detector may not be available for counting due to high activity after irradiation, and therefore will have to be put away for a couple of days for it to decay before counting. If the half-life is too short, the radioactive decay during the period between irradiation and counting would reduce the specific activity below an acceptable level and there will not be good counting gamma spectrum.

(c) design of the experiment and irradiation environment will determine the appropriate detector to be used. Detectors with short half-life are sometimes used to map neutron flux distribution in low-power reactors.

The general equations to calculate fluence and flux density from the activation of a detector can be derived as the rate of increase in product isotope concentration expressed as:

$$\frac{dN}{dt} = N_0\sigma\phi - \lambda N \tag{2.24}$$

where N is the number of product atoms; N_o is the initial number of parent isotope; assuming the flux density is constant, the solution for the number of atoms in parent isotope N is expressed as:

$$N = \left[\frac{N_o\sigma\phi}{\lambda}\right]\left[1-\exp(-\lambda t)\right] \tag{2.25}$$

The equation for the effective cross-section used to determine the fast neutron flux above the threshold energies can be expressed as:

$$\sigma(E_i) = \frac{\int_0^\infty \sigma(E)\varphi(E)dE}{\int_0^\infty \varphi(E)dE} \tag{2.26}$$

where t is the irradiation time, the neutron flux expressed as:

$$\phi = \left(\frac{N}{N_o\sigma}\right)\left[\frac{\Lambda t}{1-\exp(-\lambda t)}\right] \tag{2.27}$$

Considering the effective activity $A(Bq) = \Lambda N$, then the fast neutron fluence is given as:

$$\phi\left(n/cm^2\right) = \left(\frac{A\Lambda}{N_o\lambda}\right)\left[\frac{t}{1-\exp(-\lambda t)}\right] \tag{2.28}$$

To account for decay between the period of end of irradiation and counting, the factor *exp* $(t_o\lambda)$ is included, thus the fluence can be calculated as:

$$\phi = \left(\frac{A\Lambda}{N_o\lambda}\right)\left[\frac{t}{1-\exp(-\lambda t)}\right]\exp(\lambda t_o) \tag{2.29}$$

Fast neutron fluence is expressed as

$$\phi(n/cm^2) = \frac{A\Lambda\exp(\lambda\lambda_o)}{\lambda\sigma N\left[1-\exp(-\lambda t)\right]} \tag{2.30}$$

The production rate of the parent isotope can be expressed as:

$$\frac{dn}{dt} = N_o\sigma_m\phi_f - N_1(\lambda_1 + \sigma_1\phi_{th}) = N_o\sigma_m\phi_f - N_1\lambda \tag{2.31}$$

$$N_1 = \frac{\sigma_m\phi_f N_o}{\lambda_1}\left[1-\exp(-\lambda t\right]$$

<u>Example</u>: the application of the equations is illustrated for irradiation of sodium (Na^{23}) assuming a fast neutron flux of 1.35 x 10^{11} n/cm^2s, microscopic cross-section of Na^{23} at 0.025 eV, σ - 0.527 barns, half-life of Na^{23}, $T_{1/s}$ - 15 hours, decay constant of Na^{23}, λ -7128 x 10^{-5} sec^{-1}, and irradiation time – 360 minutes; applying equation (2.33) we obtain the molecule concentration of Na^{23} within the sample:

$$N_{Na} = \frac{\sigma_m\phi_f N_o}{\Lambda}\left[1-\exp(-\Lambda_1 t)\right]$$

$$N_{Na} = \frac{0.527\times10^{-24}cm^2\cdot1.35\times10^{11}n/cm^2s\cdot10^{22}atoms}{1.28\times10^{-5}\sec^{-1}}\cdot\left[1-\exp\left(-\left(1.28\times10^{-5}\sec^{-1}\cdot360\sec\right)\right)\right]$$

$$N_{Na} = \underline{\underline{2.514\times10^{11}\,ppm}}$$

Commonly used fast neutron threshold detectors for fast neutron flux mapping, and reactor physics calculation include $^{58}Ni\ (n, p)\ ^{58}Co$, $^{32}S\ (n, p)\ ^{32}P$, $^{27}Al\ (n, \alpha)\ ^{24}Na$, and $^{54}Fe\ (n, p)\ ^{54}Mn$.

2.5. Cyclic Activation Analysis

In CINAA, a sample is irradiated for short periods of time, and rapidly transferred to a detector to be counted. The entire process is repeated for a number of cycles (mostly about four cycles), and the gamma-ray spectrum per each cycle is summed together to create a cumulative sample spectrum [15]. During the process of cyclic irradiation, four different time periods are: t_1 – time between the end of irradiation and the start of counting, which is also considered as the decay time; t_2 – counting time; t_3 – time it took for the sample to be transferred back for irradiation; and t_4 – time in which there is decay of long-lived radionuclides. Therefore, the total cycle period time T can be calculated as [15]:

$$T = t_1 + t_2 + t_3 + t_4 \tag{2.32}$$

The first cycle could be determined by equation;

$$C_1 = \alpha \cdot F_1 \cdot F_2 \cdot F_3 \tag{2.33}$$

where C_1 is the initial activity (disintegration per second - dps) and the F_1 are the time factors;

$$\begin{aligned}\alpha &= \frac{N_T \cdot \sigma \cdot \phi \cdot \in \cdot I}{\lambda} \\ F_1 &= 1 - e^{-\lambda t_1} \\ F_2 &= e^{-\lambda t_2} \\ F_3 &= 1 - e^{-\lambda t_3} \\ F_4 &= e^{-\lambda T}\end{aligned} \tag{2.34}$$

where $\in$ is the efficiency of the detector, I is the intensity of the radiation of interest, λ is the decay constant of the isotope of interest. The second count rates can be calculated based on the first count as follows:

$$C_2 = C_1 + F_4 \cdot C_1 \tag{2.35}$$

The nth cycle could be deduced as:

$$C_n = C_1 \cdot \sum_{k=0}^{n} F_4^k = C_1 \frac{1 - F_4^{n+1}}{1 - F_4} = \alpha \cdot F_1 \cdot F_2 \cdot F_3 \cdot \frac{1 - F_4^{n+1}}{1 - F_4} \tag{2.36}$$

and the total number of accumulated counts in all the cycles could be derived as:

$$\begin{aligned}C_T &= \sum_{i=1}^{n} C_i = \frac{\alpha \cdot F_1 F_2 F_3}{1 - F_4} \cdot \sum_{i=1}^{n} \left(1 - F_4^{i+1}\right) = \frac{\alpha F_1 F_2 F_3}{1 - F_4} \left[n - \frac{F_4 \left(1 - F_4^n\right)}{1 - F_4} \right] \\ C_T &= \alpha F_1 F_2 F_3 \left[\frac{n}{1 - F_4} - \frac{F_4 \left(1 - F_4^n\right)}{\left(1 - F_4\right)^2} \right]\end{aligned} \tag{2.37}$$

The total number of counts for all the cycles can be optimized by choosing approximate irradiation and decay times which will lead to optimal time factors, and consequently lead to good experimental analysis [15].

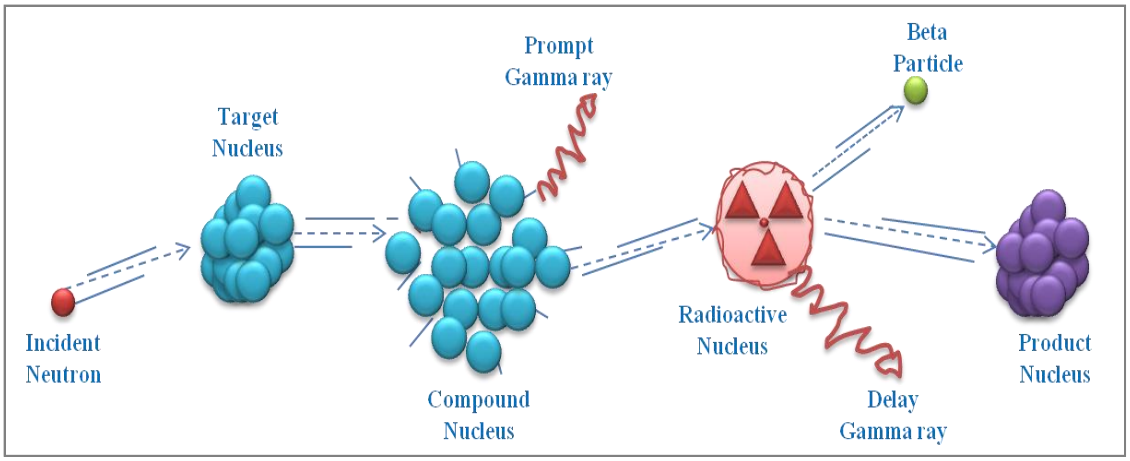

Figure 2-1. Schematic description of NAA.

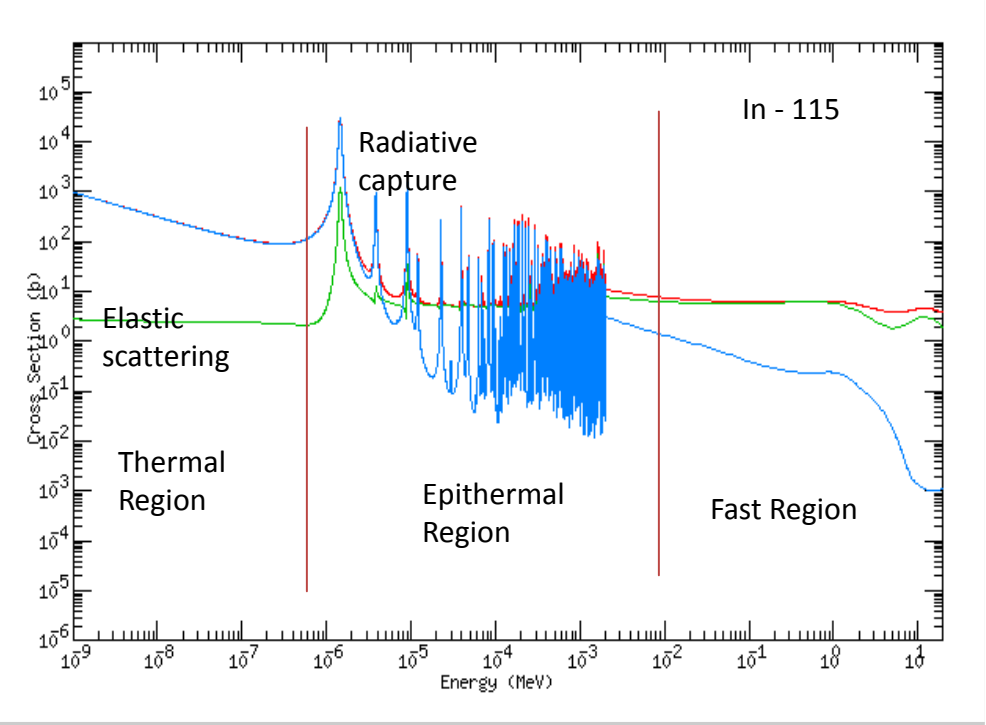

Figure 2-2. Microscopic cross-section plot of In-115 indicating thermal, epithermal, and fast region. Adapted from [6].

CHAPTER 3

COMPUTATIONAL ANALYSIS OF UNIVERSITY OF UTAH TRIGA IRRADIATION FACILITIES

3.1. UUTR Reactor Core Irradiation Channels

The University of Utah TRIGA (training, research, isotope, general, and atomics) research reactor (UUTR) is a pool type research reactor manufactured/licensed to operate at 100 kilowatt thermal power and first went critical in September 30, 1975. The UUTR uses light water as a coolant, and circulates naturally through a mixed-resin bed ion-exchange system to maintain the high purity of the pool water [16, 17]. The pool water also serves as a neutron moderator and a heat sink, and shields radiation from the core. The reactor core is of hexagonal geometry with standard TRIGA fuel elements, deuterium oxide (D_2O, or "heavy water") and graphite reflectors, and three boron carbide (B_4C) neutron absorbing control rods. The hexagonal lattice of the core has upper and lower grid plates designed to hold the assembly of fuel elements and both reflectors into position [15-18].

The UUTR has four sample irradiation channels, namely, the pneumatic irradiation facility (PI), the central irradiation (CI) facility, the thermal irradiation (TI) facility, and the fast neutron irradiation facility

(FNIF). The TI and FNIF are the main sample irradiation facilities most used for neutron activation analysis research. The thermal irradiation facility (TI) consists of a pure aluminum canister of a trapezoidal shaped tank filled with heavy water (D_2O). The heavy water within the canister moderates neutron leakage from the reactor core and also provides an isotropic thermal neutron environment well-suited for neutron activation via neutron capture (n,γ) reaction [19]. The TI has a cylindrical sample irradiation space with a 5-cm-diameter entrance and an estimated length of 60-cm, and has a polyethylene tube that extends from the TI canister to the top of the pool for insertion of experiments into the TI, Figure 3-1.

The thermalized neutrons within the TI have an estimated kinetic energy of 0.025 eV and have relative thermal neutron speed of 2,200 m/sec. This could be shown mathematically as:

$$KE = \frac{1}{2}mv^2 = kT \tag{3.1}$$

where KE is the kinetic energy and measured in *joules* or *eV (1 joule = 6.2415 x 10^{18} eV)*, m is the mass *(kg)* $m_{neutron} = 1.6749 \times 10^{-27}$ *kg*, v is velocity *(m/sec)*, k is the Boltzmann's constant *($k = 8.6173 \times 10^{-5}$ eV/K)*, and T is the temperature *(K)*.

$$v = \sqrt{\frac{2KE}{m}} = \sqrt{\frac{2(0.0252eV)}{1.6749x10^{-27}kg} * \frac{1J}{6.24151x10^{18}eV}} = 2196\,{}^{m}\!/_{s}$$

$$T = \frac{KE}{k} = \frac{0.0252eV}{8.6173x10^{-5}\,{}^{eV}\!/_{K}} - 273K = 19.4^{o}C \tag{3.2}$$

The fast neutron irradiation facility (FNIF) is located beside the reactor core opposite the thermal irradiation (TI) sample facility. The FNIF is designed to cater for high-energy neutrons emitted from the fission process within the reactor core, and to provide a neutron irradiation environment with a quasi-fission neutron energy spectrum. The FNIF is manufactured over heavy lead material to attenuate low photon component from the FNIF, and has fuel elements placed at the face surface of the FNIF at the hexagonal ring of the core to provide a planar fission neutron source to optimize for neutron hardness assurance testing of the reactor electronics components [19]. The FNIF, as shown in Figure 3-1, consists of a sample holder, inner irradiation box, and lead shielding. The FNIF irradiation sample holder is manufactured from a 0.476-cm, type-5052 pure aluminum sheet, and anodized to prevent corrosion and the material integrity of the sample holder [19].

The FNIF is manufactured with lead blocks and has rectangular dimensions of 17 cm x 25 cm x 60.96 cm for shielding against gamma radiations. Both the inner and outer irradiation boxes are assembled to form a watertight cavity to hold the irradiation sample holder and have two inches of lead shielding circumscribing the sample holder. Two machined lead bricks of dimensions 5.08 cm x 10.16 cm x 20.32 cm are placed at the bottom and top of the irradiation sample holder to provide additional shielding against vertically scattered gamma radiation from the bottom and top of the

sample holder. The configuration of the FNIF and irradiation sample holder creates a test volume of approximately 7800 cm^3 for irradiation [19].

3.2. MCNP and GEANT4 Neutron and Gamma Flux Characterization of UUTR Irradiation Channels

Fission neutrons produced within the reactor core are controlled reactions where a single neutron interacts with the nucleus of U^{235} and produces an average of two or three neutrons per fission during the de-excitation of the nuclei fragments. Fission neutrons can be classified based on the time period the neutron is born, called prompt or delayed neutrons. Prompt neutrons are born directly from a fission process in which the excitation energy of the fission fragment is much greater than the binding energy of the neutron, and it's born less than 10^{-14} seconds after fission, as explained in Figure 3-2 [20 - 22].

Delayed neutrons are born in greater than 10^{-14} seconds and are born primarily from fission fragments known as delayed neutron precursors. The fission fragments decay to excited states of neutron emitters and the energy levels of the residual nucleus also exceed the neutron binding energy. During the de-excitation of the fragments nuclei, there is the emission of gamma, beta, or a neutron. The rate of delayed neutron emission is dependent on the decay of delayed neutron precursors, basically the half-life of the precursor nuclide [20-22].

The half –life of delayed neutron precursors from U^{235} fission ranges from a minimum of 0.23 to 55.6 seconds, Figure 3-3. Delayed neutrons just like prompt neutrons also have a continuous energy spectrum but have less intense energy than prompt neutrons and have less probability of leakage from the reactor core system than prompt neutrons and are easily moderated to induce the reactor fission process. For a well-moderated thermal reactor, neutrons (prompt and delayed) born out of fission are moderated primarily by elastic-scattering collisions with moderating materials such as heavy water or graphite [20-21]. Energetic neutrons born in the reactor core may be classified based on their energy into three general categories, namely, thermal, intermediate (epithermal), and fast neutrons.

The neutron energy spectrum in an ideal thermal reactor is normally evaluated as having a Maxwellian distribution at the effective, absolute temperature of the moderator, and the neutron flux as a function of energy can be given as:

$$\Phi(E) = \frac{E}{kT^2}\exp\left(\frac{-E}{kT}\right) \tag{3.3}$$

where $\psi(E)$ is the differential neutron flux defined as:

$$\int_0^\infty \Phi(E)dE = 1 \tag{3.4}$$

Most probable velocity of a neutron in the thermal region can be expressed as:

$$v_o = \sqrt{\frac{2kT}{m}} \tag{3.5}$$

m is the neutron mass, k is Boltzmann constant, and T is the absolute moderator temperature, and the kinetic energy can be expressed as:

$$E_n = \frac{1}{2} m v_o^2 = kT \tag{3.6}$$

at moderator temperature of 20 ^{o}C, the neutron energy is 0.0253 eV and the relative neutron velocity is 2200 m.s^{-1}. At the intermediate region, the differential flux is the inverse of the neutron energy expressed as:

$$\Phi(E) \approx \frac{1}{E} \tag{3.7}$$

The intermediate region is also known as the resonance peak region of neutrons with specific energies dependent on the nucleus of the materials, which may cause neutron flux depressions. Fast energy neutrons during slowing down cross from the fast neutron region through the intermediate region to the thermal region. Neutron fission is mostly caused by thermal neutrons. An empirical analytical equation developed by Watt, who used a proton-recoil spectrometer to measure the neutron energy spectrum produced by thermal fission of U^{235}, expressed the fraction of fission neutron flux with energy E in units of MeV as; $\Phi(E) = 0.484 e^{-E} \sinh\sqrt{2E}$.

Watts determined that the most probable energy of a neutron born form U^{235} fission is approximately 0.7 MeV and as a mean energy of 2 MeV. It can be deduced from equation (3.6) that the neutron energy released has an isotropic Maxwellian velocity distribution. The concept of neutron logarithmic lethargy corresponds to the slowing down of neutrons from high energies to

lower energies. The assumption is made that fast neutrons of maximum neutron energy of 10 MeV generated in the fuel pin of a nuclear reactor are slowed down to thermal neutrons (< 0.25 eV) by a moderating material and are responsible for thermal fission within the reactor core in a ^{235}U fuel. The mechanism of energy loss is due to neutron scattering with moderating nuclei whereby the neutron loses energy, and is highly dependent on the nuclei material and energy of neutron. Since the neutron is energy-dependent, the neutron flux within the reactor is related to the energy lethargy of the neutron during the slowing down process [19-22].

The main mode of neutron energy loss is due to neutron elastic scattering. During neutron elastic scattering, the incident neutron interacts with a nucleus at rest, and the nucleus recoils from its original position of the collision at an angle relative to its position at rest. The incident neutron is also scattered at a reference angle relative to the point of collision (Figure 3-4) and loses energy in the process [20].

Energy loss by the incident neutron can be determined from the laws of conservation of energy and momentum. The energy and momentum of the incident particle is donated as E, P and that of the scattered neutron donated as E', P', respectively, scattered at an angle ϑ (Figure 3-4). The energy and momentum of the recoil nucleus is denoted as E_{nuc}, P_{nuc}, scattered at an angle φ (Figure 3-4). Based on the conservation law of energy [19-22]:

$$E = E' + E_{nuc} \tag{3.8}$$

Conservation of momentum:

$$P = P' + P_{nuc} \tag{3.9}$$

From the resultant vector diagram of the collision, the momentum equation can be expressed by the law of cosines as

$$p_{nuc}^2 = p^2 + (p')^2 - 2p' p_{nuc} \cos\vartheta \tag{3.10}$$

In classical mechanics, $p^2 = 2mE, p_{nuc}^2 = 2ME_{nuc}$, and $p'^2 = 2mE'$,

where M and m are the masses of the nucleus and neutron, respectively. Therefore, equation (3.8) can be written as

$$ME_{nuc} = mE + mE' - 2m\sqrt{EE'}\cos\vartheta \tag{3.11}$$

since M/m is approximately equal to the atomic mass number of the nucleus, A. Hence, further simplifying equation (3.10) and introducing E_A from equation (3.7) gives

$$E' = \frac{E}{(A+1)^2}\left[\cos\vartheta + \sqrt{A^2 - \sin^2\vartheta}\right]^2 \tag{3.12}$$

Assuming that the neutron scattering angle occurs when $\vartheta = \pi$, then the neutron is scattered backwards and loses maximum possible energy and the equation can be simplified as:

$$(E')_{\min} = \left(\frac{A-1}{A+1}\right)^2, E' = \alpha E, \tag{3.13},$$

where $\alpha = \left(\frac{A-1}{A+1}\right)^2$. Neutrons also lose energy through inelastic scattering collisions as a result of both recoil and internal excitation of the target nucleus and the threshold energy for inelastic scattering is high for light nuclei and low for heavy nuclei [21-23]. The slowing down of neutrons occurs during neutron collision with moderating material which is also described as

neutron *lethargy,* and the variable is denoted by the symbol u and defined [19-22] as

$$u = \ln\left(\frac{E_M}{E}\right) \tag{3.14},$$

where E_M is the initial highest energy and E is the final low energy.

The change in average fractional energy loss of the lethargy is denoted as $\bar{\Delta u}$ and also denoted as ξ and can be derived based on the mass number (A) of a target nucleus as

$$\Delta u = \xi = 1 - \frac{(A-1)^2}{2A}\ln\left(\frac{A+1}{A-1}\right) \cong \frac{2}{A+\frac{2}{3}} \tag{3.15}$$

The number of collisions (C) the neutron undergoes during moderation can be expressed as:

$$C = \frac{u}{\xi} = \frac{\ln(E_M/E)}{\left(2/\left(A+2/3\right)\right)} \tag{3.16}$$

The incremental lethargy neutron interval, du, is related to the total neutron flux which corresponds to the incremental energy interval between the flux per unit energy, $\Phi(u)$, and the flux per unit lethargy, $\Phi(u)$, and can be derived as [23]:

$$\Phi(u)du = -\Phi(E)dE \Rightarrow u\Phi(u) = E\Phi(E) \tag{3.18}$$

3.3. MCNP and GEANT4 Neutron Flux Comparison for UUTR Irradiation Channels

3.3.1. MCNP Simulation Code

The Monte Carlo N-Particle (MCNP6) and GEANT4 codes are based on Monte Carlo methods based on probability of randomization. The essence of both codes is based on a physics interaction of a neutron, charged particles (proton, electron, etc.), or photon particles. MCNP6 is currently managed by the Diagnostic Application Group (Group X-5) in the Applied Physics Division (X-Division) at the Los Alamos National Laboratory [24]. MCNP6 is a general purpose code that can be used to simulate neutron, photon, and electron transport. It is capable of modeling complex 3D geometries and utilizes extensive point-wise cross-section data libraries in a continuous energy spectrum. It is applicable to modeling nuclear interactions in medical physics, boron neutron capture therapy (BNCT), high energy physics, and radiation detection and shielding, particle accelerator models, space study analysis, nuclear reactor simulations, and criticality calculations [20-24]. MCNP6 contains comprehensive data libraries relating to the probability of unique particle interactions with elements, and has nine novel data libraries, namely, [20-24]; (a) continuous energy neutron interaction data; (b) discrete reaction neutron interaction data; (c) continuous energy photoatomic interaction data; (d) continuous energy photonuclear interaction data; (e) neutron dosimetry cross-sections; (f) neutron S(α,β) thermal data; (g) multigroup neutron, coupled neutron/photon, and charged particles

masquerading as neutrons; (h) multigroup photon; and (i) electron interaction data.

Physics interactions implemented in the MCNP code for simulations include particle weight calculation, particle tracking, neutron interactions, photon interactions, electron interactions, electromagnetic interactions, and many more. During neutron interactions, a particle may collide with a nucleus and will either be absorbed or scattered. Photon interactions include coherent scattering and account for fluorescent photons after photoelectric absorption, the Compton scattering from free electrons, photonuclear interactions, and pair production [20-24]. The transport of electrons and other charged particles is fundamentally different from that of neutrons and photons. The interaction of neutral particles is characterized by relatively infrequent isolated collisions, with simple free flight between collisions. In contrast, the transport of electrons is dominated by the Coulomb force, resulting in large numbers of small interactions, Bremsstahlung, Cerenkov radiations, and other nuclear reactions [24-26].

3.3.2. GEANT4 Simulation Code

The GEANT4 code is a successor of GEANT3 and has developed in a large international collaboration of over hundred scientists, physicists, programmers, and software engineers from a wide variety of institutions and universities participating in a wide range of research experiments in Europe, Asia, and the Americas. GEANT4 is an object oriented (OO) code based on

C++ that exploits advanced novel techniques in software programming. It is one of the largest and most ambitious open source codes in terms of the size, scope, and number of scientists helping to develop the code. The main application of GEANT4 code is its use in the study of High Energy Physics (HEP), and Large Hadron Collider (LHC) experiments, simulation of the BaBar experiment, large HEP ATLAS experiments, and space and radiation science experiments [28, 29]. GEANT4 consists of various physics models that support the interaction of ionizing and nonionizing radiation particles with matter across a wide range of energies, and provides built-in steering routines, and commands at every level of the simulation. All aspects of the simulation process can be included in the code, starting from the geometry of a system to be modeled, materials, particles of interest, generation of primary events, tracking of particles, physics processes governing particle interactions, storage of events and tracks, visualization of the detector and particle trajectories, and analysis of simulation data [29, 30].

3.3.3. MCNP and GEANT4 Neutron Flux Simulation

It is important to have a good knowledge of neutron flux profiles within the irradiation channels of the UUTR to optimize NAA experiments. MCNP (ver. 6) code was used to simulate the total neutron profile within the two main sample irradiation facilities (FNIF and TI) within the UUTR reactor core. An MCNP6 input file of the UUTR reactor had been developed previously at the Utah Nuclear Engineering Program (UNEP) and it was

used to simulate the neutron profile for various reactor power levels. The three main control rods within the reactor were withdrawn to specific positions; for example, during reactor operation, the safety control rod is withdrawn 100% out of the reactor core, the regulation control rod is withdrawn 65% out of the core, and the shim control rod, which is used to raise/lower power to the desired distance, is withdrawn at an estimate of 77% from the core. Table 3-1 shows the percent withdrawal of the three control rods from the reactor core at different reactor power levels. Knowledge of each control rod percent withdrawal within the reactor at different power levels is implemented within the simulation code to enable the realistic simulation of the total neutron flux within the neutron irradiation channels. Figure 3-5 shows the total neutron flux within the UUTR irradiation channels. As expected, the total neutron flux within the FNIF and TI increases linearly or doubles as reactor power level increases. The total neutron flux within the FNIF and TI at different power levels is highlighted in Table 3-2.

To obtain the total neutron flux within the UUTR, criticality calculations were performed in MCNP using the kcode command, i.e., kcode 100000 1.0 100 5000, where the initial value 100,000 represents the number of particle simulation per cycle, 1.0 represents the initial estimate of effective multiplication factor (k_{eff}), 100 indicates that the first 100 cycles is not included in the calculation for statistical purposes, and 5000 indicates the

number of cycle simulations to be executed. Figure 3-6 shows the neutron flux spectra within the FNIT, TI, in comparison to the central irradiation (CI) sample facility. The track length estimator tally (F4) in MCNP6 was used to track each neutron particle within the irradiation facility to generate the lethargy neutron spectrum from lower energies of 10e-9 MeV to 10 MeV, with the assumption that the minimum and maximum neutron energy generated during nuclear fission in the UUTR reactor core is 10e-9 MeV and 10 MeV, respectively.

GEANT4 simulation codes are not capable of reactor physics criticality calculations, as well as simulation of nuclear fission reactions. Hence, to simulate the neutron flux profile and characterization of the sample irradiation channels within the UUTR, and for NAA experimental simulations, the neutron flux profile obtained from MCNP simulation was imported into GEANT4, simulated, and compared with MCNP to verify the accuracy in GEANT4. Figure 3-7 shows the comparison of simulated neutron flux profile within the FNIF and TI to MCNP6. As expected the imported neutron flux profile from MCNP6 into GEANT4 yielded very good agreement between the two codes. The difference in neutron flux between MCNP and GEANT4 is because the neutron flux measurements obtained from MCNP criticality calculation were coded into GEANT4 as a volumetric isotropic source for both the FNIF and TI irradiation channels. As a result of the isotropic source definition, not all the emitted neutrons from the volumetric

source are recorded within the FNIF and TI since some neutrons were emitted away from the FNIF and TI, hence the difference in neutron flux magnitude between MCNP and GEANT4. Therefore, GEANT4 and MCNP6 could be used to simulate UUTR NAA experiments to help optimize NAA experiment.

To ascertain the axial neutron flux profile within the FNIF and TI, criticality calculations were performed using MCNP6 and MCNPX. Figures 3-8 and 3-9 present the axial flux profile within irradiation facilities. It can be seen that the neutron flux hardens in the middle of the irradiation ports and softens both at the top and bottom of both irradiation ports. As compared to the TI, the FNIF has a bit of a flux depression at the bottom of the facility compare to the top of the facility; this is due to control rod worth at the top of the FNIF due to the fast neutron leakage factor. Figure 3-10 shows the comparison of the axial profile of the FNIF and the TI.

Figure 3-11 and Table 3-3 illustrate the graphical and numerical representation of thermal to epithermal to fast neutron ratios within the FNIF at increasing UUTR power level, respectively. Estimated ratio of thermal to epithermal neutron within the FNIF at the different power levels is about 1:2, while the estimated ratio of epithermal to fast neutron within the FNIF is about 2:1. Hence, there is an abundance of epithermal neutrons in the FNIF, more than the fast neutrons. Based on numerical analysis in Table 3-4, and graphical interpretation in Figure 3-12, it can be deduced that

the thermal irradiation channel has thrice the abundance of thermal neutrons ratio as compared to fast neutrons. This is due to the fact that the TI canister is filled with heavy water moderator for abundance of thermal neutron generation. There is slight thermal neutron population in the TI as compared to epithermal neutrons.

Table 3-1. Percent withdrawal of control rod positions within the UUTR reactor core obtained University of Utah TRIGA reactor run.

Power Level (kW)	Safety CR (% out)	Shim CR (% out)	Regulation CR (% out)
1	100.00%	54.00%	65.20%
10	100.00%	58.20%	65.30%
30	100.00%	64.10%	65.00%
50	100.00%	68.70%	65.00%
70	100.00%	73.20%	65.00%
90	100.00%	77.70%	65.10%

Table 3-2 MCNP simulation of neutron flux (n/cm^{2}s) distribution at different power levels within FNFI and TI.

	1 kW	10 kW	30 kW	50 kW	70 kW	90 kW
FNIF	5.836E+09	5.864E+10	1.767E+11	2.960E+11	4.154E+11	5.356E+11
TI	6.367E+09	6.345E+10	1.887E+11	3.122E+11	4.357E+11	5.571E+11

Table 3-3 Fractions of thermal, epithermal, and fast neutron fluxes in fast neutron irradiation facility (FNIF) simulated with MCNP6.

FNIF			
Power level	Thermal - n/cm²s	Epithermal - n/cm²s	Fast - n/cm²s
1 kW	1.643512E+09	2.685916E+09	1.506554E+09
10 kW	1.650618E+10	2.699566E+10	1.514245E+10
30 kW	4.969183E+10	8.140677E+10	4.568922E+10
50 kW	8.332443E+10	1.362178E+11	7.650529E+10
70 kW	1.169020E+11	1.912351E+11	1.072771E+11
90 kW	1.506392E+11	2.467824E+11	1.382309E+11

Table 3-4 Fractions of thermal, epithermal, and fast neutron fluxes in thermal irradiation (TI) channel obtained from MCNP6 simulation.

TI			
Power level	Thermal - n/cm²s	Epithermal - n/cm²s	Fast - n/cm²s
1 kW	2.876082E+09	2.145402E+09	6.805702E+08
10 kW	2.867541E+10	2.799555E+10	6.784629E+09
30 kW	8.531250E+10	8.327898E+10	2.013647E+10
50 kW	1.411072E+11	1.377458E+11	3.337068E+10
70 kW	1.969704E+11	1.921649E+11	4.660110E+10
90 kW	2.519088E+11	2.457237E+11	5.95E+10

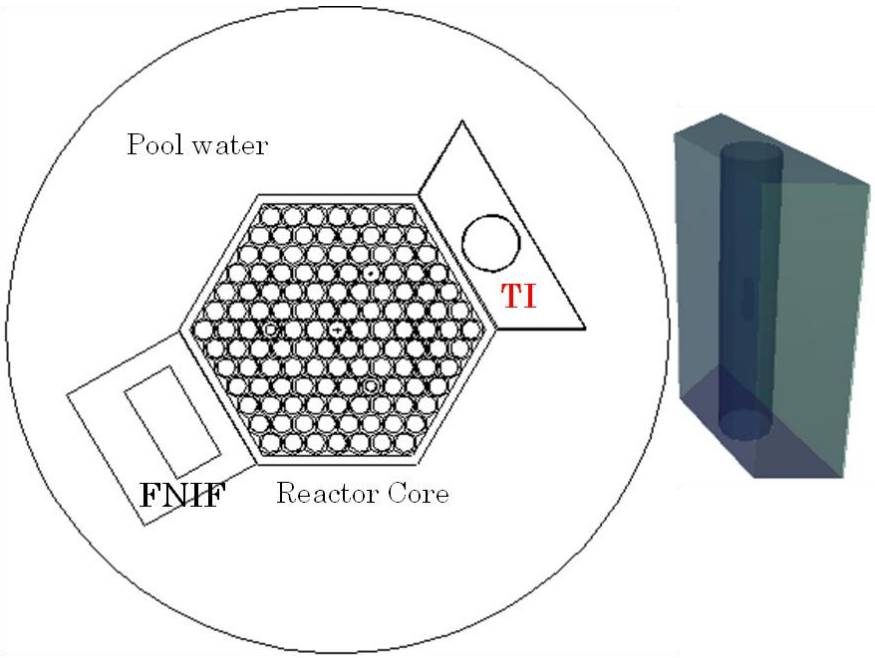

Figure 3-1. MCNP model of thermal irradiation (TI) sample unit in the reactor core.

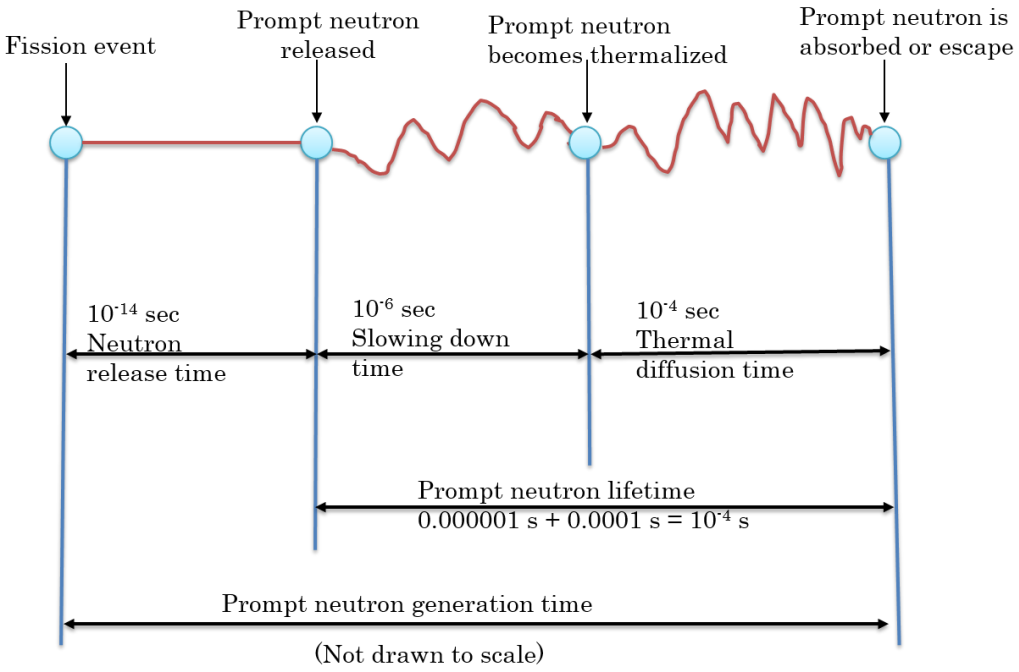

Figure 3-2. Prompt neutron generation time during fission process.

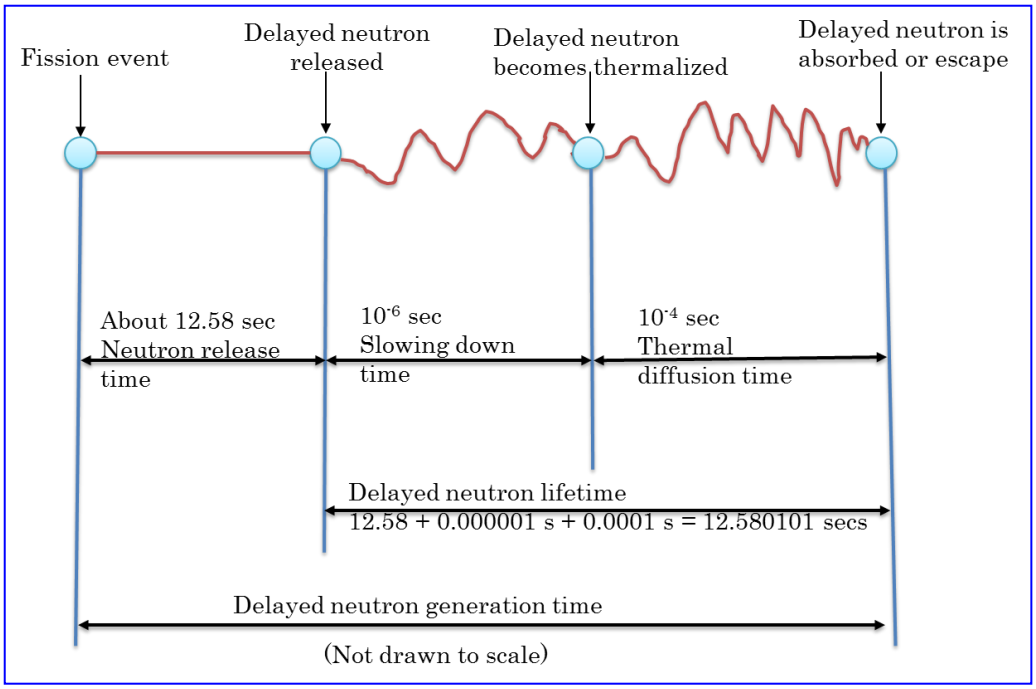

Figure 3-3. Delayed neutron generation time during fission process.

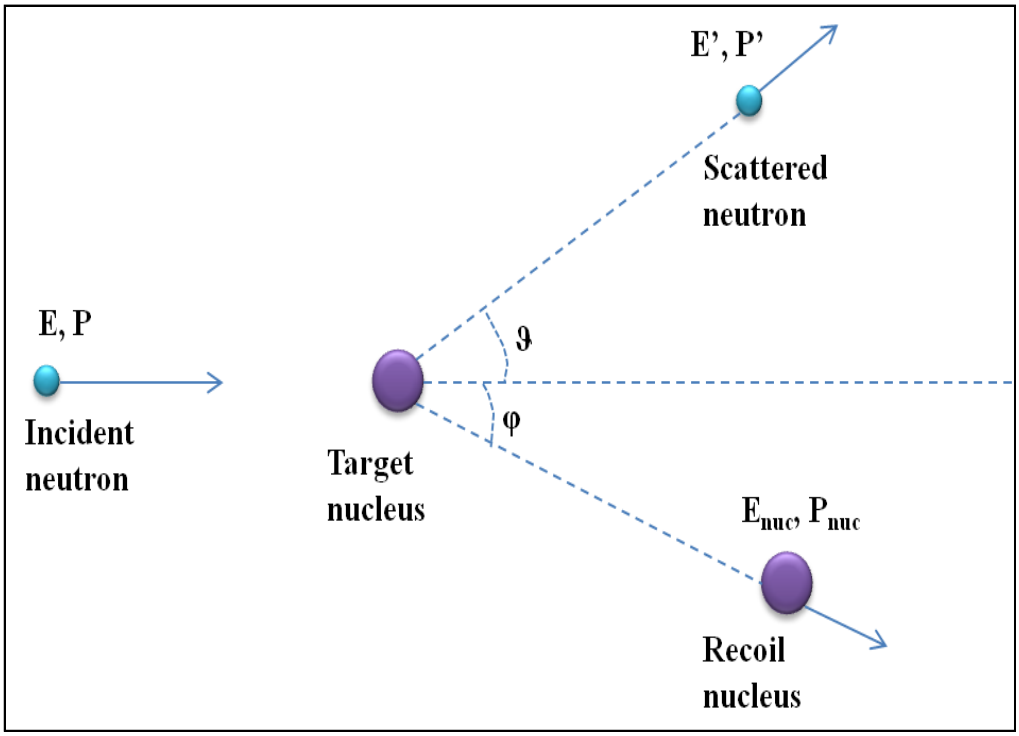

Figure 3-4. Elastic scattering of a neutron by a nucleus [not drawn to scale].

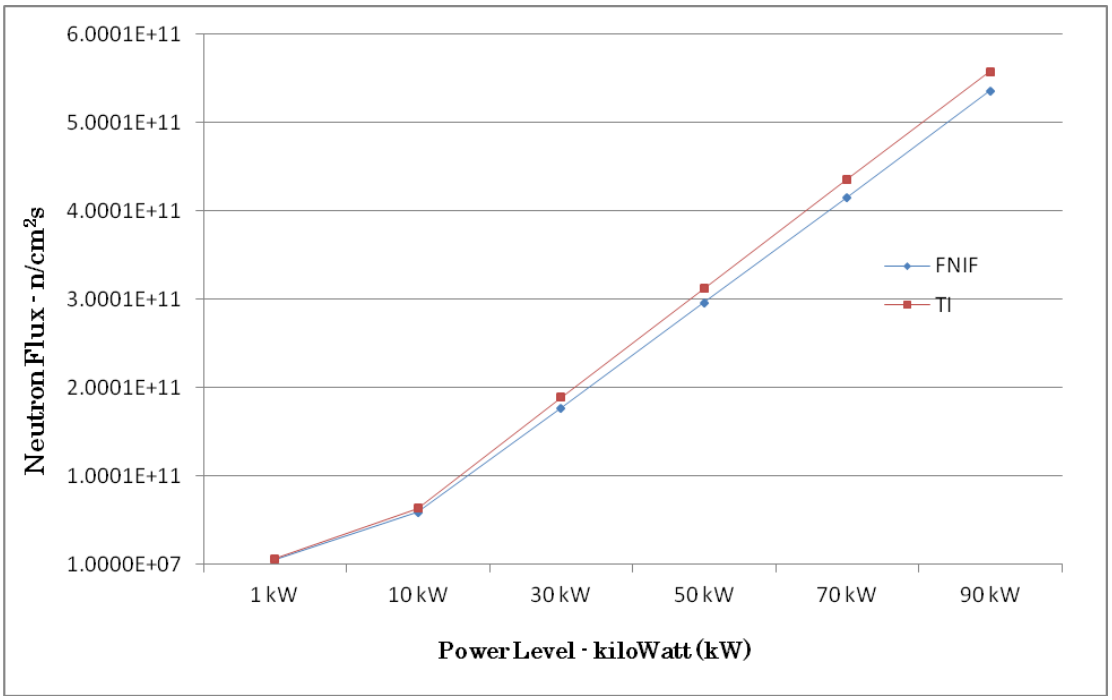

Figure 3-5. MCNP6 simulation of total neutron flux within the FNIF and TI at different power level.

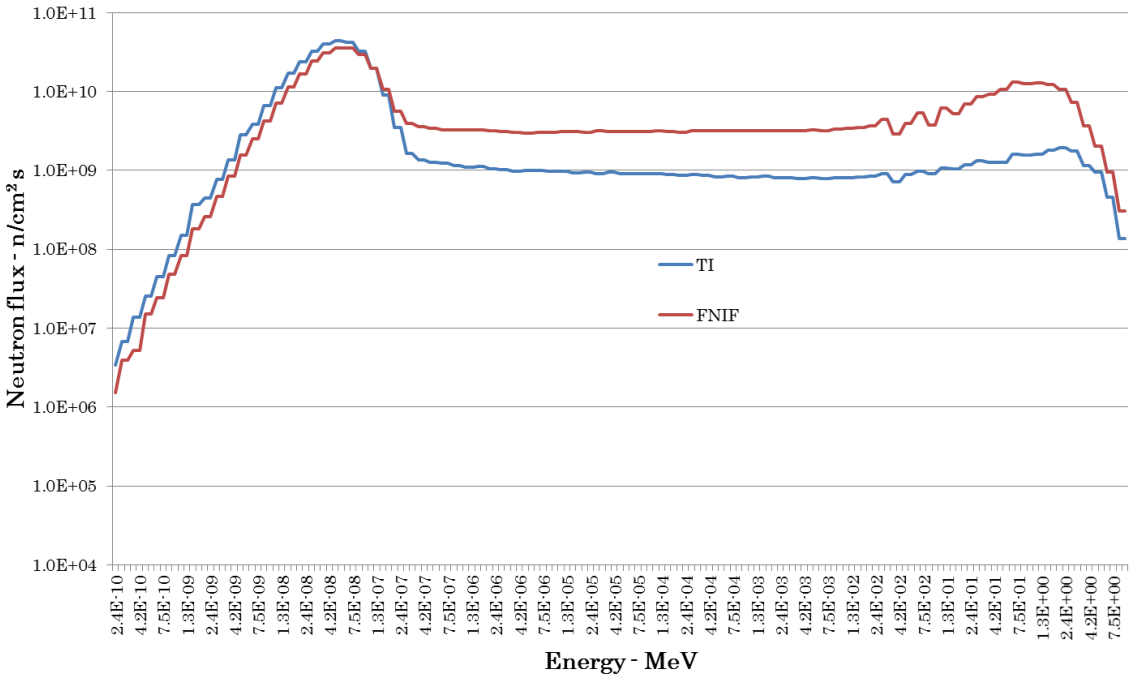

Figure 3-6. Neutron flux within the FNIF, TI, and the CI obtained from MCNP6 simulation.

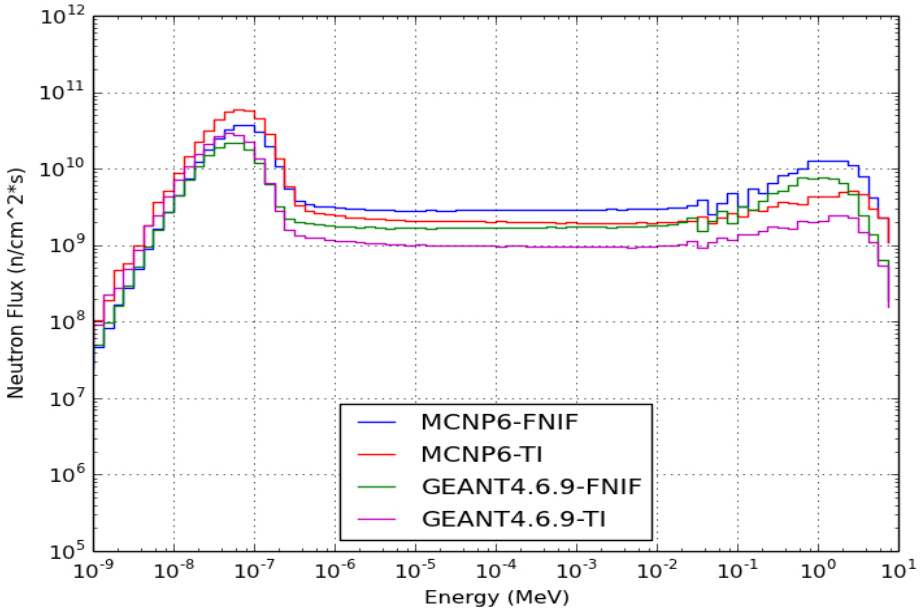

Figure 3-7 Comparison of GEANT4 and MCNP6 neutron flux within the fast neutron irradiation facility (FNIF) and thermal irradiation (TI) facility.

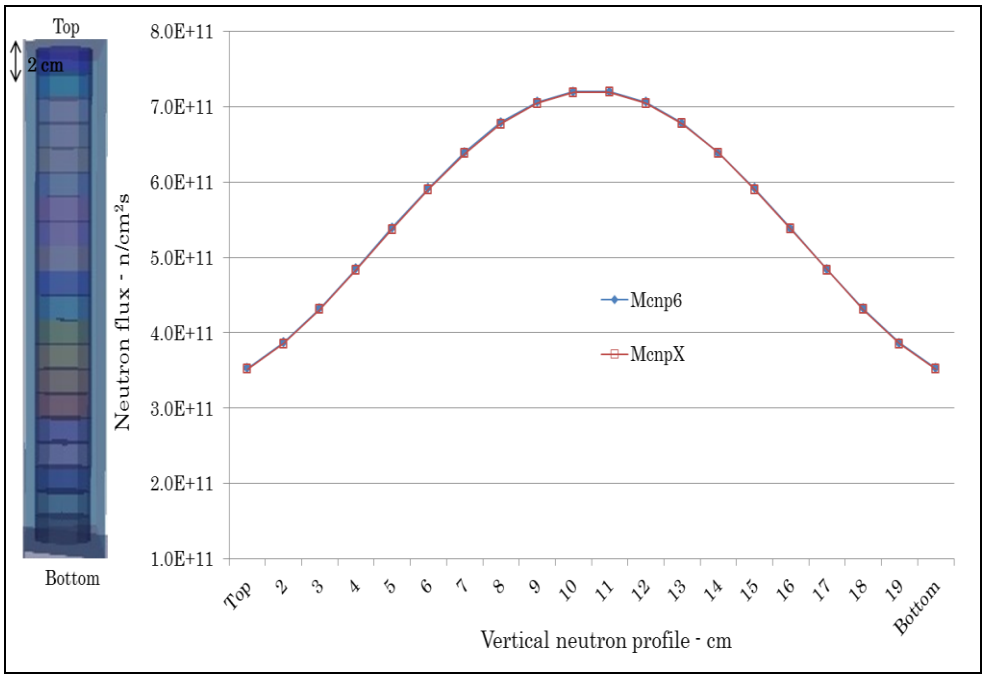

Figure 3-8. Axial neutron flux profile within thermal irradiation (TI) channel simulated from MCNP6 and MCNPX.

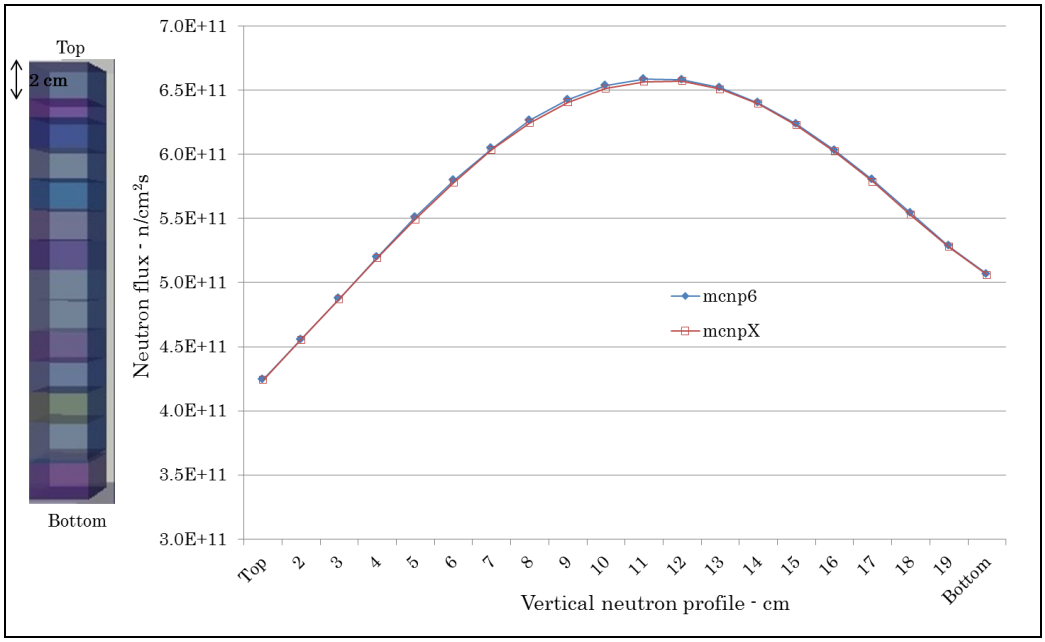

Figure 3-9. Axial neutron flux profile within fast neutron irradiation facility (FNIF) simulated from MCNP6 and MCNPX.

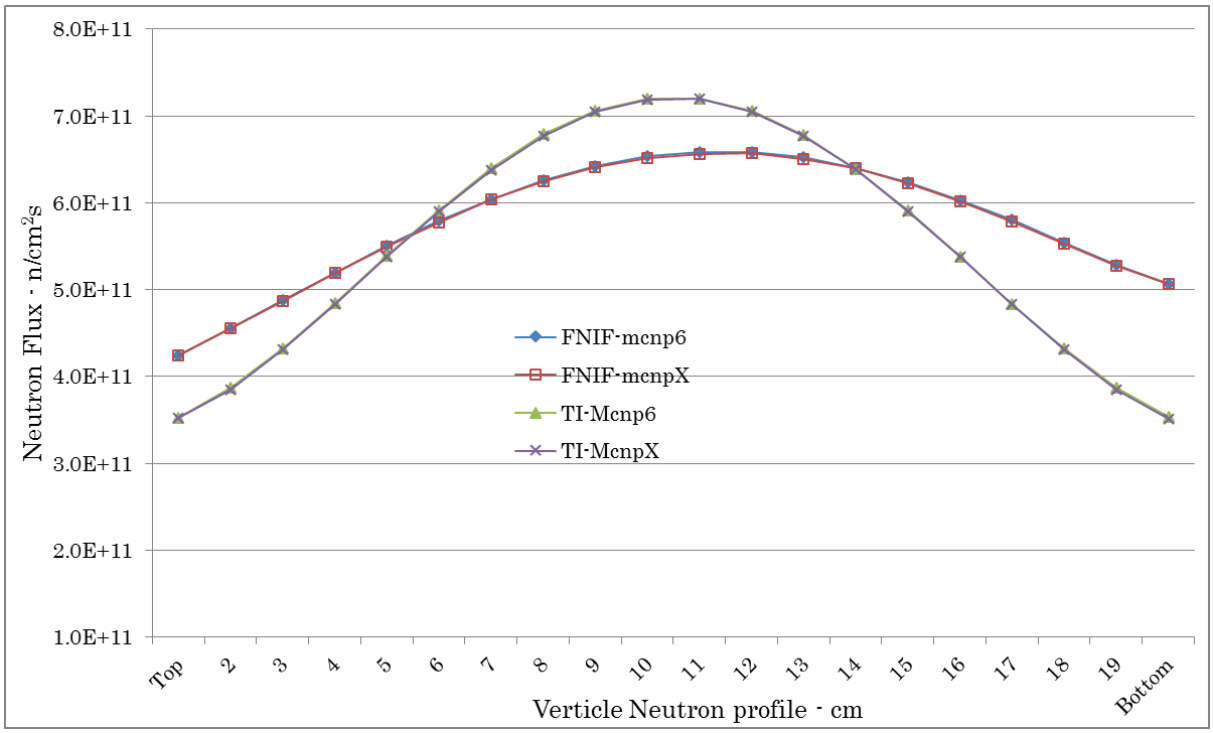

Figure 3-10. Axial neutron flux profile comparison within fast neutron irradiation facility (FNIF) and thermal irradiation (TI) simulated from MCNP6 and MCNPX.

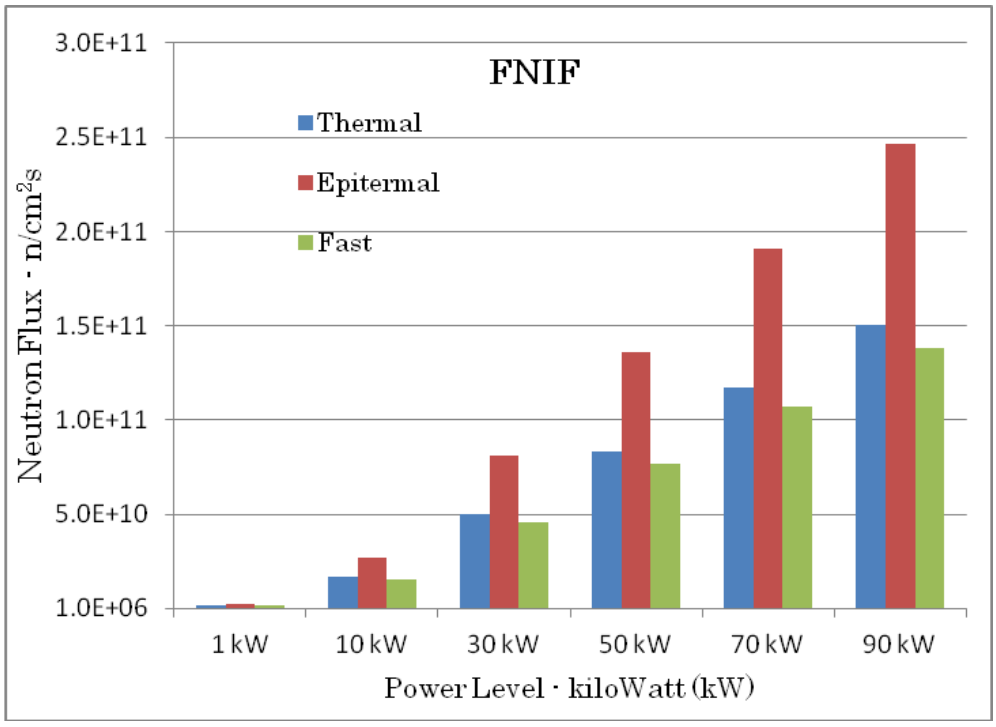

Figure 3-11. Thermal, epithermal, and fast neutron flux ratios in the FNIF obtained from MCNP6 simulation at different UUTR power levels.

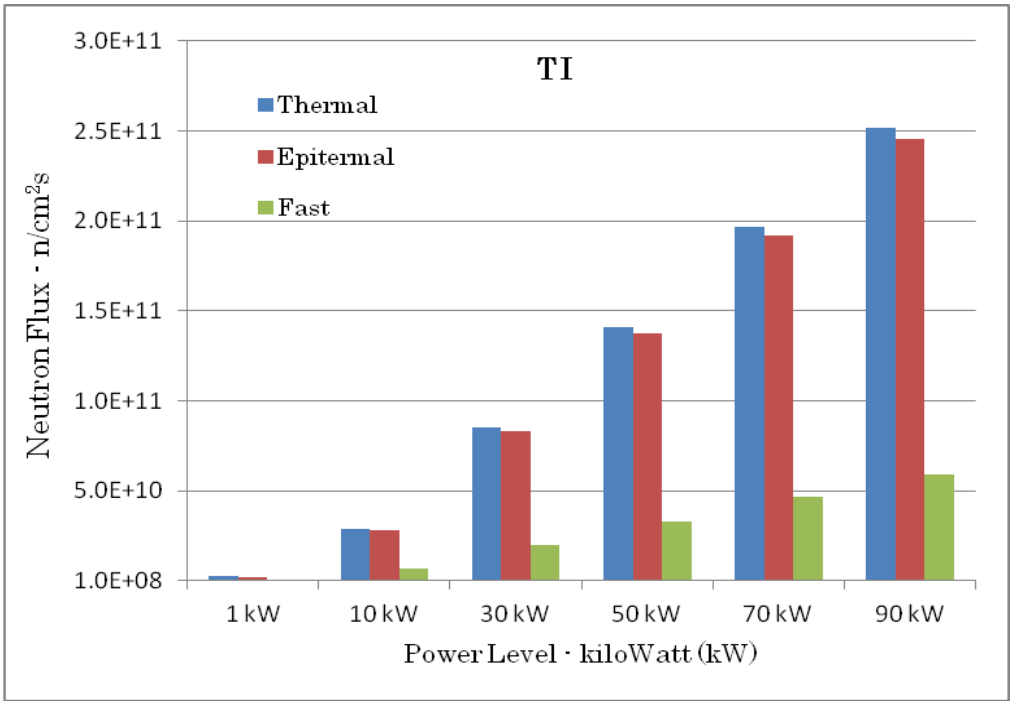

Figure 3-12. Thermal, epithermal, and fast neutron ratios in the TI obtained from MCNP6 simulation at different UUTR power levels.

CHAPTER 4

PROPOSED MODALITY OF QUALITY CONTROL AND QUALITY ASSURANCE FOR THE NAA AT RESEARCH FACILITIES

4.1. Accuracy and Precision of NAA

The accuracy and precision of NAA analysis of a sample could be enhanced greatly by limiting the errors and uncertainties associate with the measurements. The error of the measurement is related to the accuracy and precision of the true measurement. The accuracy of an experiment is determined by how close the result of the measurement is to the true value of the measured quantity, while precision of an experiment is a measure of the exactness of the measured quantity. The accuracy and precision of an experiment should be treated simultaneously since they are independent of each other. Some key factors that affect the accuracy and precision of measurements are: uncalibrated instruments or faulty instruments; reading errors by observer; uncontrolled environmental conditions, such as temperature, pressure, and humidity; sensitivity of instrument to detecting individual effects at atoms, electrons, molecules, and protons; improper method of measurement; and statistical nature of some processes (e.g., radioactive decay) [3, 4].

4.2 Error and Uncertainty Analysis in NAA

Various types of errors that affect the accuracy and precision of measurements are systematic and random errors. Systematic errors when they occur affect the results in the same manner and carry on throughout the experiments. For example, systematic errors arise from instruments, algebraic calculations and measurement errors, and imperfect techniques. Systematic errors introduce uncertainties into the measurements; therefore, the experimenter has to eliminate to the best of their ability systematic errors. Random errors can arise from the experimental apparatus, uncontrolled change in conditions such as voltage, temperature, or pressure, and probabilistic nature of the phenomenon under study. Random error can either decrease or increase the results of a measurement.

Uncertainty is not the same as the error of a measurement. Uncertainty is a quantitative declaration of confidence of a measurement. Without uncertainty, it will be difficult to understand the degree of confidence, and the accuracy and precision of the measurement will not be reliable. The uncertainty of a measurement could be used for method validation, determining the confidence limit of the measurement, and is important for measurement reports. There are two types of methods used to evaluate uncertainties – they are Type A and Type B methods [3].

Evaluation of type A standard uncertainty:

$\bar{X}_i = \frac{1}{n}\sum_{k=1}^{n} X_{i,k}$ where $\bar{X}$ is the mean of n independent observations

$u^2(x_i) = s^2(\bar{X}_i) = \frac{1}{n(n-1)}\sum_{k=1}^{n}(X_{i,k} - \bar{X}_i)^2$ - Variance of the mean

The type B evaluation of standard uncertainty assumes probability distributions given as the measured value being within an interval of uncertainty and expressed as $\mu_- \le X_i \le \mu_+$; $x_i = (\mu_+ - \mu_-)/2$; $\mu_+ - \mu_- = 2\mu$ and can be represented graphically, for rectangular -distribution $u^2(x_i) = \mu^2/3$, triangular distribution - $u^2(x_i) = \mu^2/6$, normal "3σ" - $u^2(x_i) = \mu^2/9$, normal "2 out of 3" - $u^2(x_i) = \mu^2$, normal "50%" - $u^2(x_i) = 1.48\mu^2$.

4.3. Sampling Procedures to Reduce Random and Eliminate Systematic Errors

An absolute and meticulous process is followed religiously to obtain accurate and precise NAA results to reduce and eliminate random and systematic errors. Procedures to reduce random errors are:

- The sample collected for analysis should be representative of the area/environment or material of research interest. This is very important because if the sample collected is not representative of the environment or material of interest, then the research or experimental analysis is baseless.
- The first point of random error reduction emerges from the process of sample collection. The experimenter or samples being collected should not be contaminated. This could be ensured by making sure that whoever collects the sample to be researched wears gloves, uses clean tools for the sample collection, and makes sure that all samples

collected for analysis are placed in a clean container or plastic bags. For example, if the you touch the samples with your bare hands, you can easily transfer sodium (Na) or minute residue on your hands directly to the sample, and this could easily be identified during sample analysis.

- All samples should be labeled appropriately and stored in clean areas, and not mixed with other samples to prevent cross-contamination between samples. It is very important to prevent this from happening since moving the samples around can transfer residues between samples and might introduce trace elements within your analysis which might not be explained. Residue transfer between samples can easily be caused by air circulation.
- Sample preparation is key to random error reduction. The area used for sample research, preparation, and tools needed for sample preparation (such as spartler, mortar and pestle, scissors, capsules, spoons) should be cleaned thoroughly with acetone to remove any contaminate. This is because any residue or particles left on the tools without cleaning them will be transferred into the sample, and can change the elemental analysis of the research.
- Sample homogeneity is very essential in elemental analysis, and this might depend on the nature of the sample, either biological, liquid,

geological, environmental samples, etc., keeping the sample as homogeneous as possible for absolute elemental analysis.

- Depending on the nature of the sample, the representative sample is weighed to desired mass, mostly approximately 1 gram, and placed in clear clean polyethylene bags, sealed, and further placed in polyethylene capsules for irradiation. Sometimes if the sample is powdery or liquid, it is double bagged to prevent leakage.
- Keeping track of the time period of irradiation, the time it takes for the sample to be allowed to decay before counting the sample, and the time it takes for the sample to be counted, is very crucial for the NAA analysis to help reduce the error and uncertainty.

As stated earlier, systematic errors arise from a number of scenarios, such as instruments not calibrated, incorrect measuring tools, misguided procedures, etc. Some procedures to help eliminate/reduce systematic errors are highlighted:

- Calibration of electronic beam balance to weigh the mass of samples is very crucial, as errors made for the mass of the sample will affect the concentration of isotopes present in the sample, hence skewing the experimental analysis completely. The mass of the sample is needed for quantitative analysis of concentration of isotopes present in the sample; therefore, incorrect measurement of the samples mass will result in wrong or inaccurate analysis.

- Efficiency calibration of the desired radiation detector is of empirical importance for the accuracy and precision of quantitative and qualitative analysis of isotopes present in the sample. The efficiency calibration determines how efficiently the detector accounts for the gamma energies of the spectrum. The efficiency calibration of the detector is performed by counting certified gamma source(s). The efficiency at which the detector counts each discrete energy line is calculated. The efficiency curves and calibration are different based on the geometry or setup of the detector and the distance from the sample to be counted; for example, the geometry of the sample could be considered as a point source on the surface of the detector or as a volumetric source.
- Energy calibration of the detector is equal essentially as the efficiency calibration. Every isotope has a unique gamma ray signature that it emits to become stable. The gamma rays absorbed in the detector are normally counted by the multichannel analyzer (MCA) and placed into energy bins or channels according to their specific energy groups. Energy bins or channels of most MCAs typically operates on 4096 (4K), 8192 (8K), 16,384 (16K), or 32,768 (32K) channel spectrums, and assigns energy values to these channels.
- Preirradiation of the sample is necessary for optimization of the experiment. Based on fair knowledge of decay of predicted isotopes

present in the sample, the developed pre-NAA calculator at UNEP could be used to determine the desired irradiation time, expected activity, and dose of the sample for optimum NAA experiment to enable the experimenter to plan adequately for the experiment.

- Estimated knowledge of neutron flux within the irradiation channels helps the researcher decide which irradiation port will be adequate for the experiment.

4.4. Principles of Quality Control and Quality Assurance

The main principles of quality control (QC) and quality assurance (QA) are to ensure that an organization, product, analysis, or services are precisely and accurately executed to meet standards. This embodies a complete definition of management policies, strategies, procedures, accountability, and responsibility defined for development, implementation, and monitoring of the quality assurance and control program. This is accomplished through well-defined organizational structure, functional responsibility levels of authority and interfaces, effect measures for the implementation and management of procedures and systems for an excellent QC and QA program.

Quality control is the process by which organizations, institutions, laboratories, and entities, etc. review operational techniques and activities involved in operations, production and/or manufacturing, and laboratory analysis to attain or fulfill the requirements of quality. The main idea of quality control is to ensure that processes and management methods

implemented in an organization are sufficient to assure conformance to specified requirements. Quality control places an emphasis on the following [31-34]: a) on the job management, defined and well-managed processes, performance and integrity criteria, and identification records,; b) competence, such as knowledge, skills, experience, and qualifications; c) elements such as personnel training, integrity, and well-defined organizational culture; d) personnel and staff should be trained in the work procedures, control of errors, and statistical processes for effective control of experiments or production lines; e) documentation of all activities and processes such as reactor operations, sample description, statistical analysis, safety analysis and procedures, design and design changes, and quality of material or equipment/instruments to indicate the quality of work, especially the quality of laboratory analysis, reference materials, blind samples, and reference certificates. QC includes frequent inspection or review of processes, samples, and protocols and reporting defects or any uncovered lapses and reporting to managements [1-4].

Quality assurance is a way of implementing measures to prevent mistakes or detect malfunctions or defects in products, procedures, and analysis to avoid problems when delivering solutions, services, reports, or products to customers or entities. QA is normally applied to physical products or analysis to verify that the products, analysis, or services meet specifications, standards, or prescribed requirements, by verifying test

samples or test runs to meet quality controls. QA can also be applied to software to verify features and functionalities, meet business objectives, etc. QA also refers to administrative and procedural actions implemented in a quality system so that requirements, goals, and objectives are met or fulfilled [5-7]. QA is also the systematic measurement, comparison with standards, monitoring of processes, and confirmation from feedbacks that help curtail and prevent error. QA is all the plans and systematic actions necessary to provide adequate confidence that a product or service will satisfy given requirements for quality. In general, two main principles of QA are of significant importance in the international standards: "Fit for purpose" – which is the product should be suitable for the intended purpose; and "Right first time" – which includes the mistakes and errors should be eliminated from all processes and production line to ensure quality products [35, 36]. QA also includes the management of the quality of samples, raw materials, assemblies, production lines, and instruments, services related to production, management, and inspections [31-37]. QA is usually also determined by product users and clients. One way of controlling QA is by using statistical control methods which are based on analyses of the objectives which are subjective to the data. Statistical process control is used by most entities and institutions as a tool to improve QA efforts and to track data and products.

4.5. Quality Control and Quality Assurance in NAA

QC and QA in NAA is beneficiary for most research facilities to improve their technique for commercialization activities. One principal reason for QC/QA is for internal generation of funds, due to budgets cuts and for operational continuation of research reactors. One of the major problems is that most research laboratories and facilities are having issues acquiring credibility with intended clients and beneficiaries because of lack of objective evidence on the quality and reliability of their operations; this is due to lack of quality assurance and quality control protocols [38]. There are several factors that make this issue prevalent in laboratories due to mistakes being made during analysis. These could include the determination of very low element levels and implicit problems of contamination, blank or element loss, insufficient insight into the correct operation of equipment and principles of irradiation and analytical process and statistical errors, as well as wrong interpretation of quality control and quality assurance concepts. NAA also requires co-ordination between experimentalists and reach reactor operators for appropriate and optimization of sample irradiation information and process. Quality practices of quality control and assurance systems are increasingly implemented throughout the world in research facilities, management, and analytical laboratories [39].

Management policies, strategies, and responsibilities should be clearly defined for development, monitoring, and implementation of a quality

assurance and control program, and should involve all aspects of the organizational structure or staff. Every staff member of the institution or research facility should be responsible for their specified functionality for various levels of authority to ensure adequate work. Effective measures should be implemented by management to verify effectiveness and continuous improvement of the quality control and assurance program. For example, typical items involved with quality assurance are: quality control systems, appropriate equipment, trained and skilled staff, documented and validated procedures, calibration of equipment and instruments, standards and reference materials, traceability, proficiency testing, nonconformance management, internal audits, and statistical analysis and errors. QC and QA needs commitment at all levels of staff and processes and should be followed religiously. Strategic planning is necessary to define the direction and an organization's performance as well as the work performance and effectiveness of the QA /QC systems [37-39].

The QC systems should be audited at regular intervals to determine the level of maintainability, effectiveness, implementation, and continuation so that the QC/QA system does not become redundant. It also very important to provide staff, and research state-of-the-art systems instruments, materials, and tools to perform the QA/QC. Quality control is very essential because major parts of operational techniques and activities are used to fulfill requirements to ensure that the processes and measurement methods

implemented in day-to-day work activities assure conformance to specified requirements. Adequate training should be given to staff/researchers on laboratory procedures, statistical control, and facility processes. All activities should be well documented and records kept well for future reference such as reactor operations, sample irradiation, sample documentation, statistical analysis, safety analysis, design and changes in design, and samples to be irradiated [34-39].

4.6. Sample Preparation, Irradiation, and Sample Analysis

The UNEP facilities operate under the DevonWay (i.e., corrective action software) safety culture paradigm. The research reactor is the main source of neutrons and instruments for laboratory research at the University of Utah TRIGA research (UUTR) facility. To ensure adequate and systematic reactor run for experiments, good collaboration between the reactor operators and experimentalist is very important to schedule effective, adequate, and efficient experimental procedures. This includes scheduling the reactor runs, start-up of reactor, irradiation and removal of radioactive samples and equipment, and proper documentation of times, materials, and records of the experiments [41]. For example, the reactor operations group and experimentalists must be aware of the samples to be irradiated, time, irradiation period, and whether the sample to be irradiated falls within technical specifications in order not to violate any policies or NRC requirements for safe operation of the experiment. This requires filling out a

request to irradiate samples and conduct experiments at the facility, and approval at least a week or two before the experiment is performed. Based on the organizational hierarchy, the reactor supervisor (RS) and senior reactor operator (SRO) are responsible for:

a) a complete list of personnel at the facility at the time of reactor operation and during reactor run at any time of reactor operation;

b) listing personnel trained and qualified to conduct any experiment at the facility such as operation of experimental instruments, sample preparation, and irradiation, and loading and removal of sample from the facility;

c) Safe operation of the reactor and its facilities, including scheduling and control of reactor utilization;

d) All safety aspects of preparation, implementation, and running or modification of experiments and experimentalists at the facility. This includes keeping track and keeping all staff informed about the status of the research reactor during its operation, for example, from reactor start-up to rod manipulation to change in power and reactor "shut-down".

Steps to ensure sample irradiation include [42-45]:

a) Consistent neutron flux characterization and profile of irradiation facility
b) Stock control of suitable flux monitors for flux measurements, and characterization (coding, masses, etc.)

c) Standard operating procedure (SOP) for neutron flux monitors irradiations and measurements, as well as calculation of neutron flux spectrum profile. This could be done using computer codes such as Monte Carlo n-particle codes (MCNP) and GEANT4.

d) Planning of irradiation, measurements after core changes, record keeping of critical variables and experimental conditions.

e) Calibration status of control rods, and equipment, adjustment of water level, and reactor instruments

f) Secured and unsecured experiments should not exceed a reactivity of $1.20 and $1.00, respectively

Sample preparation: it is a key process in the quality control system to help improve QA/QC at the research facility. Presence of impurities in irradiation containers contributes immensely to problems associated with blank samples and thus the accuracy of the analysis. Therefore, capsules to be used for irradiation should be clean and irradiated. Some factors that can cause contamination of samples include but are not limited to heat sealing of plastic containers to prevent accidental opening during irradiation and handling, reduction of moisture content in the sample because samples have to be dried prior to irradiation and analysis, accurate weighing of the sample to determine the true weight of the sample, evaporation loss due to drying of the sample, homogeneity of the sample, quality of standards and references, and consideration of the effects of difference between the sample and the

standards. Some steps that could be taken to improve QA and QC of sample preparation [41-44] include:

a) It is important to keep a control chart and inventory list of all the various batches of capsules available at the facility, and perform test analysis of random sample capsules before experiments.
b) The RS or SRO should be well furnished or informed with/about all samples in the facility and samples to be prepared for irradiation to determine the viability and feasibility of irradiation, as well as the time and period of irradiation. An irradiation request form with details of sample and irradiation should be submitted to the RS/SRO for approval, inspection, and audit.
c) Capsules should be kept in a well-cleaned environment and possibly washed with appropriate reagents before usage, for example, dilute HNO_3 could be used to clean polyethylene capsules.
d) For encapsulation of liquid samples, capsules should be submerged in hot water to test for leakage. If a container contains acetous or alkaline liquids, a wipe test with pH paper may also indicate leakage.
e) Samples should be cleaned, experimentalists should wear clean gloves and avoid touching samples with the hand or leaving samples in open air to avoid cross-contamination, and samples should be properly kept, stored in clean plastic bags and environment before and after irradiation.

f) Sealing of capsules should be properly done, heat seal polyethylene capsules with quartz tools, and clean capsule after sealing.

g) If possible, samples should be transferred after irradiation into a clean capsule and re-weighed and documented.

h) The moisture content of the sample should be determined by weighing the sample before and after drying in accordance with procedures in certificates. Note that the moisture content of samples should be performed with accordance to the reference standards.

i) Some elements are volatile and may be lost during drying such as As, Se, Halogens, Sb, and Hg; therefore, inspect the recommendations in certificates for use and drying of reference materials of a similar matrix composition.

j) The samples have to be weighed consistently for inspection and for development of control charts to inspect nuclides drifting with time.

k) Sample size reduction should carefully be done during sample homogeneity to prevent sample contamination – more samples should be analyzed to get a fair analysis of the sample, and if possible, apply different homogenization procedures.

l) Statistical test control and analysis should be applied to all analyzed data, and possible variance propagation could be performed to determine the uncertainties of the analysis.

m) A high tech electronic balance should be used to weigh the samples to get the true value of the sample mass – this requires consistent inspection and calibration of balance to obtain accurate weight of the sample.

n) Control calibrated masses could be used for the calibration of beam balance and development of control charts, date, and the time of calibration should be documented and monitored frequently. Balance calibration certificates from manufacturers could also be used for calibration.

o) In every research reactor, it is important to have the axial and radial neutron flux gradient. In addition, the neutron spectra ratios of the fluence rates of thermal neutrons over epithermal neutrons and fast neutrons should be determined varying with time, space, and power level. Changes in neutron flux can affect changes in activation rate between a sample and a standard for which corrections could be made. Differences in activation rate may also result from variations in the concentrations of strong neutron absorbing components such as B, Cd, and Gd.

p) Experimental verification of neutron gradients and correction should be considered in the experimental analysis and statistical control processes. This could be corrected by performing both experimental verification with multiple neutron flux monitors and computational

codes such as MCNP6/X, and the results should be well documented, recorded, and performed frequently.

All experimentalists should complete and submit an irradiation request form detailing time, schedule of irradiation, sample characteristics, capsule to be used, and samples to be irradiated to the research reactor operators as part of the QA/QC systems management process, and reviewed also by the reactor safety committee or director of the facility [41-45].

a) To improve the QA/QC of the facility, it is necessary and important to determine and calculate the expected activation of the sample based on the initial dose rate and activity of the samples. This could be done using a NAA precalculator developed at the UUTR facility to determine the estimate of activity and dose rate of the sample per specified irradiation periods based on fair knowledge of sample composition.
b) The irradiation and experiment could be greatly optimized using the NAA precalculator. During irradiation, fair knowledge of neutron flux level within irradiation channels based on core configuration could be estimated using Monte Carlo codes such as MCNP6/X, and should be monitored and documented.
c) A visual inspection of sample holders and irradiation ports could be performed using a camera to make sure no samples were left in irradiation ports to interfere with sample matrix.

d) Coincidence between reactor operation and irradiation schedule or program should be managed between reactor operators and experimenters.

e) Instructions should be clearly spelled out and explained concerning preparation, handling, packaging, irradiation, loading/unloading of samples from the reactor, and rules of conduct within the facility.

f) If the irradiated sample could release airborne contamination, a handling process to prevent this release should be clearly developed and communicated to all experimentalists. This could be done by keeping samples in a tight-leak container or by providing a system with negative pressure or filters.

g) Inventory of systems, devices, instruments/equipments, materials, and samples should be kept in the reactor facility.

h) A list of approved samples should be distributed to various laboratories and researchers, staff, and regularly updated for completeness.

i) In the event of any new development, problems, difficulties, challenges or new techniques, it should be reported and communicated to all reactor operators, researchers, and staff of the facility.

Sample analysis is the final step to having confident result and credibility of the research facility for clients and effective profitable commercialization process. The final implementation phase of the QA/QC program through the facility is confidence and accurate experimental results [39-43].

a) To accurately correct for radioactive decay, it is important to know the synchronization of start of irradiation time, period of irradiation, start of counting of sample, and duration of sample count. This is very essential for short-lived radionuclides.

b) Energy calibration and efficiency calibration of the detector is very essential for accurate and precise analysis of samples, and should ideally be performed before each and every experiment or on a consistent calendar schedule.

c) The geometry of detector, sample, and distance of sample from the detector before counting is very important to account for the detector dead-time effects.

d) It is also necessary to vary the irradiation and time rates depending on the irradiation process (Short, medium, or long irradiation). If short-lived isotopes are of interest, the total activity may decay significantly during the sample measurement. The NAA precalculator and fair knowledge of sample composition could be used to determine the irradiation times, counting times, and the half-life of radionuclides.

e) Pile-up corrections at high count rates could also be corrected since it is the consequence of the spectrometer's electronics being unable to distinguish successive pulses anymore. The detector should be adequately cooled and calibrated.

f) Coincidence or cascade summing effects, and element interference could also affect the accuracy of the results. This is due to the activated sample having multiple radionuclides; as a result, the gamma ray spectra of the sample will be more complex and challenging to detect elements present in the sample.

g) Gamma ray self-absorption effects occur in all samples, but become more dominant in materials with high average atomic numbers and materials with high density.

h) Malfunctioning of gamma ray or detector spectrometers – this could be due to either high voltage of AD/DC current input to the detector, improper maintenance of instrument, or staff and researchers not well trained on detectors (both handling and usage). Each and every member, staff, and experimentalist of the facility should be trained adequately on the handling, maintenance, operation, and appropriate methods of radiation particle detectors.

4.7. Quality Control and Quality Assurance Forms

The main principals of quality control and quality assurance are to ensure that an organization, product, analysis, or services are precisely and accurately executed to meet standards. This embodies a complete definition of management policies, strategies, procedures, accountability, and responsibility defined for development, implementation, and monitoring of the quality assurance and control program. This is accomplished through

having well-defined documentation and forms. Three main forms that must be completed to accomplish good QA/QC at the Utah Nuclear Engineering Program (UNEP) and the University of Utah TRIGA reactor (UUTR) facility are:

a) Sample collection and preparation details login form: The experimenter is required to provide details related to the location/origin of the sample(s) and a description, sample(s) weight, reason for analysis, etc.; Sample preparation includes details on how the sample was homogenized if needed.
b) NAA Request forms should be prepared at least a week before the irradiation is performed which is reviewed and authorized by the director of the UUTR and Reactor Supervisor (RS).
c) Sample analysis and report form: details of equipment, software, and analytical and statistical tools used for sample analysis and report should be highlighted in this form, and signed by personnel who performed the analysis.

Prerequisites:

- All experimentalists and personnel at the UUTR shall complete a radiation safety training and acquire a training certificate or be accompanied by an individual with unescorted access throughout the entire process.

- All experimentalists and personnel at the UUTR should be trained on each piece of equipment necessary for the completion of their NAA experiment.
- All experimentalists and personnel at the UUTR should obtain access to the DevonWay software system (an online corrective action system) by contacting the Reactor Supervisor.

Precautions and limitations: The technical specifications for the safe completion of experiments at the UUTR are as follows:

- The absolute value of the reactivity worth of any single experiment shall be less than < $ 1.00.
- The sum of the absolute values of the reactivity worth of all experiments shall be less than < $ 1.20.
- Explosive materials, such as gunpowder, TNT, nitroglycerin, of PETN, in quantities greater than > 2 milligrams TNT equivalent shall not be irradiated in the reactor or irradiation facilities; whereas, explosive materials less than < 2 milligrams TNT equivalent may be irradiated provided the pressure produced upon detonation of the explosive has been calculated and/or experimentally demonstrated to be less than half the design pressure of the container.
- Experiments containing corrosive materials shall be doubly encapsulated. NAA experiments should be <1 mrem/hr at 1 ft upon removal from the reactor tank.

- The reactivity worth of an experiment shall be determined and approved by the RS before an experiment is performed.

CHAPTER 5

PREDICTING MODELS FOR GAMMA SPECTRA FOR NEUTRON ACTIVATION ANALYSIS

5.1 Utah Nuclear Engineering Program NAA Experimental Data Library

A comprehensive NAA experimental data library, NAA calculator tools, and experimental protocols and procedures have been developed at the Utah Nuclear Engineering Program (UNEP). The NAA data libraries are continuously updated, as are the NAA calculator tools, experimental protocols, and standard operating procedures (SOP). Such tools developed are the NAA gamma spectra predicting tools. The motivation for the development of the NAA tools and experimental protocols and procedures is to have a well-established NAA system with quality control and quality assurance systems implemented. This will prepare and provide UNEP with a competitive edge to meet the commercial demands of clients, institutions, and companies. Various applications of NAA were considered and investigated, and developed for varying forms of samples including but not limited to soil and geological samples, metals and toxins in drinking water and contaminated water, precious metals and minerals such as iron ore, nutritional mineral

composition, and potential toxins in food, elemental composition of agricultural products, metal alloys, uranium content in soils, NAA of bullet lead, electric circuit, and chemical residues for forensic analysis, petroleum products such as crude oil contamination, building materials, meteorite composition, and archeological samples, heavy metal toxins in biological specimens, and radiation shielding [8].

One of the integral parts of the NAA databases is the NAA calculator which includes the *Activity Estimator* that provides the estimates of the activities for isotopes to be irradiated at the UUTR facility [8]. This provides the experimenter a fair idea of the activity of the sample to be expected and hence calculation for the estimated dose of the sample. This helps the experimenter better prevent radiation exposure and optimize his/her irradiation and decay times. Since NAA utilizes the method of isotope production, being able to predict the activities of each sample irradiated informs the experimenter of potential radiation risk, and provides the guidelines for irradiation of the samples to be altered if/when needed. Knowing the optimum activity and irradiation of an isotope allows for better elemental detection and analysis, based on the minimal detectable activity (MDA) by the high purity germanium detector spectroscopy. The activity calculator provides a safe application of NAA protocols (which never existed before over the course of 40 years) at the UUTR, and determines the most optimal irradiation conditions per sample. During the explorative study, we

selected samples data with varying matrix from the existing library of samples (over 300 samples) at UNEP to benchmark the predictive model.

Most of the data analyzed were compiled and implemented as part of the NAA database and manual for reference and studies [8]. The data library was created to serve several purposes, such as but not limited to serve as reference for future NAA experiments, improve NAA results, explore new adventures in NAA, serve as a foundation for NAA protocol and procedures to improve quality control and control assurance at the UNEP, and serve as a platform for computational NAA simulations and models. To develop the methodology for the NAA protocol, it was observed based on literature and the developed NAA calculator that by irradiating the samples for both short and long periods, it enhances the detection of many isotopes present in the sample.

The short sample irradiations normally range from 0.5 – 20 minutes at desired reactor power (preferably 90 kWth) and counted several times at different decay periods – for short-lived isotopes (time of decay t_{decay} = 1 – 10 min to decay time of t_{decay} = 1 – 4 hr) ($t_{1/2}$ = 1 – 30 min) and for medium-lived isotopes $t_{1/2}$ = 0.5 – 12 hr. Long irradiation times range from 1 – 5 hours and are allowed to decay for at least 24 hours before counting for long periods of at least 48 hours to identify long-lived isotopes. After the development of the NAA Activity Estimator and the Elemental Concentration calculator, experimental procedures and protocol commenced. A high purity germanium

detector is normally used for the detection of unique charged particles emitted from the sample during the decay process. Different ASF files are used to analyze the spectra and print out reports.

The different ASF files contain different libraries of nuclides according to the half-lives of the isotopes that may be identified. An AFS files queues the Genie 2000 ™ algorithms to: Locate the peaks; Sum the peak area counts; Subtract out background counts; Divide the sum peak areas by the efficiencies at the individual energies for the selected geometry; Correlate the peak energies to the energies available in the selected library from the listed isotopes; Calculate the activities and uncertainties of the identified isotopes. Custom ASF files are regularly used for short irradiations and long irradiations for isotopes with different have lives. When needed, additional custom ASF files can be created and used [7]. The UNEP NAA template for all methodologies created in the protocols includes but is not limited to sample preparation, sample irradiation, sample counting, and sample analysis. The protocol could be used by the experimenter to determine similar composition of samples, optimization of future experiments, and possible improvement of the experiment based on previous NAA data library.

The authentication and accuracy of NAA results and data library were proven by benchmarking the protocols with irradiation of NIST standard reference materials (SRM). The authentication and benchmarking was performed by running certified standards (SRM) subjected under the same

conditions and protocols through the NAA procedures and verifying that the results match up with the assay results of NAA experimental data at the UNEP. The matrix used for the SRM's was of similar matrix for the UNEP samples.

5.1.1 Selected UNEP Sample Data for NAA Predictive Tool

To validate the Monte Carlo predictive NAA models, certified National Institute of Standard and Technology (NIST) flyash sample and various certified NAA sample data were selected from the comprehensive UNEP NAA data library for the implementation of the NAA gamma sample spectrum predictive model. The matrix, sample property, characteristics, and sample analysis obtained from the data library were used as material sample inputs or descriptions for the simulation. The selected samples ranged from different media such as:

- Geological sample - quartz monzonite from a quarry in Utah's Little Cotton Wood Canyon. The quartz monzonite stone is normally used for building construction in Utah. The analysis of the irradiation confidently identified most of elements present.
- Liquid sample – tap water from Teton Valley Idaho were irradiated to explore the detection of various minerals present in water and to investigate heavy metal contaminates.
- Nutritional samples - red beans, broccoli, and white and brown rice from Japan and California were also considered for the validation of

the predictive tool. Irradiation of food products is normally performed to identify and quantify minerals present in nutritional products. Some agricultural food products tend to have the presence of heavy elements such as Al, V, Sc, Cs, Mo, Cd, As, Br, and possibly Hg. This is possibly due to the soil content and location where the produce is grown. Quantitative and qualitative analysis of samples are acquired with the experimental gamma spectra for all samples using a high purity germanium (HPGe) crystal detector.

5.1.2 Gamma Spectroscopy

Gamma spectroscopy is the process by which the radiation counting system detects gamma radiations. There are two main methods of operation used for radiation detection [3]: a) current-type system - the signal output is an average value resulting from the detection of particles that enter the system; b) pulse-type system - the signal output is a combination of voltage pulses relating to one pulse per particle detected within the system. The pulse-type systems are mostly used in most laboratories and also at the UUTR for gamma detection, which is the high purity germanium detector (HPGe). The function of the detector is to produce a signal for every particle that enters and interacts with the germanium crystal in the detector. Figure 5-1 illustrates the basic outline of a pulse-type detection system. Particles entering the detector and interacting with the germanium crystal generates unique pulses which are processed by the detector electronic

system to produce a gamma spectrum. Every component of the gamma spectroscopy system has a unique function. The high-voltage power supply (HVPS) provides a positive or negative voltage to the detector. Most voltage supplies to the detector are positive. The preamplifier optimizes the initial signal generated within the crystal and also minimizes any sources of noise that may change the signal generated. The initial signal pulse generated from the detector is very weak in the millivolt (mV) range and it is optimized and amplified by a factor of a thousand and more for detection. The preamplifier shapes the signal and reduces its attenuation by matching the impedance of the detector with that of the amplifier [3]. The main function of the amplifier is the amplification of the signal by a 100 times or more. The primary purpose of the oscilloscope is to smooth out the quality of the signal and the level of electronic noise to generate smooth pulse signals. The discriminator eliminates electronic noises and rejects unwanted pulses. The discriminator works with voltage pulses, and one-to-one correspondence between a pulse height and the energy of a particle. For example, if the discriminator is set to energy E=2.0 V, only pulses with height greater than 2.0 V will pass through the discriminator and pulses lower than 2.0 V will be rejected [3]. The timer and scalar are connected in series and counts every pulse that enters the system by adding a factor of one. At the end of the counting period, the total number of pulses recorded is displayed. The primary purpose of the multichannel analyzer (MCA) is to record and store

voltage pulses according to their height into each storage unit channel. The height of the pulse generated is usually proportional to the energy of the particle that enters the gamma detection system. The pulse generated is stored in a specific channel corresponding to a specific energy, in which the distribution of the generated pulses in the channels is directly proportional to the distribution of the energies of the particles [3]. At the end of a detection period, the spectrum recorded is displayed on a screen process through the MCA [3].

5.2 MCNP NAA Predictive Model

MCNP (ver. 6) and GEANT4 (ver. 4.9.6) Monte Carlo codes were used to model the NAA process as performed at the UUTR including irradiation of a sample and predictive model of gamma spectra that is analyzed using a high purity germanium (HPGe) gamma detector. The UUTR has two main neutron irradiation facilities, the fast neutron irradiation facility (FNIF) and the thermal irradiation (TI) facility, as shown in Figure 5-1. The TI is mostly used for NAA experiments at the UUTR because it has abundantly more thermal neutrons compared to the FNIF, and the neutrons have the same energy as the surrounding moderating atoms in the heavy water at an estimated temperature of 20^0C.

Experimental and MCNP6-based evaluation of neutrons in the irradiation facilities performed at the UUTR using the cadmium ratio measurement method by B. Noble et al. [44] concluded that there are far

more thermal neutrons in the TI than FNIF. Most materials have good neutron absorption cross-section for thermal neutrons which makes neutron activation via thermal neutrons more efficient and common. Neutrons, upon interactions with a nucleus of an atom within a material, are either absorbed or scattered; the most probable absorption interaction is capture after which a nucleus becomes unstable and decays through emission of γ-rays. These are the signature gamma rays for a given nucleus and are detected to identify isotopes present within the material. When the neutron is captured by a nucleus, the resulting reaction can be illustrated with a cobalt target nucleus as follows:

$$^{59}\mathrm{Co} + {}^{1}\mathrm{n} \rightarrow {}^{60}\mathrm{Co} + \gamma\text{; or} \rightarrow {}^{59}\mathrm{Co}\ (\mathrm{n}, \gamma)\ {}^{60} \qquad (5.1)$$

The ^{59}Co nucleus, upon capture of a neutron, forms unstable ^{60}Co nucleus. It decays by β− to a stable ^{60}Ni nucleus followed by the emission of γ-rays. The γ-ray is a consequence of a nucleus's transition from an excited state to a ground stable state. During the nucleus transition from excited state to ground state, energy is released in the form of two unique 1.1732 MeV and 1.3325 MeV gamma rays. Common nuclear reactions that occur in NAA include: (n, p), (n, α), (n, n'), (n, 2n); the most dominant one is radiative capture, (n, γ). MCNP (ver. 6) simulation of a NAA process includes the implementation of physics models and neutron cross-sections data libraries for neutron interaction with materials such as neutron absorption and scattering models; however, the PHYS card available within the code allows a

user to optimize simulation of neutron interactions, which include neutron capture, absorption, fission, and scattering physics models, and also setting of the cut-off energies for various radiation particles. To ascertain the possibility of a gamma predictive model, a simulation of the Co^{59} activation process leading to Co^{60} was conducted and compared with experimental measurements. Figure 5-2 shows the comparison of MCNP gamma spectra simulation of the activated cobalt (Co^{59}) leading to Co^{60} indicating the 1.1732 MeV and 1.3325 MeV gamma peaks. The simulation predicted the two main gamma peaks of Co^{60} with good agreement, as shown in Figure 5-2, which validates the possibility of the gamma predictive model.

The evaluated nuclear data files version *seven (ENDF/B-VII.0)* cross-section data libraries for gamma and neutron interactions were selected for this model. To simulate the NAA physics process with MCNP6, three separate input files were developed. The first input file (Appendix C) utilizes the criticality source *(ksrc card)* code that is comprised of the UUTR model and the encapsulated sample placed within the middle of the TI facility (Figure 5-3), imitating the realistic process of the NAA experiment at the UUTR. The criticality source file simulates the k_{eff} process of the UUTR reactor core for the production of the neutron flux. The *F4 tally* is the track length estimator tally used to track each individual neutron generated for the calculation of the neutron flux. The first input file (Appendix A) also includes all the fuel assembles within the reactor core, the three control rods, and all

four sample irradiation channels. The *SSW* card is used to track all the generated fission neutrons that interact with the sample within the thermal irradiation (TI) channel.

The second MCNP6 input file (Appendix B) includes the encapsulated sample model, and subsequently all tallied neutrons that interacted with the sample using the surface source write *SSW* card. The tallied neutrons are used as the neutron source for the sample irradiation in an *SDEF* source description format. The tallied neutron energies range from 0 – 10 MeV with respective energy probability distributions. The activation *ACT* card is implemented for sample activation and delayed gamma biasing during the interaction of the tallied neutrons with the sample since we were interested in the delayed gammas from the neutron activation of the sample. The signature delayed gammas from the radioactive samples were tallied with the *(F4:P)* track estimator tally.

The third MCNP6 input file (Appendix C) includes the geometry and specified definition of the HPGe GC4020 model detector from Canberra, as shown in Figure 5-4. High purity germanium gamma spectroscopy is the most practical device for detection and identification of emitted gamma radioactive sources. It has the ability to detect a wide range of gamma energies and has good peak resolution to distinguish different gamma energies. The HPGe detector utilizes high purity germanium crystal as a semiconductor, and when high voltage is applied across the crystal it acts as

a semiconductor; hence, when a photon particle travels within the crystal, the photon interacts with an electron within the crystal causing a Photoelectric Effect, Compton Effect, or Pair Production. During this process, the electron is knocked out of its valence bond, creating an electronic signal which is 'collected' by the electron system of the detector. The current/signal is then amplified and relayed to a multichannel analyzer (MCA) which counts and the records the signal pulses at energy bins, subsequently generating a gamma spectrum.

A complete set of the NAA detection system is shown in Figure 5-4. MCNP6 was used to model the germanium crystal system considering all of its properties and dimensions, shown in Figure 5-5. The tallied delayed gammas emitted from the sample from the second MCNP input file were used as the gamma source to be detected by the HPGe detector to predict the gamma spectrum of a sample.

5.3 GEANT4 NAA Predictive Model

Because the reactor criticality model cannot be performed in GEANT4, a neutron flux of the UUTR irradiation channels was transferred from MCNP6 into the GEANT4 model. The neutron flux within the irradiation channel were calculated using the track length estimator – F4 MCNP6 tally normalized per source neutron and averaged over the calculated volume of the irradiation channel. Based on the F4 tally, if the reactor power is known,

the estimated neutron flux within the irradiation channel can be determined as follows, [47]:

$$\phi = \frac{P\bar{\nu}}{w_f k_{eff}} \Phi_{F4} \tag{5.2}$$

where ϕ is neutron flux, P reactor power, $\bar{\nu}$ average number of neutrons produced per fission, w_f average recoverable energy per fission, k_{eff} multiplication factor obtained in MCNP6 model, and Φ_{F4} in the F4 tally in units of cm^{-2}. Even though both codes are similar and are based on Monte Carlo probabilistic methods, a couple of distinct features are unique to both codes. For example, MCNP is capable of criticality calculation and nuclear fission reactions, whereas GEANT4 does not have that capability. GEANT4 is versatile and gives the user open access to the code which enables the user to modify and program external libraries and physics routines tailored towards desired simulations of interest, which is not available with MCNP since it is developed by Los Alamos National Laboratory and requires individual licenses. Figure 3-11 in Chapter 3 shows the calculated GEANT4 and MCNP6 neutron flux of the UUTR irradiation channels – the FNIF and the TI neutron facility. Calculated neutron flux spectra within the FNIF and TI indicates the ratio of thermal neutrons to fast neutrons in the FNIF to be *(1.0 : 2.0),* and the ratio of thermal to fast neutrons in the TI to be *(1.0 : 4.23),* respectively; hence, there are more thermal neutrons than fast neutrons in the TI, and more fast neutrons than thermal neutrons in the FNIF, which is

in agreement with experimental evaluation of neutron flux with the FNIF and TI as described in [48].

Experimental discrimination between thermal and fast neutron spectra within the FNIF and TI was performed using the cadmium ratio method [48]. The cadmium ratio is defined as the ratio of the activity of a bare detector, gold foil, to the activity of gold foil covered with cadmium. The irradiated gold foil is exposed to neutrons of all energies. The cadmium-covered gold foil is activated mostly by fast neutrons, while the bare gold foil is activated by mostly thermal neutrons. This is because nearly all neutrons below the cadmium cut-off energy of 0.4 to 0.6 eV are absorbed by the cadmium foil. B. Noble *et al.* concluded that the ratio of thermal to fast neutron in the TI was *(4.18:1.01),* and the ratio of thermal to fast neutron in the FNIF was *(2.10:4.22),* respectively [48].

GEANT4 (ver. 4.9.6) Monte Carlo code (Appendix D) was used to model the NAA process as performed at the UUTR including irradiation of a sample and predictive model of gamma spectra that is analyzed using a high purity germanium (HPGe) gamma detector. The physics processes for neutrons include both neutron absorption and scattering processes and gamma interactions implemented for the simulation of neutron interactions for low energies (less than 1 MeV) of up to 20 MeV include QGSP_BERT_HP and QGSP_BIC_HP High Precision (HP) physics model libraries. GEANT4 low-energy electromagnetic physics models for gamma ray Compton

scattering, Photoelectric Effect, Pair Production, and Rayleigh (Coherent) scattering processes were implemented. Electron and positron physics processes such as multiple scattering, ionization, Bremsstrahlung, and annihilation processes, were also defined. Cross-sectional data libraries for GEANT4 is the G4NDL4.0 and also includes ENDF/B-VII.0 evaluated libraries [44, 46]. "G4RadioactiveDecayPhysics.hh" was invoked during the simulation to account for neutron interactions within the sample and the subsequent radioactive decay processes. A sensitive detector and scoring mesh macro files were implemented to evaluate the gamma rays emitted from the sample.

5.4 Data Normalization and Spectra Simulation

The elemental composition and concentrations of the samples that were obtained from the experimental neutron activation analysis served as the material sample definitions for both the MCNP6 and GEANT4 NAA modeling and simulation. A detailed model of the UUTR and an expansive NAA simulation were performed using the MCNP6 and GEANT4 Monte Carlo codes. The Neutron spectra (Chapter 3, Figure 3-11) for the UUTR irradiation channels were calculated using a tally track length estimator in MCNP6 and imported into GEANT4 to facilitate the NAA simulation. To accurately simulate the sample gamma ray spectra comparable to the detector, the HPGe detector was modeled and simulated to specifications considering the energy range and channels of the multichannel analyzer

(MCA). A set of High Precision physics models implemented in both codes enabled the simulation of radioactive decay processes during the neutron interactions with the samples, Figure 5-4. The HPGe detector was modeled in MCNP6 and defined as a sensitive detector in GEANT4. The specified detector energy ranged from 3keV to 3000 keV over the MCA specified channels of 1 to 8196. The energy range and MCA channels were considered to create energy bins in GEANT4 and MCNP6 code as

En 0 1.E-5 1.E-3 8196I 3.0

En - specifies range of low gamma energies from 0, 1.E-5, and 1.E-3MeV, 8196I is the number of energy bins, and 3.0 MeV is the maximum gamma energy. Simulated gamma spectra were obtained using the pulse height tally weight *(F8:P tally)* which tracks the collection of gamma particles per each individual energy bin in MCNP6. A particle primitive tracking scorer mesh was implemented in GEANT4 to track the collection of gamma particles per each individual energy bin. The experimental measurements and Monte Carlo code simulations were normalized to unity per the highest gamma counts obtained for each spectrum to enable comparison between simulated and experimental data. A MATLAB script is written to process the simulated data to obtain the simulated gamma spectra. The predictive models were validated with a National Institute of Standard and Technology flyash (NIST) sample, and various samples with different material matrix and multi-elemental composition from the UNEP NAA data libraries such as

quartz, tap water, red-beans, Portland cement, broccoli, and rice. Figures 5-6 to 5-12 present the overlay and comparison of experimental HPGe detector gamma spectra of neutron activation analysis with predictive gamma spectra. Figure 5-6 shows the calculated, i.e., predictive gamma spectra of certified NIST flyash sample in comparison to measured spectra. Some major predictive elements peaks identified for the NIST flyash sample include As, Na, Mn, and multiple Eu peaks. Predictive gamma spectra for quartz monzonite had elemental peaks of Na, Mn, Al, V, Si, Mg, and Ba, Figure 5-7. Predictive spectra of Portland cement and measured spectra had many Eu peaks identified, shown in Figure 5-8. Predictive spectra of the red beans sample indicates some elemental peaks such as Na, Mn, Cl, Ar, Ba, and K, Figure 5-9. Elemental composition of simulated elements in broccoli is Na, Cl, Al, K, V, Mn, Ar, and Ba, Figure 5-10. Common elements prominent in simulation of water include Na, La, Br, Sb, Se, and Ar, Figure 5-11. Figure 5-12 depicts the overlay of predictive gamma spectra of Japanese brown rice and experimental measured spectra. It is important to note that even though the predictive gamma spectra agrees well with the experimental measured spectra, the predictive spectra presents the ideal peaks of elements presents in each sample; therefore, the predictive spectrum has some peaks not present in the experimental peaks. The missing peaks are identified with an asterisk (*) sign.

GEANT4 Monte Carlo simulation codes have good physics models for the simulation of neutron capture processes during neutron interactions with matter, which can be seen with elemental peak identification in the simulated spectra based on the unique gamma energy of elements present within the samples. However, the predictive model does not consider the decay elapsed time between the period after which the sample is irradiated and measured by the detector. The HPGe detector is limited in the detection of gamma radiations between 0.001 keV to 3 keV, whereas GEANT4 codes indicate gamma counts within this range. Dead time, or resolving time, of a counting system is the minimum time that elapses between the arrivals of two successive particles at the detector. Dead time determines if the detector records one pulse for both particles, or two distinct pulses for each of the particles. The dead time of the HPGe detector was below 2%. Considering the detector dead time, the possibility exists that some of the particles emitted by the samples will not be recorded. Detector dead time correction and measurement maybe expressed as [49]:

$$n = \frac{g}{1 - g\tau} \tag{5.3}$$

where n is the true counting rate, τ is the dead time, and g is the observed counting rate of the detector system. The fraction of time during which the system is insensitive is represented in equation (2) by $g\tau$ [44]. Root mean square error (RMSE) frequently used to measure the difference between modeled and simulated data in comparison with actual experimental data

was implemented in the analysis. The RMSE of the simulation with respect to experimental value is defined as the square root of the mean squared error given as:

$$RMSE = \sqrt{\frac{\sum_{i=1}^{n}\left(X_{\exp,i} - X_{simulation,i}\right)^2}{n}} \tag{5.4}$$

where X_{exp} is the experimental value, $X_{simulation}$ is the simulated value, i denotes the ith value, and n is the number of data points.

Table 5-1 highlights RMSE values for gamma predictive values (i.e., peak count) indicating the average difference between experimental and simulated values. Quantitative analysis and comparison of predictive gamma spectra with experimental spectra values for samples are presented in Table 5-2. Analyses of some major elements present in simulated samples are also presented in Table 5-2. Sodium (Na) element present in the flyash sample has unique gamma energy of 1.369 and 2.754 MeV, respectively; from the quantitative analysis the normalized counts of experimental measurements were 0.38 and 0.36, respectively. Whereas predictive value for GEANT4 at energy peaks of 1.369 and 2.754 MeV were 0.15 and 0.11, respectively, indicating that the experimental measurement was twice that of the predictive value. Qualitatively, both experimental measurements and predictive spectra identified both gamma energies and are in good agreement. Quantitative analysis of results is similar to work done by Sahin *et al.* [50].

The Monte Carlo predictive gamma spectra models agree well with experimental measurements. However, some observations were made in comparison with the experimental measurements. The slight shift in some peak identification is due to difference in algorithms used by Genie 2000 software within the MCA for the energy channel distribution. The predictive spectra tends to have more peak counts as compared to the measured spectra since it provides the ideal counts of unique gamma particles emitted from the sample. The predictive model does not also contain possible contaminations of the sample. It was also noticed that the nuclear data, decay constants, cross-section values, and molecular weight values contain some errors, as indicated in work done Sahin *et al.*, 2009 [50] and Boson *et al.,* 2008 [51]. The predictive spectra model can be improved using more accurate nuclei data and possibly obtaining the exact MCA detector algorithm used by Genie 2000 from the manufacturers.

Table 5-1. Sample root mean sqaure error analysis.

Sample	RMSE Value
Quartz	0.03998
Redbeans	0.03203
Tapwater	0.07792
Flyash	0.04054
Broccoli	0.04826

Table 5-2. Peak analysis of experimental measurement and GEANT4 predicted values.

Sample	Energy (MeV)	Isotope	Normalized Count		Difference
			Experiment	GEANT4	
Flyash	0.837	Mn-56	1.0	1.0	0.00
	1.811	Mn-56	0.34	0.16	0.18
	0.559	As-76	0.5	0.48	0.02
	1.369	Na-24	0.38	0.15	0.23
	2.754	Na-24	0.36	0.11	0.25
Quartz	1.780	Al-28	1.0	1.0	0.00
	1.369	Na-24	0.09	0.07	0.02
	2.754	Na-24	0.24	0.2	0.04
	0.837	Mn-56	0.98	0.71	0.27
	1.811	Mn-56	0.08	0.07	0.01
	1.434	V-52	0.05		
Redbeans	0.837	Mn-56	1.0	1.0	0.00
	1.811	Mn-56	0.15	0.13	0.02
	1.600	Cl-38	0.14	0.12	0.02
	1.293	Ar-41	0.12	0.11	0.01
	1.524	K-42	0.4	0.31	0.09
Broccoli	1.293	Ar-41	1	1	0.00
	1.369	Na-24	0.4	0.29	0.11
	2.754	Na-24	0.12	0.09	0.03
	1.524	K-42	0.11		
	1.434	V-52	0.23	0.21	0.02
TapWater	0.412	Au-198	1.0	0.68	0.32
	1.369	Na-24	0.8	1.0	0.20
	2.754	Na-24	0.35	0.7	0.35
	1.293	Ar-41	0.41	0.4	0.01
	0.837	Mn-56	0.41	0.4	0.01
	0.564	Sb-122	0.17	0.11	0.06
	1.692	Sb-124	0.09	0.07	0.02

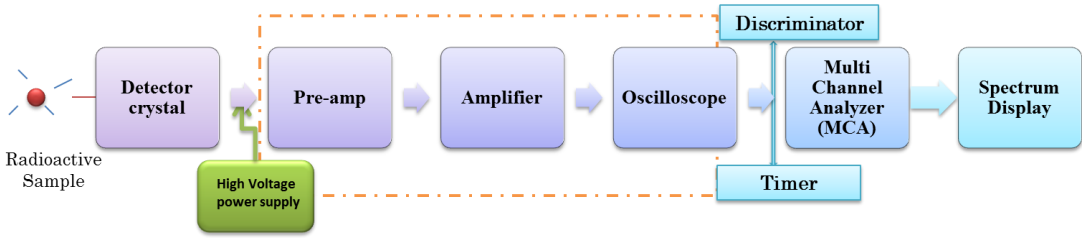

Figure 5-1. A basic outline of pulse-type detection system.

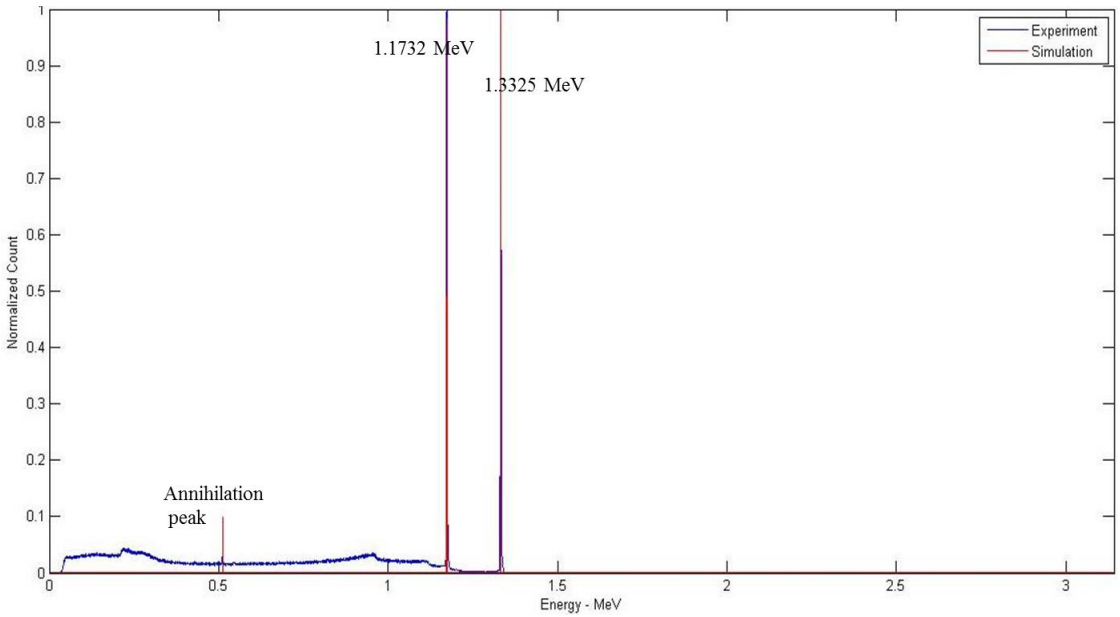

Figure 5-2. Comparison of MCNP and experimental measurement of gamma spectra of cobalt 59 activation.

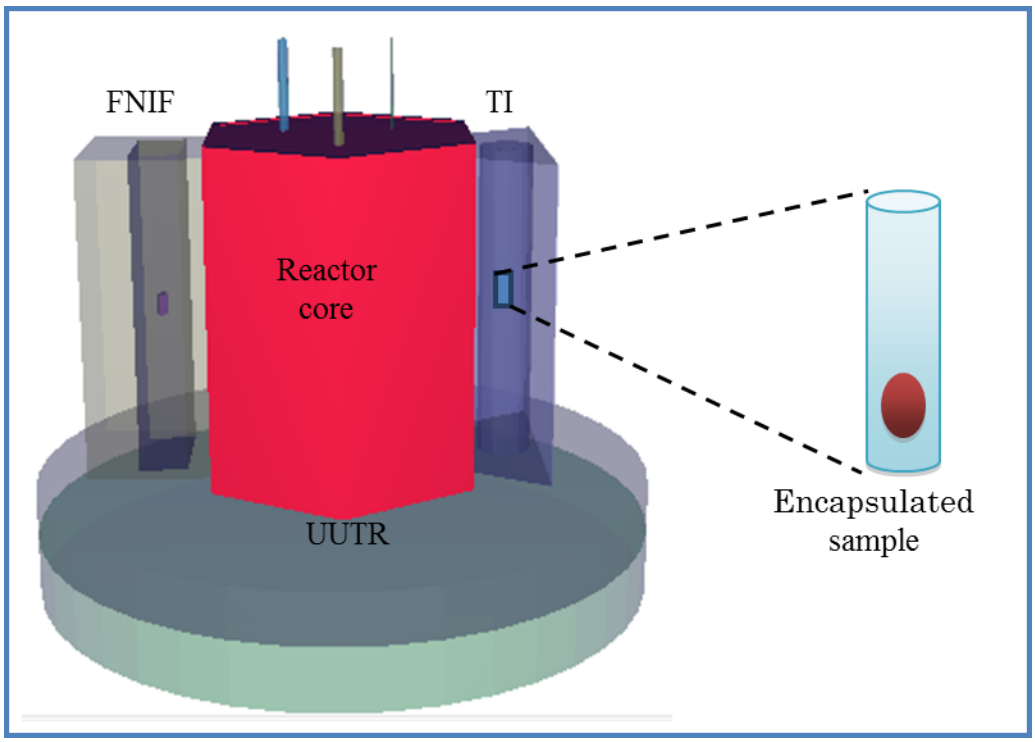

Figure 5-3. MCNP6 model of the UUTR research reactor irradiation ports (FNIF and TI).

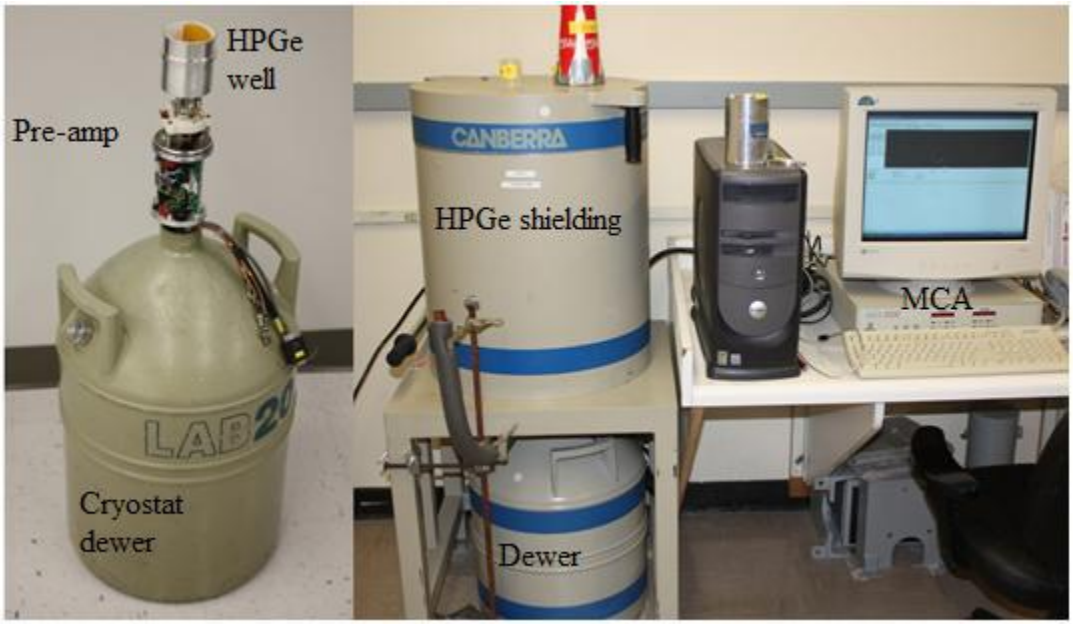

Figure 5-4. Shielded HPGe detector for counting of irradiated sample at the Utah Nuclear Engineering Program laboratory.

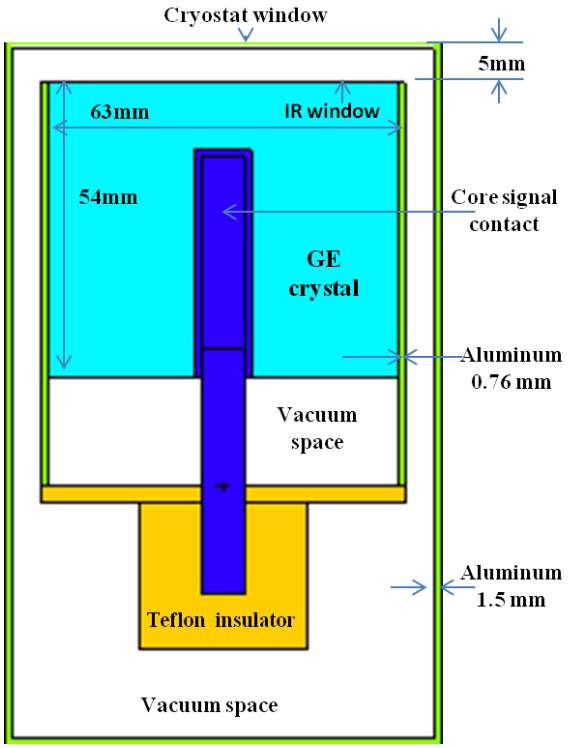

Figure 5-5. MCNP6 model of an HPGe detector at the UUTR.

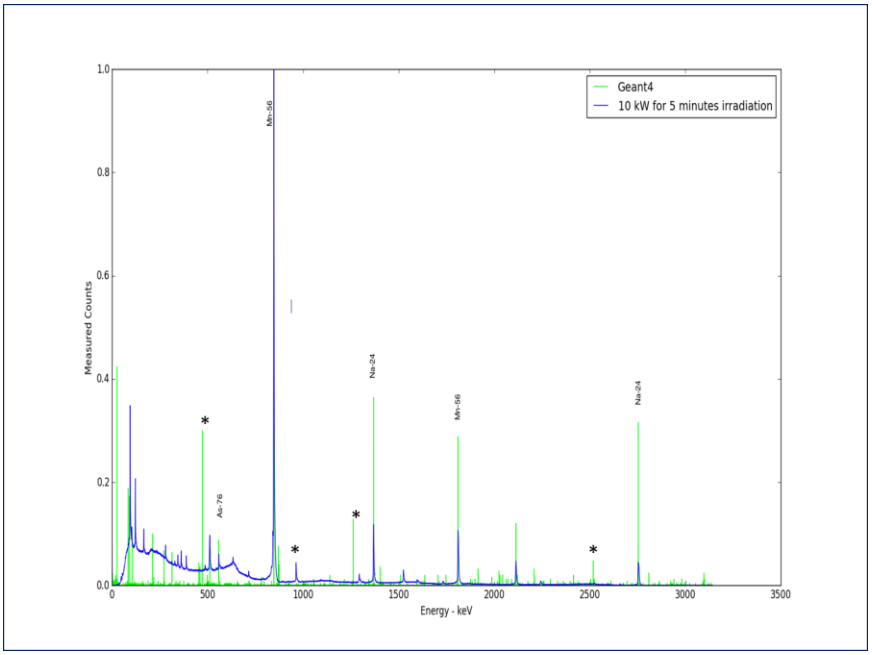

Figure 5-6. Measured, and GEANT4 predictive gamma spectrum for the certified NIST flyash sample.

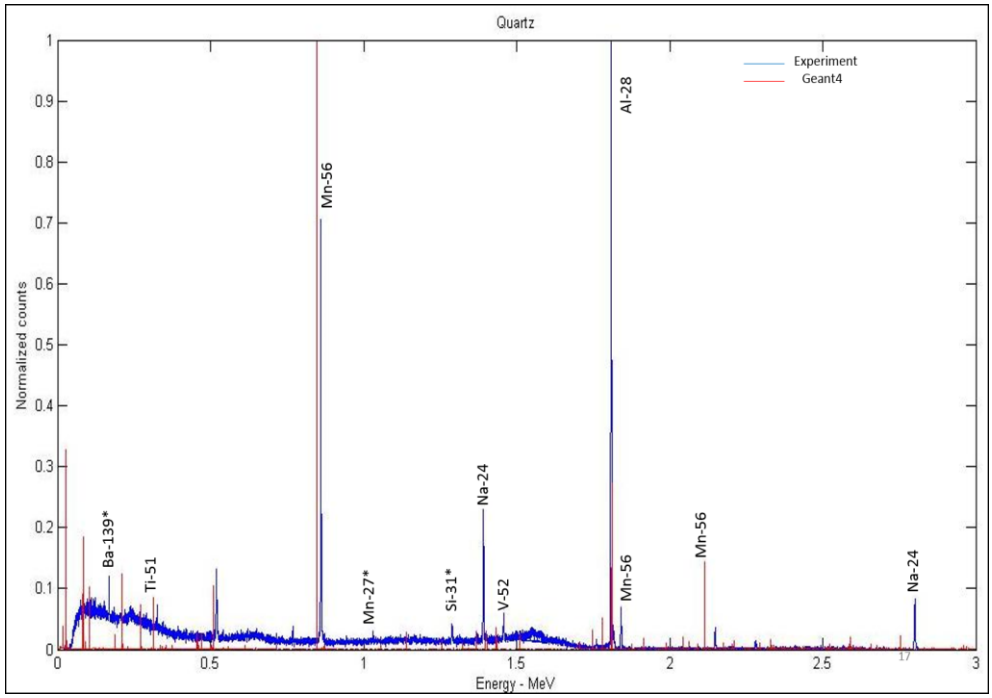

Figure 5-7. Measured, and GEANT4 predictive gamma spectrum for quartz monzonite from a quarry native to Utah's Little Cottonwood Canyon.

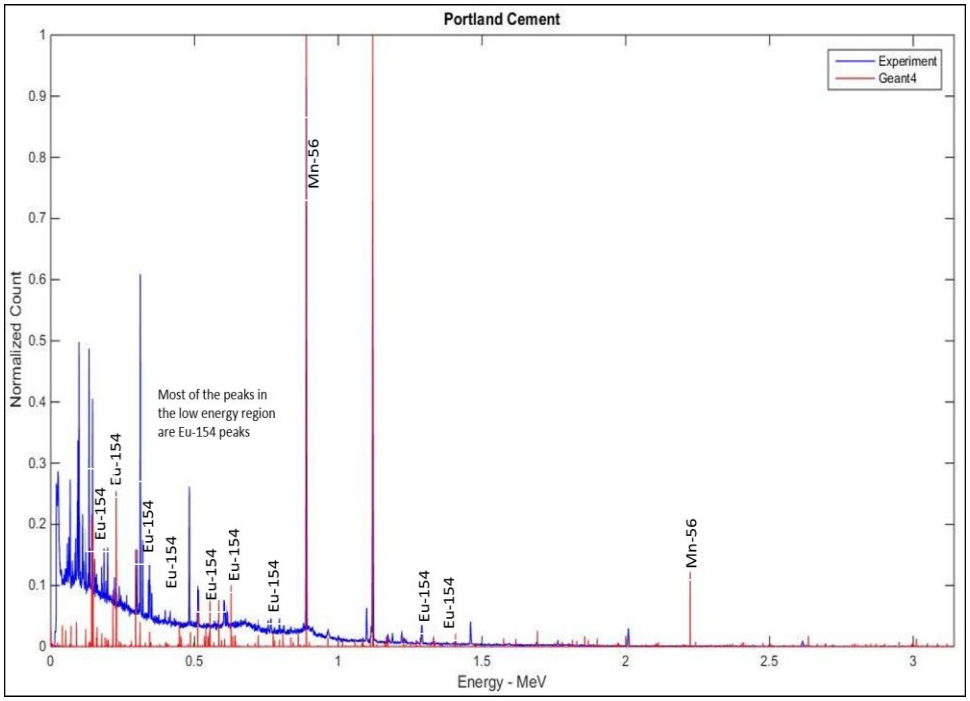

Figure 5-8. Measured, and GEANT4 predictive gamma spectra for Portland cement.

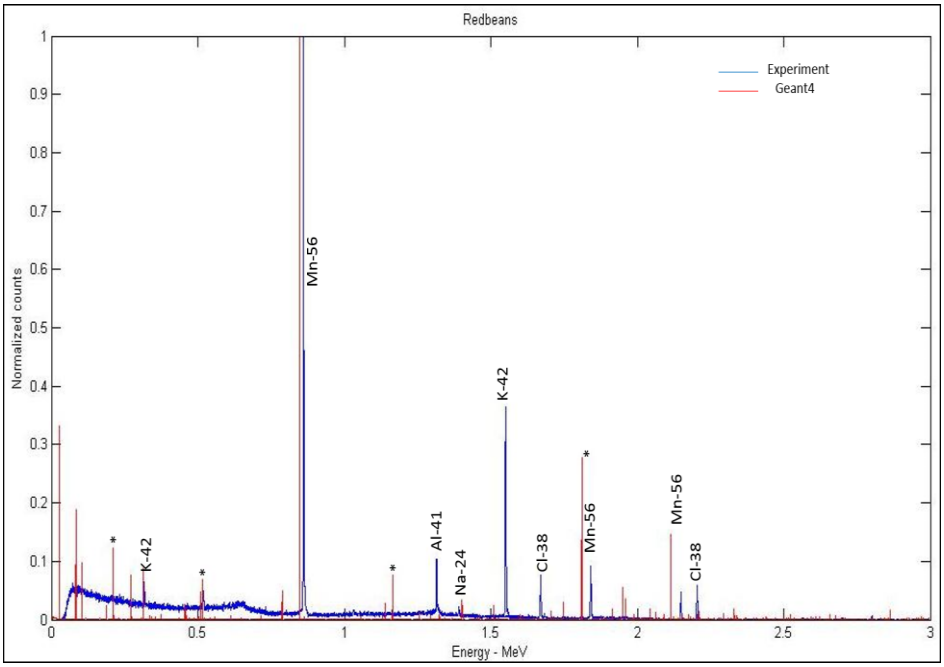

Figure 5-9. Measured, and GEANT4 predictive gamma spectra for red beans from Salt Lake Valley in Utah.

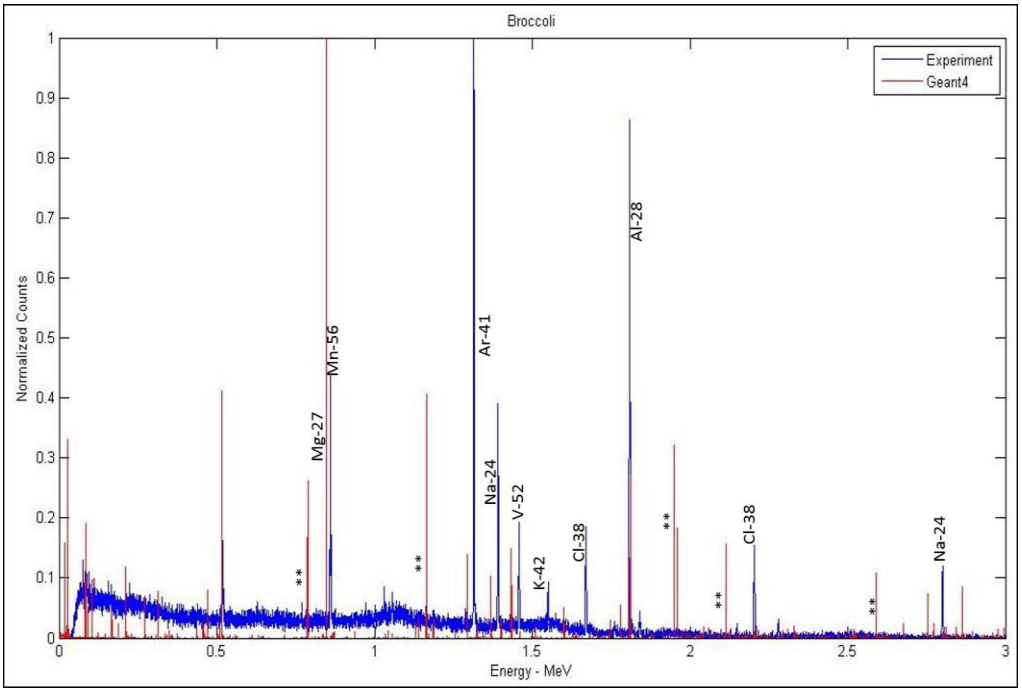

Figure 5-10. Measured, and GEANT4 predictive gamma spectrum for broccoli from Salt Lake Valley in Utah.

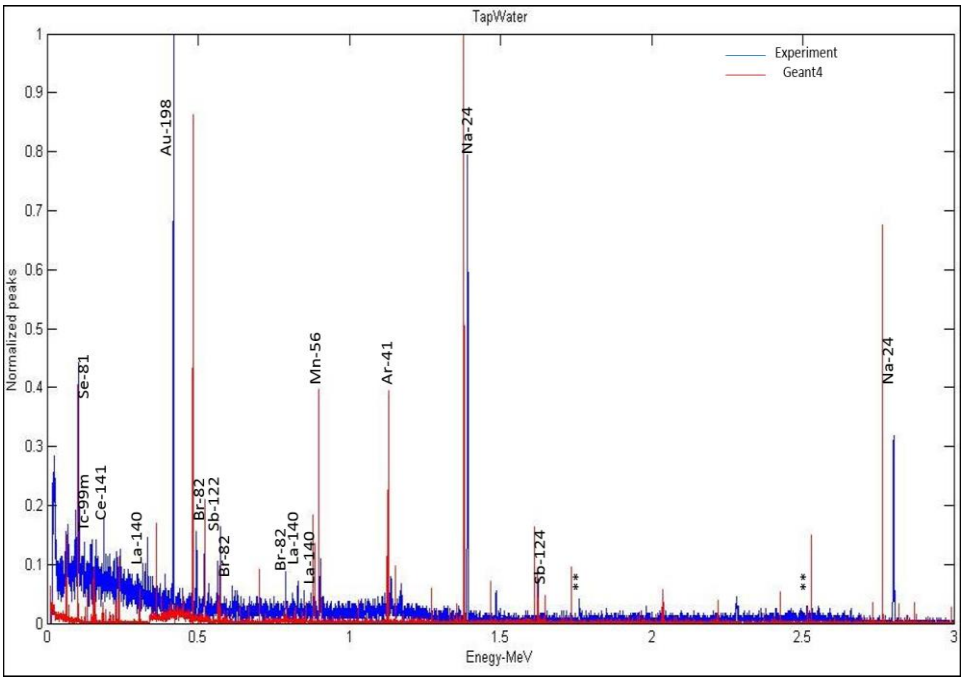

Figure 5-11. Measured, and GEANT4 predictive gamma spectrum for water from Teton Valley in Idaho.

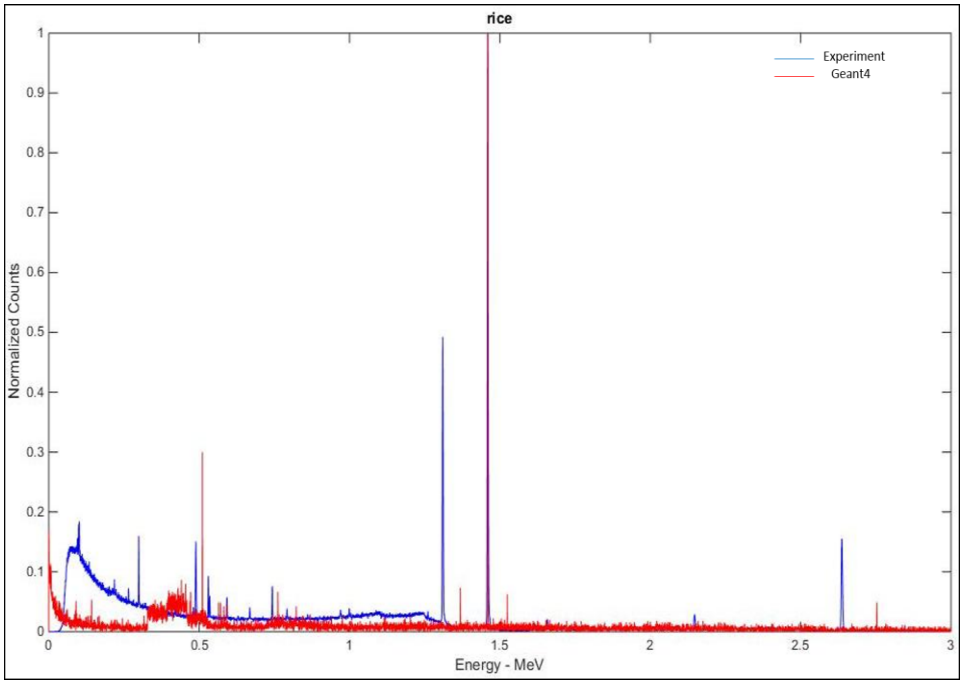

Figure 5-12. Measured, and GEANT4 predictive gamma spectrum overlay of brown Japanese rice.

CHAPTER 6

LARGE SAMPLE NEUTRON ACTIVATION ANALYSIS (LSNAA)

6.1. Large Sample Neutron Activation Analysis

Multiple elemental analysis techniques have been in existence for years and the methods keep improving rapidly as the application of computing and technology in elemental analysis have evolved. Some of the multiple elemental analysis technique include x-ray fluorescence (XRF) spectroscopy, inductively coupled plasma mass spectrometry (ICP-MS), inductively coupled plasma atomic emission spectrometry (ICP-AES), laser-ablation ICP, solid-state atomic absorption spectrometry (AAS), and instrumental neutron activation analysis (INAA). All these techniques explore the use of a small test portion size of materials, varying from a few milligrams to about a gram, from solid to liquid samples. This is a limitation to analysts during elemental analysis because the small test sample size might not be representative of the test area or material of interest, which is often the case. Small test sample size might not necessarily be representative of the test area or the sample itself. Therefore, a sample is denoted as representative when it exhibits the average properties of the test area,

environment, or material. Table 6-1 indicates the test portion size with respect to the elemental method [52]. According to Kratochvil and Taylor [53], representativeness of a test portion is a priori preserved when the sampling is performed according to specific certified norms or when a truly homogeneous material is sampled. Hence, it was in the challenge of test sample size, sample representation, and sample homogenization that the concept of large sample activation analysis (LSAA) was conceived by scientist in the late 1990s. The technique of large sample analysis is capable of direct analysis of samples with masses of hundreds of grams to several kilograms and though the principles and physics maybe understood, the method is still not versatile and applicable as compared to NAA. Peter Bode defines "large sample" as any sample material that exceeds the regular size of a test portion in the process to determine the elemental components of the material in which neutron and γ-ray self-attenuation cannot be neglected [52, 53]. The standard sample size for NAA varies from a few milligrams to 1 gram while standard size for a large sample varies from 1 gram to 10 kilograms.

6.1.1. Neutron Sources for Large Sample Analysis

The neutron source strength and energy characteristics are inherent in large sample NAA, this is because the radioactivity produced during neutron interaction is directly proportional to the neutron flux ($n/cm^{-2}s^{-1}$) and the energy-dependent neutron absorption cross-section (σ-barns) [52]. Common neutron sources for activation analysis include (a) isotopic neutron sources

such as californium (Cf^{252}) which has a relative half-life of 2.64 years with an estimated soft neutron flux distribution of less than 10^{10} n/cm^{-2} s^{-1} but are mostly limited to determination of major elements in the sample and very expensive. (b) Neutron generators such as T-D (tritium ions on a deuterium target) and/or D-D (deuterium ions on a deuterium target) normally have very high neutron energies of 3 – 14 MeV and are mostly suitable when the sample is being rotated during irradiation, but has a limitation of lower neutron flux, an estimate of 10^4 n/cm^{-2} s^{-1} which might not be enough for adequate neutron flux distribution within the sample. Therefore, some major elements may not be detected. (c) The research reactor is the most used neutron source for sample activation analysis and most widely used in the world. Most research reactors generate neutron flux over a range of 10^9 – 10^{12} n/cm^{-2} s^{-1} because they provide sufficient high neutron fluence rate for adequate neutron distribution within the sample for element activation. Literature studies indicate that an estimated neutron flux of 5 x 10^8 n/cm^{-2} s^{-1} would result in an adequate induced radioactivity during sample irradiation [52]. One factor of research reactors is that they provide a more longitudinal neutron flux gradient within the sample despite neutron flux depression within the middle of the sample because of multiple neutron scattering. Since the exploration of large sample analysis, only a few reactor facilities currently operate in the world. Some of the facilities use isotope neutron source-based facilities such as in Hungry and Japan. Table 6.2 highlights

reactor facilities in the world that explore large sample neutron activation analysis with the relevant neutron fluence rate. At the Utah Nuclear Engineering Program (UNEP), we explore the possibility of large sample NAA at the UUTR using computational and numerical Monte Carlo neutron particle code (MCNP).

6.2. Homogeneity and Inhomogeneity of Large Samples

Literature review of large sample homogeneity explains varying definitions of homogeneity. According to Kratochvil and Taylor, homogeneity is defined as "the degree to which a property or substance is randomly distributed throughout the material" [52]. Kratochvil and Taylor explain that a mixture of minerals may be inhomogeneous at the molecular or atomic level but homogenous at the particle level. This could depend on the size of the units under consideration, differences in solubility, and/or its description by the experimenter. Another quantifiable definition of homogeneity proposed by Buslik [54] is: "the negative log of the sample weight (g) required to obtain a standard deviation of 1 %"(most likely in a series of subsamples). This is related to the homogeneity index available in pharmaceutical practice: "the ratio of the standard deviation of a number of tablets measured in practice during the mixing operation, to the required standard deviation" [54]. The latter is not considered as an accurate definition of homogeneity, but rather Kratochvil and Taylors' definition is more popularly used, applicable, and explored. Therefore, during sampling, often more material is collected and

presented for analysis. The practically reality is that irrespective of the analysis technique selected, emphasis is placed on sample representation to obtain a relevant analytical portion for the collected material. This is because representation is not defined strictly and mostly depends on the researcher. To achieve homogeneity sometimes, the solid material is reduced via other processes such as crushing, milling, blending, or sieving.

Homogenization could be a limitation or could be impossible or extremely expensive depending on the nature of the material properties. For instance, it is impossible to homogenize electronic circuits on printed boards, and components of automobiles during radiation damage of materials studies [52]. Sometimes, steps taken during homogenization could often results in contamination of the sample. Contamination of the sample could be due to crushing and/or milling when the process is not controlled or different samples are crushed or milled one after the other. Therefore, when processing series of samples, careful steps are adhered to during cleaning of the work space or area before a different sample is worked on. According to Peter Bode, testing the degree of homogeneity is a common practice in the preparation of reference materials, but for routine operations, the requirement of analysis and statistical evaluation of at least five or more test portions of each sample would raise the cost of the analysis considerably [52]. Peter Bode deduced that direct analysis of voluminous solid samples might have both analytical and economical advantages, since detection limits in

trace element analysis are based on the signal-to-noise ratio. Additionally, Verheijke demonstrated in his study of assessment of impurities in silicon wafers used in the electronic industry that the detection limit for trace elements may be decreased considerably in case of high purity large samples [56, 57].

6.3. Physics of Large Sample Neutron Activation Analysis

The physics of large sample NAA is similar to instrumental neutron activation analysis. The probability of a neutron being absorbed during neutron interaction within the sample, and the subsequent release of a residual gamma particle, depends on the energy of the incoming neutron and the microscopic cross-section of the elements present within the sample. The activity equation of large sample NAA is written as follows [51-57]:

$$A_0 = \Phi_{th}\sigma_{eff}\frac{N_{Av}\theta m}{M}\left(1-e^{-\lambda_{ir}}\right)e^{-\lambda t_d}\frac{\left(1-e^{-\lambda t_m}\right)}{\lambda}\gamma\varepsilon \qquad (6.1)$$

where Φ_{th} is the thermal neutron fluence rate ($cm^{-2}s^{-1}$), σ_{eff} is the effective absorption cross-section (cm^2), N_{Av} is the Avogadro's number (mol^{-1}), θ is the isotopic abundance, m is the mass of the irradiated element (g), M is the atomic mass number (g mol^{-1}), λ is the decay constant of the radioisotope formed (s^{-1}), t_{ir} is the irradiation duration (secs), t_d is the decay time (secs), t_m is the live-time measuring time of the sample (secs), γ is the abundance in the nuclear decay of the γ-ray measured, and ε is the full energy photopeak efficiency of the detector for the energy of the γ-ray measured. The equation

to determine the mass of the element within the sample does not set a priori constraints to the mass of the sample analyzed [52]:

$$m_{unk} = m_{std} \frac{A_{o,x}}{A_s} R_\theta R_\phi R_{En} R_\sigma R_{\gamma ss} R_{inh} \quad (6.2)$$

where A_o is the area of the relevant peak in the γ-ray spectrum, corrected for differences in decay and measurement time between the unknown (x) and the standard (s), R_θ is the ratio of isotopic abundance of the element of interest in the test portion and standard which equates to 1, R_ϕ is the ratio of thermal neutron fluence rates in the test portion and standard, R_{En} is the ratio of neutron energy distribution in the test portion and standard, R_o is the ratio of the effective activation cross-section for the test portion and standard at the different neutron energy spectra, R_{nss} is the ratio of the neutron self-shielding in the test portion , R_ε is the ratio of the photopeak efficiency for the test portion and standard, $R_{\gamma ss}$ is the ratio of the γ-ray self-attenuation in the test portion and standard, and R_{inh} is the ratio of the effect of extreme inhomogeneities in the test portion and standard. During the calculation of the mass of the elements, it assumed that most of the correction terms (R) can often be neglected during NAA, but during large sample analysis, R_{nss}, $R_{\gamma ss}$, R_ε, and R_{En} are significant. This is because of the following reasons: the neutron fluence differs within the large sample, the neutron and self-shielding and attenuation within the sample, the γ-ray attenuation within the sample, and the volumetric gamma ray detection efficiency by the

detector. One of the effective and efficient ways of analyzing the neutron flux fluence and these factors is the study of large sample analysis via computation and numerical analysis [57].

6.3.1. Neutron Self-shielding in Large Samples

A couple of phenomena considered in large sample analysis are the neutron self-shielding and gamma attenuation. The neutron self-shielding during large sample irradiation depends on both the neutron energy and attenuation within the sample material properties and the dimensions of the samples [58]. The neutron attenuation and scattering properties of the sample can be evaluated by measuring the thermal neutron flux at the surface of the sample and within the sample; this has been illustrated by Overwater and Bode [59]. The neutron self-shielding will depend on the macroscopic thermal neutron absorption cross-section (Σ_a) of the sample. Thus, the relation between the microscopic (σ) and macroscopic cross-section (Σ) is; $\Sigma = N\sigma[cm^{-1}]$ which is also dependent on the energy of the neutron. If the sample is a weak thermal neutron absorber, it will not perturb the neutron flux, but if the sample has strong thermal absorbing properties, it will significantly affect flux depression within the sample. The neutron self-shielding could be determined as follows:

$I = I_0 e^{\Sigma x}$ where I_o is initial neutron flux intensity, x is the thickness of the attenuating material, and I is the final neutron flux intensity. The above equation can be expressed in terms of the attenuation factor (AF), given

as $AF = \frac{I_o}{I} = e^{\Sigma x}$. Neutron self-shielding calculations for large sample irradiation have been performed by Overwater *et al.* [57] based on neutron flux measurements at the vicinity of the sample and in comparison with the neutron flux under reference conditions [57]. Overwater *et al.* used this technique to estimate the thermal neutron diffusion length and the thermal diffusion coefficient, subsequently determining the neutron and gamma attenuation factor. The present study differs from the previous studies since it considers the realistic model neutron activation of the large sample within the irradiation channels of the reactor core and provides a graphical representation of the neutron attenuation flux distribution within the sample which could be evaluated at every layer within the sample. Based on this model, it is possible to ascertain a realistic evaluation of the neutron attenuation and distribution within the entire sample, and in the case of sample inhomogeneity, have a fair knowledge of parts of the sample that are most likely to have the maximum and minimum neutron distribution. This will help better optimize experimental procedures in LSNAA.

6.3.2. Gamma Attenuation in Large Samples

The gamma attenuation is of concern for the efficient detection of gamma ray for large sample elemental analysis. This is the attenuation of the gamma rays emerging out of the sample after sample irradiation to be determined. We assume that the gamma ray emitted from the sample is

discrete. The gamma ray linear attenuation $\mu(E_\gamma)[cm^{-1}]$ can be calculated as [57]:

$$\mu(E_\gamma) = \frac{1}{d} In\left(\frac{I_o(E_\gamma)}{I(E_\gamma)}\right) \tag{6.1}$$

where d is the path length [cm] of the gamma rays through the sample, I_o is the intensity of gammas with energy E_γ at the detector surface, and I is the intensity of gamma emitted from the sample. Overwater applied equation (6.1) in his method for the determination of the spatial averaged gamma ray attenuation in large samples, using a mixed energy gamma ray beam from a ^{152}Eu/^{154}Eu source and measuring the gamma ray spectrum. The linear attenuation is also governed by the exponential absorption law: $I = I_o e^{-\mu_l x_l}$ where μl is the linear absorption coefficient and x_l is the linear absorber thickness. The linear absorption coefficient is related to the mass absorption coefficient, μ_m, through the density of the absorber materials, ρ and be expressed as $\mu_l(cm^{-1}) = \mu_m(cm^2/g) \times \rho(g/cm^3)$. The mass thickness x_m can be defined as the mass per unit area obtained by multiplying the linear thickness x_l by the density $(x_m = \rho \cdot x_l)$; then the exponential absorption law can be modified as $I = I_o e^{-\mu_l x_l} = I_o e^{-(\mu_l/\rho)x_m}$ and μ_l / ρ can be obtained from the empirical measurements of I_o, I, and x. The linear and mass attenuation coefficient could be determined for different elements, compounds, and materials, at different energies, and could be found in literature [59]. In this work, explorative study of Monte Carlo code simulation is used to determine

and assess whether large sample NAA is possible in one of the UUTR irradiation channels by analyzing the neutron flux distribution and gamma attenuation within the sample. The advantage of using computation methods is the representation of the neutron flux distribution within the sample, flexibility in the sample geometry and composition, and the assessment of flux depression within the sample.

6.4. Methods of LSNAA

The determination of mass concentrations of elements in a large sample is very challenging because it is difficult to know the actual quantity of elements within the sample. Similar methods such as the absolute method, the comparator method, and the internal standard methods used for the elemental mass concentration in instrumental neutron activation analysis are normally employed [51-56]. The absolute method for the sample is based on the use of known values of activation cross-section and neutron flux that are derived from performed measurements and/or computational physics estimates. These various parameters are often independent measures and the imprecision of the values add up to systematic errors in the measurement. The absolute method is best applied to sample matrix that is well known and when dealing with pure materials such as alloys [51, 52, 59]. The absolute method normally has large errors when adopted for large sample analysis.

In using the comparator method, a known standardized sample with known amount of elements of interest is irradiated under the same conditions

as the experimental sample. Both samples are measured under the same conditions considering the sample-to-detector distance, and sample size. The mass concentrations of the elements of interest could be calculated by comparing the net peak areas in the two measured spectra of both the known standard and the experimental standard. However, it is not practical to use reference standard materials because aside from the economic cost of using the standard materials, the neutron flux distribution in the experimental sample might be different from the known standard sample. It also depends on the sensitivity of the elements within the experimental sample and reference standard sample [52, 53].

The application of the internal monostandard method consists of the use of one of the main radionuclides produced during the activation of the experimental sample and used as a mono energy standard. Based on literature [52, 53], the effect of neutron spectrum perturbation is the same for the parent element of the radionuclide and for other elements in the experimental sample. During the application of the internal monostandard method, it is assumed that the experimental sample is macroscopically homogeneous. Hence, the internal monostandard method either results in the ratios of the element of interest to the monostandard element or thus may serve as a comparative method [52, 53]. For instance, if the material is of high purity and known stoichiometry, the major element is used as the

monostandard element in comparison to the mass fraction of the element of interest [52, 53].

6.5. MCNP Numerical Model and Simulation of Large Sample NAA

An explorative study of the concept of large sample neutron activation analysis (LSNAA) is developed for the University of Utah TRIGA reactor (UUTR) facility using Monte Carlo computational code. This explorative study has not been performed before. Detailed descriptions of the UUTR irradiation facilities are highlighted in Chapter 3, Section 3.1.2. The fast neutron irradiation facility (FNIF) is employed to explore the viability of large sample NAA mainly due to the FNIF being spacious enough. The FNIF has a total area of 206.45 cm^2 and a total volume of 12,585.265 cm^3. In addition, the FNIF has a semi-hard neutron flux with an estimate of 10^{11} neutrons/cm^2s and has good proportions of thermal neutron flux as described in Chapter 3, Section 3.3.3. Since the sample is insert and removed from the FNIF manually and also because the FNIF canister sample holder is moveable, it is important to determine the position of the sample as accurately as possible prior to its irradiation.

To explore and study large sample NAA, the UUTR reactor core with all its components and irradiation facility were modeled using MCNP computational simulation code. The MCNP code provides the ability to visualize graphically the spatial neutron flux spread within the large sample, and provides clear estimates of the neutron flux distribution within the

sample considering both the axial and radial (x, y, and z dimensions) distribution throughout the sample. In order to derive the magnitude of the neutron flux distribution within the sample and enable a critical understanding of the neutron self-shielding, depression, and the gamma attenuation within the sample, subsequent estimates of the activity of gamma rays are produced after the sample activation. This will also be dependent on the material composition and the elemental properties as well as cross-section within the sample. Based on the sample space within the FNIF, computational calculations were performed for a series of samples. A cylindrical sample size was considered for the computation because most polyethylene sample holders and capsules tend to be cylindrical in shape. The cylindrical axis of the sample can be analyzed layer by layer. The dimensions of the sample size considered for the computation are a cylindrical shape with diameter 5.08 cm and a height of 5.08 cm as described in the MCNP model in Figure 6-1. In order to understand and explore the concept of large sample analysis at the UUTR, different materials with varying levels of homogeneities, inhomogeneities, material density, and material matrix were considered, such as wax, flyash, and Portland cement. Table 6-3 highlights the elemental composition of wax, flyash, and Portland cement.

One key factor vital to understanding the nature of neutron interaction and self-shielding, and gamma attenuation within large samples, is the neutron microscopic cross-sectional data of elements present within the

sample. Analysis of neutron interactions and neutron flux distributions within the large sample includes; a) a large sample with copper pellets embedded in the middle of the sample to access the neutron flux depression within the middle of the large sample, and (b) analysis of the sample without the copper pellet in the middle of the large sample. For instance, the elemental composition of wax (14.3 % hydrogen and 85.7 % Carbon) and a large sample with copper pellet embedded within the middle of the wax sample exhibit different probability of neutron interaction based on the element present within the wax and the neutron energies. With reference to neutron cross-sections of H, C, and Cu in Figures 6-2, 6-3, and 6-4 respectively, elastic scattering process is of high probability at varying neutron energies as compared to radiative capture for hydrogen, while a carbon atom has resonance at high specific neutron energies. Inelastic scattering cannot take place within a hydrogen element due to the fact that all states are filled within the nucleons; therefore, no excited states exist and a compound nucleus cannot be formed. Major elemental composition of Portland cement includes O, Si, Al, Na, Ca; these elements are most common to cements and have very low probability of neutron capture. Based on the neutron cross-sectional data of O, Si, Na, Ca, and Ali, all these elements have high probability of neutron elastic scattering as compared to radiative capture. For example, O, oxygen has strongly bonded nucleus and has very little affinity of neutron capture at low neutron energies. Hence, the

presence of these elements within cements and the above-mentioned property makes cement a good neutron moderating material. Since flyash is composed of residues mostly generated from combustion, it is mostly of fine particles and known to be very homogenous. Major elementals synonymous to flyash include Na, Mn, La, and Eu. Even though most of these elements do not have strongly bonded nucleus as compared to H, C, and O, they have good probability of neutron elastic scattering process, and have a fair chance of neutron capture at low neutron energy. Compared to wax and cement, flyash is the least neutron moderating material. The probability of radiation capture is dominated at very low neutron energies for copper, making it a good neutron monitor at thermal energies. Figure 6-4, indicates neutron cross-section data for Cu^{65}. The high probability of neutron interaction at thermal neutron energy with Cu^{65} is the radiative capture with the emission of a gamma ray with unique energies. The nuclear reaction could be given as $Cu^{65} + n^{1} \rightarrow Cu^{66} \rightarrow Zn^{66} + \gamma$; Cu^{65} interacts with a neutron to form Cu^{66}, forms a radioactive compound, and decays to a daughter isotope of Zn^{66}, emitting a residual gamma ray which is detected for the gamma spectrum.

In order to derive the magnitude of the effect of inhomogeneities and assess the spatial neutron distribution, a set of MCNP simulations were performed modeling different sample matrix and neutron activity distribution within the activated sample. The MCNP simulations included (a) the spatial distribution of the neutron flux on the surface of the cylindrical

sample, (b) the linear distribution of neutron flux within the main axis of the sample – the x, y and z axis, (c) the neutron flux at the center and/or middle of the sample, (d) the neutron flux at the top and bottom of the sample, and (e) random distribution of neutron flux within the sample. This was accomplished by inserting copper pellets of dimension 0.2 cm within the main axis of sample, center and/or middle of the sample, and meshed within the cylindrical sample, to form an extremely inhomogeneous sample; this is illustrated in Figure 6-5.

6.5.1. Large Sample Simulation and Analysis

A Monte Carlo model, including the reactor core, the FNIF irradiation facility, and a large sample matrix, has been developed. The effect of neutron fission generation within the reactor core was taken into account using the MCNP explicit $S(\alpha,\beta)$ capability. Calculations were performed for detailed core geometry using the MCNP criticality *mode* and core assembly with a Maxwell fission neutron source distribution within the FNIF. The number of histories simulated for the "*kcode"* criticality calculations are as follows: kcode 1000000 1.0 100 1100. The results obtained for the criticality calculation indicated that the final estimated combined collision/absorption/track-length "*keff"* = 1.00653 with an estimated standard deviation of 0.00002, signifying that the reactor core is in critical condition under steady state. Track length estimate tallies (F4) for neutron flux averaged over a cell in units of cm^{-2} per source neutron were used to track the

neutron flux distribution within the large sample. The FMESH card was invoked and superimposed over the large sample in a grid format to calculate the track length estimate of the neutron flux average over the mesh cell in the units of particles/cm^2. A MATLAB script was used to convert the results obtained from the FMESH tally into a visualize graph of the neutron flux within the large sample, and this provides a clear pictorial view of neutron flux depressions and flux attenuation distribution within the sample during large sample analysis.

Figure 6-6 depicts the neutron flux distribution within the top section of the large wax sample. The surface of the sample that is closer to the core recorded an average neutron flux of 6.2 x 10^{10} n/cm^{2}s and the section away from the core recorded an average flux of 5.2 x 10^{10} n/cm^{2}s. The pictorial view of the spatial distribution of neutron flux self-shielding as it attenuates throughout the wax sample could be seen in Figure 6-6. The relative computational error of the spatial flux distribution within the top section of wax sample is less than 2 % which is well within the MCNP error limits and presented in Figure 6-7. The middle section of the wax sample with the copper pellet in the center has different flux distribution from the top and bottom section. A pictorial view of the spatial neutron flux self-shielding and depression could be seen in the middle of the wax sample, as shown in Figure 6-8, with the relative computational error less than 2 % which is well within the MCNP error limit presented in Figure 6-9. It could be seen in Figure 6-8

that the average spatial flux distribution at the surface was 6.4 x 10^{10} n/cm^2s, more than that of the top and bottom section. This is because the neutron flux within the FNIF is hardest in the middle section of the FNIF. The spatial flux is depressed towards the middle due to elastic scattering by the H and C elements within the wax. The copper pellet in the middle has average neutron flux of 5.3 x 10^{10} n/cm^2s compared to its immediate surroundings. The bottom section of the wax sample recorded similar spatial neutron flux distribution as the top section, with an average neutron flux of 6.3 x 10^{10} n/cm^2s as depicted in Figure 6-10. The relative computational error of the spatial flux distribution within the bottom section of the wax sample is less than 2 % which is well within the MCNP error limits as presented in Figure 6-11.

The middle section of both flyash and Portland cement samples were simulated and analyzed. The flyash sample is similar to the Portland cement sample as both have the same density. One can deduce from Figures 6-12 and 6-13 that the copper pellet located in the center at (-32.5, 18.5) has the lower neutron flux. Comparing both the flyash and cement sample, the side that faces the reactor core has higher neutron flux within the flyash than cement because flyash is mostly composed of carbon and has a smooth distribution of neutron flux within it as compared to cement. This confirms that flyash is more homogenous than cement and a better moderating material. Hence, in large sample analysis, a good neutron moderator sample with hidden

elements within it could be activated with adequate neutron flux of 10^{10} n/cm^{2}s. Figures 6-14 and 6-15 indicate the the graph of relative computational error of the flyash and cement, respectively. Both relative computational errors are within 5% which is within the acceptable simulation limit of 10%. Figure 6-16 shows the graphical analysis of all three samples.

Analysis of neutron flux depression and distribution within the large sample with and without the presence of the copper pellet in the middle of the sample are analyzed and compared. Cement and flyash were simulated for this study. MCNP code was used to simulate the neutron flux depression and distribution with the cement and flyash sample without the presence of copper pellet embedded in the middle. Figure 6-17 shows the neutron flux distribution with the flyash sample, the maximum neutron flux recorded is estimated at 7.0 x 10^{10} n/cm^{2}s, and the flux distribution at the middle of the sample is estimated at 6.0 x 1010 n/cm2s. Figure 6-18 shows the relative computational error distribution within 4.9%. Figure 6-19 shows the neutron flux distribution with the flyash sample, the maximum neutron flux recorded is estimated at 7.0 x 10^{10} n/cm^{2}s, and the flux distribution at the middle of the sample is estimated at 6.5 x 10^{10} n/cm^{2}s. Figure 6-20 shows the relative computational error distribution within 5.0%. Figure 6-21 and Figure 6-22 show the comparison of neutron flux distribution and depression with and without copper pellet with both the flyash and the cement large sample. Analysis of the figures indicates there is a clear neutron flux depression

within the sample with the copper pellet in the middle. This is because based on the neutron microscopic cross-sectional data, copper is a good neutron absorbing material and absorbs the neutrons that interact with it. Hence, there is minimum record of neutron flux at the location of the copper pellet which is expected.

6.5.2. Effect of Sample Size in FNIF of the UUTR

The effect of sample size along the axial profile of the FNIF irradiation channel was examined due to different flux levels axially within the FNIF. Axial distribution of neutron flux profile within the FNIF was analyzed in Chapter 3; the maximum neutron flux was at the middle of the FNIF and reduced towards the top and bottom of the FNIF. The effect of sample size was conducted considering wax sample material with copper pellets embedded in the top, middle, and bottom of the wax sample at different sample sizes, 2 cm, 3 cm, 4 cm, and 5 cm, from the center of the FNIF, as seen in Figure 6-23.

Figure 6-23 shows the process of sample loading within the FNIF during large sample analysis. Lead bricks are placed at the bottom and top of the FNIF sample holder to enable it to sink within the pool into the reactor core. MCNP code was used to simulate reactor criticality to study the effect of sample size in relation to change in axial neutron flux. Figures 6-24, 6-25, and 6-26 highlight the effect of sample size with respect to the effective neutron flux distribution within the top, middle, and bottom of the wax

sample, respectively, along the axial neutron profile of the FNIF. Both the top of 2 cm and 3 cm sample size had an estimated maximum neutron flux of 8.5 x 10^2 n/cm^{2}s and reduced to 6.0 x 10^2 n/cm^{2}s, while sample size of 4 cm and 5 cm recorded maximum of 8.0 x 10^2 n/cm^{2}s and reduced to 5.5 x 10^2 n/cm^{2}s. The reason for less neutron flux distribution at the top of the FNIF might be due to 'control rod worth'. The control rod worth is the process by which the control rod absorbs thermal neutrons near it, hereby reducing the neutron flux within the region of the control rod which is located at the top of the reactor core. The middle section of all sample sizes (2 cm, 3 cm, 4 cm, and 5 cm) had equivalently the same estimated maximum flux of 10.5 x 10^2 n/cm^{2}s and a minimum of 6.0 x 10^2 n/cm^{2}s. The bottom portion of the wax sample sizes also recorded similar reduction in neutron flux estimated at maximum of 8 x 10^2 n/cm^{2}s and minimum of 5.5 x 10^2 n/cm^{2}s. As part of the large sample analysis, the effect of sample size with respect to the neutron flux profile within the axial length of the different sample sizes was also evaluated. The simulation results were compared with the axial neutron flux profile within the FNIF. Figure 6-27 represents a graph of the effect of sample size in relation to neutron flux profile as a function of axial sample length. It could be deduced from the graph that the peripheral of the sample size 5 cm records less neutron flux estimated at 5.81 x 10^{10} n/cm^{2}s as compared to sample sizes of 2 cm, whereas the middle of the sample size 5 cm recorded a maximum neutron flux of 6.66 x 10^{10} n/cm^{2}s which is the highest

neutron flux compared to sample size of 2 cm, 3 cm, and 4 cm. Figure 6-28 indicates the comparison of axial neutron flux profile in FNIF with the effect of sample size in relation to neutron flux profile as a function of axial sample length. The estimated axial neutron flux within the FNIF was 10^{11} n/cm^{2}s as compared to the effect of sample size with an estimated flux ~ 10^{10}. The difference in neutron flux value is due to neutron moderation and attenuation process by the sample. As a result, the size of large samples irradiated within the FNIF will have an effect on the neutron flux distribution within the sample.

Table 6-1 Analytical techniques with respect to the sample test portion size [52].

Analytical technique	Test volume
Instrumental neutron activation analysis (INAA	< 1 g
X-ray fluorescence (XRF)	1 – 50 mL
Inductively coupled plasma mass spectrometry (ICP-MS)	1 – 2 mL
Inductively coupled plasma atomic emission spectrometry (ICP-AES)	1 – 2 mL
Absorption spectrometry (AAS)	10 – 20 µL

Table 6-2. LSNAA facilities and relative neutron flux [52].

Institute	Nation	Reactor Type	Test Portion	Sample Load	Neutron Flux ($n/cm^{-2}s-1$)
Univ. of Utah TRIGA	USA	TRIGA	10 kg	Manual	7.3×10^{11}
Dalhousie University	Canada	SLOWPOKE	30 g	Rabbit system	2.5×10^{11}
International Centre for Environment and Sciences	Jamaica	SLOWPOKE	30 g	Rabbit system	2.5×10^{11}
Atominstitut	Austria	TRIGA	5 g	Rabbit system	2×10^{12}
FRG-II	Germany	TRIGA	1 kg	Manual	6×10^{9}
Delft Univesity	Netherlands	Pool type reactor	50 kg	Manual	3×10^{8}
BARC, Mumbai	India	Pool type reactor	1-4 kg	Manual	2×10^{8}
Demokritos	Greece	Pool type reactor	2 kg	Manual	2×10^{6}
Institute of Nuclear Physics	Kazakhstan	Pool type reactor	10 x mL	Manual	Low power operation

Table 6-3. Elemental composition of wax, flyash, and Portland cement.

Wax – 0.94 g/cm^3	Flyash – 2.3 0.94 g/cm^3	Portland Cement – 2.3 g/cm^3
H – 14.4 w/o	As - 0.11 w/o	H – 1.0 w/o
C – 85.6 w/o	Mn - 0.172 w/o	C - 0.1 w/o
	Na - 0.63074 w/o	O – 52.9 w/o
	Ba - 0.080 w/o	Na – 1.6 w/o
	La - 0.002 w/o	Mg - 0.2 w/o
	Hg - 0.002 w/o	Al – 3.3 w/o
	Sr - 0.0018 w/o	Si - 33.7 w/o
	Eu - 0.00028 w/o	K – 1.3 w/o
	Ce - 0.0011 w/o	Ca – 4.5 w/o
	Dy - 0.00008 w/o	Fe – 1.4 w/o

Table 6-4. Analysis of neutron interactions within the large sample.

	Number of Neutrons that react with sample	% that interact with sample
Wax	7.10 x 10^{10} n/cm^{2}s	9.59%
Flyash	5.8 x 10^{10} n/cm^{2}s	7.94%
Sample	Neutron Capture - counts	Neutron Scattering - counts
Wax	6.65 x 10^8	7.03 x 10^{10}
flyash	4.10 x 10^9	5.39 x 10^{10}

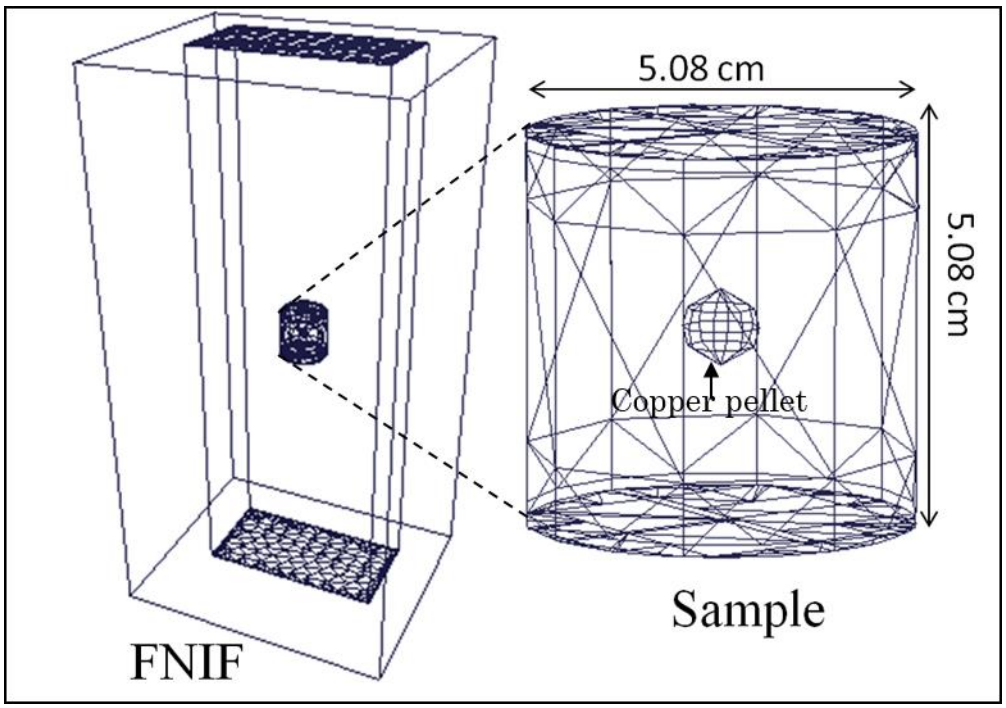

Figure 6-1. Large sample description explored at the UUTR within the FNIF (not drawn to scale), model obtained from MCNP6.

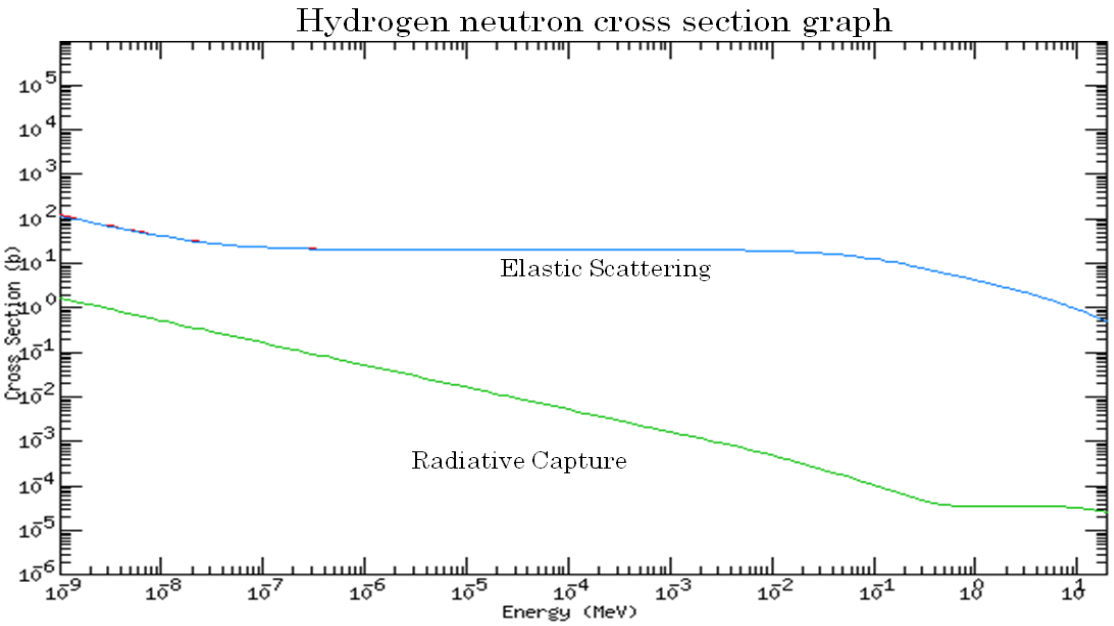

Figure 6-2. Neutron cross-section data – Hydrogen. Adapted from [60].

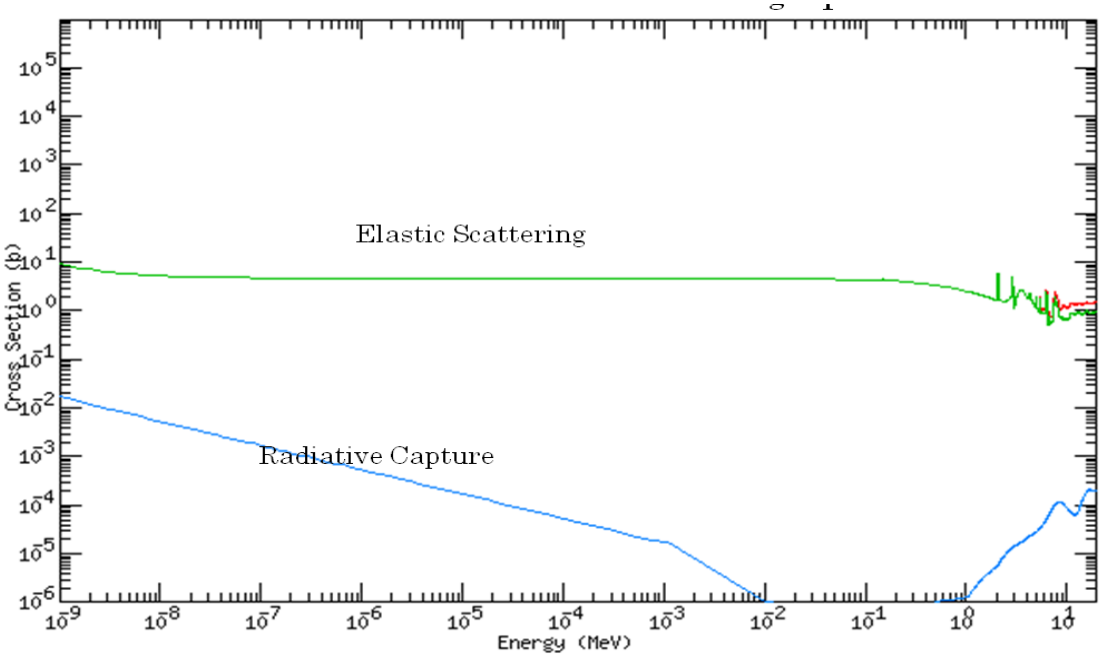

Figure 6-3. Neutron cross-section data – Carbon 12. Adapted from [60].

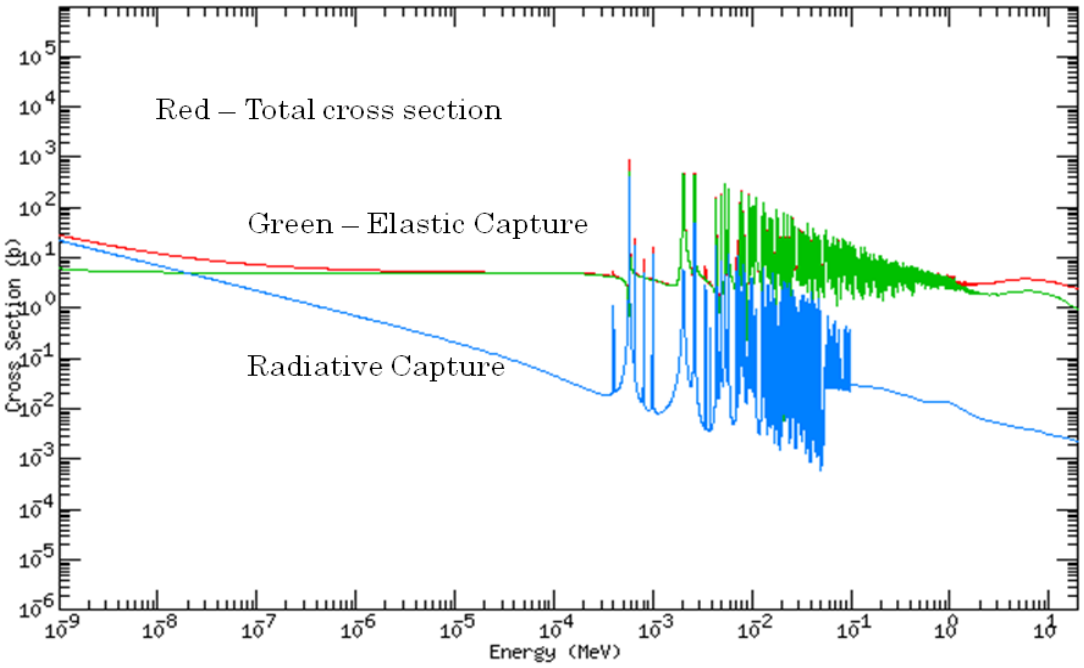

Figure 6-4. Neutron cross-section data – Copper 65. Adapted from [60].

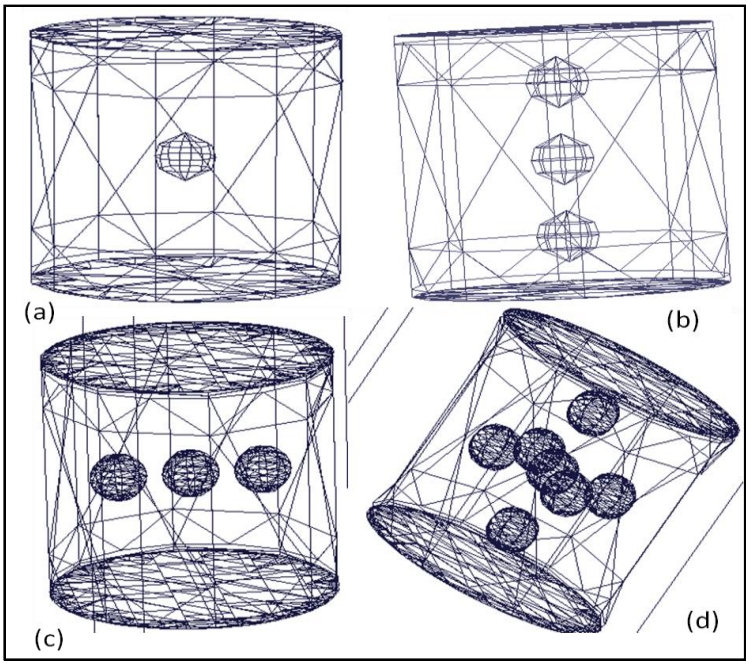

Figure 6-5. Schematic diagram of large sample (a) copper pellet embedded in the middle of sample, (b) copper pellet along z-axis, (c) copper pellet along x-axis, and (d) copper pellets meshed randomly in the sample.

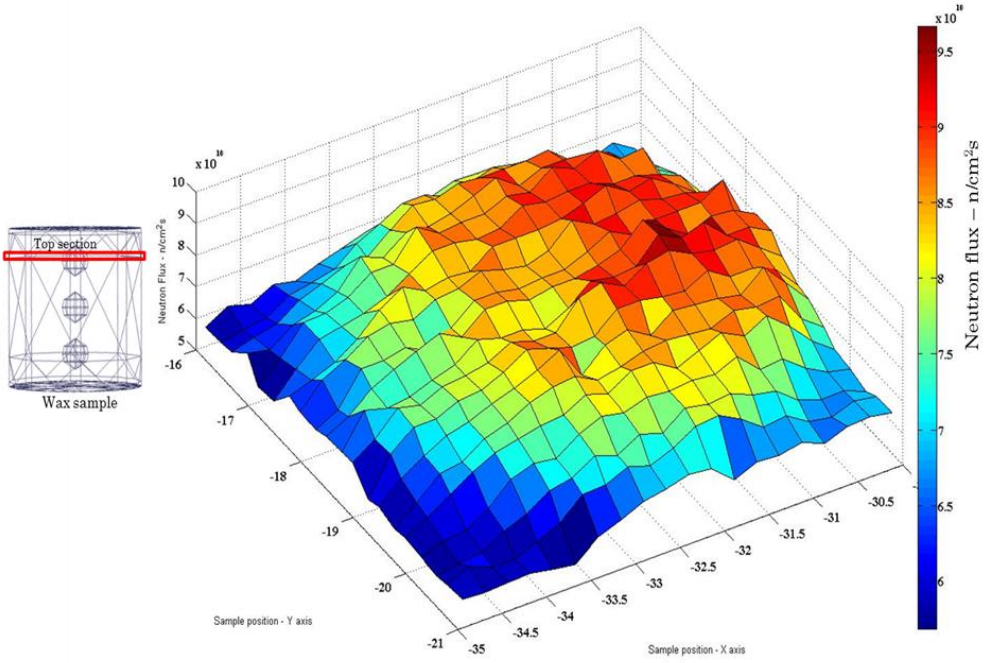

Figure 6-6. MCNP6 simulation of neutron flux (n/cm^{2}s) distribution within wax large sample – Top section.

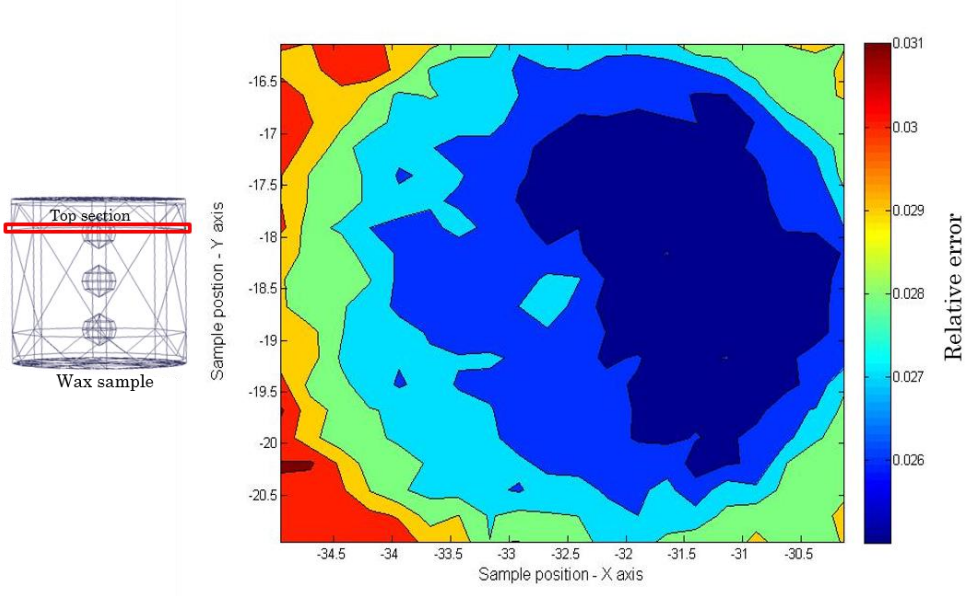

Figure 6-7. MCNP6 simulation of relative error of neutron flux distribution within wax large sample – Top section.

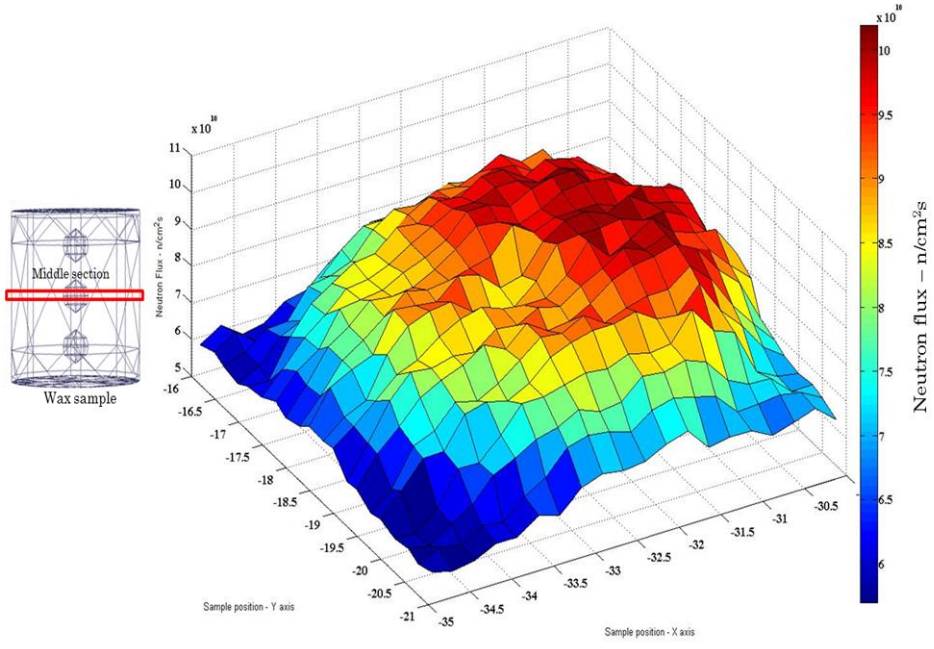

Figure 6-8. MCNP6 simulation of neutron flux (n/cm^{2}s) distribution within wax large sample – Middle section.

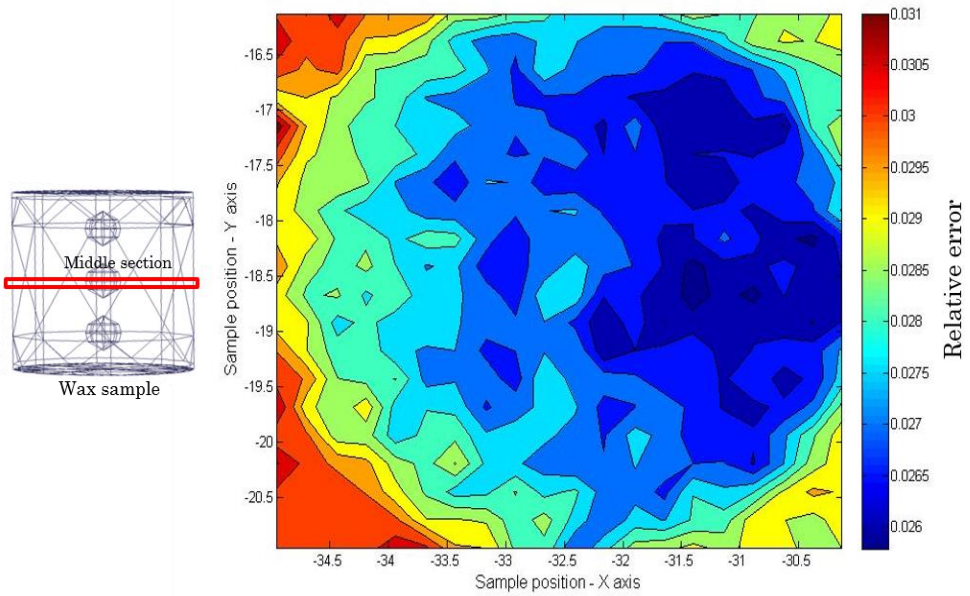

Figure 6-9. MCNP6 simulation of relative error of neutron flux distribution within wax large sample – Middle section.

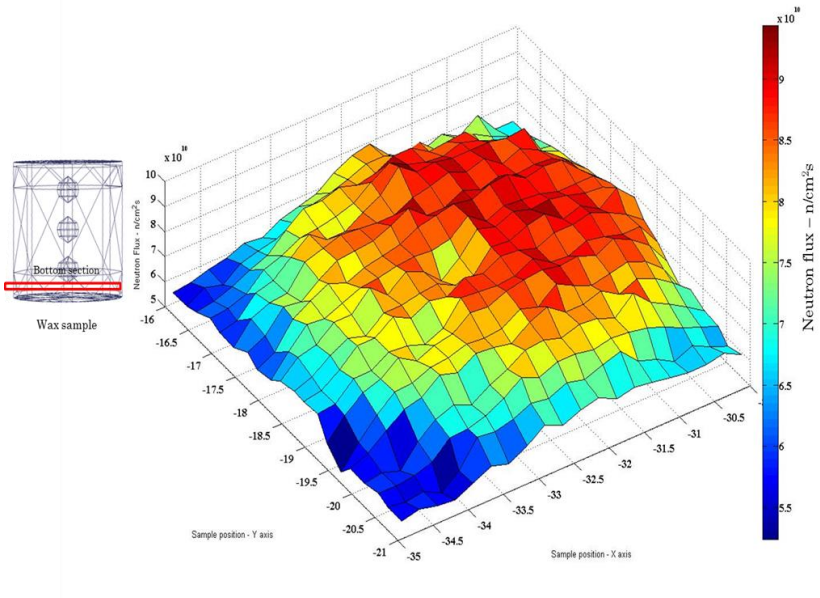

Figure 6-10. MCNP6 simulation of neutron flux (n/cm^{2}s) distribution within wax large sample – Bottom section.

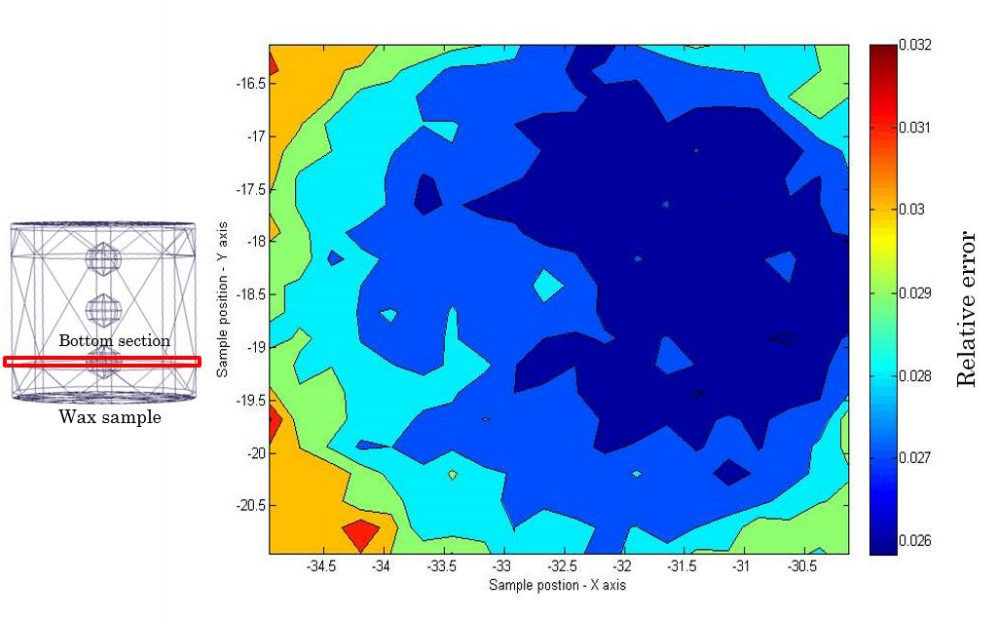

Figure 6-11. MCNP6 simulation of relative error of neutron flux distribution within wax large sample – Bottom section.

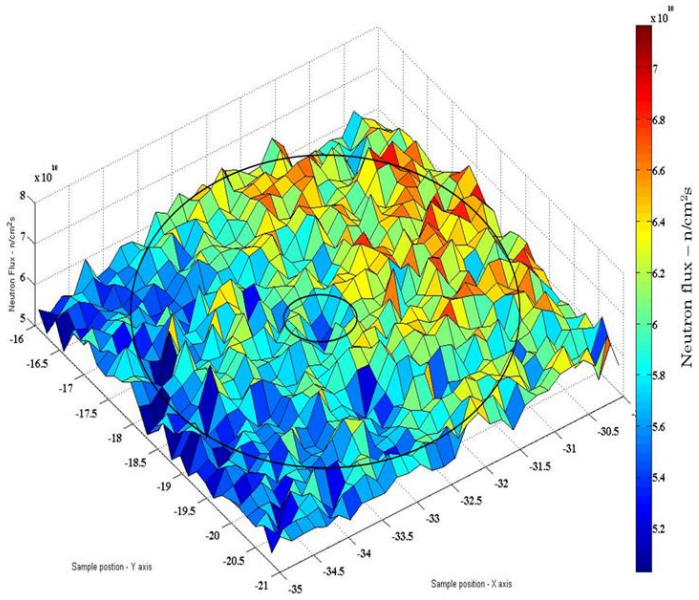

Figure 6-12. MCNP6 simulation of neutron flux (n/cm^{2}s) distribution within flyash large sample – Middle section.

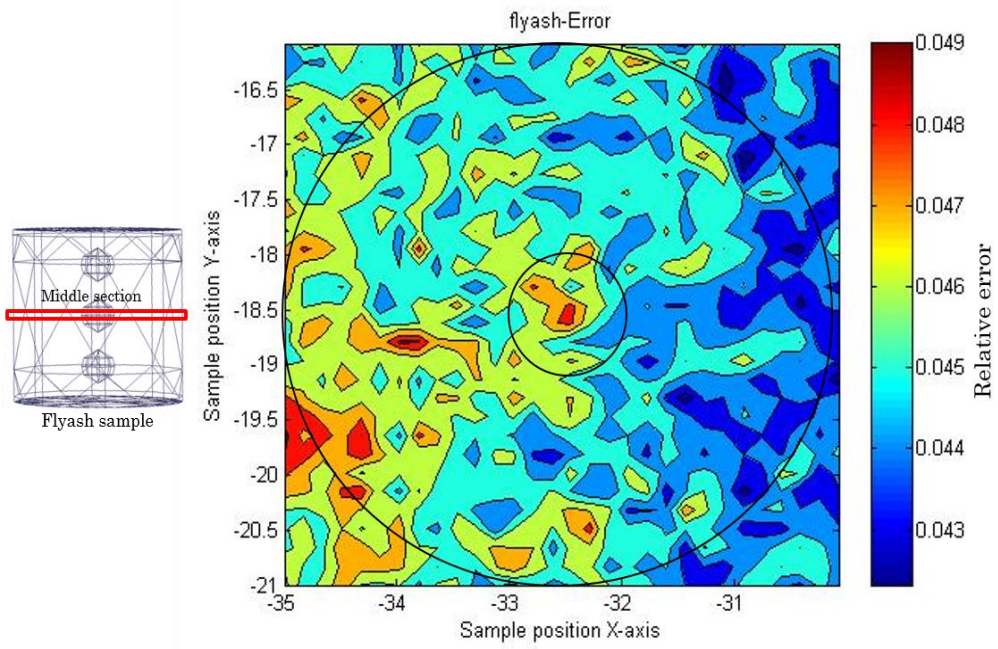

Figure 6-13. MCNP6 simulation of relative error of neutron flux distribution within flyash large sample – Middle section.

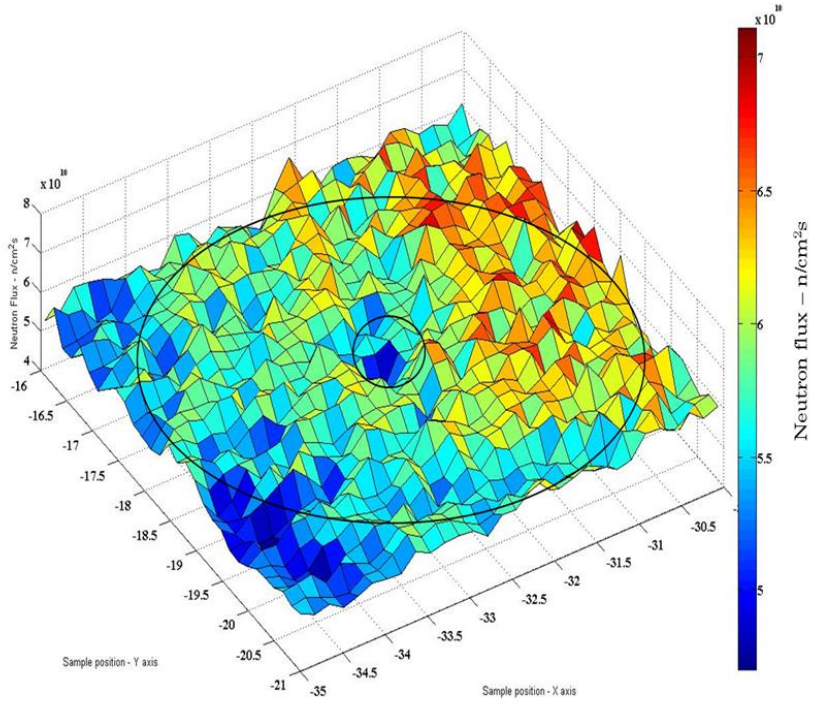

Figure 6-14. MCNP6 simulation of neutron flux (n/cm²s) distribution within Portland cement large sample – Middle section.

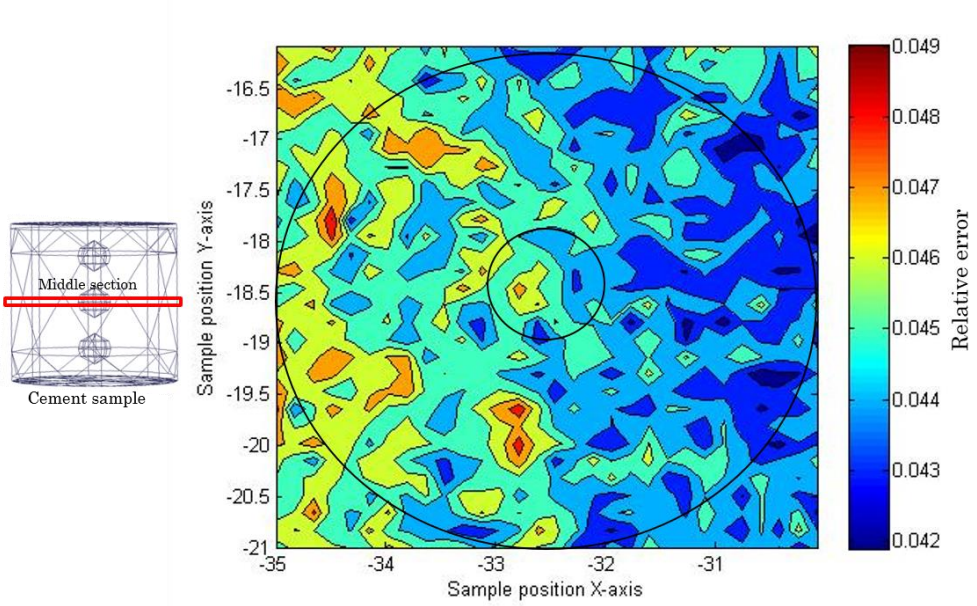

Figure 6-15. MCNP6 simulation of relative error of neutron flux distribution within Portland cement large sample – Middle section.

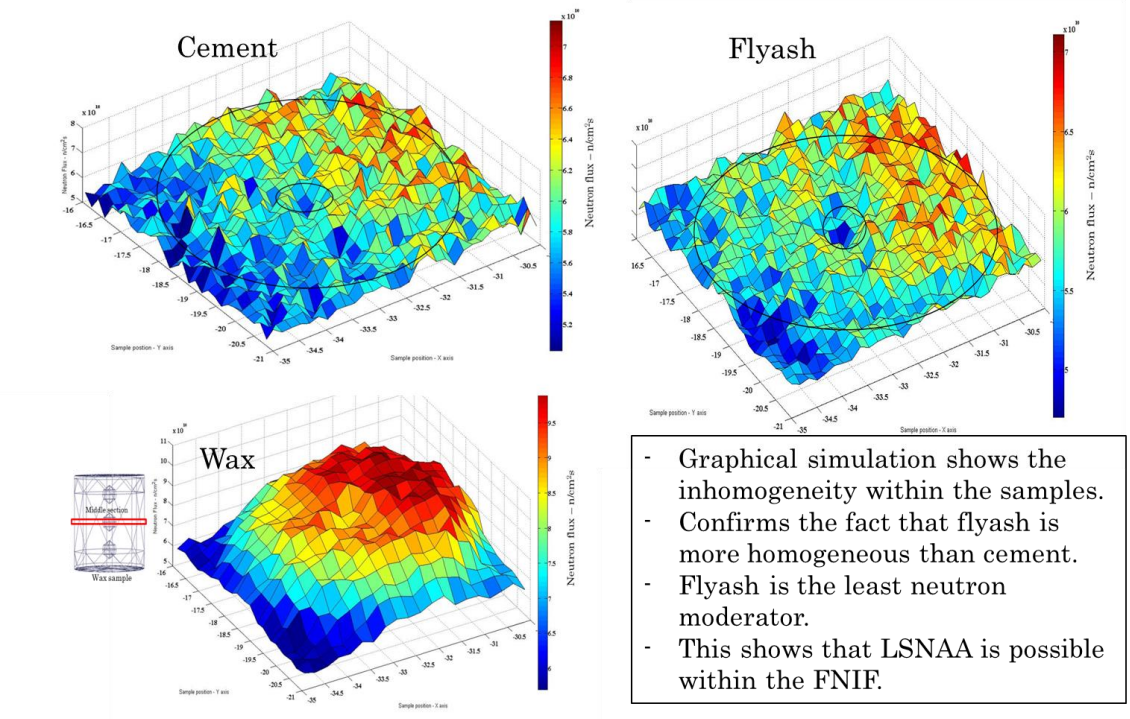

Figure 6-16. MCNP6 simulation of comparison of neutron flux distribution within Portland cement, flyash, and wax.

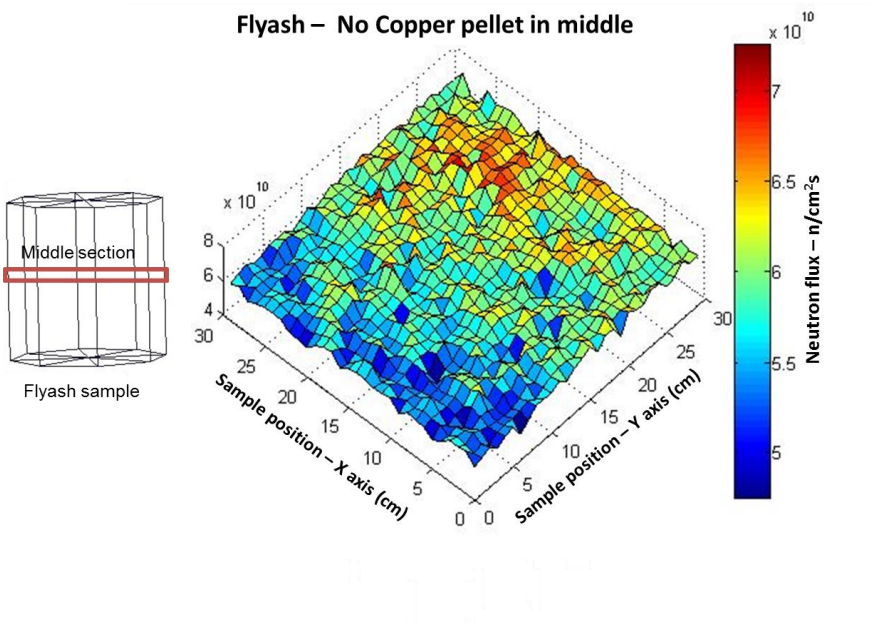

Figure 6-17. MCNP6 simulation of neutron flux distribution within flyash without the copper pellet embedded in the middle.

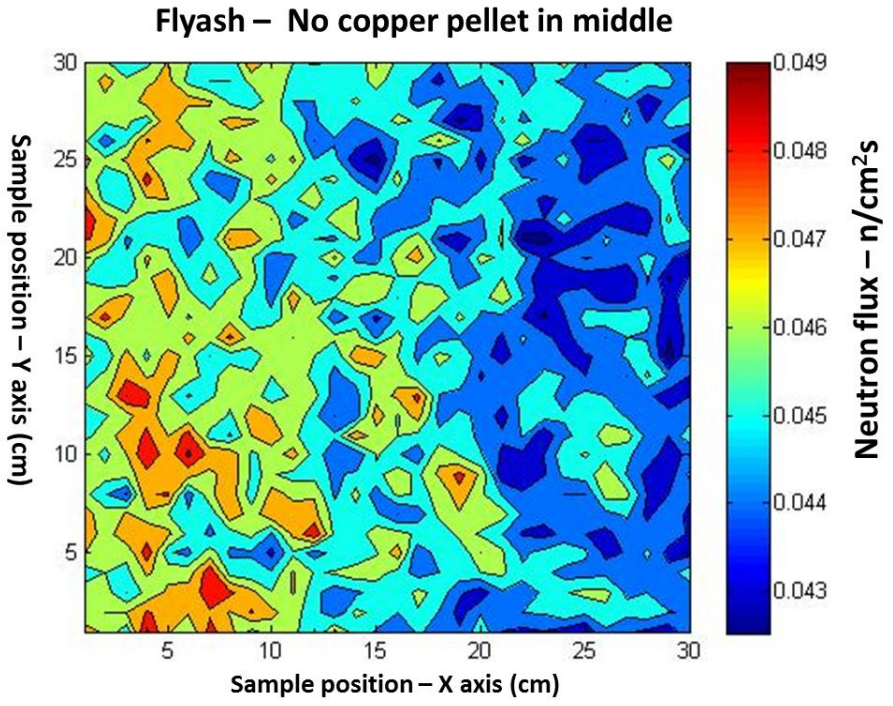

Figure 6-18. MCNP6 simulation of relative error of neutron flux distribution within flyash large sample without the copper pellet embedded in the middle.

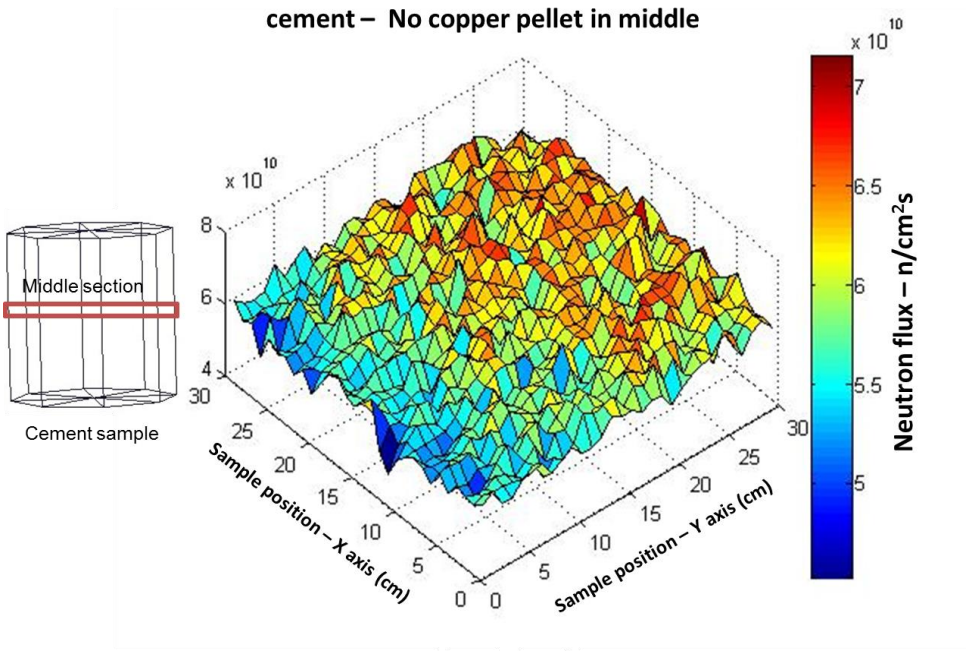

Figure 6-19. MCNP6 simulation of neutron flux distribution within cement without the copper pellet embedded in the middle.

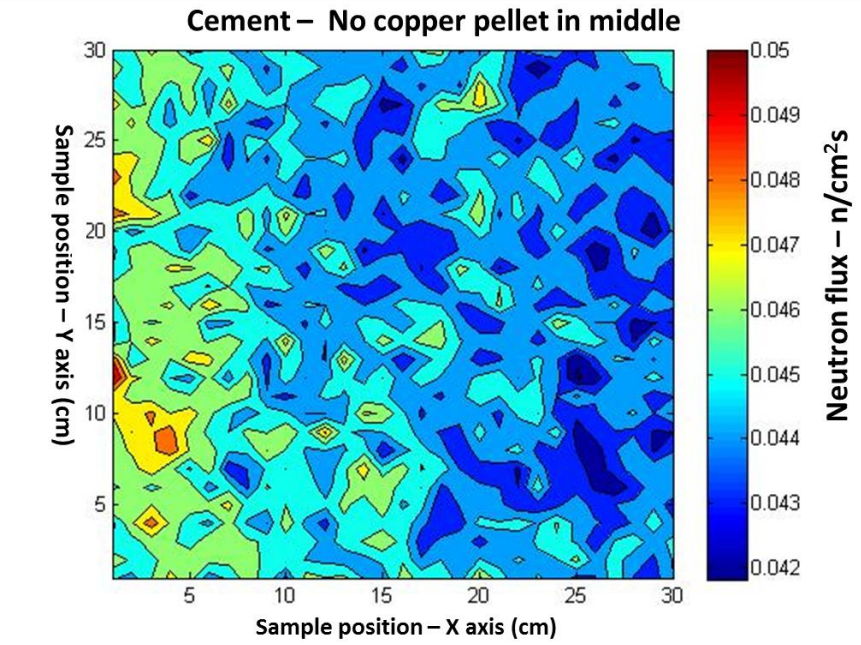

Figure 6-20. MCNP6 simulation of relative error of neutron flux distribution within cement large sample without copper pellet embedded in the middle.

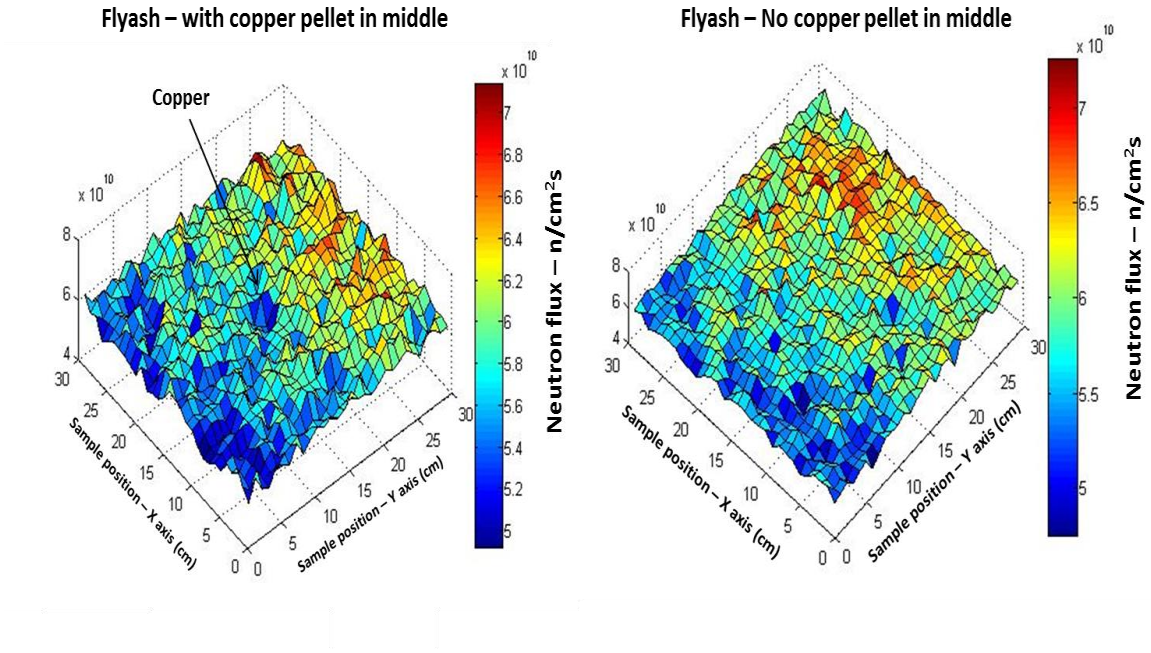

Figure 6-21. MCNP6 simulation of comparison of neutron flux distribution with and without the copper pellet within the middle of flyash sample.

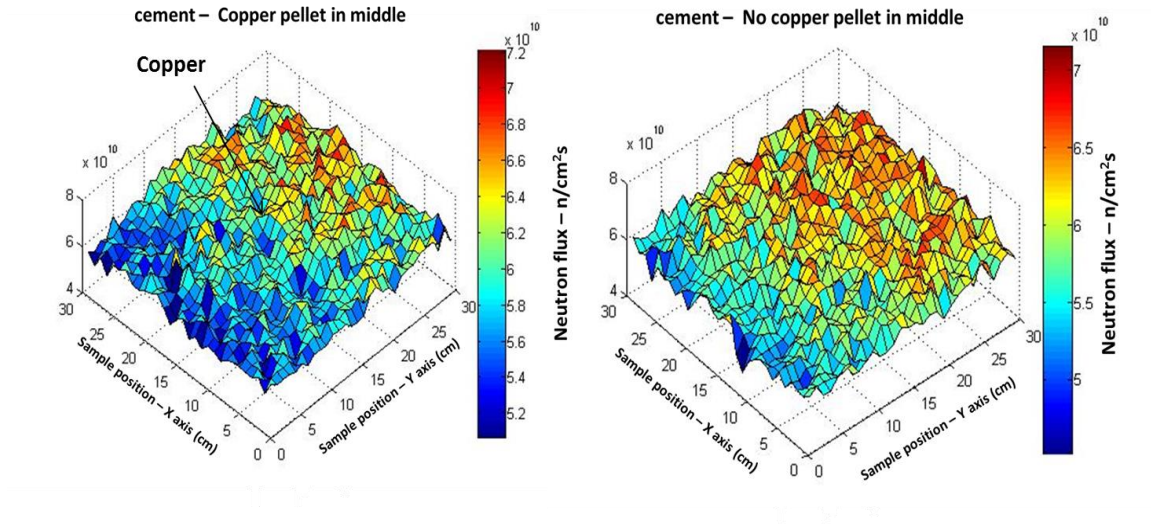

Figure 6-22. MCNP6 simulation of comparison of neutron flux distribution with and without the copper pellet within the middle of cement sample.

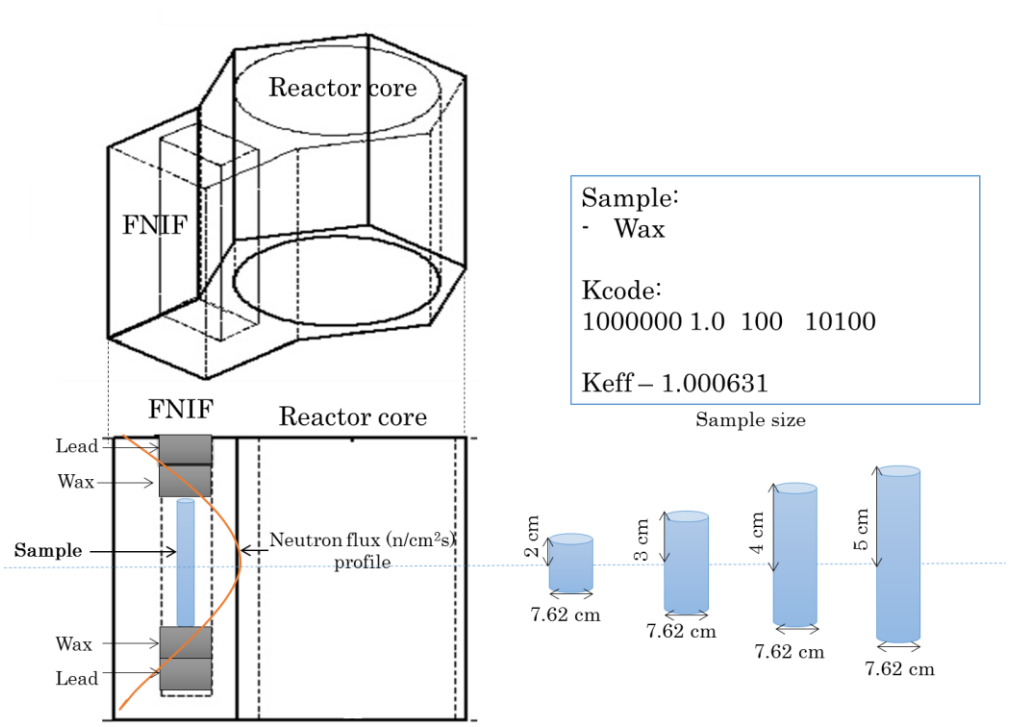

Figure 6-23. Schematic diagram of the UUTR FNIF indicating the (wax) sample location, and (wax) sample size.

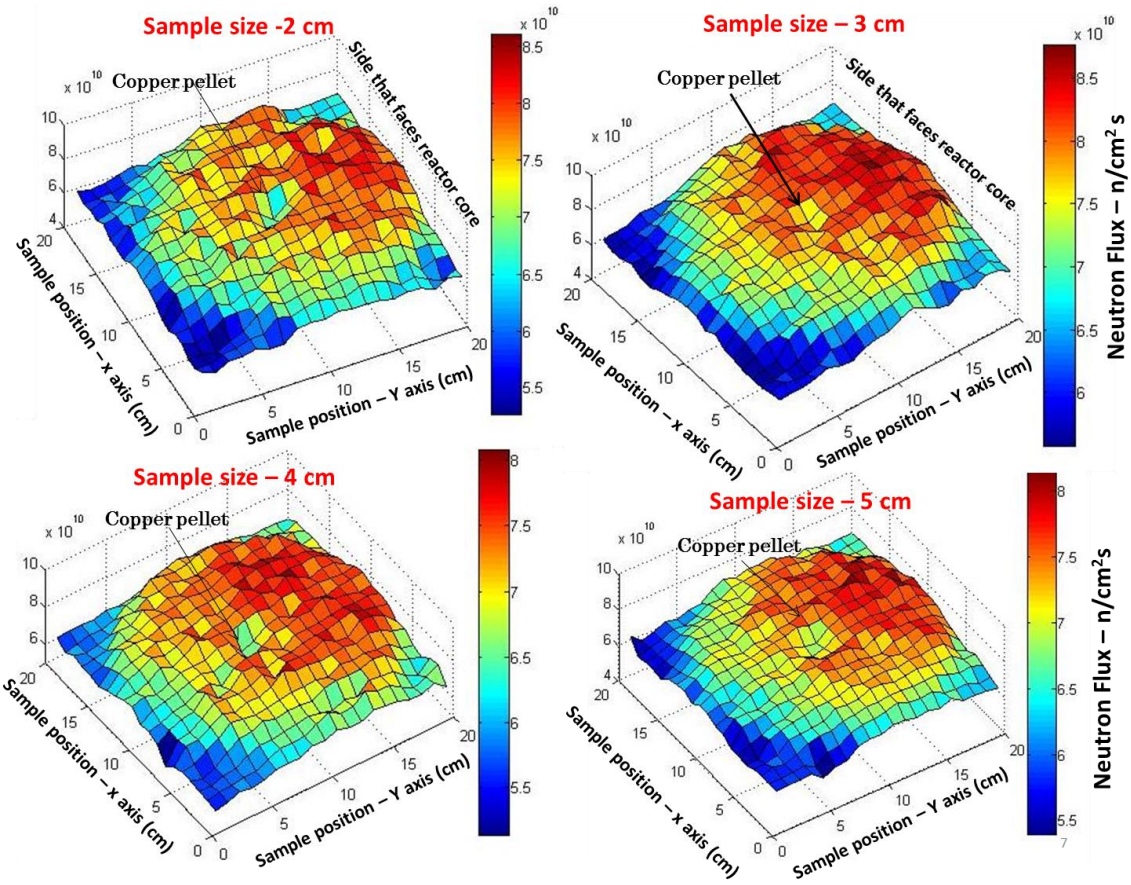

Figure 6-24. Comparison of neutron flux distribution as an effect of sample size within the FNIF – Top section.

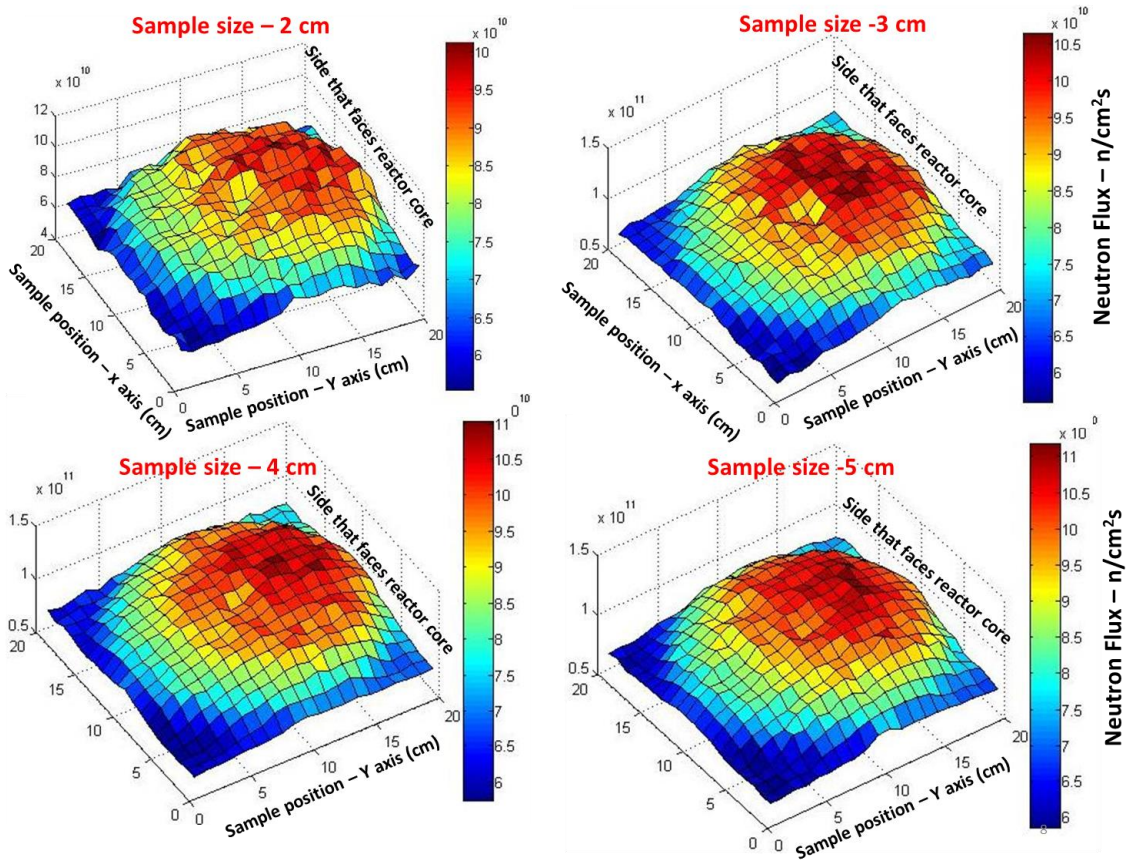

Figure 6-25. Comparison of neutron flux distribution as an effect of sample size within the FNIF – Middle section.

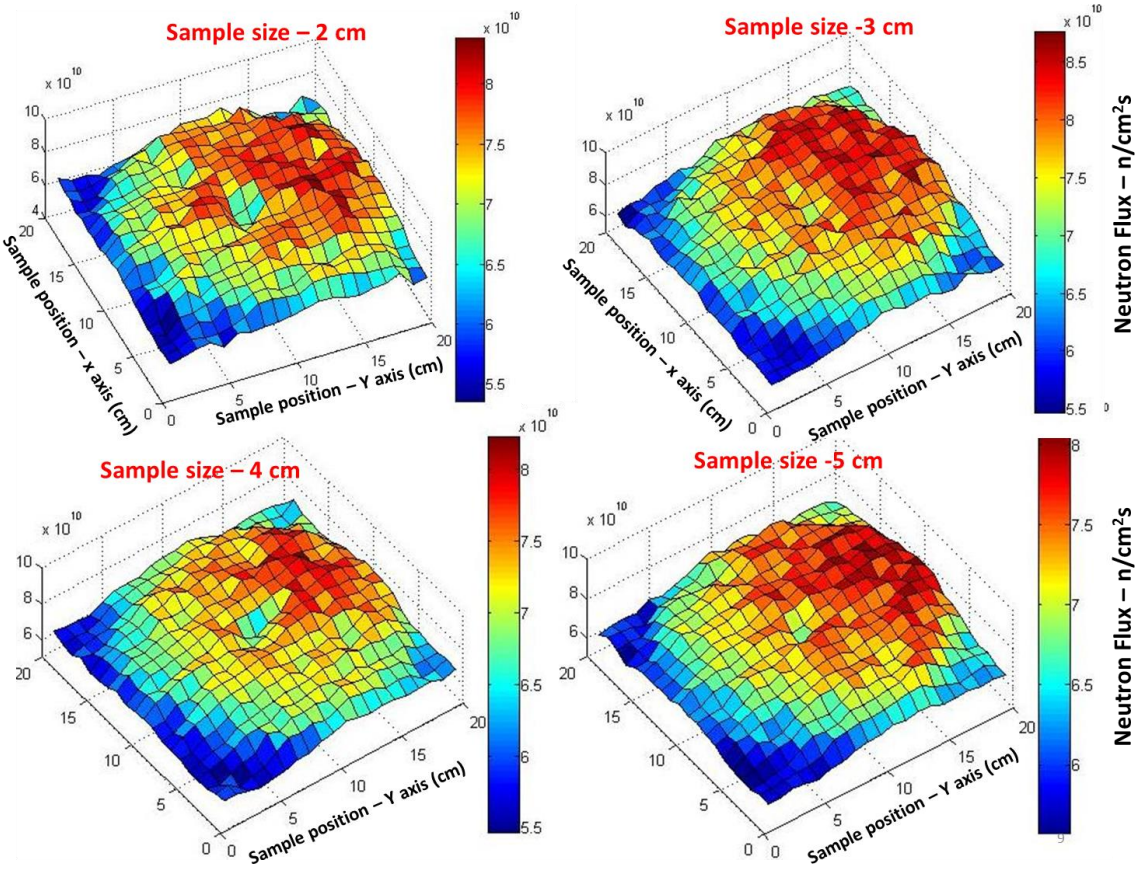

Figure 6-26. Comparison of neutron flux distribution as an effect of sample size within the FNIF – Bottom section.

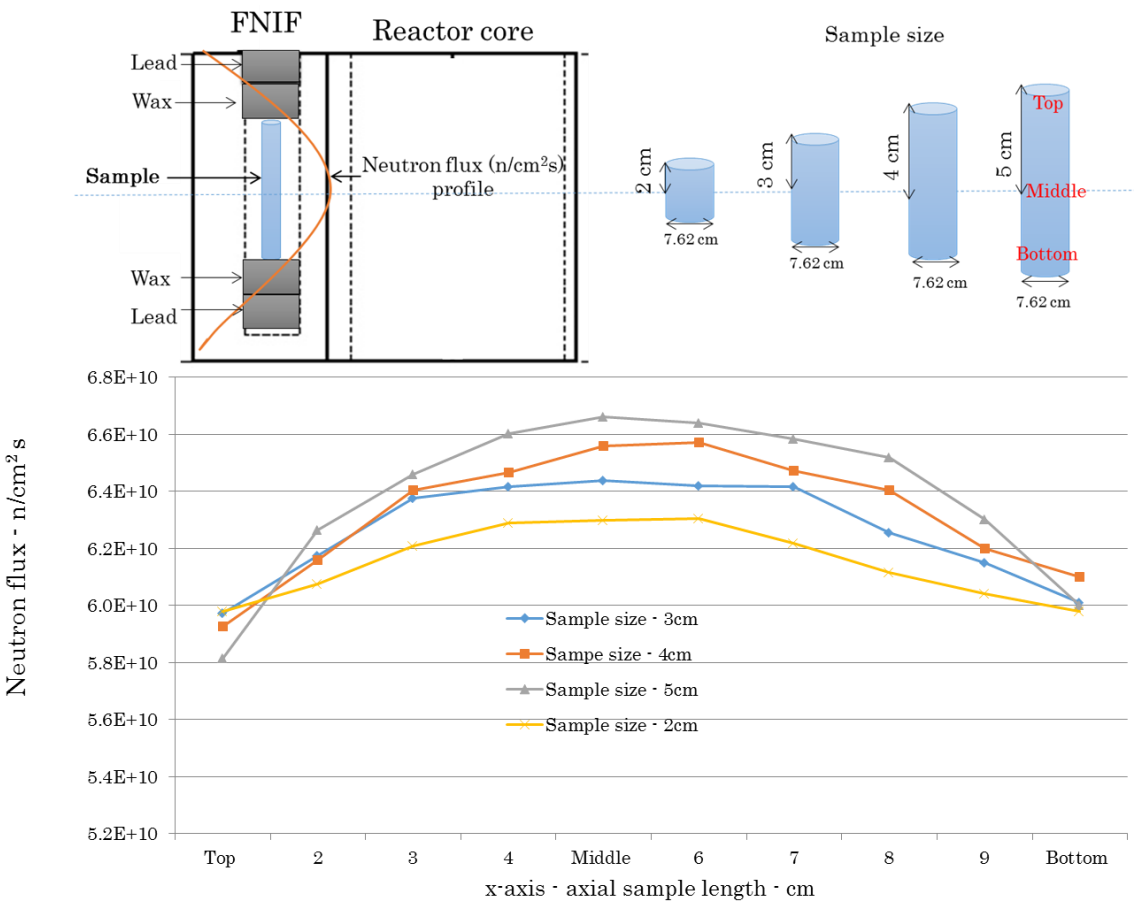

Figure 6-27. Effect of sample size in relation to neutron flux profile as a function of axial sample length.

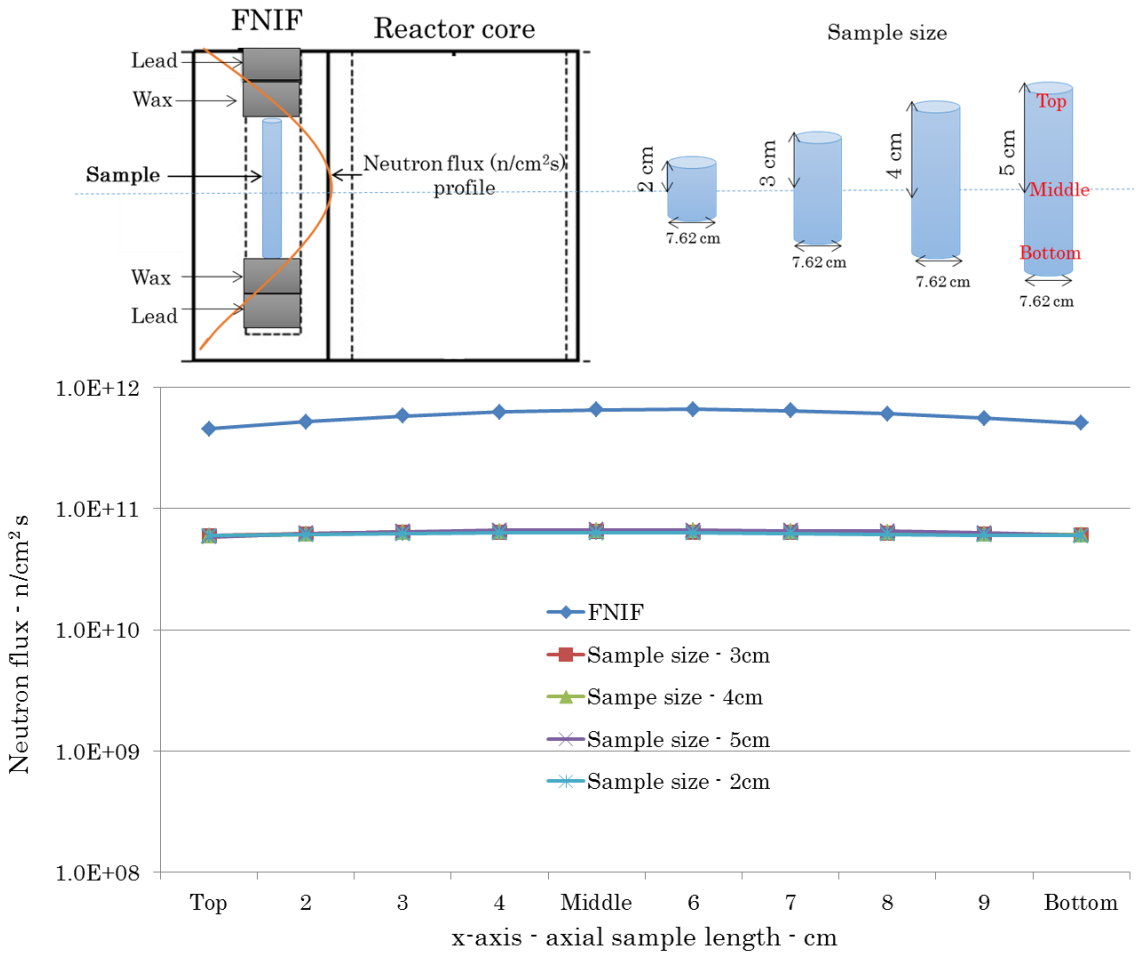

Figure 6-28. Comparison of axial neutron flux profile in FNIF with effect of sample size in relation to neutron flux profile as a function of axial sample length.

CHAPTER 7

CONCLUSION AND FUTURE WORK

7.1. Conclusion

The University of Utah's TRIGA research reactor is among others used for the irradiation of various samples for neutron activation analysis. MCNP6 and GEANT4 Monte Carlo simulation of the research reactor and neutron flux spectra in the irradiation channels have been successfully characterized. This work focused on the neutron flux profile of the irradiation channels within the UUTR, and predictive simulation of neutron activation analysis using the MCNP6 and GEANT4 Monte Carlo codes. Explorative study of the possibility of large sample neutron activation analysis at the UUTR was also studied and explored using Monte Carlo computational approaches. High Precision physics models implemented in GEANT4 to simulate the neutron interactions within various samples include radioactive decay processes. Physics models for the transport of free particle interactions in MCNP6 account for radioactive decay process of the irradiated samples. ENDF/B-VII evaluated cross-sectional data library files were used for both MCNP6 and GEANT4. The neutrons modeled ranged from the low energies of 1 eV to 20 MeV.

The Monte Carlo simulations performed for this study recorded gamma ray detection at the low energies of 1 eV to 3 keV over the MCA energy channels of 1 - 8196, which is a limitation for most HPGe detectors. The gamma ray spectrum for each of the samples obtained from the predictive spectra model simulations are in good agreement with the experimental gamma ray spectra based on the fact that the computational model identifies major elements presents within the experimental sample. Hence, Monte Carlo codes are capable of simulating NAA physics processes and can be used to predict and study gamma ray spectroscopy of NAA samples.

Explorative study of spatial neutron flux distribution within an inhomogeneous wax sample has been presented. The relative computational errors for all simulations were kept well below 5 % which is well within the MCNP error limit of 10 %. All MCNP statistical tests for both the track estimator tally (F4) and the FMESH card were passed. Based on literature, the average neutron source flux needed for adequate large sample irradiation ranges from 10^8 to 10^{12} n/cm^{2}s [51], hence, the explorative study of large sample analysis at the UUTR depicts that there is adequate neutron flux within the FNIF to carry out large sample NAA.

7.2. Recommendations for Future Work

Large sample analysis is taking root in the scientific world and very useful, especially for analysis of archeological artifacts, environmental, and geological samples. This is due to the nondestructive nature of NAA and the fact that large sample analysis provides the ability to analyze the whole sample. However, determination of the exact mass concentrations of elements present within the large sample tends to be very challenging. Hence, some relevant areas that are not well developed and still need further research include but are not limited to:

- The development of algorithms to determine the mass element concentrations within large samples.
- Further experimental research of irregular large samples.
- Development of a graphic user interface or software for large sample analysis that requires little or no experience in computer programming.
- Development of additional larger sample irradiation ports at the UUTR for LSNAA

Thus, comprehensive research and large sample data base analysis will have to be performed to fully understand the impacts and process of large sample neutron activation analysis.

APPENDIX A

MCNP6 INPUT FILE FOR PREDICTIVE GAMMA SPECTRA

TRIGGA 3D Model

```
c New SS Fuel
     100   1   -5.636 -2 11 -12              u=1   imp:n=1 imp:p=0 $Fuel Meat
     101   2   -1.70  -2 12 -14              u=1   imp:n=1 imp:p=0 $Up Graphite
     102   2   -1.70  -2 13 -11              u=1   imp:n=1 imp:p=0$Down
     Graphite
     103   3   -7.92  (-1 15 -16) (2:-13:14)   u=1   imp:n=1 imp:p=0 $Cladding
     104   4   -1.0   1:-15:16 92 -93         u=1   imp:n=1 imp:p=0 $H2O
     c Old SS Fuel
     110 like 100 but mat=12 rho=-5.636       u=2   imp:n=1 imp:p=0 $Fuel
     Meat
111 like 101 but                    u=2   imp:n=1 imp:p=0 $Up Graphite
     112 like 102 but                    u=2   imp:n=1 imp:p=0 $Down
     Graphite
     113 like 103 but                    u=2   imp:n=1 imp:p=0 $Cladding
     114 like 104 but                    u=2   imp:n=1 imp:p=0 $H2O
     c Al Fuel
     120   5   -6.143 -3 21 -22              u=3   imp:n=1 imp:p=0 $Fuel Meat
     121   2   -1.70  -3 22 -24              u=3   imp:n=1 imp:p=0 $Up Graphite
     122   2   -1.70  -3 23 -21              u=3   imp:n=1 imp:p=0 $Down
     Graphite
```

123 6 -2.70 (-1 25 -26) (3:-23:24) u=3 imp:n=1 imp:p=0 $Cladding

124 4 -1.0 1:-25:26 92 -93 u=3 imp:n=1 imp:p=0 $H2O

c Instrumental Fuel

130 like 110 but u=4 imp:n=1 imp:p=0 $Fuel Meat

131 like 111 but u=4 imp:n=1 imp:p=0 $Up Graphite

132 like 112 but u=4 imp:n=1 imp:p=0 $Down Graphite

133 like 113 but u=4 imp:n=1 imp:p=0 $Cladding

134 like 114 but u=4 imp:n=1 imp:p=0 $H2O

c Graphite

140 2 -1.70 -3 23 -24 u=6 imp:n=1 imp:p=0 $Graphite

143 like 123 but u=6 imp:n=1 imp:p=0 $Cladding

144 like 124 but u=6 imp:n=1 imp:p=0 $H2O

c Heavy Water

150 7 -1.056 -3 23 -24 u=7 imp:n=1 imp:p=0 $D2O

153 like 123 but u=7 imp:n=1 imp:p=0 $Cladding

154 like 124 but u=7 imp:n=1 imp:p=0 $H2O

c Water

160 4 -1.0 -1 92 -93 u=8 imp:n=1 imp:p=0 $H2O

161 4 -1.0 1 92 -93 u=8 imp:n=1 imp:p=0 $H2O

c Safety Control Rod

170 9 -2.52 -46 11 -93 u=10 imp:n=1 imp:p=0 $B4C

171 6 -2.7 46 -47 11 -93 u=10 imp:n=1 imp:p=0 $Al Cladding

172 4 -1.0 (47 -50 11 -93):(-50 -11 92) u=10 imp:n=1 imp:p=0 $H2O

173 6 -2.7 50 -1 92 -93 u=10 imp:n=1 imp:p=0 $Al Tube

174 4 -1.0 1 92 -93 u=10 imp:n=1 imp:p=0 $H2O

```
c Shim Control Rod
180   9   -2.52   -46 11 -93            u=11  imp:n=1 imp:p=0 $B4C
181   6   -2.7     46 -47 11 -93         u=11  imp:n=1 imp:p=0 $Al Cladding
182   4   -1.0    (47 -50 11 -93):(-50 -11 92)  u=11  imp:n=1 imp:p=0
$H2O
183   6   -2.7     50 -1 92 -93          u=11  imp:n=1 imp:p=0 $Al Tube
184   4   -1.0     1 92 -93             u=11  imp:n=1 imp:p=0 $H2O
c Reg Control Rod
190   9   -2.52   -48 11 -93            u=12  imp:n=1 imp:p=0 $B4C
191   6   -2.7     48 -49 11 -93         u=12  imp:n=1 imp:p=0 $Al Cladding
192   4   -1.0    (49 -50 11 -93):(-50 -11 92)  u=12  imp:n=1 imp:p=0
$H2O
193   6   -2.7     50 -1 92 -93          u=12  imp:n=1 imp:p=0 $Al Tube
194   4   -1.0     1 92 -93             u=12  imp:n=1 imp:p=0 $H2O
c Empty Control Rod
196   4   -1.0    -50 92 -93            u=5   imp:n=1 imp:p=0 $H2O
197   6   -2.7     50 -1 92 -93          u=5   imp:n=1 imp:p=0 $Al Tube
198   4   -1.0     1 92 -93             u=5   imp:n=1 imp:p=0 $H2O
c Brand New SS Fuel, more U235
c 310 like 100 but mat=5  rho=-5.781       u=15   imp:n=1 imp:p=0
$Fuel Meat
c 311 like 101 but                         u=15   imp:n=1 imp:p=0 $Up
Graphite
c 312 like 102 but                         u=15   imp:n=1 imp:p=0 $Down
Graphite
c 313 like 103 but                         u=15   imp:n=1 imp:p=0 $Cladding
c 314 like 104 but                         u=15   imp:n=1 imp:p=0 $H2O
c Lattice
```

```
200   4   -1.0   -101 102 -103 104 -105 106 92 -93    lat=2    u=9
               fill=-7:7 -7:7 0:0
               0 0 0 0 0 0 0 9 9 9 9 9 9 9 9
                0 0 0 0 0 0 9 8 7 8 7 8 7 8 9
                 0 0 0 0 0 9 3 2 3 1 1 3 2 7 9
                  0 0 0 0 9 1 3 1 1 1 1 3 3 8 9
                   0 0 0 9 1 1 3 1 3 1 5 3 3 7 9
                    0 0 9 3 1 1 4 1 2 2 1 2 3 7 9
                     0 9 3 3 1 3 2 2 2 4 2 3 3 7 9
                      9 8 7 2 5 1 1 5 1 1 8 3 1 6 9
                       9 8 7 1 2 2 1 1 1 2 1 3 6 9 0
                        9 8 7 1 3 8 2 2 1 3 1 6 9 0 0
                         9 8 7 1 1 2 2 5 3 3 6 9 0 0 0
                          9 8 7 8 1 1 1 1 1 6 9 0 0 0 0
                           9 8 6 6 6 6 6 6 6 9 0 0 0 0 0
                            9 8 8 8 8 8 8 8 9 0 0 0 0 0 0
                             9 9 9 9 9 9 9 9 0 0 0 0 0 0 0 imp:n=1 imp:p=0
201   4   -1.0   -111 112 -113 114 -115 116 92 -93  fill=9  imp:n=1
imp:p=0 $Lattices

202   6   -2.7   (-121 122 -123 124 -125 126) 91 -94
              (111:-112:113:-114:115:-116)              imp:n=1 imp:p=0
$Al Wall

203   6   -2.7   -111 112 -113 114 -115 116 91 -92          imp:n=1 imp:p=0
$Lower Al Plate

204   6   -2.7   -111 112 -113 114 -115 116 93 -94 41 43 45 imp:n=1
imp:p=0      $Upper Al Plate

206   4   -1.0   -131 94 -97 41 43 45 imp:n=1 imp:p=0              $Top
Water
```

```
207   4   -1.0   -131 96 -91                          imp:n=1 imp:p=0
$Bottom Water

208   10  -2.30  -131 -96 95                          imp:n=1 imp:p=0
$Bottom Concrete

301   9   -2.52  -40 93 -97      imp:n=1 imp:p=0 $Safety Rod above core
region

302   6   -2.7    40 -41 93 -97  imp:n=1 imp:p=0

303   9   -2.52  -42 93 -97      imp:n=1 imp:p=0 $Shim Rod above core
region

304   6   -2.7    42 -43 93 -97  imp:n=1 imp:p=0

305   9   -2.52  -44 93 -97      imp:n=1 imp:p=0 $Reg Rod above core
region

306   6   -2.7    44 -45 93 -97  imp:n=1 imp:p=0

c FNIF

400   11  -0.00115   -141 #402 #403 #410 #404 imp:n=1 imp:p=1 $ FNIF
Air

401   8  -11.34  -140 141  imp:n=1 imp:p=1 $ FNIF Pb

410   14   -8.96   -240  imp:n=1 imp:p=1

402   15   -0.94  -142 143 -144 #410 #403 #404 imp:n=1 imp:p=1

403   14   -8.96   -241  imp:n=1 imp:p=1

404   14   -8.96   -242  imp:n=1 imp:p=1

c Heavy water block

500   11  -0.00115   -159 160 -161 imp:n=1 imp:p=0 $ Heavy water Air

501   6   -2.7   159 -158 160 -161 imp:n=1 imp:p=0

502   7   -1.056 158 154 -155 156 157 160 -161  imp:n=1 imp:p=0

503   6   -2.7   (-154:155:-156:-157)
                150 -151 152 153 160 -161    imp:n=1 imp:p=0

c

900   4   -1.0   -131 91 -94 140
```

(-150:151:-152:-153:-160:161)

(121:-122:123:-124:125:-126) imp:n=1 imp:p=0
$Water Arround Core

999 0 131:-95:97 imp:n=0 imp:p=0

C Surface Cards

1 cz 1.873 $Outer Radius

2 cz 1.82 $Inner Radius

3 cz 1.79 $Inner Radius for Aluminum Container

11 pz -19.05 $SS Fuel Meat Bottom (7.5 inch * 2)

12 pz 19.05 $SS Fuel Meat Top

13 pz -29.21 $SS Fuel Graphite Bottom (4 inch)

14 pz 29.21 $SS Fuel Graphite Top

15 pz -30.39 $SS Cladding Bottom (1.18 cm)

16 pz 30.39 $SS Cladding Top (1.18 cm)

21 pz -17.78 $Al Fuel Meat Bottom (7 inch * 2)

22 pz 17.78 $Al Fuel Meat Top

23 pz -27.94 $Al Fuel Graphite Bottom (4 inch)

24 pz 27.94 $Al Fuel Graphite Top

25 pz -29.12 $Al Cladding Bottom (1.18 cm)

26 pz 29.12 $Al Cladding Top (1.18 cm)

40 c/z 6.555 -11.354 1.00 $Safety Control Rod

41 c/z 6.555 -11.354 1.11 $Safety Control Rod Cladding

42 c/z -13.11 0.0 1.00 $Shim Control Rod

43 c/z -13.11 0.0 1.11 $Shim Control Rod Cladding

44 c/z 6.555 11.354 0.200 $Reg Control Rod

45 c/z 6.555 11.354 0.318 $Reg Control Rod Cladding

```
46    cz     1.00   $ Safety and Shim Rod in Unit
47    cz     1.11   $ Safety and Shim Rod in Unit Cladding
48    cz     0.200  $ Reg Rod in Unit
49    cz     0.318  $ Reg Rod in Unit Cladding
50    cz     1.750  $ Inner radius of Al tube for control rod
91    pz   -33.43   $Lower Plate Bottom
92    pz   -30.89   $Lower Plate Top (1 inch)
93    pz    30.89   $Upper Plate Bottom
94    pz    32.79   $Upper Plate Top (0.75 inch)
95    pz   -55.0    $Concrete Bottom
96    pz   -43.09   $Water Bottom (2 inch)
97    pz    50.0    $Water Top
C Lattice Cells
101   px    2.185
102   px   -2.185
103   p     0.5   0.8660254  0   2.185
104   p     0.5   0.8660254  0  -2.185
105   p    -0.5   0.8660254  0   2.185
106   p    -0.5   0.8660254  0  -2.185
c Frame Boundary
111   p     1.732038    1   0    50.460
112   p     1.732038    1   0   -50.460
113   p     1.732038   -1   0    50.460
114   p     1.732038   -1   0   -50.460
115   py   25.230
116   py  -25.230
```

```
c Al Wall
121   p     1.732038    1   0    54.270
122   p     1.732038    1   0   -54.270
123   p     1.732038   -1   0    54.270
124   p     1.732038   -1   0   -54.270
125   py   27.135
126   py  -27.135
C Reflector Surfaces
131   cz   65.0       $ Water reflector
c 131   p     1.732038    1    0  83.259682
c 132   p     1.732038    1    0 -83.259682
c 133   p     1.732038   -1    0  83.259682
c 134   p     1.732038   -1    0 -83.259682
c 135   py   41.629841
c 136   py  -41.629841
c FNIF
140   BOX -15.88 -26.77 -30.48   -15.24 26.40 0  -22.00 -12.7 0    0 0
60.96
141   BOX -22.82 -24.91 -30.48   -10.16 17.60 0   -8.80  -5.1 0    0 0 60.96
c Concrete cube
142   pz   2.54
143   pz   -2.54
144   c/z  -32.54 -18.54 2.54
c 145   px  -35.08
c 146   py  -16.00
c 147   py  -21.08
240   S   -32.54 -18.54 0 0.25
```

```
241   S   -32.54 -18.54 1.8 0.25
242   S   -32.54 -18.54 -1.8 0.25
c Heavy water beside core
150   p     1.732038    1   0    54.270  $ Al outer
151   p     1.732038    1   0    84.670
152   py    0.0
153   p     1.732038   -1   0     0.0
154   p     1.732038    1   0    54.670  $ Al outer
155   p     1.732038    1   0    84.270
156   py    0.2
157   p     1.732038   -1   0     0.4
158   c/z   30.08 17.37 5.7  $ Air tub Al wall
159   c/z   30.08 17.37 5.5  $ Air tub
160   pz   -30.0           $ Heavy water top
161   pz    30.0           $ Heavy water bottom
201 pz -18.5
202 pz -17.5
203 pz -16.5
204 pz -15.5
205 pz -14.5
206 pz -13.5
207 pz -12.5
208 pz -11.5
209 pz -10.5
210 pz -9.5
211 pz -8.5
```

212 pz -7.5

213 pz -6.5

214 pz -5.5

215 pz -4.5

216 pz -3.5

217 pz -2.5

218 pz -1.5

219 pz -0.5

220 pz 0.5

221 pz 1.5

222 pz 2.5

223 pz 3.5

224 pz 4.5

225 pz 5.5

226 pz 6.5

227 pz 7.5

228 pz 8.5

229 pz 9.5

230 pz 10.5

231 pz 11.5

232 pz 12.5

233 pz 13.5

234 pz 14.5

235 pz 15.5

236 pz 16.5

237 pz 17.5

```
238 pz 18.5


mode n p
SSW      142 -143 -144 (402)  CEL 100 110 120 130 PTY=n
kcode 1000000 1.0 100 1100
ksrc   -15.2950   -18.9227     0.0000
      -10.9250   -18.9227     0.0000
       -6.5550   -18.9227     0.0000
       -2.1850   -18.9227     0.0000
        2.1850   -18.9227     0.0000
        6.5550   -18.9227     0.0000
       10.9250   -18.9227     0.0000
      -17.4800   -15.1381     0.0000
      -13.1100   -15.1381     0.0000
       -8.7400   -15.1381     0.0000
       -4.3700   -15.1381     0.0000
        0.0000   -15.1381     0.0000
        4.3700   -15.1381     0.0000
        8.7400   -15.1381     0.0000
       13.1100   -15.1381     0.0000
      -19.6650   -11.3536     0.0000
      -15.2950   -11.3536     0.0000
      -10.9250   -11.3536     0.0000
       -6.5550   -11.3536     0.0000
       -2.1850   -11.3536     0.0000
        2.1850   -11.3536     0.0000
```

10.9250	-11.3536	0.0000
15.2950	-11.3536	0.0000
-21.8500	-7.5691	0.0000
-17.4800	-7.5691	0.0000
-13.1100	-7.5691	0.0000
-8.7400	-7.5691	0.0000
-4.3700	-7.5691	0.0000
0.0000	-7.5691	0.0000
4.3700	-7.5691	0.0000
8.7400	-7.5691	0.0000
13.1100	-7.5691	0.0000
17.4800	-7.5691	0.0000
-24.0350	-3.7845	0.0000
-19.6650	-3.7845	0.0000
-15.2950	-3.7845	0.0000
-10.9250	-3.7845	0.0000
-6.5550	-3.7845	0.0000
-2.1850	-3.7845	0.0000
2.1850	-3.7845	0.0000
6.5550	-3.7845	0.0000
10.9250	-3.7845	0.0000
15.2950	-3.7845	0.0000
19.6650	-3.7845	0.0000
-17.4800	0.0000	0.0000
-8.7400	0.0000	0.0000
-4.3700	0.0000	0.0000

4.3700	0.0000	0.0000
8.7400	0.0000	0.0000
17.4800	0.0000	0.0000
21.8500	0.0000	0.0000
-15.2950	3.7845	0.0000
-10.9250	3.7845	0.0000
-6.5550	3.7845	0.0000
-2.1850	3.7845	0.0000
2.1850	3.7845	0.0000
6.5550	3.7845	0.0000
10.9250	3.7845	0.0000
15.2950	3.7845	0.0000
19.6650	3.7845	0.0000
-13.1100	7.5691	0.0000
-8.7400	7.5691	0.0000
0.0000	7.5691	0.0000
4.3700	7.5691	0.0000
8.7400	7.5691	0.0000
13.1100	7.5691	0.0000
17.4800	7.5691	0.0000
-10.9250	11.3536	0.0000
-6.5550	11.3536	0.0000
-2.1850	11.3536	0.0000
2.1850	11.3536	0.0000
10.9250	11.3536	0.0000
15.2950	11.3536	0.0000

```
      -4.3700    15.1381     0.0000
       0.0000    15.1381     0.0000
       4.3700    15.1381     0.0000
       8.7400    15.1381     0.0000
      13.1100    15.1381     0.0000
m1     1001.66c    -0.015896   $ new SS meat, H/Zr=1.6. 0.59% burn-up
     40000.66c    -0.899104
     92235.66c    -0.016728
     92238.66c    -0.068272
mt1    h/zr.60t
      zr/h.60t
m2     6000.66c     1.0        $ graphite
mt2    grph.60t
m3     6000.66c    -0.0004     $ ss cladding
     14000.60c    -0.0046
     24000.50c    -0.190
     25055.66c    -0.009
     26000.50c    -0.699
     28000.50c    -0.097
m4     1001.66c     2.0        $ H2O
      8016.66c     1.0
mt4    lwtr.60t
m5     1001.66c    -0.010   $ Al meat, H/Zr=1.0, 8.91% burnup
     40000.66c    -0.905
     92235.66c    -0.01533
     92238.66c    -0.06967
```

```
mt5    h/zr.60t
       zr/h.60t
m6    13027.66c     1.0        $ Al
m7     1001.66c     0.64       $ D20 (68% atom)
       1002.66c     1.36
       8016.66c     1.00
mt7    lwtr.60t
       hwtr.60t
m8    82000.50c     1.0        $ Pb
m9     5010.66c    -0.1566     $ b4c
       5011.66c    -0.6264
       6000.66c    -0.217
m10    1001.66c    -0.00619    $ Concrete
       6000.66c    -0.17520
       8016.66c    -0.41020
      11023.66c    -0.00027
      12000.66c    -0.03265
      13027.66c    -0.01083
      14000.60c    -0.03448
      19000.66c    -0.00114
      20000.66c    -0.32130
      26000.50c    -0.00778
m11    7014.66c     0.0000381259 $Air
       8016.66c     0.0000095012
      18000.59c     0.0000001664
m12    1001.66c    -0.015896   $ Old SS meat, H/Zr=1.6, 8.77% burnup
```

```
     40000.66c    -0.899104
     92235.66c    -0.015354
     92238.66c    -0.069646
mt12   h/zr.60t
      zr/h.60t
c ################################
c CONCRETE CUBE MATERIAL
c ################################
 m13    21045.70c  -0.0000017132
      51123.70c  -0.0000008072
      56130.70c  -0.0001308765
      55133.70c  -0.0000007725
      57139.70c  -0.0000088666
      58140.70c  -0.0000240198
      62152.70c  -0.0000010743
      63151.66c  -0.0000000501
      64153.70c  -0.0000046425
      65159.70c  -0.0000002731
      72180.70c  -0.0000000607
      14000.60c  -0.034316367
      19000.66c  -0.00113459
      20000.66c  -0.319775191
      26000.50c  -0.007743078
C Copper Cu-63 Naturally occuring isotope (rho = 8.96 g/cc)
M14   29063     -1.0
M15   1001.66c -0.143711        $polyethylene - density 0.94
```

```
      8016.66c -0.856289
M16   6000.70c   -0.986487598872   $ flyash - rho - 2.3 g/cc
      33074.70c  -0.00154
      25055.70c  -0.00241
      11023.70c  -0.00894
      56137.70c  -0.00056232
      57138.70c  -0.0000306
      80200.70c  -0.000002950168
      38090.70c  -0.000025143
      63152.70c  -0.00000039196
      58140.70c  -0.00000015
      66162.70c  -0.000000846
c act nonfiss = p dg = lines
c F74:p 402
c E74 1e-6 8192i 3
c T74 1e6 1e18 T
F14:n 402
FM14 7.5461e15
F24:n 410
FM24 7.5461e15
FMESH84:n GEOM=rec ORIGIN=-35.08 -21.08 -2.54
         IMESH=-30.00 IINTS=30
         JMESH=-16.00 JINTS=30
         KMESH=2.54   KINTS=30
         EMESH=2.5E-8 6.25E-7 0.1 10 EINTS=1 1 1 1 OUT=ij
```

APPENDIX B

MCNP6 ACTIVATION FILE

LaBr3 detector simulation

```
C  ***SECTION 1. CELL DEFINITION*********************************
10    2  -8.90    -1                imp:n=1 imp:p=1 $ sample
20    1  -0.00115  -10 -30 20 #10     imp:n=1 imp:p=1 $ Ti air space
30    1  -0.00115  60 -70 40 -50 20 -30 #10 #20 imp:n=1 imp:p=1
90    0           -60:70:-40:50:-20:30 imp:n=0 imp:p=0

C  ***SECTION 2. SURFACE
SPECIFICATION**************************
C
1   so  1
10  cz  5.5
20  pz  -30.0
30  pz   30.0
40  py  -15.24
50  py   15.24
60  px  -8.04
70  px   8.04

C  ******SECTION 4. MATERIAL DEFINITIONS************************
```

```
C
C    AIR NEAR SEA LEVEL (dry, rho=0.00115 g/cc)
M1   7014.50c  -0.742     $N
     8016.50c  -0.246     $O
C
C    Cobalt-59 (rho=8.90 g/cc)
M2   27059.70c -1.0
C
C  ******SECTION 5 SOURCE
DEFINITION*********************************
C
SDEF   POS=0 0 0 x=-2 y=d1 z=d2 par=N ERG=d3
       AXS= 1 0 0 Vec= 1 0 0 DIR=1
SI1 -1 1
SP1 0 1
SI2 -1 1
SP2 0 1
si3  H    1.00E-11  $ specify energy of neutron flux
     1.33E-11
     1.78E-11
     2.37E-11
     3.16E-11
     4.22E-11
C
sp3  0.00E+00    $specify distribution of neutron flux relative to each neutron
energy
     2.32E-09
```

```
    1.67E-08

    1.03E-07

    1.48E-07

C

C  ******SECTION 6 TALLY
SPECIFICATION*******************************

C

act nonfiss=p dg=lines

F4:p 20

E4   0.000 $ specify energy bin based on MCA number of channels of detector
- normal 0-3MeV | 8192 channels

    0.000383557

    0.000767114

    0.001150671

MODE N P

NPS  1E+9

PRINT
```

APPENDIX C

MCNP6 HPGE DETCTOR FILE

HPGe detector simulation

```
C
C  ***SECTION 1. CELL  DEFINITION**********************************
C
1    0          -1 2 -3 #3 #4 #5 imp:p=1   $ vacuum base
2    2  -5.323    -4 3 -5 #4 #3 #5 imp:p=1   $ Ge crystal
3    1  -0.001205 -6 7 -8 imp:p=1 $ inner core
4    1  -0.001205 -9 3 -10 #3 #5 imp:p=1 $outter core
5    1  -0.001205 -6 -7 12 imp:p=1  $ ext core
6    3  -2.6989   -13 2 -5 #1 #2 #4 #3 #5 imp:p=1 $ crystal holder
7    4  -2.200    -13 -2 14 #5 imp:p=1 $ teflon
8    4  -2.200    -15 -14 16 #5 imp:p=1 $ teflon holder
10   0          -17 -18 19 #1 #2 #3 #4 #5 #6 #7 #8 imp:p=1 $ Vacuum space
20   3  -2.6989   -20 -21 22 #1 #2 #3 #4 #5 #6 #7 #8 #10 imp:p=1 $ Aluminum
housin
30   1  -0.001205 -25 22 -23 #1 #2 #3 #4 #5 #6 #7 #8 #10 #20 imp:p=1
40   5  -8.96     -26 22 -27 #1 #2 #3 #4 #5 #6 #7 #8 #10 #20 #30 imp:p=1 $
copper
60   0          26:-22:27 imp:p=0 $void
```

```
C  ***SECTION 2. SURFACE
SPECIFICATION**************************

C

1    cz  3.15   $ vacuum

2    pz  0

3    pz  2

4    cz  3.15   $ Ge crystal

5    pz  7.4

6    cz  0.375  $ inner core

7    pz  2.5

8    pz  6.05

9    cz  0.5    $ outer core

10   pz  6.2

12   pz  -2

13   cz  3.3    $crystal holder

14   pz  -0.32  $teflon

15   cz  1.5

16   pz -3

17   cz  3.8    $ vacuum space

18   pz  8.05

19   pz  -4.65

20   cz  3.95   $ Aluminum housing

21   pz  8.15

22   pz  -4.8

25   cz  15.24  $ Air

23   pz  35

26   cz  15.494 $ copper
```

```
27   pz  35.254


C  ******SECTION 3. MATERIAL DEFINITIONS************************
C    AIR NEAR SEA LEVEL (dry, rho=0.001205 g/cc)
M1   7000.04p  -0.742     $N
     8000.04p  -0.246     $O
     18000.04p -0.012     $Ar
C    GERMANIUM (rho=5.323 g/cc)
M2   32000.04p  -1.00
c
C    Aluminum (rho=2.6989 g/cc)
M3   13000.04p  -1.00
C
c    Teflon (rho=2.200 g/cc)
M4   6000.04p   -0.240183  $ C
     9000.04p   -0.759818  $ F
c
C    Copper (rho=8.96 g/cc)
M5   29000.04p  -1.00
c
C  ******SECTION 4 SOURCE
DEFINITION*********************************
C
mode p
SDEF   POS=0 0 0 z=8.151 x=d1 y=d2 par=2 ERG=d3
       AXS= 0 0 1 Vec= 0 0 1 DIR=-1
SI1 -1 1
```

```
SP1 0 1

SI2 -1 1

SP2 0 1

C -----------------------------------------

C  ENERGY OF DECAY GAAMMA FROM ACTIVATED SAMPLE (Insert
desired energy)

C -----------------------------------------

si3  L  3.8356E-04

     7.6711E-04

     1.1507E-03

     1.5342E-03

     1.9178E-03

C ----------------------------------------

C DISTRIBUTION OF DECAY GAMMA  (Insert desired distribution)

C ----------------------------------------

sp3 D  0.00E+00

     0.00E+00

     0.00E+00

     4.97E-05

     1.88E-04

C

C  ******SECTION 6 TALLY SPECIFICATION**************************

C   Gamma Energy Bin   (Insert desired energy bin)

c ************************************************************PHYS:P
10 0 0 0 0

F8:P 2

E8   3.8356E-04
```

7.6711E-04

1.1507E-03

1.5342E-03

1.9178E-03

FT8 GEB 0 0.0752 -0.121

NPS 1E

APPENDIX D

GEANT4 SOURCE CODES FOR PREDICTIVE GAMMA SPECTRA

```
// $Id: ExN02DetectorConstruction.cc,v 1.22 2010/01/22 11:57:03 maire Exp $
// GEANT4 tag $Name: geant4-09-04-beta-01 $
//....oooOO0OOooo........oooOO0OOooo........oooOO0OOooo........oooOO0OOooo...
...
#include "ExN02DetectorConstruction.hh"
#include "G4Material.hh"
#include "G4Element.hh"
#include "G4Box.hh"
#include "G4Trd.hh"
#include "G4VSolid.hh"
#include "G4Tubs.hh"
#include "G4Polyhedra.hh"
#include "G4LogicalVolume.hh"
#include "G4ThreeVector.hh"
#include "G4RotationMatrix.hh"
#include "G4PVPlacement.hh"
#include "G4NistManager.hh"
#include "G4VisAttributes.hh"
#include "G4GeometryManager.hh"
#include "G4PhysicalVolumeStore.hh"
```

```
#include "G4LogicalVolumeStore.hh"
#include "G4SolidStore.hh"
#include "G4Colour.hh"
#include "G4SDManager.hh"
#include "G4MultiFunctionalDetector.hh"
#include "G4VPrimitiveScorer.hh"
#include "G4PSEnergyDeposit.hh"
#include "G4PSDoseDeposit.hh"
#include "G4PSCellFlux.hh"
#include "G4SDParticleFilter.hh"
//....oooOO0OOooo........oooOO0OOooo........oooOO0OOooo........oooOO0OOooo...
...
ExN02DetectorConstruction::ExN02DetectorConstruction()
{
  //Reactor Pool tank
  world_x = 0*cm;
  world_y = 100*cm;
  world_z = 300*cm;
  world_a = 0*deg;
  world_b = 360*deg;
// FNIF- Fastlead
  FNIF_x = 13.7*cm;
  FNIF_y = 14.5*cm;
  FNIF_z = 30.48*cm;
// FNIF- sample space Air
  FNIFa_x = 5.08*cm;
  FNIFa_y = 8.42*cm;
```

```
  FNIFa_z = 27.58*cm;
  //TI - Thermal irradiation channel
  TI_x = 0.*cm;
  TI_y = 5.5*cm;
  TI_z = 30.48*cm;
  TI_a = 0*deg;
  TI_b = 360.*deg;
  //Concrete floor
  concrete_x = 0*cm;
  concrete_y = 65*cm;
  concrete_z = 5*cm;
  concrete_a = 0.*deg;
  concrete_b = 360.*deg;
//Control rod
  CR_x = 0.*cm;
  CR_y = 1.75*cm;
  CR_z = 20*cm;
  CR_a = 0*deg;
  CR_b = 360.*deg;
//Shim rod
  shim_x = 0.*cm;
  shim_y = 1.5*cm;
  shim_z = 20*cm;
  shim_a = 0*deg;
  shim_b = 360.*deg;
  //Safety rod
```

```
  safe_x = 0.*cm;
  safe_y = 1*cm;
  safe_z = 20*cm;
  safe_a = 0*deg;
  safe_b = 360.*deg;

//------ sample -----
//Ti
  sample_x = 2*cm;
  sample_y = 2*cm;
  sample_z = 2*cm;
}
//....oooOO0OOooo........oooOO0OOooo........oooOO0OOooo........oooOO0OOooo...
...
ExN02DetectorConstruction::~ExN02DetectorConstruction(){;}
//....oooOO0OOooo........oooOO0OOooo........oooOO0OOooo........oooOO0OOooo...
...
G4VPhysicalVolume* ExN02DetectorConstruction::Construct()
{
//         ------------ Materials ------------
  G4double a, z, density;
  G4String symbol;
  G4int nelements, natoms;
  G4int ncomponents;
  G4double fractionmass, temperature, pressure;
//Vacuum
pressure = 3.e-18*pascal; temperature = 293.15*kelvin;
```

```
density = universe_mean_density;

G4Material* Vacuum = new G4Material("Vacuum", 1., 1.01*g/mole, density,
kStateGas,temperature,pressure);

// Use NIST database for elements and materials whereever possible.

        G4NistManager* man = G4NistManager::Instance();

        man->SetVerbose(1);


        G4Element* C  = man->FindOrBuildElement("C");

        G4Element* Si = man->FindOrBuildElement("Si");

        G4Element* Cr = man->FindOrBuildElement("Cr");

        G4Element* Mn = man->FindOrBuildElement("Mn");

      G4Element* Mg = man->FindOrBuildElement("Mg");

        G4Element* Fe = man->FindOrBuildElement("Fe");

        //G4Element* Ni = man->FindOrBuildElement("Ni");

        G4Element* Na = man->FindOrBuildElement("Na");

        G4Element* I  = man->FindOrBuildElement("I");

        G4Element* Cd = man->FindOrBuildElement("Cd");

        G4Element* Al = man->FindOrBuildElement("Al");

      G4Element* B  = man->FindOrBuildElement("B");

      G4Element* Ti = man->FindOrBuildElement("Ti");

      G4Element* V  = man->FindOrBuildElement("V");

      G4Element* Ba = man->FindOrBuildElement("Ba");

        G4Element* Cu = man->FindOrBuildElement("Cu");

        G4Element* K = man->FindOrBuildElement("K");

        G4Element* Cl = man->FindOrBuildElement("Cl");

        G4Element* Sc = man->FindOrBuildElement("Sc");

        G4Element* Zn  = man->FindOrBuildElement("Zn");
```

```
G4Element* As = man->FindOrBuildElement("As");
  G4Element* La = man->FindOrBuildElement("La");
  G4Element* Sm = man->FindOrBuildElement("Sm");
  G4Element* Hf = man->FindOrBuildElement("Hf");
  G4Element* Hg = man->FindOrBuildElement("Hg");
  G4Element* Br = man->FindOrBuildElement("Br");
  G4Element* Rb = man->FindOrBuildElement("Rb");
  G4Element* Mo = man->FindOrBuildElement("Mo");
  G4Element* Sb = man->FindOrBuildElement("Sb");
  G4Element* Tc = man->FindOrBuildElement("Tc");
G4Element* Ca = man->FindOrBuildElement("Ca");
G4Element* S = man->FindOrBuildElement("S");
G4Element* P = man->FindOrBuildElement("P");
G4Element* Co = man->FindOrBuildElement("Co");
G4Element* Dy = man->FindOrBuildElement("Dy");
G4Element* Lu = man->FindOrBuildElement("Lu");
G4Element* Ta = man->FindOrBuildElement("Ta");
G4Element* Se = man->FindOrBuildElement("Se");
G4Element* Tb = man->FindOrBuildElement("Tb");
G4Element* U = man->FindOrBuildElement("U");
G4Element* Th = man->FindOrBuildElement("Th");
G4Element* Sr = man->FindOrBuildElement("Sr");
G4Element* Ce = man->FindOrBuildElement("Ce");
G4Element* Eu = man->FindOrBuildElement("Eu");
  G4Element* Ar = man->FindOrBuildElement("Ar");
G4Element* Au = man->FindOrBuildElement("Au");
```

```
        G4Element* Sn = man->FindOrBuildElement("Sn");

// Sample - Quartz

        G4Material* Quartz = new G4Material("Quartz", density= 2.74*g/cm3,
ncomponents=8);

            Quartz->AddElement(Na, fractionmass=0.026);

            Quartz->AddElement(Si, fractionmass=0.77753);

            Quartz->AddElement(Mg, fractionmass=0.024);

            Quartz->AddElement(Mn, fractionmass=0.00083);

            Quartz->AddElement(Al, fractionmass=0.16);

            Quartz->AddElement(V, fractionmass=0.00014);

        Quartz->AddElement(Ti, fractionmass=0.0045);

        Quartz->AddElement(Ba, fractionmass=0.007);

// Sample - Redbeans

        G4Material* Redbeans = new G4Material("Redbeans", density=
1.13*g/cm3, ncomponents=7);

            Redbeans->AddElement(Cl, fractionmass=0.0153);

            Redbeans->AddElement(K, fractionmass=0.8993);

            Redbeans->AddElement(Mg, fractionmass=0.0814);

            Redbeans->AddElement(Mn, fractionmass=0.0005);

            Redbeans->AddElement(Al, fractionmass=0.0028);

            Redbeans->AddElement(V, fractionmass=0.0001);

        Redbeans->AddElement(Cu, fractionmass=0.0006);

// Sample - drinkWater

        G4Material* drinkwater = new G4Material("drinkwater", density=
1*g/cm3, ncomponents=9);

            drinkwater->AddElement(Na, fractionmass=0.2375);

            drinkwater->AddElement(Sc, fractionmass=0.0500);

            drinkwater->AddElement(Fe, fractionmass=0.1375);
```

```
        drinkwater->AddElement(Zn, fractionmass=0.3000);
        drinkwater->AddElement(As, fractionmass=0.0625);
        drinkwater->AddElement(La, fractionmass=0.0625);
      drinkwater->AddElement(Sm, fractionmass=0.0500);
        drinkwater->AddElement(Hf, fractionmass=0.0500);
      drinkwater->AddElement(Hg, fractionmass=0.0500);



// Sample - rice
     G4Material* rice = new G4Material("rice", density= 0.9*g/cm3,
ncomponents=11);
        rice->AddElement(Na, fractionmass=0.01765);
        rice->AddElement(K, fractionmass=0.95294);
        rice->AddElement(Zn, fractionmass=0.01429);
        rice->AddElement(As, fractionmass=0.00084);
        rice->AddElement(Br, fractionmass=0.00168);
        rice->AddElement(Rb, fractionmass=0.00504);
      rice->AddElement(Mo, fractionmass=0.00252);
        rice->AddElement(Sb, fractionmass=0.00084);
      rice->AddElement(La, fractionmass=0.00084);
        rice->AddElement(Sm, fractionmass=0.00084);
      rice->AddElement(Tc, fractionmass=0.00252);
// Sample - Broccoli
     G4Material* Broccoli = new G4Material("Broccoli", density=
0.465*g/cm3, ncomponents=8);
        Broccoli->AddElement(Na, fractionmass=0.116);
        Broccoli->AddElement(Mg, fractionmass=0.0632);
```

```
        Broccoli->AddElement(Al, fractionmass=0.258);
        Broccoli->AddElement(Cl, fractionmass=0.056);
        Broccoli->AddElement(Ar, fractionmass=0.284);
      Broccoli->AddElement(K, fractionmass=0.0304);
        Broccoli->AddElement(V, fractionmass=0.0608);
      Broccoli->AddElement(Mn, fractionmass=0.1316);


// Cesium
G4Element* Cs = new G4Element("Cesium", "Cs", z = 55, a = 137*g/mole);
G4Material* Cesium = new G4Material("Cesium", density = 1.873*g/cm3,
nelements=1);
Cesium->AddElement(Cs,100.*perCent);
// Sample - nickel
   G4Element* Ni = new G4Element("nickel", "Ni", z = 28, a = 65*g/mole);
   G4Material* nickel = new G4Material("nickel", density= 8.908*g/cm3,
nelements=1);
   nickel->AddElement(Ni, fractionmass=1.0);
// Sodium Iodide
        G4Material* SodiumIodide = new G4Material("SodiumIodide",
density= 3.667*g/cm3, ncomponents=2);
        SodiumIodide->AddElement(Na, fractionmass=0.153373);
        SodiumIodide->AddElement(I, fractionmass=0.846627);
// Water
  G4Element* H = new G4Element("Hydrogen", "H", z=1 , a=1.01*g/mole);
  G4Material* H2O = new G4Material("H2O", density= 1.0*g/cm3,
nelements=2);
  H2O->AddElement(H, 2);
  H2O->AddElement(O, 1);
```

```
  G4Material* Sapphire = new G4Material("Sapphire",density= 4.*g/cm3,
ncomponents=2);

  Sapphire->AddElement(Al, natoms=2);

  Sapphire->AddElement(O , natoms=3);

// Heavy water

 G4Element* D  = new G4Element("Deuterium", "D" , z= 1., a = 2.01*g/mole);

 G4Material* D2O = new G4Material("D2O", density= 1.056*g/cm3,
nelements=2);

  D2O->AddElement(D, 2);

  D2O->AddElement(O, 1);


// Sample - cement - portland-white

  G4Material* WhitePortland = new G4Material("WhitePortland", density=
2.3*g/cm3, nelements=10);

       WhitePortland->AddElement(H, fractionmass=0.010000);

          WhitePortland->AddElement(C, fractionmass=0.001000);

       WhitePortland->AddElement(O, fractionmass=0.529107);

          WhitePortland->AddElement(Na, fractionmass=0.016000);

       WhitePortland->AddElement(Mg, fractionmass=0.002000);

          WhitePortland->AddElement(Al, fractionmass=0.033872);

       WhitePortland->AddElement(Si, fractionmass=0.337021);

          WhitePortland->AddElement(K, fractionmass=0.013000);

       WhitePortland->AddElement(Ca, fractionmass=0.044000);

          WhitePortland->AddElement(Fe, fractionmass=0.014000);

// Sample - Flyash

    G4Material* flyash = new G4Material("flyash", density= 2.3*g/cm3,
nelements=10);

    flyash->AddElement(C, fractionmass=0.986487598872);
```

```
    flyash->AddElement(As, fractionmass=0.00154);
    flyash->AddElement(Mn, fractionmass=0.00241);
    flyash->AddElement(Na, fractionmass=0.00894);
    flyash->AddElement(Ba, fractionmass=0.00056232);
    flyash->AddElement(La, fractionmass=0.0000306);
    flyash->AddElement(Hg, fractionmass=0.000002950168);
    flyash->AddElement(Sr, fractionmass=0.000025143);
    flyash->AddElement(Ce, fractionmass=0.00000015);
    flyash->AddElement(Dy, fractionmass=0.000000846);
 flyash->AddElement(Eu, fractionmass=0.00000039196);


//-----------Geometry definition ----------
// The world volume
  G4Tubs* world_box = new G4Tubs("World",world_x,world_y,world_z,
world_a, world_b);
  G4LogicalVolume* world_log  = new
G4LogicalVolume(world_box,Air,"World",0,0,0);
  G4VPhysicalVolume* world_phys = new
G4PVPlacement(0,G4ThreeVector(),world_log,"World",0,false,0);
// Reactor core
  G4double startAngle = 90.*deg;
  G4double totalAngle = 360.*deg;
  G4int NumberOfSide = 6;
  G4int NumberOfPlane = 2;
  const G4double Z[2]= {-30.48*cm, 30.48*cm};
  const G4double rInner[2]= {0*cm, 0*cm};
  const G4double rOuter[2]= {27.48*cm, 27.48*cm};
    G4Polyhedra* reactor_core = new G4Polyhedra("core", startAngle,
```

```
                                        totalAngle,NumberOfSide,

                                        NumberOfPlane, Z, rInner, rOuter);

  G4LogicalVolume* reactor_log = new
G4LogicalVolume(reactor_core,Air,"core",0,0,0);

  G4VPhysicalVolume* reactor_phys = new
G4PVPlacement(0,G4ThreeVector(0,0,-20*cm),reactor_log,"core",

                world_log,false,0);

// FNIF-Lead

  G4VSolid* FNIFLead_box = new G4Box("FNIF", FNIF_x, FNIF_y, FNIF_z);

  G4LogicalVolume* FNIFLead_log = new
G4LogicalVolume(FNIFLead_box,Air,"FNIF",0,0,0);

  G4VPhysicalVolume* FNIFLead_phys = new
G4PVPlacement(0,G4ThreeVector(-41.596*cm,0,-
20*cm),FNIFLead_log,"FNIF",

                world_log,false,0);

// FNIF-Air

  G4VSolid* FNIF_Box = new G4Box("FNIF-
air",FNIFa_x,FNIFa_y,FNIFa_z);

  G4LogicalVolume* FNIF_log

        = new G4LogicalVolume(FNIF_Box,Air,"FNIF-air",0,0,0);

  G4VPhysicalVolume* FNIF_phys = new G4PVPlacement(0,G4ThreeVector(-
39*cm,0,-17.1*cm),FNIF_log,"FNIF-air",world_log,false,0);

// TI-thermal Heavy water box

G4double  dx1 = 30.48*cm;

          G4double  dx2 = 30.48*cm;

         G4double  dy1 = 20*cm;

         G4double  dy2 = 15*cm;

         G4double  dz = 8.24*cm;

G4RotationMatrix* xRot = new G4RotationMatrix;
```

```
xRot->rotateY(90*deg);

G4Trd* TI_Box = new G4Trd("TI", dx1, dx2, dy1, dy2, dz);

G4LogicalVolume* TI_log

        = new G4LogicalVolume(TI_Box,Air,"TI",0,0,0);

  G4VPhysicalVolume* TI_phys = new
G4PVPlacement(xRot,G4ThreeVector(36*cm,0,-
20*cm),TI_log,"TI",world_log,false,0);

// TI - Thermal irradiation channel

  G4Tubs* TIsample_box = new G4Tubs("TI-channel", TI_x, TI_y, TI_z, TI_a,
TI_b);

  G4LogicalVolume* TIsample_log  = new
G4LogicalVolume(TIsample_box,Air,"TI-channel",0,0,0);

  G4VPhysicalVolume* TIsample_phys = new
G4PVPlacement(0,G4ThreeVector(36*cm,0,-20*cm),TIsample_log,"TI-
channel",world_log,false,0);

// Concrete floor

  G4Tubs* concrete_floor = new G4Tubs("concrete", concrete_x, concrete_y,
concrete_z, concrete_a, concrete_b);


  G4LogicalVolume* concrete_log  = new
G4LogicalVolume(concrete_floor,Air,"concrete",0,0,0);

  G4VPhysicalVolume* concrete_phys = new
G4PVPlacement(0,G4ThreeVector(0,0,-
57*cm),concrete_log,"concrete",world_log,false,0);

// Control Rod

  G4Tubs* Control_rod = new G4Tubs("CR", CR_x, CR_y, CR_z, CR_a, CR_b);

  G4LogicalVolume* CR_log  = new
G4LogicalVolume(Control_rod,Air,"CR",0,0,0);

  G4VPhysicalVolume* CR_phys = new G4PVPlacement(0,G4ThreeVector(0,-
12.24*cm,31*cm),CR_log,"CR",world_log,false,0);

// Shim Rod
```

```
  G4Tubs* shim_rod = new G4Tubs("shim", shim_x, shim_y, shim_z, shim_a,
shim_b);

  G4LogicalVolume* shim_log  = new
G4LogicalVolume(shim_rod,Air,"shim",0,0,0);

  G4VPhysicalVolume* shim_phys = new G4PVPlacement(0,G4ThreeVector(-
12*cm,8*cm,31*cm),shim_log,"shim",world_log,false,0);

// Shim Rod

  G4Tubs* safe_rod = new G4Tubs("safe", safe_x, safe_y, safe_z, safe_a,
safe_b);

  G4LogicalVolume* safe_log  = new
G4LogicalVolume(safe_rod,Air,"safe",0,0,0);

  G4VPhysicalVolume* safe_phys = new
G4PVPlacement(0,G4ThreeVector(12*cm,8*cm,31*cm),safe_log,"safe",world_l
og,false,0);

//--------------sample definition-----------------------

  G4VSolid* sample_Box = new
G4Box("sample",sample_x,sample_y,sample_z);

  G4LogicalVolume* sample_log

        = new G4LogicalVolume(sample_Box,drinkwater,"sample",0,0,0);

  G4VPhysicalVolume* sample_phys = new
G4PVPlacement(0,G4ThreeVector(36*cm,0,-
20*cm),sample_log,"sample",world_log,false,0);

//====================================

//Sensitive detector

//====================================


// Create a new sensitive detector named "MyDetector"

  G4MultiFunctionalDetector* detector =

    new G4MultiFunctionalDetector("MyDetector");

   // Get pointer to detector manager

  G4SDManager* manager = G4SDManager::GetSDMpointer();
```

```
  // Register detector with manager
  manager->AddNewDetector(detector);
  // Attach detector to scoring volume
  FNIF_log->SetSensitiveDetector(detector);
  // Create a primitive Scorer energy deposit
  G4PSEnergyDeposit* energyDeposit = new G4PSEnergyDeposit("eDep");
  detector->RegisterPrimitive(energyDeposit);
  // Create a primitive Scorer Dose deposit
  G4PSDoseDeposit* DoseDeposit = new G4PSDoseDeposit("Dose");
  detector->RegisterPrimitive(DoseDeposit);
   // Create a primitive Scorer CellFul deposit
  G4PSCellFlux* CellFlux = new G4PSCellFlux("Flux");
  detector->RegisterPrimitive(CellFlux);
 //==============================
 //   Visualization attributes
  //==============================
// Mother volume of WaterPhantom
  {G4VisAttributes* BoxVisAtt= new
G4VisAttributes(G4Colour(0.0,1.0,1.0,0.1));
  //BoxVisAtt->SetForceSolid(true);
  world_log  ->SetVisAttributes(BoxVisAtt);}
  //logicWorld->SetVisAttributes(G4VisAttributes::Invisible);


  // Reactor core - water
 {G4VisAttributes* reactorcore = new
G4VisAttributes(G4Colour(1.0,1.0,0.0,1.0));
  reactorcore->SetForceSolid(true);
```

```
  reactor_log->SetVisAttributes(reactorcore);}

  // FNIF lead block

 {G4VisAttributes* FNIFLead = new
G4VisAttributes(G4Colour(1.0,1.0,1.0,0.2));

  FNIFLead->SetForceSolid(true);

  FNIFLead_log->SetVisAttributes(FNIFLead);}

 // FNIF sample space

  {G4VisAttributes* FNIFair = new
G4VisAttributes(G4Colour(1.0,0.0,1.0,0.2));

  FNIFair->SetForceSolid(true);

  FNIF_log->SetVisAttributes(FNIFair);}

 // Ti - heavy water

 {G4VisAttributes* TiBox = new G4VisAttributes(G4Colour(1.0,1.0,1.0,0.2));

  TiBox->SetForceSolid(true);

  TI_log->SetVisAttributes(TiBox);}

 // Ti - Air sample space

 {G4VisAttributes* TiAir = new G4VisAttributes(G4Colour(1.0,1.0,1.0,0.2));

  TiAir->SetForceSolid(true);

  TIsample_log->SetVisAttributes(TiAir);}

//concrete floor

 {G4VisAttributes* concretefloor= new
G4VisAttributes(G4Colour(0.0,1.0,1.0,1.0));

  concretefloor->SetForceSolid(true);

  concrete_log  ->SetVisAttributes(concretefloor);}


//Control rod

 {G4VisAttributes* controlR= new
G4VisAttributes(G4Colour(0.5,1.0,0.5,1.0));
```

```
  controlR->SetForceSolid(true);
  CR_log  ->SetVisAttributes(controlR);}
//Control rod
 {G4VisAttributes* shimR= new G4VisAttributes(G4Colour(0.5,1.0,0.5,1.0));
  shimR->SetForceSolid(true);
  shim_log  ->SetVisAttributes(shimR);}
//Control rod
{G4VisAttributes* safeR= new G4VisAttributes(G4Colour(0.5,1.0,0.5,1.0));
  safeR->SetForceSolid(true);
  safe_log  ->SetVisAttributes(safeR);}
//sample
{G4VisAttributes* samp= new G4VisAttributes(G4Colour(0.5,1.0,1.0,1.0));
  samp->SetForceSolid(true);
  sample_log  ->SetVisAttributes(samp);}
//always return the physical World
  return world_phys;
}


// $Id: ExN02PhysicsList.cc 69899 2013-05-17 10:05:33Z gcosmo $
//....oooOO0OOooo........oooOO0OOooo........oooOO0OOooo........oooOO0OOooo...
...
//....oooOO0OOooo........oooOO0OOooo........oooOO0OOooo........oooOO0OOooo...
...
#include "globals.hh"
#include "ExN02PhysicsList.hh"
```

```
#include "G4ProcessManager.hh"
#include "G4ParticleTypes.hh"
#include "G4SystemOfUnits.hh"
#include "G4IonConstructor.hh"
//....oooOO0OOooo........oooOO0OOooo........oooOO0OOooo........oooOO0OOooo...
...
ExN02PhysicsList::ExN02PhysicsList():  G4VUserPhysicsList()
{
  defaultCutValue = 1.0*cm;
   SetVerboseLevel(1);
}
//....oooOO0OOooo........oooOO0OOooo........oooOO0OOooo........oooOO0OOooo...
...
ExN02PhysicsList::~ExN02PhysicsList()
{}
//....oooOO0OOooo........oooOO0OOooo........oooOO0OOooo........oooOO0OOooo...
...
void ExN02PhysicsList::ConstructParticle()
{
  // In this method, static member functions should be called
  // for all particles which you want to use.
  // This ensures that objects of these particle types will be
  // created in the program.
  ConstructBosons();
  ConstructLeptons();
```

```
  ConstructMesons();
  ConstructBaryons();
  G4IonConstructor pIonConstructor;
  pIonConstructor.ConstructParticle();
}
//....oooOO0OOooo........oooOO0OOooo........oooOO0OOooo........oooOO0OOooo...
...
void ExN02PhysicsList::ConstructBosons()
{
  // pseudo-particles
  G4Geantino::GeantinoDefinition();
  G4ChargedGeantino::ChargedGeantinoDefinition();
  // gamma
  G4Gamma::GammaDefinition();
}
//....oooOO0OOooo........oooOO0OOooo........oooOO0OOooo........oooOO0OOooo...
...
void ExN02PhysicsList::ConstructLeptons()
{
  // leptons
  //  e+/-
  G4Electron::ElectronDefinition();
  G4Positron::PositronDefinition();
  // mu+/-
  G4MuonPlus::MuonPlusDefinition();
```

```
  G4MuonMinus::MuonMinusDefinition();
  // nu_e
  G4NeutrinoE::NeutrinoEDefinition();
  G4AntiNeutrinoE::AntiNeutrinoEDefinition();
  // nu_mu
  G4NeutrinoMu::NeutrinoMuDefinition();
  G4AntiNeutrinoMu::AntiNeutrinoMuDefinition();
}
//....oooOO0OOooo.....oooOO0OOooo.....oooOO0OOooo.....oooOO0OOooo...
...
void ExN02PhysicsList::ConstructMesons()
{
  //  mesons
  //    light mesons
  G4PionPlus::PionPlusDefinition();
  G4PionMinus::PionMinusDefinition();
  G4PionZero::PionZeroDefinition();
  G4Eta::EtaDefinition();
  G4EtaPrime::EtaPrimeDefinition();
  G4KaonPlus::KaonPlusDefinition();
  G4KaonMinus::KaonMinusDefinition();
  G4KaonZero::KaonZeroDefinition();
  G4AntiKaonZero::AntiKaonZeroDefinition();
  G4KaonZeroLong::KaonZeroLongDefinition();
  G4KaonZeroShort::KaonZeroShortDefinition();
```

```
}

//....oooOO0OOooo........oooOO0OOooo........oooOO0OOooo........oooOO0OOooo...
...


void ExN02PhysicsList::ConstructBaryons()
{
  //  barions
  G4Proton::ProtonDefinition();
  G4AntiProton::AntiProtonDefinition();
  G4Neutron::NeutronDefinition();
  G4AntiNeutron::AntiNeutronDefinition();
}

//....oooOO0OOooo........oooOO0OOooo........oooOO0OOooo........oooOO0OOooo...
...
void ExN02PhysicsList::ConstructProcess()
{
  AddTransportation();
  ConstructEM();
  ConstructGeneral();
  AddStepMax();
}

//....oooOO0OOooo........oooOO0OOooo........oooOO0OOooo........oooOO0OOooo...
...
#include "G4PhysicsListHelper.hh"
#include "G4ComptonScattering.hh"
```

```
#include "G4GammaConversion.hh"
#include "G4PhotoElectricEffect.hh"
#include "G4eMultipleScattering.hh"
#include "G4eIonisation.hh"
#include "G4eBremsstrahlung.hh"
#include "G4eplusAnnihilation.hh"
#include "G4MuMultipleScattering.hh"
#include "G4MuIonisation.hh"
#include "G4MuBremsstrahlung.hh"
#include "G4MuPairProduction.hh"
#include "G4hMultipleScattering.hh"
#include "G4hIonisation.hh"
#include "G4hBremsstrahlung.hh"
#include "G4hPairProduction.hh"
#include "G4ionIonisation.hh"
//....oooOO0OOooo........oooOO0OOooo........oooOO0OOooo........oooOO0OOooo...
...
void ExN02PhysicsList::ConstructEM()
{
  G4PhysicsListHelper* ph = G4PhysicsListHelper::GetPhysicsListHelper();
    theParticleIterator->reset();
  while( (*theParticleIterator)() ){
    G4ParticleDefinition* particle = theParticleIterator->value();
    G4String particleName = particle->GetParticleName();
        if (particleName == "gamma") {
```

```
  // gamma
  ph->RegisterProcess(new G4PhotoElectricEffect, particle);
  ph->RegisterProcess(new G4ComptonScattering,   particle);
  ph->RegisterProcess(new G4GammaConversion,     particle);

} else if (particleName == "e-") {
  //electron
  ph->RegisterProcess(new G4eMultipleScattering, particle);
  ph->RegisterProcess(new G4eIonisation,         particle);
  ph->RegisterProcess(new G4eBremsstrahlung,     particle);
} else if (particleName == "e+") {
  //positron
  ph->RegisterProcess(new G4eMultipleScattering, particle);
  ph->RegisterProcess(new G4eIonisation,         particle);
  ph->RegisterProcess(new G4eBremsstrahlung,     particle);
  ph->RegisterProcess(new G4eplusAnnihilation,   particle);
   } else if( particleName == "mu+" ||
         particleName == "mu-"    ) {
  //muon
  ph->RegisterProcess(new G4MuMultipleScattering, particle);
  ph->RegisterProcess(new G4MuIonisation,         particle);
  ph->RegisterProcess(new G4MuBremsstrahlung,     particle);
  ph->RegisterProcess(new G4MuPairProduction,     particle);
         } else if( particleName == "proton" ||
```

```
            particleName == "pi-" ||
            particleName == "pi+"    ) {
    //proton
    ph->RegisterProcess(new G4hMultipleScattering, particle);
    ph->RegisterProcess(new G4hIonisation,         particle);
    ph->RegisterProcess(new G4hBremsstrahlung,     particle);
    ph->RegisterProcess(new G4hPairProduction,     particle);
      } else if( particleName == "alpha" ||
            particleName == "He3" )     {
    //alpha
    ph->RegisterProcess(new G4hMultipleScattering, particle);
    ph->RegisterProcess(new G4ionIonisation,       particle);
      } else if( particleName == "GenericIon" ) {
    //Ions
    ph->RegisterProcess(new G4hMultipleScattering, particle);
    ph->RegisterProcess(new G4ionIonisation,       particle);
        } else if ((!particle->IsShortLived()) &&
            (particle->GetPDGCharge() != 0.0) &&
            (particle->GetParticleName() != "chargedgeantino")) {
    //all others charged particles except geantino
    ph->RegisterProcess(new G4hMultipleScattering, particle);
    ph->RegisterProcess(new G4hIonisation,         particle);
  }
}
```

```
}

//....oooOO0OOooo........oooOO0OOooo........oooOO0OOooo........oooOO0OOooo...
...
#include "G4Decay.hh"
void ExN02PhysicsList::ConstructGeneral()
{
  G4PhysicsListHelper* ph = G4PhysicsListHelper::GetPhysicsListHelper();
    // Add Decay Process
  G4Decay* theDecayProcess = new G4Decay();
  theParticleIterator->reset();
  while( (*theParticleIterator)() ){
    G4ParticleDefinition* particle = theParticleIterator->value();
    if (theDecayProcess->IsApplicable(*particle)) {
      ph->RegisterProcess(theDecayProcess, particle);
    }
  }
}

//....oooOO0OOooo........oooOO0OOooo........oooOO0OOooo........oooOO0OOooo...
...
#include "G4StepLimiter.hh"
#include "G4UserSpecialCuts.hh"
void ExN02PhysicsList::AddStepMax()
{
  // Step limitation seen as a process
```

```
  G4StepLimiter* stepLimiter = new G4StepLimiter();
  ////G4UserSpecialCuts* userCuts = new G4UserSpecialCuts();
    theParticleIterator->reset();
  while ((*theParticleIterator)()){
      G4ParticleDefinition* particle = theParticleIterator->value();
      G4ProcessManager* pmanager = particle->GetProcessManager();

      if (particle->GetPDGCharge() != 0.0)
        {
          pmanager ->AddDiscreteProcess(stepLimiter);
          ////pmanager ->AddDiscreteProcess(userCuts);
        }
  }
}
//....oooOO0OOooo.....oooOO0OOooo.....oooOO0OOooo.....oooOO0OOooo...
...
void ExN02PhysicsList::SetCuts()
{
  //G4VUserPhysicsList::SetCutsWithDefault method sets
  //the default cut value for all particle types
  //
  SetCutsWithDefault();
      if (verboseLevel>0) DumpCutValuesTable();
}
```

//....oooOO0OOooo.....oooOO0OOooo.....oooOO0OOooo.....oooOO0OOooo...
...

//------------------------------Macro file----------------------

/control/verbose 1
/run/verbose 2
/event/verbose 0
/tracking/verbose 0
/run/initialize
#####################################
Source the source
#####################################
Neutron spectrum in Ti
#####################################
/gps/particle neutron
/gps/pos/type Beam
/gps/pos/shape Square
/gps/pos/centre 33. 0. -20. cm
/gps/pos/halfx 13. cm
/gps/pos/halfz 31. cm
/gps/direction 1 0 0
/gps/ang/type iso
/gps/ene/type User
/gps/hist/type energy

/gps/hist/point 0.0000000000237 1.03211596473167E-07
/gps/hist/point 0.0000000000316 1.47799725929044E-07
/gps/hist/point 0.0000000000422 1.61306090752751E-07
/gps/hist/point 0.0000000000562 2.56692982009653E-07
/gps/hist/point 0.000000000075 6.86279671461966E-07
/gps/hist/point 0.0000000001 1.54258732879304E-06
/gps/hist/point 0.000000000133 2.41497235396662E-06
/gps/hist/point 0.000000000178 4.89113320394458E-06
/gps/hist/point 0.000000000237 7.91203459637131E-06
/gps/hist/point 0.000000000316 1.58177693120882E-05
/gps/hist/point 0.000000000422 3.38133421952305E-05
/gps/hist/point 0.000000000562 5.69746361839445E-05
/gps/hist/point 0.00000000075 0.000100041380667989
/gps/hist/point 0.000000001 0.00019209386095438
/gps/hist/point 0.00000000133 0.000343546250445615
/gps/hist/point 0.00000000178 0.000861537644460567
/gps/hist/point 0.00000000237 0.00106116963847386
/gps/hist/point 0.00000000316 0.00180887495662696
/gps/hist/point 0.00000000422 0.00325895722750039

/gps/hist/point 0.00000000562 0.00673775856611367
/gps/hist/point 0.0000000075 0.00926220039800352
/gps/hist/point 0.00000001 0.0160582328601706
/gps/hist/point 0.0000000133 0.0265043944497827
/gps/hist/point 0.0000000178 0.040591506892438
/gps/hist/point 0.0000000237 0.057579098870873
/gps/hist/point 0.0000000316 0.0795378035725951
/gps/hist/point 0.0000000422 0.0995754067368255
/gps/hist/point 0.0000000562 0.109178198958485
/gps/hist/point 0.000000075 0.104513571808414
/gps/hist/point 0.0000001 0.0830146859820435
/gps/hist/point 0.000000133 0.0512013748635384
/gps/hist/point 0.000000178 0.0248258745236968
/gps/hist/point 0.000000237 0.010496868387638
/gps/hist/point 0.000000316 0.00591404917054816
/gps/hist/point 0.000000422 0.00506514025236496
/gps/hist/point 0.000000562 0.00473443272421852
/gps/hist/point 0.00000075 0.00456035326337683
/gps/hist/point 0.000001 0.00439559690177946
/gps/hist/point 0.00000133 0.00419812822885296
/gps/hist/point 0.00000178 0.00418500347748959
/gps/hist/point 0.0000023714 0.00406206528920174
/gps/hist/point 0.0000031623 0.00399258557094982
/gps/hist/point 0.000004217 0.00394157102013328
/gps/hist/point 0.0000056234 0.00384942621400971
/gps/hist/point 0.0000074989 0.00377815428833024
/gps/hist/point 0.00001 0.00376968203503636
/gps/hist/point 0.000013335 0.0037751310697 4033
/gps/hist/point 0.000017783 0.00373570250633422
/gps/hist/point 0.000023714 0.00375777019173002
/gps/hist/point 0.000031623 0.00370972455018739
/gps/hist/point 0.00004217 0.00371195123214284
/gps/hist/point 0.000056234 0.00368481467725497
/gps/hist/point 0.000074989 0.00367346403021382
/gps/hist/point 0.0001 0.00369091542375078
/gps/hist/point 0.00013335 0.00363115707306042
/gps/hist/point 0.00017783 0.0036450964641636
/gps/hist/point 0.00023714 0.00363914054251042
/gps/hist/point 0.00031623 0.00359533102761474
/gps/hist/point 0.0004217 0.00361220312178117
/gps/hist/point 0.00056234 0.00355850931137597
/gps/hist/point 0.00074989 0.00358300281288583
/gps/hist/point 0.001 0.00357183319689796
/gps/hist/point 0.0013335 0.00353750970919456

```
/gps/hist/point 0.0017783 0.00354869742828776
/gps/hist/point 0.0023714 0.00356642036840465
/gps/hist/point 0.0031623 0.00357501934343583
/gps/hist/point 0.004217 0.00355213701830023
/gps/hist/point 0.0056234 0.00359882492694319
/gps/hist/point 0.0074989 0.00353048570432699
/gps/hist/point 0.01 0.00360814802618752
/gps/hist/point 0.013335 0.00363803625308537
/gps/hist/point 0.017783 0.00371072022098048
/gps/hist/point 0.023714 0.00379468242349543
/gps/hist/point 0.031623 0.00430404949813174
/gps/hist/point 0.04217 0.00346857308410251
/gps/hist/point 0.056234 0.00414494130539696
/gps/hist/point 0.074989 0.00470601084885232
/gps/hist/point 0.1 0.00434546940312403
/gps/hist/point 0.13335 0.00524626182117956
/gps/hist/point 0.17783 0.00510239644313162
/gps/hist/point 0.23714 0.00577121566950396
/gps/hist/point 0.31623 0.0065526905203374
/gps/hist/point 0.4217 0.00634079367246385
/gps/hist/point 0.56234 0.00620060322479766
/gps/hist/point 0.74989 0.0078479677066127
/gps/hist/point 1 0.00772774498412417
/gps/hist/point 1.3335 0.00785423138105647
/gps/hist/point 1.7783 0.00909208551722883
/gps/hist/point 2.3714 0.00916218074106193
/gps/hist/point 3.1623 0.00848889004767337
/gps/hist/point 4.217 0.0054117604100954
/gps/hist/point 5.6234 0.00414481458365966
/gps/hist/point 7.4989 0.00199431049544141
/gps/hist/point 10 0.000582452931469726

#
######################################
##          Score mesh for Ti    ##
######################################
/score/create/cylinderMesh boxMesh_1

/score/mesh/cylinderSize 5 30 cm
/score/mesh/translate/xyz 36 0 -20 cm
/score/mesh/nBin 5 5 5

/score/quantity/doseDeposit doseDep
/score/filter/particle gammafilter gamma
```

/score/quantity/nOfSecondary
NStepGamma0.02197265625MeV_0.0223388671875MeV
/score/filter/particleWithKineticEnergy Gammafilter60 0.02197265625
0.0223388671875 MeV gamma
/score/quantity/nOfSecondary
NStepGamma0.0223388671875MeV_0.022705078125MeV
/score/filter/particleWithKineticEnergy Gammafilter61 0.0223388671875
0.022705078125 MeV gamma
/score/quantity/nOfSecondary
NStepGamma0.022705078125MeV_0.0230712890625MeV
/score/filter/particleWithKineticEnergy Gammafilter62 0.022705078125
0.0230712890625 MeV gamma
/score/quantity/nOfSecondary
NStepGamma0.0230712890625MeV_0.0234375MeV
/score/filter/particleWithKineticEnergy Gammafilter63 0.0230712890625
0.0234375 MeV gamma
/score/quantity/nOfSecondary
NStepGamma0.0234375MeV_0.0238037109375MeV
/score/filter/particleWithKineticEnergy Gammafilter64 0.0234375
0.0238037109375 MeV gamma
/score/quantity/nOfSecondary
NStepGamma0.0238037109375MeV_0.024169921875MeV
/score/filter/particleWithKineticEnergy Gammafilter65 0.0238037109375
0.024169921875 MeV gamma
/score/quantity/nOfSecondary
NStepGamma0.0703125MeV_0.0706787109375MeV
/score/filter/particleWithKineticEnergy Gammafilter192 0.0703125
0.0706787109375 MeV gamma
/score/quantity/nOfSecondary
NStepGamma0.0706787109375MeV_0.071044921875MeV
/score/filter/particleWithKineticEnergy Gammafilter193 0.0706787109375
0.071044921875 MeV gamma
/score/quantity/nOfSecondary
NStepGamma0.071044921875MeV_0.0714111328125MeV
/score/filter/particleWithKineticEnergy Gammafilter194 0.071044921875
0.0714111328125 MeV gamma
/score/quantity/nOfSecondary
NStepGamma0.0714111328125MeV_0.07177734375MeV
/score/filter/particleWithKineticEnergy Gammafilter195 0.0714111328125
0.07177734375 MeV gamma
/score/quantity/nOfSecondary
NStepGamma0.07177734375MeV_0.0721435546875MeV

/score/filter/particleWithKineticEnergy Gammafilter196 0.07177734375 0.0721435546875 MeV gamma
/score/quantity/nOfSecondary NStepGamma0.0721435546875MeV_0.072509765625MeV
/score/filter/particleWithKineticEnergy Gammafilter197 0.0721435546875 0.072509765625 MeV gamma
/score/filter/particleWithKineticEnergy Gammafilter7466 2.734130859375 2.7344970703125 MeV gamma
/score/quantity/nOfSecondary NStepGamma2.7344970703125MeV_2.73486328125MeV
/score/filter/particleWithKineticEnergy Gammafilter7467 2.7344970703125 2.73486328125 MeV gamma
/score/quantity/nOfSecondary NStepGamma2.73486328125MeV_2.7352294921875MeV
/score/filter/particleWithKineticEnergy Gammafilter7468 2.73486328125 2.7352294921875 MeV gamma
/score/quantity/nOfSecondary NStepGamma2.7352294921875MeV_2.735595703125MeV
/score/filter/particleWithKineticEnergy Gammafilter7469 2.7352294921875 2.735595703125 MeV gamma
/score/quantity/nOfSecondary NStepGamma2.735595703125MeV_2.7359619140625MeV
/score/filter/particleWithKineticEnergy Gammafilter7470 2.735595703125 2.7359619140625 MeV gamma
/score/quantity/nOfSecondary NStepGamma2.7359619140625MeV_2.736328125MeV
/score/filter/particleWithKineticEnergy Gammafilter7471 2.7359619140625 2.736328125 MeV gamma
/score/quantity/nOfSecondary NStepGamma2.736328125MeV_2.7366943359375MeV
/score/filter/particleWithKineticEnergy Gammafilter7472 2.736328125 2.7366943359375 MeV gamma
/score/quantity/nOfSecondary NStepGamma2.7366943359375MeV_2.737060546875MeV
/score/filter/particleWithKineticEnergy Gammafilter7473 2.7366943359375 2.737060546875 MeV gamma
/score/quantity/nOfSecondary NStepGamma2.737060546875MeV_2.7374267578125MeV
/score/filter/particleWithKineticEnergy Gammafilter7474 2.737060546875 2.7374267578125 MeV gamma
/score/quantity/nOfSecondary NStepGamma2.7374267578125MeV_2.73779296875MeV
/score/filter/particleWithKineticEnergy Gammafilter7475 2.7374267578125 2.73779296875 MeV gamma

/score/quantity/nOfSecondary
NStepGamma2.73779296875MeV_2.7381591796875MeV
/score/filter/particleWithKineticEnergy Gammafilter7476 2.73779296875
2.7381591796875 MeV gamma
/score/quantity/nOfSecondary
NStepGamma2.7381591796875MeV_2.738525390625MeV
/score/filter/particleWithKineticEnergy Gammafilter7477 2.7381591796875
2.738525390625 MeV gamma
/score/quantity/nOfSecondary
NStepGamma2.738525390625MeV_2.7388916015625MeV
/score/filter/particleWithKineticEnergy Gammafilter7478 2.738525390625
2.7388916015625 MeV gamma
/score/quantity/nOfSecondary
NStepGamma2.7388916015625MeV_2.7392578125MeV
/score/filter/particleWithKineticEnergy Gammafilter7479 2.7388916015625
2.7392578125 MeV gamma
/score/quantity/nOfSecondary
NStepGamma2.7392578125MeV_2.7396240234375MeV
/score/filter/particleWithKineticEnergy Gammafilter7480 2.7392578125
2.7396240234375 MeV gamma
/score/quantity/nOfSecondary
NStepGamma2.7396240234375MeV_2.739990234375MeV
/score/filter/particleWithKineticEnergy Gammafilter7481 2.7396240234375
2.739990234375 MeV gamma
/score/quantity/nOfSecondary
NStepGamma2.739990234375MeV_2.7403564453125MeV
/score/filter/particleWithKineticEnergy Gammafilter7482 2.739990234375
2.7403564453125 MeV gamma
/score/quantity/nOfSecondary
NStepGamma2.7403564453125MeV_2.74072265625MeV
/score/filter/particleWithKineticEnergy Gammafilter7483 2.7403564453125
2.74072265625 MeV gamma
/score/quantity/nOfSecondary
NStepGamma2.74072265625MeV_2.7410888671875MeV
/score/filter/particleWithKineticEnergy Gammafilter7484 2.74072265625
2.7410888671875 MeV gamma
/score/quantity/nOfSecondary
NStepGamma2.7410888671875MeV_2.741455078125MeV
/score/filter/particleWithKineticEnergy Gammafilter7485 2.7410888671875
2.741455078125 MeV gamma
/score/quantity/nOfSecondary
NStepGamma2.741455078125MeV_2.7418212890625MeV
/score/filter/particleWithKineticEnergy Gammafilter7486 2.741455078125
2.7418212890625 MeV gamma

/score/quantity/nOfSecondary
NStepGamma2.7418212890625MeV_2.7421875MeV
/score/filter/particleWithKineticEnergy Gammafilter7487 2.7418212890625
2.7421875 MeV gamma
/score/quantity/nOfSecondary
NStepGamma2.7421875MeV_2.7425537109375MeV
/score/filter/particleWithKineticEnergy Gammafilter7488 2.7421875
2.7425537109375 MeV gamma
/score/quantity/nOfSecondary
NStepGamma2.7425537109375MeV_2.742919921875MeV
/score/filter/particleWithKineticEnergy Gammafilter7489 2.7425537109375
2.742919921875 MeV gamma
/score/quantity/nOfSecondary
NStepGamma2.742919921875MeV_2.7432861328125MeV
/score/filter/particleWithKineticEnergy Gammafilter7490 2.742919921875
2.7432861328125 MeV gamma
/score/quantity/nOfSecondary
NStepGamma2.7432861328125MeV_2.74365234375MeV
/score/filter/particleWithKineticEnergy Gammafilter7491 2.7432861328125
2.74365234375 MeV gamma
/score/quantity/nOfSecondary
NStepGamma2.74365234375MeV_2.7440185546875MeV
/score/filter/particleWithKineticEnergy Gammafilter7492 2.74365234375
2.7440185546875 MeV gamma
/score/quantity/nOfSecondary
NStepGamma2.7440185546875MeV_2.744384765625MeV
/score/filter/particleWithKineticEnergy Gammafilter7493 2.7440185546875
2.744384765625 MeV gamma
/score/quantity/nOfSecondary
NStepGamma2.744384765625MeV_2.7447509765625MeV
/score/filter/particleWithKineticEnergy Gammafilter7494 2.744384765625
2.7447509765625 MeV gamma
/score/quantity/nOfSecondary
NStepGamma2.7447509765625MeV_2.7451171875MeV
/score/filter/particleWithKineticEnergy Gammafilter7495 2.7447509765625
2.7451171875 MeV gamma
/score/quantity/nOfSecondary
NStepGamma2.7451171875MeV_2.7454833984375MeV
/score/filter/particleWithKineticEnergy Gammafilter7496 2.7451171875
2.7454833984375 MeV gamma
/score/quantity/nOfSecondary
NStepGamma2.7454833984375MeV_2.745849609375MeV
/score/filter/particleWithKineticEnergy Gammafilter7497 2.7454833984375
2.745849609375 MeV gamma

/score/quantity/nOfSecondary
NStepGamma2.745849609375MeV_2.7462158203125MeV
/score/filter/particleWithKineticEnergy Gammafilter7498 2.745849609375
2.7462158203125 MeV gamma
/score/quantity/nOfSecondary
NStepGamma2.7462158203125MeV_2.74658203125MeV
/score/filter/particleWithKineticEnergy Gammafilter7499 2.7462158203125
2.74658203125 MeV gamma
/score/quantity/nOfSecondary
NStepGamma2.74658203125MeV_2.7469482421875MeV
/score/filter/particleWithKineticEnergy Gammafilter7500 2.74658203125
2.7469482421875 MeV gamma
/score/quantity/nOfSecondary
NStepGamma2.7469482421875MeV_2.747314453125MeV
/score/filter/particleWithKineticEnergy Gammafilter7501 2.7469482421875
2.747314453125 MeV gamma
/score/quantity/nOfSecondary
NStepGamma2.747314453125MeV_2.7476806640625MeV
/score/filter/particleWithKineticEnergy Gammafilter7502 2.747314453125
2.7476806640625 MeV gamma
/score/quantity/nOfSecondary
NStepGamma2.7476806640625MeV_2.748046875MeV
/score/filter/particleWithKineticEnergy Gammafilter7503 2.7476806640625
2.748046875 MeV gamma
/score/quantity/nOfSecondary
NStepGamma2.748046875MeV_2.7484130859375MeV
/score/filter/particleWithKineticEnergy Gammafilter7504 2.748046875
2.7484130859375 MeV gamma
/score/quantity/nOfSecondary
NStepGamma2.7484130859375MeV_2.748779296875MeV
/score/filter/particleWithKineticEnergy Gammafilter7505 2.7484130859375
2.748779296875 MeV gamma
/score/quantity/nOfSecondary
NStepGamma2.748779296875MeV_2.7491455078125MeV
/score/filter/particleWithKineticEnergy Gammafilter7506 2.748779296875
2.7491455078125 MeV gamma
/score/quantity/nOfSecondary
NStepGamma2.7491455078125MeV_2.74951171875MeV
/score/filter/particleWithKineticEnergy Gammafilter7507 2.7491455078125
2.74951171875 MeV gamma
/score/quantity/nOfSecondary
NStepGamma2.74951171875MeV_2.7498779296875MeV
/score/filter/particleWithKineticEnergy Gammafilter7508 2.74951171875
2.7498779296875 MeV gamma

/score/quantity/nOfSecondary
NStepGamma2.7498779296875MeV_2.750244140625MeV
/score/filter/particleWithKineticEnergy Gammafilter7509 2.7498779296875
2.750244140625 MeV gamma
/score/quantity/nOfSecondary
NStepGamma2.750244140625MeV_2.7506103515625MeV
/score/filter/particleWithKineticEnergy Gammafilter7510 2.750244140625
2.7506103515625 MeV gamma
/score/quantity/nOfSecondary
NStepGamma2.7506103515625MeV_2.7509765625MeV
/score/filter/particleWithKineticEnergy Gammafilter7511 2.7506103515625
2.7509765625 MeV gamma
/score/quantity/nOfSecondary
NStepGamma2.7509765625MeV_2.7513427734375MeV
/score/filter/particleWithKineticEnergy Gammafilter7512 2.7509765625
2.7513427734375 MeV gamma
/score/quantity/nOfSecondary
NStepGamma2.7513427734375MeV_2.751708984375MeV
/score/filter/particleWithKineticEnergy Gammafilter7513 2.7513427734375
2.751708984375 MeV gamma
/score/quantity/nOfSecondary
NStepGamma2.751708984375MeV_2.7520751953125MeV
/score/filter/particleWithKineticEnergy Gammafilter7514 2.751708984375
2.7520751953125 MeV gamma
/score/quantity/nOfSecondary
NStepGamma2.7520751953125MeV_2.75244140625MeV
/score/filter/particleWithKineticEnergy Gammafilter7515 2.7520751953125
2.75244140625 MeV gamma
/score/quantity/nOfSecondary
NStepGamma2.75244140625MeV_2.7528076171875MeV
/score/filter/particleWithKineticEnergy Gammafilter7516 2.75244140625
2.7528076171875 MeV gamma
/score/quantity/nOfSecondary
NStepGamma2.7528076171875MeV_2.753173828125MeV
/score/filter/particleWithKineticEnergy Gammafilter7517 2.7528076171875
2.753173828125 MeV gamma
/score/quantity/nOfSecondary
NStepGamma2.753173828125MeV_2.7535400390625MeV
/score/filter/particleWithKineticEnergy Gammafilter7518 2.753173828125
2.7535400390625 MeV gamma
/score/quantity/nOfSecondary
NStepGamma2.7535400390625MeV_2.75390625MeV
/score/filter/particleWithKineticEnergy Gammafilter7519 2.7535400390625
2.75390625 MeV gamma

/score/quantity/nOfSecondary
NStepGamma2.75390625MeV_2.7542724609375MeV
/score/filter/particleWithKineticEnergy Gammafilter7520 2.75390625
2.7542724609375 MeV gamma
/score/quantity/nOfSecondary
NStepGamma2.7542724609375MeV_2.754638671875MeV
/score/filter/particleWithKineticEnergy Gammafilter7521 2.7542724609375
2.754638671875 MeV gamma
/score/quantity/nOfSecondary
NStepGamma2.754638671875MeV_2.7550048828125MeV
/score/filter/particleWithKineticEnergy Gammafilter7522 2.754638671875
2.7550048828125 MeV gamma
/score/quantity/nOfSecondary
NStepGamma2.7550048828125MeV_2.75537109375MeV
/score/filter/particleWithKineticEnergy Gammafilter7523 2.7550048828125
2.75537109375 MeV gamma
/score/quantity/nOfSecondary
NStepGamma2.75537109375MeV_2.7557373046875MeV
/score/filter/particleWithKineticEnergy Gammafilter7524 2.75537109375
2.7557373046875 MeV gamma
/score/quantity/nOfSecondary
NStepGamma2.7557373046875MeV_2.756103515625MeV
/score/filter/particleWithKineticEnergy Gammafilter7525 2.7557373046875
2.756103515625 MeV gamma
/score/quantity/nOfSecondary
NStepGamma2.756103515625MeV_2.7564697265625MeV
/score/filter/particleWithKineticEnergy Gammafilter7526 2.756103515625
2.7564697265625 MeV gamma
/score/quantity/nOfSecondary
NStepGamma2.7564697265625MeV_2.7568359375MeV
/score/filter/particleWithKineticEnergy Gammafilter7527 2.7564697265625
2.7568359375 MeV gamma
/score/quantity/nOfSecondary
NStepGamma2.7568359375MeV_2.7572021484375MeV
/score/filter/particleWithKineticEnergy Gammafilter7528 2.7568359375
2.7572021484375 MeV gamma
/score/quantity/nOfSecondary
NStepGamma2.7572021484375MeV_2.757568359375MeV
/score/filter/particleWithKineticEnergy Gammafilter7529 2.7572021484375
2.757568359375 MeV gamma
/score/quantity/nOfSecondary
NStepGamma2.757568359375MeV_2.7579345703125MeV
/score/filter/particleWithKineticEnergy Gammafilter7530 2.757568359375
2.7579345703125 MeV gamma

/score/quantity/nOfSecondary
NStepGamma2.7579345703125MeV_2.75830078125MeV
/score/filter/particleWithKineticEnergy Gammafilter7531 2.7579345703125
2.75830078125 MeV gamma
/score/quantity/nOfSecondary
NStepGamma2.75830078125MeV_2.7586669921875MeV
/score/filter/particleWithKineticEnergy Gammafilter7532 2.75830078125
2.7586669921875 MeV gamma
/score/quantity/nOfSecondary
NStepGamma2.7586669921875MeV_2.759033203125MeV
/score/filter/particleWithKineticEnergy Gammafilter7533 2.7586669921875
2.759033203125 MeV gamma
/score/quantity/nOfSecondary
NStepGamma2.759033203125MeV_2.7593994140625MeV
/score/filter/particleWithKineticEnergy Gammafilter7534 2.759033203125
2.7593994140625 MeV gamma
/score/quantity/nOfSecondary
NStepGamma2.7593994140625MeV_2.759765625MeV
/score/filter/particleWithKineticEnergy Gammafilter7535 2.7593994140625
2.759765625 MeV gamma
/score/quantity/nOfSecondary
NStepGamma2.759765625MeV_2.7601318359375MeV
/score/filter/particleWithKineticEnergy Gammafilter7536 2.759765625
2.7601318359375 MeV gamma
/score/quantity/nOfSecondary
NStepGamma2.7601318359375MeV_2.760498046875MeV
/score/filter/particleWithKineticEnergy Gammafilter7537 2.7601318359375
2.760498046875 MeV gamma
/score/quantity/nOfSecondary
NStepGamma2.760498046875MeV_2.7608642578125MeV
/score/filter/particleWithKineticEnergy Gammafilter7538 2.760498046875
2.7608642578125 MeV gamma
/score/quantity/nOfSecondary
NStepGamma2.7608642578125MeV_2.76123046875MeV
/score/filter/particleWithKineticEnergy Gammafilter7539 2.7608642578125
2.76123046875 MeV gamma
/score/quantity/nOfSecondary
NStepGamma2.76123046875MeV_2.7615966796875MeV
/score/filter/particleWithKineticEnergy Gammafilter7540 2.76123046875
2.7615966796875 MeV gamma
/score/quantity/nOfSecondary
NStepGamma2.7615966796875MeV_2.761962890625MeV
/score/filter/particleWithKineticEnergy Gammafilter7541 2.7615966796875
2.761962890625 MeV gamma

/score/quantity/nOfSecondary
NStepGamma2.761962890625MeV_2.7623291015625MeV
/score/filter/particleWithKineticEnergy Gammafilter7542 2.761962890625
2.7623291015625 MeV gamma
/score/quantity/nOfSecondary
NStepGamma2.7623291015625MeV_2.7626953125MeV
/score/filter/particleWithKineticEnergy Gammafilter7543 2.7623291015625
2.7626953125 MeV gamma
/score/quantity/nOfSecondary
NStepGamma2.7626953125MeV_2.7630615234375MeV
/score/filter/particleWithKineticEnergy Gammafilter7544 2.7626953125
2.7630615234375 MeV gamma
/score/quantity/nOfSecondary
NStepGamma2.7630615234375MeV_2.763427734375MeV
/score/filter/particleWithKineticEnergy Gammafilter7545 2.7630615234375
2.763427734375 MeV gamma
/score/quantity/nOfSecondary
NStepGamma2.763427734375MeV_2.7637939453125MeV
/score/filter/particleWithKineticEnergy Gammafilter7546 2.763427734375
2.7637939453125 MeV gamma
/score/quantity/nOfSecondary
NStepGamma2.7637939453125MeV_2.76416015625MeV
/score/filter/particleWithKineticEnergy Gammafilter7547 2.7637939453125
2.76416015625 MeV gamma
/score/quantity/nOfSecondary
NStepGamma2.76416015625MeV_2.7645263671875MeV
/score/filter/particleWithKineticEnergy Gammafilter7548 2.76416015625
2.7645263671875 MeV gamma
/score/quantity/nOfSecondary
NStepGamma2.7645263671875MeV_2.764892578125MeV
/score/filter/particleWithKineticEnergy Gammafilter7549 2.7645263671875
2.764892578125 MeV gamma
/score/quantity/nOfSecondary
NStepGamma2.764892578125MeV_2.7652587890625MeV
/score/filter/particleWithKineticEnergy Gammafilter7550 2.764892578125
2.7652587890625 MeV gamma
/score/quantity/nOfSecondary
NStepGamma2.7652587890625MeV_2.765625MeV
/score/filter/particleWithKineticEnergy Gammafilter7551 2.7652587890625
2.765625 MeV gamma
/score/quantity/nOfSecondary
NStepGamma2.765625MeV_2.7659912109375MeV
/score/filter/particleWithKineticEnergy Gammafilter7552 2.765625
2.7659912109375 MeV gamma

/score/quantity/nOfSecondary
NStepGamma2.7659912109375MeV_2.766357421875MeV
/score/filter/particleWithKineticEnergy Gammafilter7553 2.7659912109375
2.766357421875 MeV gamma
/score/quantity/nOfSecondary
NStepGamma2.766357421875MeV_2.7667236328125MeV
/score/filter/particleWithKineticEnergy Gammafilter7554 2.766357421875
2.7667236328125 MeV gamma
/score/quantity/nOfSecondary
NStepGamma2.7667236328125MeV_2.76708984375MeV
/score/filter/particleWithKineticEnergy Gammafilter7555 2.7667236328125
2.76708984375 MeV gamma
/score/quantity/nOfSecondary
NStepGamma2.76708984375MeV_2.7674560546875MeV
/score/filter/particleWithKineticEnergy Gammafilter7556 2.76708984375
2.7674560546875 MeV gamma
/score/quantity/nOfSecondary
NStepGamma2.7674560546875MeV_2.767822265625MeV
/score/filter/particleWithKineticEnergy Gammafilter7557 2.7674560546875
2.767822265625 MeV gamma
/score/quantity/nOfSecondary
NStepGamma2.767822265625MeV_2.7681884765625MeV
/score/filter/particleWithKineticEnergy Gammafilter7558 2.767822265625
2.7681884765625 MeV gamma
/score/quantity/nOfSecondary
NStepGamma2.7681884765625MeV_2.7685546875MeV
/score/filter/particleWithKineticEnergy Gammafilter7559 2.7681884765625
2.7685546875 MeV gamma
/score/quantity/nOfSecondary
NStepGamma2.7685546875MeV_2.7689208984375MeV
/score/filter/particleWithKineticEnergy Gammafilter7560 2.7685546875
2.7689208984375 MeV gamma
/score/quantity/nOfSecondary
NStepGamma2.7689208984375MeV_2.769287109375MeV
/score/filter/particleWithKineticEnergy Gammafilter7561 2.7689208984375
2.769287109375 MeV gamma
/score/quantity/nOfSecondary
NStepGamma2.769287109375MeV_2.7696533203125MeV
/score/filter/particleWithKineticEnergy Gammafilter7562 2.769287109375
2.7696533203125 MeV gamma
/score/quantity/nOfSecondary
NStepGamma2.7696533203125MeV_2.77001953125MeV
/score/filter/particleWithKineticEnergy Gammafilter7563 2.7696533203125
2.77001953125 MeV gamma

/score/quantity/nOfSecondary
NStepGamma2.77001953125MeV_2.7703857421875MeV
/score/filter/particleWithKineticEnergy Gammafilter7564 2.77001953125
2.7703857421875 MeV gamma
/score/quantity/nOfSecondary
NStepGamma2.7703857421875MeV_2.770751953125MeV
/score/filter/particleWithKineticEnergy Gammafilter7565 2.7703857421875
2.770751953125 MeV gamma
/score/quantity/nOfSecondary
NStepGamma2.770751953125MeV_2.7711181640625MeV
/score/filter/particleWithKineticEnergy Gammafilter7566 2.770751953125
2.7711181640625 MeV gamma
/score/quantity/nOfSecondary
NStepGamma2.7711181640625MeV_2.771484375MeV
/score/filter/particleWithKineticEnergy Gammafilter7567 2.7711181640625
2.771484375 MeV gamma
/score/quantity/nOfSecondary
NStepGamma2.771484375MeV_2.7718505859375MeV
/score/filter/particleWithKineticEnergy Gammafilter7568 2.771484375
2.7718505859375 MeV gamma
/score/quantity/nOfSecondary
NStepGamma2.7718505859375MeV_2.772216796875MeV
/score/filter/particleWithKineticEnergy Gammafilter7569 2.7718505859375
2.772216796875 MeV gamma
/score/quantity/nOfSecondary
NStepGamma2.772216796875MeV_2.7725830078125MeV
/score/filter/particleWithKineticEnergy Gammafilter7570 2.772216796875
2.7725830078125 MeV gamma
/score/quantity/nOfSecondary
NStepGamma2.7725830078125MeV_2.77294921875MeV
/score/filter/particleWithKineticEnergy Gammafilter7571 2.7725830078125
2.77294921875 MeV gamma
/score/quantity/nOfSecondary
NStepGamma2.77294921875MeV_2.7733154296875MeV
/score/filter/particleWithKineticEnergy Gammafilter7572 2.77294921875
2.7733154296875 MeV gamma
/score/quantity/nOfSecondary
NStepGamma2.7733154296875MeV_2.773681640625MeV
/score/filter/particleWithKineticEnergy Gammafilter7573 2.7733154296875
2.773681640625 MeV gamma
/score/quantity/nOfSecondary
NStepGamma2.773681640625MeV_2.7740478515625MeV
/score/filter/particleWithKineticEnergy Gammafilter7574 2.773681640625
2.7740478515625 MeV gamma

/score/quantity/nOfSecondary
NStepGamma2.7740478515625MeV_2.7744140625MeV
/score/filter/particleWithKineticEnergy Gammafilter7575 2.7740478515625
2.7744140625 MeV gamma
/score/quantity/nOfSecondary
NStepGamma2.7744140625MeV_2.7747802734375MeV
/score/filter/particleWithKineticEnergy Gammafilter7576 2.7744140625
2.7747802734375 MeV gamma
/score/quantity/nOfSecondary
NStepGamma2.7747802734375MeV_2.775146484375MeV
/score/filter/particleWithKineticEnergy Gammafilter7577 2.7747802734375
2.775146484375 MeV gamma
/score/quantity/nOfSecondary
NStepGamma2.775146484375MeV_2.7755126953125MeV
/score/filter/particleWithKineticEnergy Gammafilter7578 2.775146484375
2.7755126953125 MeV gamma
/score/quantity/nOfSecondary
NStepGamma2.7755126953125MeV_2.77587890625MeV
/score/filter/particleWithKineticEnergy Gammafilter7579 2.7755126953125
2.77587890625 MeV gamma
/score/quantity/nOfSecondary
NStepGamma2.77587890625MeV_2.7762451171875MeV
/score/filter/particleWithKineticEnergy Gammafilter7580 2.77587890625
2.7762451171875 MeV gamma
/score/quantity/nOfSecondary
NStepGamma2.7762451171875MeV_2.776611328125MeV
/score/filter/particleWithKineticEnergy Gammafilter7581 2.7762451171875
2.776611328125 MeV gamma
/score/quantity/nOfSecondary
NStepGamma2.776611328125MeV_2.7769775390625MeV
/score/filter/particleWithKineticEnergy Gammafilter7582 2.776611328125
2.7769775390625 MeV gamma
/score/quantity/nOfSecondary
NStepGamma2.7769775390625MeV_2.77734375MeV
/score/filter/particleWithKineticEnergy Gammafilter7583 2.7769775390625
2.77734375 MeV gamma
/score/quantity/nOfSecondary
NStepGamma2.77734375MeV_2.7777099609375MeV
/score/filter/particleWithKineticEnergy Gammafilter7584 2.77734375
2.7777099609375 MeV gamma
/score/quantity/nOfSecondary
NStepGamma2.7777099609375MeV_2.778076171875MeV
/score/filter/particleWithKineticEnergy Gammafilter7585 2.7777099609375
2.778076171875 MeV gamma

/score/quantity/nOfSecondary
NStepGamma2.778076171875MeV_2.7784423828125MeV
/score/filter/particleWithKineticEnergy Gammafilter7586 2.778076171875
2.7784423828125 MeV gamma
/score/quantity/nOfSecondary
NStepGamma2.7784423828125MeV_2.77880859375MeV
/score/filter/particleWithKineticEnergy Gammafilter7587 2.7784423828125
2.77880859375 MeV gamma
/score/quantity/nOfSecondary
NStepGamma2.77880859375MeV_2.7791748046875MeV
/score/filter/particleWithKineticEnergy Gammafilter7588 2.77880859375
2.7791748046875 MeV gamma
/score/quantity/nOfSecondary
NStepGamma2.7791748046875MeV_2.779541015625MeV
/score/filter/particleWithKineticEnergy Gammafilter7589 2.7791748046875
2.779541015625 MeV gamma
/score/quantity/nOfSecondary
NStepGamma2.779541015625MeV_2.7799072265625MeV
/score/filter/particleWithKineticEnergy Gammafilter7590 2.779541015625
2.7799072265625 MeV gamma
/score/quantity/nOfSecondary
NStepGamma2.7799072265625MeV_2.7802734375MeV
/score/filter/particleWithKineticEnergy Gammafilter7591 2.7799072265625
2.7802734375 MeV gamma
/score/quantity/nOfSecondary
NStepGamma2.7802734375MeV_2.7806396484375MeV
/score/filter/particleWithKineticEnergy Gammafilter7592 2.7802734375
2.7806396484375 MeV gamma
/score/quantity/nOfSecondary
NStepGamma2.7806396484375MeV_2.781005859375MeV
/score/filter/particleWithKineticEnergy Gammafilter7593 2.7806396484375
2.781005859375 MeV gamma
/score/quantity/nOfSecondary
NStepGamma2.781005859375MeV_2.7813720703125MeV
/score/filter/particleWithKineticEnergy Gammafilter7594 2.781005859375
2.7813720703125 MeV gamma
/score/quantity/nOfSecondary
NStepGamma2.7813720703125MeV_2.78173828125MeV
/score/filter/particleWithKineticEnergy Gammafilter7595 2.7813720703125
2.78173828125 MeV gamma
/score/quantity/nOfSecondary
NStepGamma2.78173828125MeV_2.7821044921875MeV
/score/filter/particleWithKineticEnergy Gammafilter7596 2.78173828125
2.7821044921875 MeV gamma

/score/quantity/nOfSecondary
NStepGamma2.7821044921875MeV_2.782470703125MeV
/score/filter/particleWithKineticEnergy Gammafilter7597 2.7821044921875
2.782470703125 MeV gamma
/score/quantity/nOfSecondary
NStepGamma2.782470703125MeV_2.7828369140625MeV
/score/filter/particleWithKineticEnergy Gammafilter7598 2.782470703125
2.7828369140625 MeV gamma
/score/quantity/nOfSecondary
NStepGamma2.7828369140625MeV_2.783203125MeV
/score/filter/particleWithKineticEnergy Gammafilter7599 2.7828369140625
2.783203125 MeV gamma
/score/quantity/nOfSecondary
NStepGamma2.783203125MeV_2.7835693359375MeV
/score/filter/particleWithKineticEnergy Gammafilter7600 2.783203125
2.7835693359375 MeV gamma
/score/quantity/nOfSecondary
NStepGamma2.7835693359375MeV_2.783935546875MeV
/score/filter/particleWithKineticEnergy Gammafilter7601 2.7835693359375
2.783935546875 MeV gamma
/score/quantity/nOfSecondary
NStepGamma2.783935546875MeV_2.7843017578125MeV
/score/filter/particleWithKineticEnergy Gammafilter7602 2.783935546875
2.7843017578125 MeV gamma
/score/quantity/nOfSecondary
NStepGamma2.7843017578125MeV_2.78466796875MeV
/score/filter/particleWithKineticEnergy Gammafilter7603 2.7843017578125
2.78466796875 MeV gamma
/score/quantity/nOfSecondary
NStepGamma2.78466796875MeV_2.7850341796875MeV
/score/filter/particleWithKineticEnergy Gammafilter7604 2.78466796875
2.7850341796875 MeV gamma
/score/quantity/nOfSecondary
NStepGamma2.7850341796875MeV_2.785400390625MeV
/score/filter/particleWithKineticEnergy Gammafilter7605 2.7850341796875
2.785400390625 MeV gamma
/score/quantity/nOfSecondary
NStepGamma2.785400390625MeV_2.7857666015625MeV
/score/filter/particleWithKineticEnergy Gammafilter7606 2.785400390625
2.7857666015625 MeV gamma
/score/quantity/nOfSecondary
NStepGamma2.7857666015625MeV_2.7861328125MeV
/score/filter/particleWithKineticEnergy Gammafilter7607 2.7857666015625
2.7861328125 MeV gamma

/score/quantity/nOfSecondary
NStepGamma2.7861328125MeV_2.7864990234375MeV
/score/filter/particleWithKineticEnergy Gammafilter7608 2.7861328125
2.7864990234375 MeV gamma
/score/quantity/nOfSecondary
NStepGamma2.7864990234375MeV_2.786865234375MeV
/score/filter/particleWithKineticEnergy Gammafilter7609 2.7864990234375
2.786865234375 MeV gamma
/score/quantity/nOfSecondary
NStepGamma2.786865234375MeV_2.7872314453125MeV
/score/filter/particleWithKineticEnergy Gammafilter7610 2.786865234375
2.7872314453125 MeV gamma
/score/quantity/nOfSecondary
NStepGamma2.7872314453125MeV_2.78759765625MeV
/score/filter/particleWithKineticEnergy Gammafilter7611 2.7872314453125
2.78759765625 MeV gamma
/score/quantity/nOfSecondary
NStepGamma2.78759765625MeV_2.7879638671875MeV
/score/filter/particleWithKineticEnergy Gammafilter7612 2.78759765625
2.7879638671875 MeV gamma
/score/quantity/nOfSecondary
NStepGamma2.7879638671875MeV_2.788330078125MeV
/score/filter/particleWithKineticEnergy Gammafilter7613 2.7879638671875
2.788330078125 MeV gamma
/score/quantity/nOfSecondary
NStepGamma2.788330078125MeV_2.7886962890625MeV
/score/filter/particleWithKineticEnergy Gammafilter7614 2.788330078125
2.7886962890625 MeV gamma
/score/quantity/nOfSecondary
NStepGamma2.7886962890625MeV_2.7890625MeV
/score/filter/particleWithKineticEnergy Gammafilter7615 2.7886962890625
2.7890625 MeV gamma
/score/quantity/nOfSecondary
NStepGamma2.7890625MeV_2.7894287109375MeV
/score/filter/particleWithKineticEnergy Gammafilter7616 2.7890625
2.7894287109375 MeV gamma
/score/quantity/nOfSecondary
NStepGamma2.7894287109375MeV_2.789794921875MeV
/score/filter/particleWithKineticEnergy Gammafilter7617 2.7894287109375
2.789794921875 MeV gamma
/score/quantity/nOfSecondary
NStepGamma2.789794921875MeV_2.7901611328125MeV
/score/filter/particleWithKineticEnergy Gammafilter7618 2.789794921875
2.7901611328125 MeV gamma

/score/quantity/nOfSecondary
NStepGamma2.7901611328125MeV_2.79052734375MeV
/score/filter/particleWithKineticEnergy Gammafilter7619 2.7901611328125
2.79052734375 MeV gamma
/score/quantity/nOfSecondary
NStepGamma2.79052734375MeV_2.7908935546875MeV
/score/filter/particleWithKineticEnergy Gammafilter7620 2.79052734375
2.7908935546875 MeV gamma
/score/quantity/nOfSecondary
NStepGamma2.7908935546875MeV_2.791259765625MeV
/score/filter/particleWithKineticEnergy Gammafilter7621 2.7908935546875
2.791259765625 MeV gamma
/score/quantity/nOfSecondary
NStepGamma2.791259765625MeV_2.7916259765625MeV
/score/filter/particleWithKineticEnergy Gammafilter7622 2.791259765625
2.7916259765625 MeV gamma
/score/quantity/nOfSecondary
NStepGamma2.7916259765625MeV_2.7919921875MeV
/score/filter/particleWithKineticEnergy Gammafilter7623 2.7916259765625
2.7919921875 MeV gamma
/score/quantity/nOfSecondary
NStepGamma2.7919921875MeV_2.7923583984375MeV
/score/filter/particleWithKineticEnergy Gammafilter7624 2.7919921875
2.7923583984375 MeV gamma
/score/quantity/nOfSecondary
NStepGamma2.7923583984375MeV_2.792724609375MeV
/score/filter/particleWithKineticEnergy Gammafilter7625 2.7923583984375
2.792724609375 MeV gamma
/score/quantity/nOfSecondary
NStepGamma2.792724609375MeV_2.7930908203125MeV
/score/filter/particleWithKineticEnergy Gammafilter7626 2.792724609375
2.7930908203125 MeV gamma
/score/quantity/nOfSecondary
NStepGamma2.7930908203125MeV_2.79345703125MeV
/score/filter/particleWithKineticEnergy Gammafilter7627 2.7930908203125
2.79345703125 MeV gamma
/score/quantity/nOfSecondary
NStepGamma2.79345703125MeV_2.7938232421875MeV
/score/filter/particleWithKineticEnergy Gammafilter7628 2.79345703125
2.7938232421875 MeV gamma
/score/quantity/nOfSecondary
NStepGamma2.7938232421875MeV_2.794189453125MeV
/score/filter/particleWithKineticEnergy Gammafilter7629 2.7938232421875
2.794189453125 MeV gamma

/score/quantity/nOfSecondary
NStepGamma2.794189453125MeV_2.7945556640625MeV
/score/filter/particleWithKineticEnergy Gammafilter7630 2.794189453125
2.7945556640625 MeV gamma
/score/quantity/nOfSecondary
NStepGamma2.7945556640625MeV_2.794921875MeV
/score/filter/particleWithKineticEnergy Gammafilter7631 2.7945556640625
2.794921875 MeV gamma
/score/quantity/nOfSecondary
NStepGamma2.794921875MeV_2.7952880859375MeV
/score/filter/particleWithKineticEnergy Gammafilter7632 2.794921875
2.7952880859375 MeV gamma
/score/quantity/nOfSecondary
NStepGamma2.7952880859375MeV_2.795654296875MeV
/score/filter/particleWithKineticEnergy Gammafilter7633 2.7952880859375
2.795654296875 MeV gamma
/score/quantity/nOfSecondary
NStepGamma2.795654296875MeV_2.7960205078125MeV
/score/filter/particleWithKineticEnergy Gammafilter7634 2.795654296875
2.7960205078125 MeV gamma
/score/quantity/nOfSecondary
NStepGamma2.7960205078125MeV_2.79638671875MeV
/score/filter/particleWithKineticEnergy Gammafilter7635 2.7960205078125
2.79638671875 MeV gamma
/score/quantity/nOfSecondary
NStepGamma2.79638671875MeV_2.7967529296875MeV
/score/filter/particleWithKineticEnergy Gammafilter7636 2.79638671875
2.7967529296875 MeV gamma
/score/quantity/nOfSecondary
NStepGamma2.7967529296875MeV_2.797119140625MeV
/score/filter/particleWithKineticEnergy Gammafilter7637 2.7967529296875
2.797119140625 MeV gamma
/score/quantity/nOfSecondary
NStepGamma2.797119140625MeV_2.7974853515625MeV
/score/filter/particleWithKineticEnergy Gammafilter7638 2.797119140625
2.7974853515625 MeV gamma
/score/quantity/nOfSecondary
NStepGamma2.7974853515625MeV_2.7978515625MeV
/score/filter/particleWithKineticEnergy Gammafilter7639 2.7974853515625
2.7978515625 MeV gamma
/score/quantity/nOfSecondary
NStepGamma2.7978515625MeV_2.7982177734375MeV
/score/filter/particleWithKineticEnergy Gammafilter7640 2.7978515625
2.7982177734375 MeV gamma

/score/quantity/nOfSecondary
NStepGamma2.7982177734375MeV_2.798583984375MeV
/score/filter/particleWithKineticEnergy Gammafilter7641 2.7982177734375
2.798583984375 MeV gamma
/score/quantity/nOfSecondary
NStepGamma2.798583984375MeV_2.7989501953125MeV
/score/filter/particleWithKineticEnergy Gammafilter7642 2.798583984375
2.7989501953125 MeV gamma
/score/quantity/nOfSecondary
NStepGamma2.7989501953125MeV_2.79931640625MeV
/score/filter/particleWithKineticEnergy Gammafilter7643 2.7989501953125
2.79931640625 MeV gamma
/score/quantity/nOfSecondary
NStepGamma2.79931640625MeV_2.7996826171875MeV
/score/filter/particleWithKineticEnergy Gammafilter7644 2.79931640625
2.7996826171875 MeV gamma
/score/quantity/nOfSecondary
NStepGamma2.7996826171875MeV_2.800048828125MeV
/score/filter/particleWithKineticEnergy Gammafilter7645 2.7996826171875
2.800048828125 MeV gamma
/score/quantity/nOfSecondary
NStepGamma2.800048828125MeV_2.8004150390625MeV
/score/filter/particleWithKineticEnergy Gammafilter7646 2.800048828125
2.8004150390625 MeV gamma
/score/quantity/nOfSecondary
NStepGamma2.8004150390625MeV_2.80078125MeV
/score/filter/particleWithKineticEnergy Gammafilter7647 2.8004150390625
2.80078125 MeV gamma
/score/quantity/nOfSecondary
NStepGamma2.80078125MeV_2.8011474609375MeV
/score/filter/particleWithKineticEnergy Gammafilter7648 2.80078125
2.8011474609375 MeV gamma
/score/quantity/nOfSecondary
NStepGamma2.8011474609375MeV_2.801513671875MeV
/score/filter/particleWithKineticEnergy Gammafilter7649 2.8011474609375
2.801513671875 MeV gamma
/score/quantity/nOfSecondary
NStepGamma2.801513671875MeV_2.8018798828125MeV
/score/filter/particleWithKineticEnergy Gammafilter7650 2.801513671875
2.8018798828125 MeV gamma
/score/quantity/nOfSecondary
NStepGamma2.8018798828125MeV_2.80224609375MeV
/score/filter/particleWithKineticEnergy Gammafilter7651 2.8018798828125
2.80224609375 MeV gamma

/score/quantity/nOfSecondary
NStepGamma2.80224609375MeV_2.8026123046875MeV
/score/filter/particleWithKineticEnergy Gammafilter7652 2.80224609375
2.8026123046875 MeV gamma
/score/quantity/nOfSecondary
NStepGamma2.8026123046875MeV_2.802978515625MeV
/score/filter/particleWithKineticEnergy Gammafilter7653 2.8026123046875
2.802978515625 MeV gamma
/score/quantity/nOfSecondary
NStepGamma2.802978515625MeV_2.8033447265625MeV
/score/filter/particleWithKineticEnergy Gammafilter7654 2.802978515625
2.8033447265625 MeV gamma
/score/quantity/nOfSecondary
NStepGamma2.8033447265625MeV_2.8037109375MeV
/score/filter/particleWithKineticEnergy Gammafilter7655 2.8033447265625
2.8037109375 MeV gamma
/score/quantity/nOfSecondary
NStepGamma2.8037109375MeV_2.8040771484375MeV
/score/filter/particleWithKineticEnergy Gammafilter7656 2.8037109375
2.8040771484375 MeV gamma
/score/quantity/nOfSecondary
NStepGamma2.8040771484375MeV_2.804443359375MeV
/score/filter/particleWithKineticEnergy Gammafilter7657 2.8040771484375
2.804443359375 MeV gamma
/score/quantity/nOfSecondary
NStepGamma2.804443359375MeV_2.8048095703125MeV
/score/filter/particleWithKineticEnergy Gammafilter7658 2.804443359375
2.8048095703125 MeV gamma
/score/quantity/nOfSecondary
NStepGamma2.8048095703125MeV_2.80517578125MeV
/score/filter/particleWithKineticEnergy Gammafilter7659 2.8048095703125
2.80517578125 MeV gamma
/score/quantity/nOfSecondary
NStepGamma2.80517578125MeV_2.8055419921875MeV
/score/filter/particleWithKineticEnergy Gammafilter7660 2.80517578125
2.8055419921875 MeV gamma
/score/quantity/nOfSecondary
NStepGamma2.8055419921875MeV_2.805908203125MeV
/score/filter/particleWithKineticEnergy Gammafilter7661 2.8055419921875
2.805908203125 MeV gamma
/score/quantity/nOfSecondary
NStepGamma2.805908203125MeV_2.8062744140625MeV
/score/filter/particleWithKineticEnergy Gammafilter7662 2.805908203125
2.8062744140625 MeV gamma

/score/quantity/nOfSecondary
NStepGamma2.8062744140625MeV_2.806640625MeV
/score/filter/particleWithKineticEnergy Gammafilter7663 2.8062744140625
2.806640625 MeV gamma
/score/quantity/nOfSecondary
NStepGamma2.806640625MeV_2.8070068359375MeV
/score/filter/particleWithKineticEnergy Gammafilter7664 2.806640625
2.8070068359375 MeV gamma
/score/quantity/nOfSecondary
NStepGamma2.8070068359375MeV_2.807373046875MeV
/score/filter/particleWithKineticEnergy Gammafilter7665 2.8070068359375
2.807373046875 MeV gamma
/score/quantity/nOfSecondary
NStepGamma2.807373046875MeV_2.8077392578125MeV
/score/filter/particleWithKineticEnergy Gammafilter7666 2.807373046875
2.8077392578125 MeV gamma
/score/quantity/nOfSecondary
NStepGamma2.8077392578125MeV_2.80810546875MeV
/score/filter/particleWithKineticEnergy Gammafilter7667 2.8077392578125
2.80810546875 MeV gamma
/score/quantity/nOfSecondary
NStepGamma2.80810546875MeV_2.8084716796875MeV
/score/filter/particleWithKineticEnergy Gammafilter7668 2.80810546875
2.8084716796875 MeV gamma
/score/quantity/nOfSecondary
NStepGamma2.8084716796875MeV_2.808837890625MeV
/score/filter/particleWithKineticEnergy Gammafilter7669 2.8084716796875
2.808837890625 MeV gamma
/score/quantity/nOfSecondary
NStepGamma2.808837890625MeV_2.8092041015625MeV
/score/filter/particleWithKineticEnergy Gammafilter7670 2.808837890625
2.8092041015625 MeV gamma
/score/quantity/nOfSecondary
NStepGamma2.8092041015625MeV_2.8095703125MeV
/score/filter/particleWithKineticEnergy Gammafilter7671 2.8092041015625
2.8095703125 MeV gamma
/score/quantity/nOfSecondary
NStepGamma2.8095703125MeV_2.8099365234375MeV
/score/filter/particleWithKineticEnergy Gammafilter7672 2.8095703125
2.8099365234375 MeV gamma
/score/quantity/nOfSecondary
NStepGamma2.8099365234375MeV_2.810302734375MeV
/score/filter/particleWithKineticEnergy Gammafilter7673 2.8099365234375
2.810302734375 MeV gamma

/score/quantity/nOfSecondary
NStepGamma2.810302734375MeV_2.8106689453125MeV
/score/filter/particleWithKineticEnergy Gammafilter7674 2.810302734375
2.8106689453125 MeV gamma
/score/quantity/nOfSecondary
NStepGamma2.8106689453125MeV_2.81103515625MeV
/score/filter/particleWithKineticEnergy Gammafilter7675 2.8106689453125
2.81103515625 MeV gamma
/score/quantity/nOfSecondary
NStepGamma2.81103515625MeV_2.8114013671875MeV
/score/filter/particleWithKineticEnergy Gammafilter7676 2.81103515625
2.8114013671875 MeV gamma
/score/quantity/nOfSecondary
NStepGamma2.8114013671875MeV_2.811767578125MeV
/score/filter/particleWithKineticEnergy Gammafilter7677 2.8114013671875
2.811767578125 MeV gamma
/score/quantity/nOfSecondary
NStepGamma2.811767578125MeV_2.8121337890625MeV
/score/filter/particleWithKineticEnergy Gammafilter7678 2.811767578125
2.8121337890625 MeV gamma
/score/quantity/nOfSecondary
NStepGamma2.8121337890625MeV_2.8125MeV
/score/filter/particleWithKineticEnergy Gammafilter7679 2.8121337890625
2.8125 MeV gamma
/score/quantity/nOfSecondary
NStepGamma2.8125MeV_2.8128662109375MeV
/score/filter/particleWithKineticEnergy Gammafilter7680 2.8125
2.8128662109375 MeV gamma
/score/quantity/nOfSecondary
NStepGamma2.8128662109375MeV_2.813232421875MeV
/score/filter/particleWithKineticEnergy Gammafilter7681 2.8128662109375
2.813232421875 MeV gamma
/score/quantity/nOfSecondary
NStepGamma2.813232421875MeV_2.8135986328125MeV
/score/filter/particleWithKineticEnergy Gammafilter7682 2.813232421875
2.8135986328125 MeV gamma
/score/quantity/nOfSecondary
NStepGamma2.8135986328125MeV_2.81396484375MeV
/score/filter/particleWithKineticEnergy Gammafilter7683 2.8135986328125
2.81396484375 MeV gamma
/score/quantity/nOfSecondary
NStepGamma2.81396484375MeV_2.8143310546875MeV
/score/filter/particleWithKineticEnergy Gammafilter7684 2.81396484375
2.8143310546875 MeV gamma

/score/quantity/nOfSecondary
NStepGamma2.8143310546875MeV_2.814697265625MeV
/score/filter/particleWithKineticEnergy Gammafilter7685 2.8143310546875
2.814697265625 MeV gamma
/score/quantity/nOfSecondary
NStepGamma2.814697265625MeV_2.8150634765625MeV
/score/filter/particleWithKineticEnergy Gammafilter7686 2.814697265625
2.8150634765625 MeV gamma
/score/quantity/nOfSecondary
NStepGamma2.8150634765625MeV_2.8154296875MeV
/score/filter/particleWithKineticEnergy Gammafilter7687 2.8150634765625
2.8154296875 MeV gamma
/score/quantity/nOfSecondary
NStepGamma2.8154296875MeV_2.8157958984375MeV
/score/filter/particleWithKineticEnergy Gammafilter7688 2.8154296875
2.8157958984375 MeV gamma
/score/quantity/nOfSecondary
NStepGamma2.8157958984375MeV_2.816162109375MeV
/score/filter/particleWithKineticEnergy Gammafilter7689 2.8157958984375
2.816162109375 MeV gamma
/score/quantity/nOfSecondary
NStepGamma2.816162109375MeV_2.8165283203125MeV
/score/filter/particleWithKineticEnergy Gammafilter7690 2.816162109375
2.8165283203125 MeV gamma
/score/quantity/nOfSecondary
NStepGamma2.8165283203125MeV_2.81689453125MeV
/score/filter/particleWithKineticEnergy Gammafilter7691 2.8165283203125
2.81689453125 MeV gamma
/score/quantity/nOfSecondary
NStepGamma2.81689453125MeV_2.8172607421875MeV
/score/filter/particleWithKineticEnergy Gammafilter7692 2.81689453125
2.8172607421875 MeV gamma
/score/quantity/nOfSecondary
NStepGamma2.8172607421875MeV_2.817626953125MeV
/score/filter/particleWithKineticEnergy Gammafilter7693 2.8172607421875
2.817626953125 MeV gamma
/score/quantity/nOfSecondary
NStepGamma2.817626953125MeV_2.8179931640625MeV
/score/filter/particleWithKineticEnergy Gammafilter7694 2.817626953125
2.8179931640625 MeV gamma
/score/quantity/nOfSecondary
NStepGamma2.8179931640625MeV_2.818359375MeV
/score/filter/particleWithKineticEnergy Gammafilter7695 2.8179931640625
2.818359375 MeV gamma

/score/quantity/nOfSecondary
NStepGamma2.818359375MeV_2.8187255859375MeV
/score/filter/particleWithKineticEnergy Gammafilter7696 2.818359375
2.8187255859375 MeV gamma
/score/quantity/nOfSecondary
NStepGamma2.8187255859375MeV_2.819091796875MeV
/score/filter/particleWithKineticEnergy Gammafilter7697 2.8187255859375
2.819091796875 MeV gamma
/score/quantity/nOfSecondary
NStepGamma2.819091796875MeV_2.8194580078125MeV
/score/filter/particleWithKineticEnergy Gammafilter7698 2.819091796875
2.8194580078125 MeV gamma
/score/quantity/nOfSecondary
NStepGamma2.8194580078125MeV_2.81982421875MeV
/score/filter/particleWithKineticEnergy Gammafilter7699 2.8194580078125
2.81982421875 MeV gamma
/score/quantity/nOfSecondary
NStepGamma2.81982421875MeV_2.8201904296875MeV
/score/filter/particleWithKineticEnergy Gammafilter7700 2.81982421875
2.8201904296875 MeV gamma
/score/quantity/nOfSecondary
NStepGamma2.8201904296875MeV_2.820556640625MeV
/score/filter/particleWithKineticEnergy Gammafilter7701 2.8201904296875
2.820556640625 MeV gamma
/score/quantity/nOfSecondary
NStepGamma2.820556640625MeV_2.8209228515625MeV
/score/filter/particleWithKineticEnergy Gammafilter7702 2.820556640625
2.8209228515625 MeV gamma
/score/quantity/nOfSecondary
NStepGamma2.8209228515625MeV_2.8212890625MeV
/score/filter/particleWithKineticEnergy Gammafilter7703 2.8209228515625
2.8212890625 MeV gamma
/score/quantity/nOfSecondary
NStepGamma2.8212890625MeV_2.8216552734375MeV
/score/filter/particleWithKineticEnergy Gammafilter7704 2.8212890625
2.8216552734375 MeV gamma
/score/quantity/nOfSecondary
NStepGamma2.8216552734375MeV_2.822021484375MeV
/score/filter/particleWithKineticEnergy Gammafilter7705 2.8216552734375
2.822021484375 MeV gamma
/score/quantity/nOfSecondary
NStepGamma2.822021484375MeV_2.8223876953125MeV
/score/filter/particleWithKineticEnergy Gammafilter7706 2.822021484375
2.8223876953125 MeV gamma

/score/quantity/nOfSecondary
NStepGamma2.8223876953125MeV_2.82275390625MeV
/score/filter/particleWithKineticEnergy Gammafilter7707 2.8223876953125
2.82275390625 MeV gamma
/score/quantity/nOfSecondary
NStepGamma2.82275390625MeV_2.8231201171875MeV
/score/filter/particleWithKineticEnergy Gammafilter7708 2.82275390625
2.8231201171875 MeV gamma
/score/quantity/nOfSecondary
NStepGamma2.8231201171875MeV_2.823486328125MeV
/score/filter/particleWithKineticEnergy Gammafilter7709 2.8231201171875
2.823486328125 MeV gamma
/score/quantity/nOfSecondary
NStepGamma2.823486328125MeV_2.8238525390625MeV
/score/filter/particleWithKineticEnergy Gammafilter7710 2.823486328125
2.8238525390625 MeV gamma
/score/quantity/nOfSecondary
NStepGamma2.8238525390625MeV_2.82421875MeV
/score/filter/particleWithKineticEnergy Gammafilter7711 2.8238525390625
2.82421875 MeV gamma
/score/quantity/nOfSecondary
NStepGamma2.82421875MeV_2.8245849609375MeV
/score/filter/particleWithKineticEnergy Gammafilter7712 2.82421875
2.8245849609375 MeV gamma
/score/quantity/nOfSecondary
NStepGamma2.8245849609375MeV_2.824951171875MeV
/score/filter/particleWithKineticEnergy Gammafilter7713 2.8245849609375
2.824951171875 MeV gamma
/score/quantity/nOfSecondary
NStepGamma2.824951171875MeV_2.8253173828125MeV
/score/filter/particleWithKineticEnergy Gammafilter7714 2.824951171875
2.8253173828125 MeV gamma
/score/quantity/nOfSecondary
NStepGamma2.8253173828125MeV_2.82568359375MeV
/score/filter/particleWithKineticEnergy Gammafilter7715 2.8253173828125
2.82568359375 MeV gamma
/score/quantity/nOfSecondary
NStepGamma2.82568359375MeV_2.8260498046875MeV
/score/filter/particleWithKineticEnergy Gammafilter7716 2.82568359375
2.8260498046875 MeV gamma
/score/quantity/nOfSecondary
NStepGamma2.8260498046875MeV_2.826416015625MeV
/score/filter/particleWithKineticEnergy Gammafilter7717 2.8260498046875
2.826416015625 MeV gamma

/score/quantity/nOfSecondary
NStepGamma2.826416015625MeV_2.8267822265625MeV
/score/filter/particleWithKineticEnergy Gammafilter7718 2.826416015625
2.8267822265625 MeV gamma
/score/quantity/nOfSecondary
NStepGamma2.8267822265625MeV_2.8271484375MeV
/score/filter/particleWithKineticEnergy Gammafilter7719 2.8267822265625
2.8271484375 MeV gamma
/score/quantity/nOfSecondary
NStepGamma2.8271484375MeV_2.8275146484375MeV
/score/filter/particleWithKineticEnergy Gammafilter7720 2.8271484375
2.8275146484375 MeV gamma
/score/quantity/nOfSecondary
NStepGamma2.8275146484375MeV_2.827880859375MeV
/score/filter/particleWithKineticEnergy Gammafilter7721 2.8275146484375
2.827880859375 MeV gamma
/score/quantity/nOfSecondary
NStepGamma2.827880859375MeV_2.8282470703125MeV
/score/filter/particleWithKineticEnergy Gammafilter7722 2.827880859375
2.8282470703125 MeV gamma
/score/quantity/nOfSecondary
NStepGamma2.8282470703125MeV_2.82861328125MeV
/score/filter/particleWithKineticEnergy Gammafilter7723 2.8282470703125
2.82861328125 MeV gamma
/score/quantity/nOfSecondary
NStepGamma2.82861328125MeV_2.8289794921875MeV
/score/filter/particleWithKineticEnergy Gammafilter7724 2.82861328125
2.8289794921875 MeV gamma
/score/quantity/nOfSecondary
NStepGamma2.8289794921875MeV_2.829345703125MeV
/score/filter/particleWithKineticEnergy Gammafilter7725 2.8289794921875
2.829345703125 MeV gamma
/score/quantity/nOfSecondary
NStepGamma2.829345703125MeV_2.8297119140625MeV
/score/filter/particleWithKineticEnergy Gammafilter7726 2.829345703125
2.8297119140625 MeV gamma
/score/quantity/nOfSecondary
NStepGamma2.8297119140625MeV_2.830078125MeV
/score/filter/particleWithKineticEnergy Gammafilter7727 2.8297119140625
2.830078125 MeV gamma
/score/quantity/nOfSecondary
NStepGamma2.830078125MeV_2.8304443359375MeV
/score/filter/particleWithKineticEnergy Gammafilter7728 2.830078125
2.8304443359375 MeV gamma

/score/filter/particleWithKineticEnergy Gammafilter8054 2.949462890625 2.9498291015625 MeV gamma
/score/quantity/nOfSecondary NStepGamma2.9498291015625MeV_2.9501953125MeV
/score/filter/particleWithKineticEnergy Gammafilter8055 2.9498291015625 2.9501953125 MeV gamma
/score/quantity/nOfSecondary NStepGamma2.9501953125MeV_2.9505615234375MeV
/score/filter/particleWithKineticEnergy Gammafilter8056 2.9501953125 2.9505615234375 MeV gamma
/score/quantity/nOfSecondary NStepGamma2.9505615234375MeV_2.950927734375MeV
/score/filter/particleWithKineticEnergy Gammafilter8057 2.9505615234375 2.950927734375 MeV gamma
/score/quantity/nOfSecondary NStepGamma2.950927734375MeV_2.9512939453125MeV
/score/filter/particleWithKineticEnergy Gammafilter8058 2.950927734375 2.9512939453125 MeV gamma
/score/quantity/nOfSecondary NStepGamma2.9512939453125MeV_2.95166015625MeV
/score/filter/particleWithKineticEnergy Gammafilter8059 2.9512939453125 2.95166015625 MeV gamma
/score/quantity/nOfSecondary NStepGamma2.95166015625MeV_2.9520263671875MeV
/score/filter/particleWithKineticEnergy Gammafilter8060 2.95166015625 2.9520263671875 MeV gamma
/score/quantity/nOfSecondary NStepGamma2.9520263671875MeV_2.952392578125MeV
/score/filter/particleWithKineticEnergy Gammafilter8061 2.9520263671875 2.952392578125 MeV gamma
/score/quantity/nOfSecondary NStepGamma2.952392578125MeV_2.9527587890625MeV
/score/filter/particleWithKineticEnergy Gammafilter8062 2.952392578125 2.9527587890625 MeV gamma
/score/quantity/nOfSecondary NStepGamma2.9527587890625MeV_2.953125MeV
/score/filter/particleWithKineticEnergy Gammafilter8063 2.9527587890625 2.953125 MeV gamma
/score/quantity/nOfSecondary NStepGamma2.953125MeV_2.9534912109375MeV
/score/filter/particleWithKineticEnergy Gammafilter8064 2.953125 2.9534912109375 MeV gamma
/score/quantity/nOfSecondary NStepGamma2.9534912109375MeV_2.953857421875MeV

/score/filter/particleWithKineticEnergy Gammafilter8065 2.9534912109375 2.953857421875 MeV gamma
/score/quantity/nOfSecondary NStepGamma2.953857421875MeV_2.9542236328125MeV
/score/filter/particleWithKineticEnergy Gammafilter8066 2.953857421875 2.9542236328125 MeV gamma
/score/quantity/nOfSecondary NStepGamma2.9542236328125MeV_2.95458984375MeV
/score/filter/particleWithKineticEnergy Gammafilter8067 2.9542236328125 2.95458984375 MeV gamma
/score/quantity/nOfSecondary NStepGamma2.95458984375MeV_2.9549560546875MeV
/score/filter/particleWithKineticEnergy Gammafilter8068 2.95458984375 2.9549560546875 MeV gamma
/score/quantity/nOfSecondary NStepGamma2.9549560546875MeV_2.955322265625MeV
/score/filter/particleWithKineticEnergy Gammafilter8069 2.9549560546875 2.955322265625 MeV gamma
/score/quantity/nOfSecondary NStepGamma2.955322265625MeV_2.9556884765625MeV
/score/filter/particleWithKineticEnergy Gammafilter8070 2.955322265625 2.9556884765625 MeV gamma
/score/quantity/nOfSecondary NStepGamma2.9556884765625MeV_2.9560546875MeV
/score/filter/particleWithKineticEnergy Gammafilter8071 2.9556884765625 2.9560546875 MeV gamma
/score/quantity/nOfSecondary NStepGamma2.9560546875MeV_2.9564208984375MeV
/score/filter/particleWithKineticEnergy Gammafilter8072 2.9560546875 2.9564208984375 MeV gamma
/score/quantity/nOfSecondary NStepGamma2.9564208984375MeV_2.956787109375MeV
/score/filter/particleWithKineticEnergy Gammafilter8073 2.9564208984375 2.956787109375 MeV gamma
/score/quantity/nOfSecondary NStepGamma2.956787109375MeV_2.9571533203125MeV
/score/filter/particleWithKineticEnergy Gammafilter8074 2.956787109375 2.9571533203125 MeV gamma
/score/quantity/nOfSecondary NStepGamma2.9571533203125MeV_2.95751953125MeV
/score/filter/particleWithKineticEnergy Gammafilter8075 2.9571533203125 2.95751953125 MeV gamma
/score/quantity/nOfSecondary NStepGamma2.95751953125MeV_2.9578857421875MeV

/score/filter/particleWithKineticEnergy Gammafilter8076 2.95751953125 2.9578857421875 MeV gamma
/score/quantity/nOfSecondary NStepGamma2.9578857421875MeV_2.958251953125MeV
/score/filter/particleWithKineticEnergy Gammafilter8077 2.9578857421875 2.958251953125 MeV gamma
/score/quantity/nOfSecondary NStepGamma2.958251953125MeV_2.9586181640625MeV
/score/filter/particleWithKineticEnergy Gammafilter8078 2.958251953125 2.9586181640625 MeV gamma
/score/quantity/nOfSecondary NStepGamma2.9586181640625MeV_2.958984375MeV
/score/filter/particleWithKineticEnergy Gammafilter8079 2.9586181640625 2.958984375 MeV gamma
/score/quantity/nOfSecondary NStepGamma2.958984375MeV_2.9593505859375MeV
/score/filter/particleWithKineticEnergy Gammafilter8080 2.958984375 2.9593505859375 MeV gamma
/score/quantity/nOfSecondary NStepGamma2.9593505859375MeV_2.959716796875MeV
/score/filter/particleWithKineticEnergy Gammafilter8081 2.9593505859375 2.959716796875 MeV gamma
/score/quantity/nOfSecondary NStepGamma2.959716796875MeV_2.9600830078125MeV
/score/filter/particleWithKineticEnergy Gammafilter8082 2.959716796875 2.9600830078125 MeV gamma
/score/quantity/nOfSecondary NStepGamma2.9600830078125MeV_2.96044921875MeV
/score/filter/particleWithKineticEnergy Gammafilter8083 2.9600830078125 2.96044921875 MeV gamma
/score/quantity/nOfSecondary NStepGamma2.96044921875MeV_2.9608154296875MeV
/score/filter/particleWithKineticEnergy Gammafilter8084 2.96044921875 2.9608154296875 MeV gamma
/score/quantity/nOfSecondary NStepGamma2.9608154296875MeV_2.961181640625MeV
/score/filter/particleWithKineticEnergy Gammafilter8085 2.9608154296875 2.961181640625 MeV gamma
/score/quantity/nOfSecondary NStepGamma2.961181640625MeV_2.9615478515625MeV
/score/filter/particleWithKineticEnergy Gammafilter8086 2.961181640625 2.9615478515625 MeV gamma
/score/quantity/nOfSecondary NStepGamma2.9615478515625MeV_2.9619140625MeV

/score/filter/particleWithKineticEnergy Gammafilter8087 2.9615478515625 2.9619140625 MeV gamma
/score/quantity/nOfSecondary NStepGamma2.9619140625MeV_2.9622802734375MeV
/score/filter/particleWithKineticEnergy Gammafilter8088 2.9619140625 2.9622802734375 MeV gamma
/score/quantity/nOfSecondary NStepGamma2.9622802734375MeV_2.962646484375MeV
/score/filter/particleWithKineticEnergy Gammafilter8089 2.9622802734375 2.962646484375 MeV gamma
/score/quantity/nOfSecondary NStepGamma2.962646484375MeV_2.9630126953125MeV
/score/filter/particleWithKineticEnergy Gammafilter8090 2.962646484375 2.9630126953125 MeV gamma
/score/quantity/nOfSecondary NStepGamma2.9630126953125MeV_2.96337890625MeV
/score/filter/particleWithKineticEnergy Gammafilter8091 2.9630126953125 2.96337890625 MeV gamma
/score/quantity/nOfSecondary NStepGamma2.96337890625MeV_2.9637451171875MeV
/score/filter/particleWithKineticEnergy Gammafilter8092 2.96337890625 2.9637451171875 MeV gamma
/score/quantity/nOfSecondary NStepGamma2.9637451171875MeV_2.964111328125MeV
/score/filter/particleWithKineticEnergy Gammafilter8093 2.9637451171875 2.964111328125 MeV gamma
/score/quantity/nOfSecondary NStepGamma2.964111328125MeV_2.9644775390625MeV
/score/filter/particleWithKineticEnergy Gammafilter8094 2.964111328125 2.9644775390625 MeV gamma
/score/quantity/nOfSecondary NStepGamma2.9644775390625MeV_2.96484375MeV
/score/filter/particleWithKineticEnergy Gammafilter8095 2.9644775390625 2.96484375 MeV gamma
/score/quantity/nOfSecondary NStepGamma2.96484375MeV_2.9652099609375MeV
/score/filter/particleWithKineticEnergy Gammafilter8096 2.96484375 2.9652099609375 MeV gamma
/score/quantity/nOfSecondary NStepGamma2.9652099609375MeV_2.965576171875MeV
/score/filter/particleWithKineticEnergy Gammafilter8097 2.9652099609375 2.965576171875 MeV gamma
/score/quantity/nOfSecondary NStepGamma2.965576171875MeV_2.9659423828125MeV

/score/filter/particleWithKineticEnergy Gammafilter8098 2.965576171875 2.9659423828125 MeV gamma
/score/quantity/nOfSecondary NStepGamma2.9659423828125MeV_2.96630859375MeV
/score/filter/particleWithKineticEnergy Gammafilter8099 2.9659423828125 2.96630859375 MeV gamma
/score/quantity/nOfSecondary NStepGamma2.96630859375MeV_2.9666748046875MeV
/score/filter/particleWithKineticEnergy Gammafilter8100 2.96630859375 2.9666748046875 MeV gamma
/score/quantity/nOfSecondary NStepGamma2.9666748046875MeV_2.967041015625MeV
/score/filter/particleWithKineticEnergy Gammafilter8101 2.9666748046875 2.967041015625 MeV gamma
/score/quantity/nOfSecondary NStepGamma2.967041015625MeV_2.9674072265625MeV
/score/filter/particleWithKineticEnergy Gammafilter8102 2.967041015625 2.9674072265625 MeV gamma
/score/quantity/nOfSecondary NStepGamma2.9674072265625MeV_2.9677734375MeV
/score/filter/particleWithKineticEnergy Gammafilter8103 2.9674072265625 2.9677734375 MeV gamma
/score/quantity/nOfSecondary NStepGamma2.9677734375MeV_2.9681396484375MeV
/score/filter/particleWithKineticEnergy Gammafilter8104 2.9677734375 2.9681396484375 MeV gamma
/score/quantity/nOfSecondary NStepGamma2.9681396484375MeV_2.968505859375MeV
/score/filter/particleWithKineticEnergy Gammafilter8105 2.9681396484375 2.968505859375 MeV gamma
/score/quantity/nOfSecondary NStepGamma2.968505859375MeV_2.9688720703125MeV
/score/filter/particleWithKineticEnergy Gammafilter8106 2.968505859375 2.9688720703125 MeV gamma
/score/quantity/nOfSecondary NStepGamma2.9688720703125MeV_2.96923828125MeV
/score/filter/particleWithKineticEnergy Gammafilter8107 2.9688720703125 2.96923828125 MeV gamma
/score/quantity/nOfSecondary NStepGamma2.96923828125MeV_2.9696044921875MeV
/score/filter/particleWithKineticEnergy Gammafilter8108 2.96923828125 2.9696044921875 MeV gamma
/score/quantity/nOfSecondary NStepGamma2.9696044921875MeV_2.969970703125MeV

/score/filter/particleWithKineticEnergy Gammafilter8109 2.9696044921875 2.969970703125 MeV gamma
/score/quantity/nOfSecondary NStepGamma2.969970703125MeV_2.9703369140625MeV
/score/filter/particleWithKineticEnergy Gammafilter8110 2.969970703125 2.9703369140625 MeV gamma
/score/quantity/nOfSecondary NStepGamma2.9703369140625MeV_2.970703125MeV
/score/filter/particleWithKineticEnergy Gammafilter8111 2.9703369140625 2.970703125 MeV gamma
/score/quantity/nOfSecondary NStepGamma2.970703125MeV_2.9710693359375MeV
/score/filter/particleWithKineticEnergy Gammafilter8112 2.970703125 2.9710693359375 MeV gamma
/score/quantity/nOfSecondary NStepGamma2.9710693359375MeV_2.971435546875MeV
/score/filter/particleWithKineticEnergy Gammafilter8113 2.9710693359375 2.971435546875 MeV gamma
/score/quantity/nOfSecondary NStepGamma2.971435546875MeV_2.9718017578125MeV
/score/filter/particleWithKineticEnergy Gammafilter8114 2.971435546875 2.9718017578125 MeV gamma
/score/quantity/nOfSecondary NStepGamma2.9718017578125MeV_2.97216796875MeV
/score/filter/particleWithKineticEnergy Gammafilter8115 2.9718017578125 2.97216796875 MeV gamma
/score/quantity/nOfSecondary NStepGamma2.97216796875MeV_2.9725341796875MeV
/score/filter/particleWithKineticEnergy Gammafilter8116 2.97216796875 2.9725341796875 MeV gamma
/score/quantity/nOfSecondary NStepGamma2.9725341796875MeV_2.972900390625MeV
/score/filter/particleWithKineticEnergy Gammafilter8117 2.9725341796875 2.972900390625 MeV gamma
/score/quantity/nOfSecondary NStepGamma2.972900390625MeV_2.9732666015625MeV
/score/filter/particleWithKineticEnergy Gammafilter8118 2.972900390625 2.9732666015625 MeV gamma
/score/quantity/nOfSecondary NStepGamma2.9732666015625MeV_2.9736328125MeV
/score/filter/particleWithKineticEnergy Gammafilter8119 2.9732666015625 2.9736328125 MeV gamma
/score/quantity/nOfSecondary NStepGamma2.9736328125MeV_2.9739990234375MeV

/score/filter/particleWithKineticEnergy Gammafilter8120 2.9736328125 2.9739990234375 MeV gamma
/score/quantity/nOfSecondary NStepGamma2.9739990234375MeV_2.974365234375MeV
/score/filter/particleWithKineticEnergy Gammafilter8121 2.9739990234375 2.974365234375 MeV gamma
/score/quantity/nOfSecondary NStepGamma2.974365234375MeV_2.9747314453125MeV
/score/filter/particleWithKineticEnergy Gammafilter8122 2.974365234375 2.9747314453125 MeV gamma
/score/quantity/nOfSecondary NStepGamma2.9747314453125MeV_2.97509765625MeV
/score/filter/particleWithKineticEnergy Gammafilter8123 2.9747314453125 2.97509765625 MeV gamma
/score/quantity/nOfSecondary NStepGamma2.97509765625MeV_2.9754638671875MeV
/score/filter/particleWithKineticEnergy Gammafilter8124 2.97509765625 2.9754638671875 MeV gamma
/score/quantity/nOfSecondary NStepGamma2.9754638671875MeV_2.975830078125MeV
/score/filter/particleWithKineticEnergy Gammafilter8125 2.9754638671875 2.975830078125 MeV gamma
/score/quantity/nOfSecondary NStepGamma2.975830078125MeV_2.9761962890625MeV
/score/filter/particleWithKineticEnergy Gammafilter8126 2.975830078125 2.9761962890625 MeV gamma
/score/quantity/nOfSecondary NStepGamma2.9761962890625MeV_2.9765625MeV
/score/filter/particleWithKineticEnergy Gammafilter8127 2.9761962890625 2.9765625 MeV gamma
/score/quantity/nOfSecondary NStepGamma2.9765625MeV_2.9769287109375MeV
/score/filter/particleWithKineticEnergy Gammafilter8128 2.9765625 2.9769287109375 MeV gamma
/score/quantity/nOfSecondary NStepGamma2.9769287109375MeV_2.977294921875MeV
/score/filter/particleWithKineticEnergy Gammafilter8129 2.9769287109375 2.977294921875 MeV gamma
/score/quantity/nOfSecondary NStepGamma2.977294921875MeV_2.9776611328125MeV
/score/filter/particleWithKineticEnergy Gammafilter8130 2.977294921875 2.9776611328125 MeV gamma
/score/quantity/nOfSecondary NStepGamma2.9776611328125MeV_2.97802734375MeV

/score/filter/particleWithKineticEnergy Gammafilter8131 2.9776611328125 2.97802734375 MeV gamma
/score/quantity/nOfSecondary NStepGamma2.97802734375MeV_2.9783935546875MeV
/score/filter/particleWithKineticEnergy Gammafilter8132 2.97802734375 2.9783935546875 MeV gamma
/score/quantity/nOfSecondary NStepGamma2.9783935546875MeV_2.978759765625MeV
/score/filter/particleWithKineticEnergy Gammafilter8133 2.9783935546875 2.978759765625 MeV gamma
/score/quantity/nOfSecondary NStepGamma2.978759765625MeV_2.9791259765625MeV
/score/filter/particleWithKineticEnergy Gammafilter8134 2.978759765625 2.9791259765625 MeV gamma
/score/quantity/nOfSecondary NStepGamma2.9791259765625MeV_2.9794921875MeV
/score/filter/particleWithKineticEnergy Gammafilter8135 2.9791259765625 2.9794921875 MeV gamma
/score/quantity/nOfSecondary NStepGamma2.9794921875MeV_2.9798583984375MeV
/score/filter/particleWithKineticEnergy Gammafilter8136 2.9794921875 2.9798583984375 MeV gamma
/score/quantity/nOfSecondary NStepGamma2.9798583984375MeV_2.980224609375MeV
/score/filter/particleWithKineticEnergy Gammafilter8137 2.9798583984375 2.980224609375 MeV gamma
/score/quantity/nOfSecondary NStepGamma2.980224609375MeV_2.9805908203125MeV
/score/filter/particleWithKineticEnergy Gammafilter8138 2.980224609375 2.9805908203125 MeV gamma
/score/quantity/nOfSecondary NStepGamma2.9805908203125MeV_2.98095703125MeV
/score/filter/particleWithKineticEnergy Gammafilter8139 2.9805908203125 2.98095703125 MeV gamma
/score/quantity/nOfSecondary NStepGamma2.98095703125MeV_2.9813232421875MeV
/score/filter/particleWithKineticEnergy Gammafilter8140 2.98095703125 2.9813232421875 MeV gamma
/score/quantity/nOfSecondary NStepGamma2.9813232421875MeV_2.981689453125MeV
/score/filter/particleWithKineticEnergy Gammafilter8141 2.9813232421875 2.981689453125 MeV gamma
/score/quantity/nOfSecondary NStepGamma2.981689453125MeV_2.9820556640625MeV

/score/filter/particleWithKineticEnergy Gammafilter8142 2.981689453125 2.9820556640625 MeV gamma
/score/quantity/nOfSecondary NStepGamma2.9820556640625MeV_2.982421875MeV
/score/filter/particleWithKineticEnergy Gammafilter8143 2.9820556640625 2.982421875 MeV gamma
/score/quantity/nOfSecondary NStepGamma2.982421875MeV_2.9827880859375MeV
/score/filter/particleWithKineticEnergy Gammafilter8144 2.982421875 2.9827880859375 MeV gamma
/score/quantity/nOfSecondary NStepGamma2.9827880859375MeV_2.983154296875MeV
/score/filter/particleWithKineticEnergy Gammafilter8145 2.9827880859375 2.983154296875 MeV gamma
/score/quantity/nOfSecondary NStepGamma2.983154296875MeV_2.9835205078125MeV
/score/quantity/nOfSecondary NStepGamma2.9959716796875MeV_2.996337890625MeV
/score/filter/particleWithKineticEnergy Gammafilter8181 2.9959716796875 2.996337890625 MeV gamma
/score/quantity/nOfSecondary NStepGamma2.996337890625MeV_2.9967041015625MeV
/score/filter/particleWithKineticEnergy Gammafilter8182 2.996337890625 2.9967041015625 MeV gamma
/score/quantity/nOfSecondary NStepGamma2.9967041015625MeV_2.9970703125MeV
/score/filter/particleWithKineticEnergy Gammafilter8183 2.9967041015625 2.9970703125 MeV gamma
/score/quantity/nOfSecondary NStepGamma2.9970703125MeV_2.9974365234375MeV
/score/filter/particleWithKineticEnergy Gammafilter8184 2.9970703125 2.9974365234375 MeV gamma
/score/quantity/nOfSecondary NStepGamma2.9974365234375MeV_2.997802734375MeV
/score/filter/particleWithKineticEnergy Gammafilter8185 2.9974365234375 2.997802734375 MeV gamma
/score/quantity/nOfSecondary NStepGamma2.997802734375MeV_2.9981689453125MeV
/score/filter/particleWithKineticEnergy Gammafilter8186 2.997802734375 2.9981689453125 MeV gamma
/score/quantity/nOfSecondary NStepGamma2.9981689453125MeV_2.99853515625MeV
/score/filter/particleWithKineticEnergy Gammafilter8187 2.9981689453125 2.99853515625 MeV gamma

```
/score/quantity/nOfSecondary
NStepGamma2.99853515625MeV_2.9989013671875MeV
/score/filter/particleWithKineticEnergy Gammafilter8188 2.99853515625
2.9989013671875 MeV gamma
/score/quantity/nOfSecondary
NStepGamma2.9989013671875MeV_2.999267578125MeV
/score/filter/particleWithKineticEnergy Gammafilter8189 2.9989013671875
2.999267578125 MeV gamma
/score/quantity/nOfSecondary
NStepGamma2.999267578125MeV_2.9996337890625MeV
/score/filter/particleWithKineticEnergy Gammafilter8190 2.999267578125
2.9996337890625 MeV gamma
/score/quantity/nOfSecondary NStepGamma2.9996337890625MeV_3MeV
/score/filter/particleWithKineticEnergy Gammafilter8191 2.9996337890625 3
MeV gamma

/score/close
#
#####################################
/score/list
#
/run/beamOn 1000000
#
#####################################
##         Write data to files    ###
#####################################
#
/score/dumpAllQuantitiesToFile boxMesh_1 filename.txt
```

APPENDIX E

FLOW CHART OF PREDICTIVE MODEL

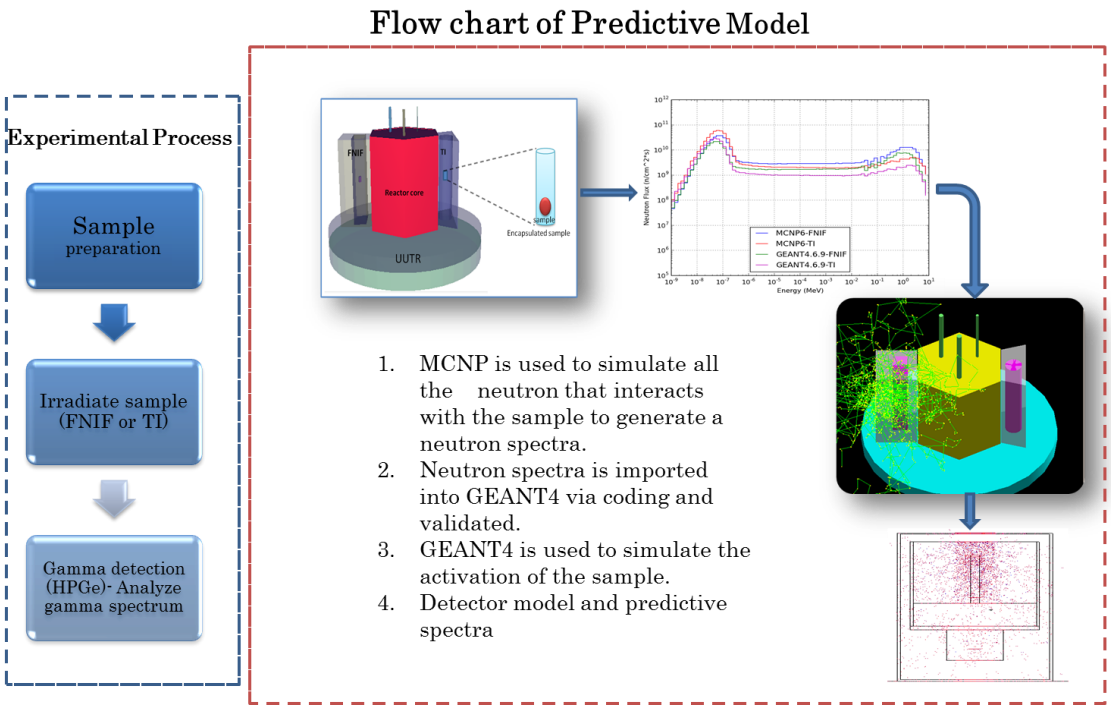

APPENDIX F

NEUTRON PHYSICS PROCESS WITHIN SAMPLE

Screen shot list of neutron possible interaction in GEANT4

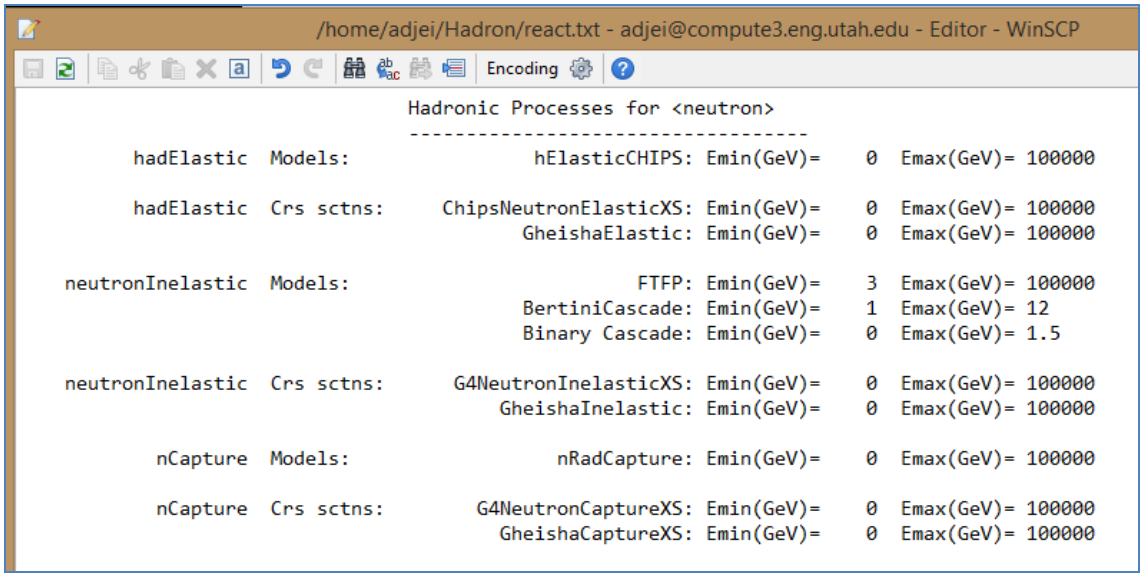

REFERENCES

1. H. Levi, G. de Hevesy: life and work: a biography. A. Hilger, 1985.

2. L. Hamidatou, H. Slamane, T. Akhal, B. Zouranen, Concepts, Instrumentation and Techniques of Neutron Activation Analysis, Chapter 6.IAEA-TECDOC-1215, Use of research reactors for neutron activation analysis, report of an advisory group meeting held in Vienna, 22-26 June 1998.

3. N. Tsoulfanidis, Measurement and Detection of Radiation, second edition. Taylor and Francis Ltd. 1995.

4 P. Bode, Instrumental and organizational aspects of a neutron activation analysis laboratory, Ph.D. dissertation, Delft University of Technology, Delft (1996).

5 G. Molnar, T. Belgya, L. Dabolczi, B. Fazekas, Z. Revay, A. Veres, I Bikit, Z. Kiss, J. Ostor, The new prompt gamma activation analysis facility at Budapest, J. Radioanal. Nucl. Chem. 215 (1997) 111–115.

6 http://atom.kaeri.re.kr/cgi-bin/endfplot.pl

7 T. Jevremovic, Nuclear Principles in Engineering. Springer, 2009.

8 T. Sherman. Advanced Neutron Activation Analysis Protocol for the University of Utah Nuclear Engineering Program. Master's Thesis. University of Utah; 2012.

9 R. Leslie, Potential for Produciton of Porliferation Sensitive Materials in Research Reactors. Australian Government, Australian Safegruards Support Program, 2008.

10 IAEA Technical report series No. 107, Neutron Fluence Measurements, 1970.

11 E. Steinnes, INAA of geological materials using a combination of epithermal activation and Compton suppression: Prediction of

possibilities. Journal of Radioanalytical and Nuclear Chemistry, Vol.278, No.2 (2008) 313-317.

12 PUN, T.H., LANDSBERGER, S., "Determination of silver using cyclic epithermal neutron activation analysis," J. Radioanal. Nucl. Chem. (2012).

13 S. Glasstone, M. C. Edlund, Nuclear Reactor Theory, Van Nostrand, 1955.

14 D. DODOO-AMOO, S. LANDSBERGER, "Gamma-ray self-attenuation calculations in neutron activation analysis," J. Radioanal. Nucl. Chem. 248 (2001) 327-332.

15 B. Zeev. Alfassi *et al*, "Activation Analysis – Volume II" – CRC Press, Inc., Florida, 1990.

16 J. D. Bess, Designing a High-Flux Trap in the University of Utah TRIGA Reactor. Masters Thesis. University of Utah; 2005

17 C. A. Adjei. MCNP5 and GEANT4 Comparison for Preliminary Fast Neutron Pencil Beam Design at the University of Utah TRIGA System. Master's Thesis. The University of Utah; 2012.

18 A. Cutic. Feasibility Study of the University of Utah TRIGA Reactor Power Upgrade in Respect to Control Rod System. Master's Thesis. The University of Utah; 2012

19 J. S. Bennion. Characterization and Qualification of a Quasi-Fission Neutron Irradiaiton Environment for Neutron Hardness Assurance Testing of Electric Devices and other Materials Damage Investigations. Doctoral Thesis. The University of Utah; 1996.

20 J. R. Lamarsh, A. J. Baratta, Introduction to Nuclear Engineering – Third Edition, Prentice Hall Inc, Upper Saddle River, New Jersey 07458, 2001. pg 68 – 75.

21 W. M. Stacey, Nuclear Reactor Physics – second edition, wiley-vch 2007.

22 J. J. Duderstadt, L. J. Hamilton, Nuclear Reactor Analysis, John Wiley & Sons Inc, 1976.

23 G. I. Bell, S. Glasstone, Nuclear Reactor Theory, Van Nostrand Reinhold Company, NY, 1970.

24 Monte Carlo Method, 2012 Web, http://en.wikipedia.org/wiki/Monte_Carlo_method

25 Berg, A. Bernd, Markov Chain Monte Carlo Simulations and Their Statistical Analysis (With Web-Based FORTRAN Code). Hackensack, NJ: World Scientific. ISBN 981-238-935-0 (2004).

26 P. Arce, et al., Nucl. Instr. and Meth. A 502 (2003) 687.

27 Geant4 Collaboration (S. Agostinelli et al.), Nucl. Instr. and Meth. A 506 (2003) 250.

28 BABAR Computing Group (D.H. Wright et al.), CHEP-2003-TUMT006, May 2003, 7pp. Proceedings of the International Conference CHEP'03, La Jolla,California, 2003, e-Print Archive: hep-ph/0305240.

29 GEANT4 Simulation code, 2012. Web, http:://www.info.cern.ch/asd/geant4/

30 GEANT4 Simulation code, Introduction to GEANT4 – Physics references, 2012. Web,http://geant4.web.cern.ch/geant4/UserDocumentation/UsersGuides /PhysicsReference

31 F. De corte, I. Moens, A. Simonits, De Wispelaere, A., hoste, J., J.Radioanal. Chem. 52 (1979) 295–304.

32 I. M. Cohen, J. C. Furnari, E. H. Montoya,P. A. Mendoza, M. S. Ubillus, B. J. Torres, J. Radioanal. Nucl. Chem.

33 F. Baumgärtner, Kerntechnik 3 (1961) 356–369.

34 J. V. Sandford, P. D. Lund, J. Radioanal. Chem. 76 (1983) 151–170.

35 W. N. Mc.Elroy, S. Berg, G. Gigas, Nucl. Sc. Eng. 27 (1967) 533–541.

36 W. N. McElroy, S. Berg, T. B. Crockett, Turtle, J., Nucl. Sci. Eng. 36 (1969) 15–27.

37 W. Z. Zijp, Review of Activation Methods for the Determination of Neutron Flux Spectra, RCN-report 241, Petten, Netherlands (1976).

38 S. M. Jefferies, Characterization of thermal and epithermal neutron spectra, PhD thesis, University of London (1983).

39 International Atomic Energy Agency, Neutron Fluence Measurements, Technical Reports Series No. 107, IAEA, Vienna (1970).

40 American Society for Testing And Materials, Standard Method for Determining Neutron Flux, Fluence and Spectra by Radioactivation Techniques, ASTM Standard Designation E261.

41 American Society for Testing And Materials, Standard Method for Determining Thermal Neutron Reaction and Fluence Rates by Radioactivation Techniques, ASTM Standard Designation E262.

42 G. Erdtmann, Neutron Activation Tables, Verlag Chemie, Weinheim, New York (1976).

43 J. R. Moody, R. R. Greenberg, K. W. Pratt, T. C. Rains, Anal. Chem., Nov. 1988) 1203A–1218A.

44 F. De Cort, A. Simonits, A. De Wispelaere, A. ELEK, J. Radioanal. Nucl. Chem. 133 (1989) 3–41 & 43–130.

45 D. Pelowitz (Ed.). MCNPX User's Manual, Ver. 2.7.0, Los Alamos National Laboratory, 2011 LA-CP-11-00438.

46 Geant4.9.6 Physics Reference Manual. http://geant4.web.cern.ch/geant4/UserDocumentation/UserGuides/PhysicsReferenceManual/BackupVersions/V9.6/fo/PhysicsReferenceManual.Pdf, October 2013.

47 L. Snoj, M. Ravnik. Calculation of Power density with MCNP in TRIGA reactor. In: Proceedings of the International Conference Nuclear Energy for New Europe 2006, Portoroz, Slovenia, Paper no. 102.

48 B. Noble, D. Choe, T. Jevremovic. Experimental and MCNP5 based evaluation of neutron and gamma flux in the irradiation ports of The University of Utah research reactor. Nucl. Tech. & Rad, 27 (2012) 222 – 228.

49 N. Tsoulfanidis, S. Landsberger, Measurement and Detection of Radiation: Third Edition. CRC press – Taylor & Francis group, 2011.

50 D. Sahin, K. Unlu. Modeling a gamma spectroscopy system and predicting spectra with Geant4. J. Radioanal Nucl Chem (2009) 282:167-172

51 J. Boson, G. Agren, L. Johansson. A detailed investigation of HPGe detector response for improved Movte Carlo efficiency calculations. Nucl Instrum Methods Phys Res A (2008) 587: 304-314.

52 P. Bode, Activation Analysis of Large Samples, Ency. of Anal Chem, John Wiley & Sons. Ltd. 2008.

53 B. Kratochvil, J.K. Taylor, 'Sampling for Chemical Analysis', Anal. Chem., 54, 924A (1981).

54 D. Buslik, A proposed universal homogeneity and mixing index, Powder Tech. 7 (1973) 111-116

55 J.A. Hersey, Assessment of homogeneity of powder mixtures, J. Pharm. Pharmacol. 19 (1967) 168S-176S

56 M.I. Verheijke, H.J.J. Jaspers, J.M.G. Hanssen, 'Neutron Activation of Very Pure Silicon Wafers', *J. Radioanal. Nucl. Chem.*, **131**, 197 (1989).

57 R.M.W. Overwater, The physics of Big Sample Instrumental Neutron Activation Analysis, thesis, Delft 1994

58 R.M.W. Overwater, P. Bode, J.J.M. De Goeij, J.E. Hoogenboom (1996) Feasibility of elemental analysis of kilogram-size samples by instrumental neutron activation analysis. Anal Chem 68:341–348

59 H. Cember, T. E. Johnson, 'Introduction to Health Physics – fourth edition'. McGrawHill Medical companies, Inc, 2009.

60 http://atom.kaeri.re.kr/cgi-bin/endfform.pl